Modelling and optimization of electrospun materials for technical applications

Ahsan Nazir

UNIVERSITÉ DE HAUTE-ALSACE

École Doctorale : Mathématiques, Sciences de l'Information et de l'Ingénieur (MSII)

Laboratoire de Physique et Mécanique Textile - LPMT (EA-4365)

Thèse en cotutelle

entre l'Université de Haute-Alsace, France et la National Textile University, Pakistan

présentée par :

Ahsan NAZIR

soutenue le : **10 septembre 2016**

pour obtenir le grade de : **Docteur de l'Université de Haute-Alsace**

Discipline/ Spécialité : MECANIQUE

Modelling and Optimization of Electrospun Materials for Technical Applications

Thèse dirigée par :

Mme Laurence **SCHACHER**	Professeur, Université de Haute-Alsace, France
Mr. Dominique C. **ADOLPHE**	Professeur, Université de Haute-Alsace, France
Mr. Tanveer **HUSSAIN**	Professeur, National Textile University, Faisalabad, Pakistan

Et co-encadrée

Mr. Nabyl **KHENOUSSI**	Maître de conférences, Université de Haute-Alsace, France

Rapporteurs **:**

Mr. Bernard **MARTEL**	Professeur, Université de Lille 1, France
Mr. Muhammad **TAUSIF**	Chercheur, University of Leeds, UK

Autres membres du jury

Mr. Niaz Ahmed **AKHTAR**	Professeur/ Vice Chancellor, University of Engineering and Technology, Taxila, Pakistan

Dedication

This modest effort is dedicated to my parents and family members, teachers and supervisors and all those who helped me to accomplish it.

Acknowledgement

I am thankful to the management and technical team of Honeywell, France and Frima, France for providing the technical support needed for this study. I am also thankful to staff and management of collaborating labs including Institut de Science des Matériaux de Mulhouse (IS2M), Laboratoire des Multimatériaux et Interfaces (LMI) Lyon and Laboratoire Gestion des Risques et Environnement (GRE) Mulhouse.

Ahsan NAZIR

MODELLING AND OPTIMIZATION OF ELECTROSPUN MATERIALS FOR TECHNICAL APPLICATIONS

Résumé

Ce travail de recherche traite de l'optimisation et de la modélisation de nanofibres obtenues par filage électrostatique pour des applications techniques en tant que, a) cellules résistives pour génération de chaleur et b) couche ultra filtrante pour système de protection respiratoire. Afin d'intégrer ces matériaux nanofibreux aux applications visées, deux procédés de production ont été mis en œuvre, à savoir mono-aiguille et multijets. Une étude statistique a été réalisée pour modéliser et optimiser les non-tissés de nanofibres pour des productions à échelle laboratoire et semi-industrielle. L'outil statistique c'est révélé pertinent pour anticiper la morphologie des matériaux produits et assurer une homogénéité optimale. Les non-tissés présentant les caractéristiques morphologiques souhaitées ont été sélectionnés, testés, et les résultats ont révélé leur fort potentiel pour les champs applicatifs visés. Ces travaux valident deux pistes de recherche qui déboucheraient sur une intégration concrète de ces matériaux innovants.

Mots clés: Modélisation, optimisation, filage électrostatique, génération de chaleur, protection respiratoire, caractérisation morphologique, nanocomposite, nanofibers

Abstract

Optimization and modelling of electrospun nanofibrous nonwovens and their technical applications, i-e heat generation and respiratory protection, were studied in this work. For utilization in these applications, nanowebs were statistically modelled and optimized using different electrospinning techniques i-e needle and needleless setups based on significance of these techniques for lab and bulk scale production of nanowebs. Moreover, quantitative impact of different electrospinning parameters was also observed. Statistical analysis was found to be a useful tool for study of electrospinning process and production of nanowebs with minimum defects. The optimized nanowebs were used for selected applications and based on results it was concluded that they can be a potential material for both, heat generation and respiratory protection. These observations are expected to initiate more focused studies in both the fields.

Keywords: Modelling, optimization, electrospinning, heat generation, respiratory protection, morphological characterization, nanocomposite, nanofibres

Table of Contents

List of Figures

List of Tables

List of Equations

Abbreviations

PAN	= Polyacrylonitrile
DMF	= Dimethylformamide
CNT	= Carbon nanotube
CNF	= Carbon nanofibers
MWCNT	= Multi walled carbon nanotube
SWCNT	= Single walled carbon nanotube
PAN/CNT	= Nanofibrous Composite with PAN and CNTs
CNF/CNT	= Nanofibrous Composite with CNF and CNTs
PA-6	= Polyamide 6
DOE	= Design of experiments
ANOVA	= Analysis of variance
FF	= Full factorial
RS	= Response surface
St. Dev.	= Standard Deviation
C	= Concentration
D	= Distance
V	= Voltage
C_{CNT}	= CNT content in fiber
Cs	= Carrier speed
Ss	= Substrate speed
Af	= Air flow
TGA	= Thermogravimetric analysis
SEM	= Scanning electron microscope
TEM	= Transmission electron microscope
mB	= millibar

Resume des chapitres en Francais

Chapitre 1: Introduction

Les nanofibres sont des structures fines et allongés, ayant des diamètres dans l'échelle nanométrique [1]. Elles peuvent être produites par de nombreuses techniques de fabrication [2, 3], dont l'électrofilage. L'électrofilage est technique la plus pratique et la plus simple qui permette de produire, à vitesse élevée et à partir d'un grand nombre de polymères, des nanofibres ayant des propriétés spécifiques, En outre, cette technique peut permettre une production à l'échelle industrielle de nanofibres [4, 5].

La théorie de l'électrofilage est basée sur l'utilisation de la force électrostatique afin de produire des nanofibres à partir d'une solution de polymères, délivrée par une buse. Le processus d'électrofilage est constitué d'une seringue contenant une solution de polymère ou de polymère fondu, d'une source de haute tension et d'un collecteur. En appliquant une différence de potentiel suffisante, la solution se charge, développant ainsi une répulsion coulombienne. Cette dernière surmonte la tension superficielle et permet la production d'un jet, qui se déplace vers le collecteur sous la force électrostatique. Au cours de ce mouvement, ou "fuite", le solvant s'évapore et le jet se transforme en nanofibres qui sont déposées sur le collecteur.

Les propriétés des fibres produites par électrofilage dépendent de différents paramètres, tel que cela est décrit dans la bibliographie [6-11]. Ces paramètres peuvent être classés comme : les propriétés de la solution, les paramètres du procédé et les paramètres ambiants [12].

Les matériaux issus de l'électrofilage de polymères ont,déjà été étudiés pour diverses applications et des résultats très prometteurs ont été obtenus. Les plus importants domaines d'application des nanofibres sont les suivants : production et stockage de l'énergie, électronique, protection de l'environnement, transport de catalyseurs et d'enzymes, médical, ingénierie tissulaire, les capteurs et les filtres [13].

Il est primordial de bien prendre conscience des propriétés et du comportement de ces matériaux afin de les intégrer de façn optimum dans les divers domains d'application visés. De

meilleures performances peuvent ainsi être obtenues en optimisant les procédés de fabrication pour et obtenir des adaptées à l'application finale. Ceci peut être réalisé en utilisant différentes techniques de modélisation qui, non seulement, permettent d'étudier le comportement des nanofibres mais aussi d'optimiser et de prédire leurs propriétés.

Ce travail de thèse a pour but de fournir un point de départ pour deux nouvelles applications de matériaux électrofilées, à savoir la production thermique et la protection respiratoire. Pour atteindre cet objectif, les réseaux de nanofibres ont été étudiés, optimisés et modélisés pour produire de meilleurs matériaux en qualité et en quantité. La modélisation et l'optimisation ont été étudiés en considérant que les résultats seront meilleurs et plus reproductibles que ceux obtenus à partir de réseaux non optimisés,. De plus, l'optimisation, la modélisation et la comparaison des résultats obtenus par le procédé d'électrofilage réalisé sur le dispositif du laboratoire qui est constitué d'un système à aiguille avec celui réalisé sur le dispositif semi-industriel sans aiguille, ont permis de mieux comprendre les processus. En effet, pour le cas de l'électrofilage sans aiguille, aucune référence n'est disponible car très peu d'études ont été réalisées à ce jour sur un tel dispsitif. La modélisation et l'optimisation de ces configurations sera donc intéressante, une fois la production en masse sera obtenue. Cette approche donne un nouveau départ, prometteur, pour les applications visées qui pourraient être étudié plus profondément par la suite. En outre, ce manuscrit permet de mieux comprendre le processus d'électrofilage dans son ensemble.

Chapitre 2 : Bibliographie

La technique d'électro-filage peut être classée, selon la géométrie du générateur de nanofibres, en électro-filage capillaire et non-capillaire. Les nanofibres produites par l'électro-filage capillaire sont générées à partir d'une goutte de polymère, généralement en solution, écoulant d'un capillaire (une aiguille, par exemple), alors qu'à l'électro-filage non-capillaire, d'autres types de sources d'alimentation de solution polymérique sont employées [13].

Les caractéristiques de nanofibres produites et les nappes de matériaux nanofibreux résultantes, ainsi que leurs applications, dépendent fortement sur l'ensemble des paramètres gouvernant le procédé d'électro-filage. Ces paramètres incluent, entre autres, la concentration du polymère (ainsi que sa viscosité), le diamètre du capillaire, le débit de solution, la tension

appliquée, la distance entre le capillaire et le collecteur, ainsi que les conditions de l'environnement comme l'humidité relative et la température de l'air l'ambiant [14-20].

Différents outils de modélisation et d'optimisation sont utilisés dans des champs d'application divers [21]. Ces outils peuvent être envisagés pour la production des nanofibres afin de prévoir et d'optimiser le procédé d'électro-filage et les matériaux obtenus par ce procédé. Il existe différents types de méthodes de modélisation statistique. Le plus important d'entre eux comprend l'analyse de variance (ANOVA) et le modèle de régression [22]. Afin d'utiliser ces méthodes de modélisation, un plan d'expériences (Design Of Experience, DOE) est nécessaire. Ce dernier est un ensemble d'expériences, avec différentes combinaisons de niveaux (combinaison de valeurs ou paramètres) de variables d'entrée [23]. Certains types importants du plan d'expériences comprennent le plan factoriel, de la surface de réponse et celui de Taguchi.

Un nombre limité d'études a été réalisé pour l'optimisation et la modélisation du processus d'électro-filage. Certaines des études emploient des approches simples pour développer de simples modèles exponentiels. Ces études ne peuvent pas parfaitement représenter le comportement du processus. Pour d'autres études, des plans d'expériences ont été conçus en utilisant un Plan Factoriel complet. Cependant, le nombre de ces études est très limité. En outre, le plan factoriel complet peut ne pas couvrir l'ensemble du comportement complexe attendu pour le processus d'électro-filage et il est plus difficile à mettre en oeuvre en raison du grand nombre d'essais expérimentaux à mener qu'il exige.

Un nombre limité d'études de recherches a utilisé des méthodes statistiques pour l'optimisation et la modélisation des processus d'électro-filage capillaire [24], alors qu'aucune étude n'a été faite pour modéliser et optimiser l'électro-filage non-capillaire. Ainsi, ce domaine doit être explorée pour évaluer ses avantages et/ou ses inconvénients pour électro-filage. Dans le cadre de cette étudse, différents plans d'expériences ont été utilisés pour la modélisation et l'optimisation du processus de l'électro-filage en utilisant différents polymères. Les polymères sélectionnés à cet effet sont le Polyacrylonitrile (PAN) et le Polyamide-6 (PA-6).

En ce qui concerne les applications spécifiques ciblées dans ce travail, le Polyacrylonitrile (PAN) a été sélectionné pour la production de chaleur et le Polyamide-6 (PA-6) pour la protection

respiratoire. Le PAN a été sélectionné car il a une bonne capacité à être électrofilé et il peut être utilisé dans la production de chaleur grâce au processus de carbonisation qui le peut le convertir en nanofibres de carbone conductrices de l'électricité [25-26].

De plus, de nombreux travaux montrent que l'ajout d'additifs tels que des nanotubes de carbone (NTC) peut modifier les propriétés électriques des nanofibres de PAN grâce à leurs propriétés exceptionnelles. Ainsi, PAN et PAN/NTC peuvent être envisagés pour une utilisation dans le cadre d'applications de production de chaleur. De même, PA-6 est également connu pour sa bonne aptitude à être électrofilé et pour la production de fibres très fines [27, 28]. Ce matériaux, a déjà été étudié pour différentes applications de filtration [29]. Ces observations ont justifié le choix de l'utilisation de PA-6 nanofibres pour le développement des filtres de protection des voies respiratoires.

L'objectif de ce travail de recherche est d'approuver l'utilisation des nanowebs optimisés et produits par l'électro-filage dans ces deux domaines d'application. Cela conduira aux résultats reproductibles avec possibilité de se concentrer et d'optimiser les propriétés autres que la morphologie, dans des études ultérieures.

Chapitre 3 : Matériaux et Méthodes

Le second chapitre expose le choix des matériaux (type de polymère et solvant associé) pour les deux applications retenues ainsi que les méthodes de filage et de caractérisation appliquées afin d'atteindre les objectifs fixés. Les matériaux ont été électrofilés en utilisant un procédé conventionnel avec aiguille et une ligne de production semi-industrielle sans aiguille. Un plan d'expériences a été établi afin d'obtenir des jeux de paramètres optimum pour la prédiction des sorties.

En ce qui concerne l'application *Générateur de chaleur*, le polymère utilisé est le Polyacrylonitrile (PAN) dont le solvant associé est le dimethylformamide (DMF). Pour l'application *Masque de protection*, le Polyamide 6 a été choisi avec pour solvant l'acide formique. Pour le composite PAN/CNT, les nanotubes de carbone ont tout d'abord été dispersés dans le DMF avant l'ajout des granulés de polymère.

Les matériels d'électrofilage utilisés furent ceux disponibles au Laboratoire. Le dispositif avec aiguille est un dispositif conçu en interne dont le filage est vertical (du haut vers le bas). Les paramètres contrôlables sont les suivants : tension, distance aiguille/collecteur, débit. Le dispositif semi-industriel est la machine Nanospider NS500 de la société Elmarco qui est également un dispositif de filage vertical, mais dont le sens de filage est du bas vers le haut. Dans ce dispositif, il y a lieu de contrôler les trois paramètres additionnels suivants : taux de recouvrement du fil (via la vitesse du chariot), vitesse de défilement du substrat et vitesse d'extraction de l'air.

L'électrofilage a été réalisé en appliquant plusieurs plans d'expérience. Pour l'application *Générateur de chaleur*, qui est basée sur la mise en œuvre de nano non-tissés de PAN et PAN / CNT, des plans factoriel complets et des plans de surface de réponses ont été appliqués pour le dispositif de filage avec aiguille ; tandis que seuls des plans de surface de réponse ont été appliqués pour la configuration sans aiguille, compte tenu du grand nombre d'essais qui auraient été à réaliser sur le dispositif semi-industriel dans le cas de plans factoriels complets. Pour l'application *Masque de protection*, les plans factoriels et Taguchi complets ont été utilisés pour la configuration d'électrofilage avec aiguille, tandis que, seule la conception Taguchi a été appliquée pour la configuration sans aiguille.

Utiliser la méthode Taguchi a permis de mener à bien l'étude avec un nombre réduit d'expériences. Les données obtenues après la réalisation des expériences ont été analysées par analyse de la variance, ANOVA (pour déterminer les facteurs importants) et par régression, afin d'établir des relations entre les entrées et sorties.

Les nanofibres électrofilées selon les plans d'expériences ont été recueillies sur des feuilles d'aluminium. Les échantillons PAN et PAN / CNT obtenus après optimisation ont été déposés sur des feuilles de téflon, afin de pouvoir être aisément retirés du collecteur, ce qui n'était pas été possible en utilisant des feuilles d'aluminium. Les nanofibres de PA-6 ont été déposées sur des supports de filtre non-tissés « melt-blown » et prises en sandwich entre les médias filtrants « spunbond ». Ces deux types de médias filtrants, couramment utilisé comme pour les masques faciaux de protection respiratoire, ont été fournis par le partenaire industriel de l'étude.

Les nano-non-tissés PAN et PAN / CNT ont été carbonisés pour les rendre électriquement conducteurs. A cet effet, les échantillons ont d'abord été stabilisés en les maintenant dans un cadre en acier avant d'être maintenu à 300 °C pendant une heure dans l'air dans un four à moufle. Après stabilisation, les nano-non-tissés ont été carbonisées à 1000 ° C pendant une heure dans un environnement d'azote à l'aide d'un four rotatif.

Après leur production et leurs différents traitements, les matériaux obtenus ont été caractérisés, en fonction des applications requises, pour déterminer leurs propriétés. La morphologie a été étudiée pour tous les types de matériaux. Pour l'application *Génération de chaleur,* les propriétés étudiées sont les suivantes : structure interne, conductivité électrique, stabilité thermique ainsi que les propriétés de génération de chaleur. Pour l'application *Masque de protection*, la protection respiratoire, l'efficacité de filtration respiratoire, la gestion de l'humidité, le transfert de vapeur d'eau, la perméabilité à l'air et la conductivité thermique. ont été mesurées.

Chapitre 4 : Résultats et Discussions

Pour les deux applications sélectionnées, l'effet des paramètres d'entrée sur la morphologie des nanofibres a été étudié. A cet effet, les diamètres et leur distribution ont été analysés pour tous les types de matériaux.

Pour l'application *Production de chaleur*, il a été observé que le paramètre qui impacte de manière significative le diamètre et sa distribution est la concentration. Des résultats obtenus par l'application des plans d'expérience et des plans d'estimation de la surface de réponse, le carré de la concentration a également un impact significatif sur le diamètre des fibres. Ceci est confirmé par le facteur significatif du terme au second degré (C^2) pour la prédiction des sorties du processus d'électrofilage. Quel que soit le modèle expérimental appliqué, les échantillons sont dits optimisés lorsqu'ils sont sans défauts et avec une dispersion en diamètre la plus faible possible. La même méthodologie a été appliquée pour l'électrofilage sans aiguille du PAN. Cependant, dans ce cas, seul le plan de la surface de réponse a été appliqué. Il a de nouveau été observé que la concentration a un impact - non linéaire- sur le diamètre des nanofibres. De ces résultats, certains modèles statistiques ont été obtenus, qui semblent acceptable si l'on considère leur valeur de R-sq. Les

modèles obtenus à partir de modèles de surface de réponse ont été jugés plus valables que les plans factoriels complets.

Les nanowebs composites PAN/CNT ont été étudiés en utilisant les mêmes méthodes que pour les nanofibres de PAN. Cependant, pour électrofilage avec aiguille, il était nécessaire d'obtenir le réglage optimisé à la fois de la concentration de PAN et de la quantité de CNT. La concentration en PAN ayant déjà été optimisée dans l'une des études antérieures de notre groupe de recherche, nous avons donc optimisé seulement la quantité de CNT. En ce qui concerne l'électrofilage du PAN, nous avons constaté que la distance d'électrofilage n'a pas d'influence significative sur la morphologie. La durée d'électrofilage a donc été contrôlée. Il a été observé que ces deux paramètres, quantité de CNT et durée d'électrofilage, impactent de manière significative la morphologie. Pour l'électrofilage sans aiguille du composite PAN / CNT, la concentration de PAN et la quantité de CNT ont toutes deux été optimisées.. Des échantillons optimisés pour ces deux matériaux ont été obtenus et les modèles pour leur prédiction ont également été développés. Nous avons obtenu des modèles valides pour le processus d'électrofilage avec aiguille (valeur de R-sq importante). Ceci a confirmé que la réalisation de nanowebs uniforme est possible pour des configurations sans aiguille à condition d'effectuer un choix pertinent de paramètres.

Pour l'électrofilage de PA-6, dans le cadre de l'application *Masque de protection*, la même méthodologie a été suivie.

Pour évaluer la possibilité d'utilisation des matériaux réalisés dans les conditions précitées pour les applications sélectionnées, certaines propriétés importantes ont été étudiées. Pour la production de chaleur, la structure interne du nano-non-tissé PAN et PAN / CNT a été étudiée en utilisant la microscopie électronique à transmission Il a été observé que les nano-non-tissés de PAN avait une très faible cristallinité. Les NTC, dans le cas des composites PAN / CNT se sont révélés être alignés le long des nanofibres avec les extrémités de certains d'entre eux émergeant à la surface. Certains CNTs ont également été observés sous forme de spirales à l'intérieur des nanofibres. La stabilité thermique des nanowebs, qui a été effectuée en utilisant l'analyse thermogravimétrique, montre une perte de poids plus faible pour les échantillons incluant des nanotubes de carbone. L'ajout de nanotubes de carbone a également entraîné une augmentation de la conductivité électrique des nano-non-tissés, même si elle est très faible. La carbonisation qui a

été réalisée afin d'améliorer la conductivité électrique, a entraîné une diminution du diamètre des nanofibres. On rappelle que les nanowebs conducteurs sont étudiés pour leurs propriétés de production de chaleur. On a pu observer que nanowebs carbonisés étaient capables de produire de la chaleur. Les nano-non-tissés sans CNTs ont produit une température plus élevée, cependant, ceux qui contenaient des CNT ont donné lieu à une augmentation uniforme de la température. Ces résultats peuvent être attribués à une résistance électrique élevée pour les nanowebs sans CNTs.

Pour l'application *Masque de protection*,les tests de pénétration de la paraffine ont été réalisés selon la norme ASTM 149. Il a été observé que l'ajout de la couche de nanofibres dans le complexe multi-couche a fait fortement chuter la pénétration de la brume de paraffine. Cependant, cette couche a également augmenté la chute de pression, qui est néanmoins restée dans des limites acceptables pour certains des échantillons. L'addition de nanofibres a également augmenté la conductivité et la perméabilité à la vapeur d'eau, et provoqué une diminution de la perméabilité à l'air. Ceci peut être attribué à une conductivité thermique plus élevée du PA-6 (par rapport à l'air, qu'il remplace), un diamètre de fibre inférieur, et surtout une taille des pores très faible.

Ces études démontrent que les matériaux nanofibreux peuvent être utilisés pour les deux applications envisagées : la production de chaleur et la protection respiratoire.

Chapitre 5 : Conclusions et Perspectives

Dans ce travail, les matériaux fibreux à base de nonanofibres non-tissées optimisés ont été étudiés pour deux applications techniques : la production de chaleur, les matériaux utilisés étant le PAN et des composites PAN / nanotubes de carbone et la protection respiratoire, les nanofibres étant en polyamide 6. Les matériaux électrofilées ont été obtenus à partir de différentes configurations d'électrofilage L'optimisation et la modélisation des processus d'électrofilage ont été réalisées en appliquant diverses méthodes (plans d'expériences notamment).

Il a été conclu que la modélisation statistique est un outil efficace pour l'obtention de structure optimum de nanofibres (absence de défaut, diamètre et dispersion des diamètres des nanofibres). Grâce à ces outils, une optimisation des plages de paramètres de contrôle du procédé d'électrofilage a été possible. Il a été obtenu que la concentration est le paramètre qui a le plus d'impact. Cependant, l'effet d'autres paramètres peut être amplifié en maintenant constante la

concentration. Dans cette étude, certaines interactions du second degré ont été observées, et ont été mises en évidence par application de plans d'expériences particuliers (surface de réponses).

Il a été observé que le comportement du procédé d'électrofilage à aiguille est très semblable à celui sans aiguille. Cependant, il a été constaté une différence dans l'ampleur des effets entre les deux procédés, le procédé sans aiguille présentant un comportement plus complexe (défini par l'équation quadratique).

Les études sur la modélisation et l'optimisation qui ont été menées, ont permis d'obtenir des matériaux nanofibreux en PAN et composites PAN / CNT optimisés. Dans ce dernier cas, les CNT se sont révélés être présents à la surface de nanofibres, bien que recouvert par le polymère. Dans le cas du procédé sans aiguille, certains CNTs ont été observées sous forme de spirales. Les composites PAN / CNT non carbonisés ont présenté une mauvaise conductivité électrique.

Les fibres de carbone obtenues par carbonisation de PAN et PAN / CNT ont montré qu'elles pouvaient composer des systèmes hautement efficaces de production de chaleur. Leurs propriétés électriques et leur capacité à produire de la chaleur pourraient être améliorées par une augmentation de la quantité de CNT. D'autres études dans ce domaine devraient conduire à la production de matériaux des produits industrialisables.

En ce qui concerne l'application de protection respiratoire, des matériaux non fibreux à base de PA-6 ont été obtenus et ont été incorporés dans des couches de masque de protection respiratoire non-tissés. Il a été observé que l'ajout de nanofibres de PA-6 améliore de façon notable la protection respiratoire. Les propriétés globales pourraient être améliorées en appliquant différents paramètres d'électrofilage. Les propriétés de confort ont également été étudiées et leur évaluation les positionne dans une gamme acceptable. Cependant, d'autres études dans ce domaine pourraient être envisagées et se traduire par la mise sur le marché de masques faciaux de protection respiratoire très efficaces.

De nombreuses perspectives s'ouvrent à l'issue de ce travail, qui pourraient conduire à améliorer encore les propriétés des matériaux nanofibreux étudiés. Ainsi, par exemple, des études sur l'influence des paramètres d'impacts plus faibles du procédé d'électrofilage, mais en gardant

les paramètres d'impact élevés constants, pourraient être menées. De même, les études sur la distribution du diamètre de la fibre avec un peu plus de paramètres pourraient être approfondies.

Pour la l'application *Production de chaleur*, l'influence de l'addition de plus grandes quantités de NTC sur la conductivité électrique et l'efficacité de la production de chaleur doit être étudiée. Par ailleurs, une étude d'optimisation de la carbonisation pourrait être certainement être réalisée.

Pour l'application *Protection respiratoire*, des améliorations peuvent être apportées en affinant les paramètres du procédé d'électrofilage pour améliorer la chute de pression. Il serait également possible d'envisager une fonctionnalisation des nanofibres pour utiliser les masques faciaux de protections dans ces environnements spécifiques.

References

[1] S. Ramakrishna, *An Introduction to Electrospinning and Nanofibers*: World Scientific, 2005.

[2] J. Fang, H. Niu, T. Lin, and X. Wang, "Applications of electrospun nanofibers," *Chinese Science Bulletin,* vol. 53, pp. 2265-2286, 2008/08/01 2008.

[3] F. L. Zhou and R. H. Gong, "Manufacturing technologies of polymeric nanofibres and nanofibre yarns," *Polymer International,* vol. 57, pp. 837-845, 2008.

[4] H. S. Wang, G. D. Fu, and X. S. Li, "Functional polymeric nanofibers from electrospinning," *Recent Pat Nanotechnol,* vol. 3, pp. 21-31, 2009.

[5] A. Greiner and J. H. Wendorff, "Electrospinning: a fascinating method for the preparation of ultrathin fibers," *Angew Chem Int Ed Engl,* vol. 46, pp. 5670-703, 2007.

[6] P. Supaphol, C. Mit-Uppatham, and M. Nithitanakul, "Ultrafine electrospun polyamide-6 fibers: Effect of emitting electrode polarity on morphology and average fiber diameter," *Journal of Polymer Science Part B: Polymer Physics,* vol. 43, pp. 3699-3712, 2005.

[7] W. Wei, J. T. Yeh, P. Li, M. R. Li, W. Li, and X. L. Wang, "Effect of nonsolvent on morphologies of polyamide 6 electrospun fibers," *Journal of applied polymer science,* vol. 118, pp. 3005-3012, 2010.

[8] J. Zeleny, "The role of surface instability in electrical discharges from drops of alcohol and water in air at atmospheric pressure," *Journal of the Franklin Institute,* vol. 219, pp. 659-675, 1935.

[9] T. J. Sill and H. A. von Recum, "Electrospinning: Applications in drug delivery and tissue engineering," *Biomaterials,* vol. 29, pp. 1989-2006, 2008.

[10] W. K. Son, J. H. Youk, T. S. Lee, and W. H. Park, "The effects of solution properties and polyelectrolyte on electrospinning of ultrafine poly (ethylene oxide) fibers," *Polymer,* vol. 45, pp. 2959-2966, 2004.

[11] S. N. Arshad, "High strength carbon nanofibers derived from electrospun polyacrylonitrile," University of Illinois at Urbana-Champaign, 2010.
[12] Z. Li and C. Wang, "Effects of working parameters on electrospinning," in *One-Dimensional Nanostructures*, ed: Springer, 2013, pp. 15-28.
[13] H. Niu and T. Lin, "Fiber generators in needleless electrospinning," *Journal of nanomaterials,* vol. 2012, p. 12, 2012.
[14] V. Pillay, C. Dott, Y. E. Choonara, C. Tyagi, L. Tomar, P. Kumar*, et al.*, "A Review of the Effect of Processing Variables on the Fabrication of Electrospun Nanofibers for Drug Delivery Applications," *Journal of Nanomaterials,* vol. 2013, p. 22, 2013.
[15] J. M. Deitzel, J. Kleinmeyer, D. Harris, and N. C. Beck Tan, "The effect of processing variables on the morphology of electrospun nanofibers and textiles," *Polymer,* vol. 42, pp. 261-272, 2001.
[16] P. K. Baumgarten, "Electrostatic spinning of acrylic microfibers," *Journal of Colloid and Interface Science,* vol. 36, pp. 71-79, 1971.
[17] L. Huang, K. Nagapudi, R. P. Apkarian, and E. L. Chaikof, "Engineered collagen-PEO nanofibers and fabrics," *J Biomater Sci Polym Ed,* vol. 12, pp. 979-93, 2001.
[18] Y. Wang, Y. Li, G. Sun, G. Zhang, H. Liu, J. Du*, et al.*, "Fabrication of Au/PVP nanofiber composites by electrospinning," *Journal of Applied Polymer Science,* vol. 105, pp. 3618-3622, 2007.
[19] M. M. Demir, M. A. Gulgun, Y. Z. Menceloglu, B. Erman, S. S. Abramchuk, E. E. Makhaeva*, et al.*, "Palladium Nanoparticles by Electrospinning from Poly(acrylonitrile-co-acrylic acid)−PdCl2 Solutions. Relations between Preparation Conditions, Particle Size, and Catalytic Activity," *Macromolecules,* vol. 37, pp. 1787-1792, 2004/03/01 2004.
[20] M. M. Khan, M. Tsukada, X. Zhang, and H. Morikawa, "Preparation and characterization of electrospun nanofibers based on silk sericin powders," *Journal of Materials Science,* vol. 48, pp. 3731-3736, 2013/05/01 2013.
[21] P. D. Cha, J. J. Rosenberg, and C. L. Dym, *Fundamentals of modeling and analyzing engineering systems*: Cambridge University Press, 2000.
[22] XLSTAT. (2015, 02 April). *What is statistical modeling?* Available: https://help.xlstat.com
[23] M. A. Bezerra, R. E. Santelli, E. P. Oliveira, L. S. Villar, and L. A. Escaleira, "Response surface methodology (RSM) as a tool for optimization in analytical chemistry," *Talanta,* vol. 76, pp. 965-977, 9/15/ 2008.
[24] S. Gu, J. Ren, and G. Vancso, "Process optimization and empirical modeling for electrospun polyacrylonitrile (PAN) nanofiber precursor of carbon nanofibers," *European polymer journal,* vol. 41, pp. 2559-2568, 2005.
[25] S. Nataraj, K. Yang, and T. Aminabhavi, "Polyacrylonitrile-based nanofibers—a state-of-the-art review," *Progress in polymer science,* vol. 37, pp. 487-513, 2012.
[26] T. Maitra, S. Sharma, A. Srivastava, Y.-K. Cho, M. Madou, and A. Sharma, "Improved graphitization and electrical conductivity of suspended carbon nanofibers derived from carbon nanotube/polyacrylonitrile composites by directed electrospinning," *Carbon,* vol. 50, pp. 1753-1761, 2012.
[27] Y. Ahn, S. Park, G. Kim, Y. Hwang, C. Lee, H. Shin*, et al.*, "Development of high efficiency nanofilters made of nanofibers," *Current Applied Physics,* vol. 6, pp. 1030-1035, 2006.

[28] S. Zhang, W. S. Shim, and J. Kim, "Design of ultra-fine nonwovens via electrospinning of Nylon 6: Spinning parameters and filtration efficiency," *Materials & Design,* vol. 30, pp. 3659-3666, 2009.
[29] X. H. Qin and S. Y. Wang, "Filtration properties of electrospinning nanofibers," *Journal of Applied Polymer Science,* vol. 102, pp. 1285-1290, 2006.

Chapter 1 INTRODUCTION

"Textile is something made of fibers, yarns or fabrics". Fibers are basic building block of any textile product. Textile fibers are long flexible materials whose length is at least 100 times their diameter. They can be converted into yarn or different types of fabric or other textile products such as felts, laces etc. Textile fibers should be strong, flexible and elastic apart from being uniform, lustrous, fine and crimpy. They may be classified as macro, micro and nanofibers on basis of their diameter [1].

Nanofibers are slender and elongated structures whose diameter is in nanometer range (10-500 nm in this case) [2]. They can be produced using a number of fabrication techniques, which include electrospinning, melt blowing, phase separation and self-assembly [3, 4]. Among these, electrospinning is the most feasible and simpler technique that allows producing nanofibers with customized properties, at much higher rate, using a large number of fiber forming materials. Besides, it also has the potential to produce nanofibers on bulk scale [5, 6].

Electrospinning principle is based on utilization of electrostatic force to draw polymer solution into nanofibers, as they are released by a nozzle. The fundamental electrospinning setup consists of a nozzle or syringe, containing a polymer solution or melt, a high-voltage source and a collector. On applying a sufficient potential difference, the solution gets charged, thus developing a Coulombic repulsion within it. This repulsion overcomes the surface tension within the liquid and allows production of a jet, which moves towards the collector under the electrostatic force. During this movement, or "flight", the solvent evaporates and the jet is converted into nanofibers due to the electrostatic drawing force applied by the collector and the repulsion within the polymer jet. Finally, the jet is deposited on the collector, resulting in a nanofibrous nonwoven.

Electrospinning can be classified according to type of fiber generator. Conventionally, nozzle or needle has been used as fiber generator, hence termed as "needle electrospinning". More recently, different setups have been developed, that employ fiber generators other than

needle (such as cylinder, wire, disc etc.), and hence the process is termed as needleless electrospinning, which is mostly used for production of nanofibers in larger quantities [7].

The properties of the nanofibrous nonwoven web are strongly dependent on different electrospinning parameters. These include polymer solution concentration (and hence the viscosity), diameter of nozzle or needle, flow rate of solution, applied voltage, distance between needle and collector, and environmental conditions such as humidity and temperature. All these parameters strongly affect the properties of electrospun nanowebs, and hence the end use applications [8-14].

Electrospun materials have, extensively, been studied for various applications and have been found to show very promising results. Some important application areas of electrospun nanofibers include energy generation and storage, electronics, environmental protection, carriers for entities like catalysts and enzymes, drug delivery, tissue engineering, sensing and filtration [7].

The potential, shown by electrospun materials in different fields, have attracted researchers to carry out extensive studies on electrospun materials. Nevertheless, use of electrospun materials in different fields can be explored better if the process is understood well. These materials can show better performance, if they have been optimized and fine-tuned morphologically with respect to the specific end use. This can be accomplished by using different modelling techniques that, not only, allow to study the behavior of nanofibers and optimize their properties but also to predict these properties.

Diverse modelling and optimization tools have been used by process experts and researchers in different fields including textiles. These tools gained considerable importance for process optimization and improvement. They have, also, been found useful for improving the reproducibility of processes and thus resulted in better quality control along with improved productivity. Moreover, they have been applied for scale up of processes from lab trials to bulk production. Some important modelling and optimization tools include differential equations, dynamic systems, statistical, game theoretic models, artificial neural networks and fuzzy logic. For engineering problems, statistical modelling and optimization have long been proven to be a valuable tool for fine tuning, optimization and modelling [15].

Current work aims to provide a start point for two novel applications of electrospun materials i-e heat generation and respiratory protection. To achieve this aim, the electrospun webs were studied, optimized and modelled to produce better electrospun materials and get maximum output from them. The nanowebs were optimized and modelled with the fact in mind that they will produce better and more reproducible results than that obtained from non-optimized webs, thus providing a better start point for selected applications. Moreover, their modelling led to observe and predict their behavior for any fine tuning needed for the selected applications. Furthermore, the optimization, modelling and comparison of lab scale needle electrospinning with semi-industrial needleless electrospinning allowed better understanding of processes. Specially, for needleless electrospinning, which is important for commercial production of nanofibers, no literature in this field is available. Modelling and optimization of such setups can be useful, once their bulk production is started. This approach was expected to give a better start for selected applications that could be, then, studied more extensively. Moreover, it was expected to help better understand the electrospinning process, as a whole.

For optimization and modelling of electrospun nanowebs, different statistical tools were utilized. However, these tools are known to work better with a proper experimental design. To fulfil this goal, the designs considered in this study included full factorial, response surface and Taguchi designs. Each design was studied to give its own optimized results and the resultant outcomes were compared to suggest one that better fitted the electrospinning process.

The polymeric materials selected for this works were polyacrylonitrile for heat generation and polyamide-6 for respiratory protection face mask. Polyacrylonitrile was selected, as for heat generation, the nanowebs needed to be electrically conductive. This was possible by use of conductive fibers, such as carbon fibers, achievable from polyacrylonitrile. Similarly, for respiratory protection, a material with maximum filtration performance was needed. This purpose could be well served by a nanoweb with very small pore size, achievable by finer fibers. Polyamide-6 has been known to produce very fine nanofibers through electrospinning and thus was selected for this study.

For heat generation application, polyacrylonitrile was not only used alone, but was also reinforced with carbon nanotubes, as they are known to carry interesting properties, such as excellent electrical and thermal conductivity. Nanowebs, constituting both these materials, were modelled and optimized to get defect free fine-tuned products. For this purpose, full factorial (for needle electrospinning) and response surface (for needle and needleless setups)

designs were utilized. The nanowebs were optimized with respect to their morphology and their properties related to heat generation (such as electrical and thermal conductivity etc.) were studied. Moreover, the effect of addition of carbon nanotubes was also investigated. Finally, the nanowebs were evaluated for possibility to generate heat through them.

For respiratory protection filter, polyamide-6 was electrospun, both on needle and needleless electrospinning. However, in this case Taguchi approach was used instead of response surface technique, along with the full factorial design. This was accomplished as some extra control parameters, offered by needleless electrospinning, were expected to affect filtration efficiency. However, studying these parameters through response surface design was not feasible because a large number of experiments were needed for this. So, Taguchi methodology was utilized to study the process, with a minimum number of experiments. Both the Taguchi (used for needle and needleless setups) and full factorials designs (used only for needle electrospinning) allowed to optimize the processes, quite well. The optimized webs were then utilized for study of performance and comfort properties of nanofiber incorporated face mask filters developed thereof.

From investigations carried out in this work, it was observed that statistical modelling is a useful tool to study and optimize the properties of electrospun nanowebs. All the experimental tools, i-e full factorial, response surface and Taguchi, allowed detailed insight into the process, along with development of prediction models. Response surface experimental tool fitted the electrospinning process better than other tools. This is because it, not only, allowed to study the linear relationships between the variables, but also the relationships that were more complex than that. However, Taguchi design was found useful because it produced acceptable optimization and modelling of process with very low number of experiments. Optimization allowed to utilize defect free and reproducible nanowebs for selected applications with minimum chance of inaccuracy in further studies.

Moreover, it was observed that needleless electrospinning, though, a more complex process, was governed by almost the same parameters, as utilized by needle electrospinning. Hence, scale-up studies were suggested to be carried out to develop exact mathematical relationships between the two processes.

Finally, the developed nanowebs were found to show promising results for heat generation as well as for respiratory protection. These results can be utilized as start point to carry out extensive studies in both the fields, with sufficient reproducibility.

Chapter 2 Literature Review

Electrospinning, although a simple looking process, is a complex technique that involves many inter-related parameters. As discussed in previous chapter, it works by drawing out a polymer jet from the liquid meniscus through a needle or spinneret. The polymer jet, after leaving the tip of Taylor cone, moves towards the collector. The meniscus at the needle tip has a stress due its surface tension that allows it to oppose the drawing force exerted by electric field. This force is equal to the ratio of surface tension of liquid (γ) and the principle curvature of meniscus (R) i-e γ/R, termed as capillary stress. For an electric field to draw out the liquid jet, it must exert force greater that this capillary stress. The electrical stress, produced by electric field, is given by $\varepsilon V^2/d^2$, where ε is the permittivity, V represents the voltage applied and d is the separation between electrodes. So the electrospinning process parameters can be estimated by balancing the capillary stress and electrical stress [16]. Normally six forces are active during electrospinning, i-e i) Electrostatic force that transmits the jet from fiber generator to the collector, ii) the gravitational force, iii) the coulombic forces that stretch the jet during its flight by pushing apart the segments in the jet, iv) the surface tension of solution that opposes the stretching of the jet surface, v) viscoelastic forces inhibiting the jet from stretching and vi) the friction of air particles, opposing the movement of jet [17]. The morphology of fibers is majorly determined by these forces.

So, during its flight, the jet is exposed to a number of forces due to which it follows a 3D path with bending, spiraling and winding paths, termed as "Bending instability" as a whole. These bending instabilities, due to the forces involved, reduce the diameter of the jet, and hence the fiber, to nanometer range. The drawing rate for the final fiber may be as high as 1,000,000 sec^{-1}, thus reducing the diameter and increasing the molecular orientation [18]. The diameters of the fibers obtained by electrospinning range between 50 nm to 10 microns [16].

2.1 Types of Electrospinning

Electrospinning may be classified according to the types of liquid being used, the direction of nanofiber production or type of fiber generators. Following paragraphs give a brief introduction to these classes.

Different types of liquids may be used in electrospinning for production of nanofibers such as solutions of different polymers in appropriate solvents, emulsions and melts. So, the electrospinning process can be divided according to the type of liquid being electrospun. According to this classification, the technique can be categorized as solution electrospinning, melt electrospinning and emulsion electrospinning [19-26]. Similarly, the process may be divided into different classes according to direction of fiber generation, which may be vertical or horizontal. In most of the conventional vertical setups, the collector for electrospun fibers is placed at the bottom while the fiber generator is at top, such as setup may be termed as downward electrospinning. An inverse case included in same class is the one where collector is at top, while polymer jet and fibers are generated from the bottom. This type of system may be called as upward electrospinning. A third type of setup has the collector and fiber generator at the same level from the ground, kept parallel to each other. Such type of setup may be termed as horizontal electrospinning [27-32]. Pictorial representation of these setups is shown in Figure 1.

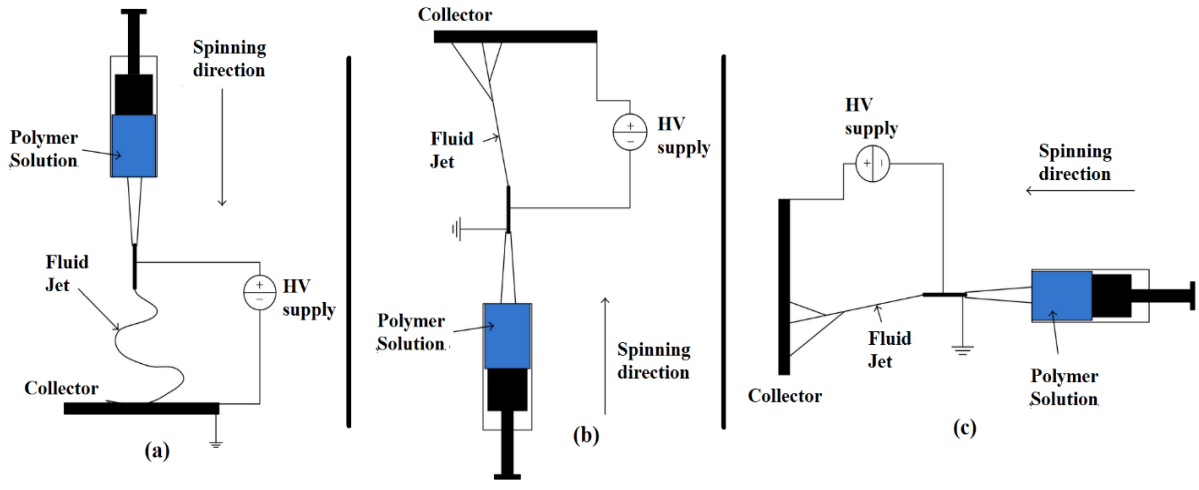

Figure 1: Types of electrospinning setups with respect to spinning direction showing (a) upward, (b) downward and (c) horizontal electrospinning [33]

Another important classification of electrospinning is the one based on types of fiber generator and can be divided into nozzle/needle electrospinning and needless electrospinning. As the name suggests, needle based electrospinning is the one where polymer jet is produced from the solution flowing through a needle or nozzle. Such setups are basic electrospinning systems, mostly for lab scale studies and research, though some bulk scale setups with multiple needles have also been developed [34]. They may be subdivided based on type of nozzle being used such as hollow nozzle and co-axial electrospinning [35]. The options for modification of needle electrospinning, however, are limited. Needless electrospinning includes all type of electrospinning techniques that do not use needle as fiber generator. Many diverse needless setups have been developed by different researchers. These can be subdivided to electrospinning with rotating fiber generators and electrospinning with stationary fiber generators. Examples of these type of setups are shown in Figure 2 and Figure 3 [7, 29, 36-38].

Rotating fiber generator needleless electrospinning setups use the polymer solution distributed over a rotating surface to produce nanofibers as electrostatic force is applied on them. The polymer solution on surface replenishes as the surface rotates and comes in contact with solution. Each of these setups produces its own set of properties. Based on high productivity, some of these techniques have been commercialized for development of nanofibrous materials on bulk scale. One of such systems includes Nanospider™ by Elmarco, which offers a set of rotating and stationary fiber generators. One of rotating fiber generators included with this system consists of a rotating cylinder partially dipped in polymer solution as one shown in Figure 2.

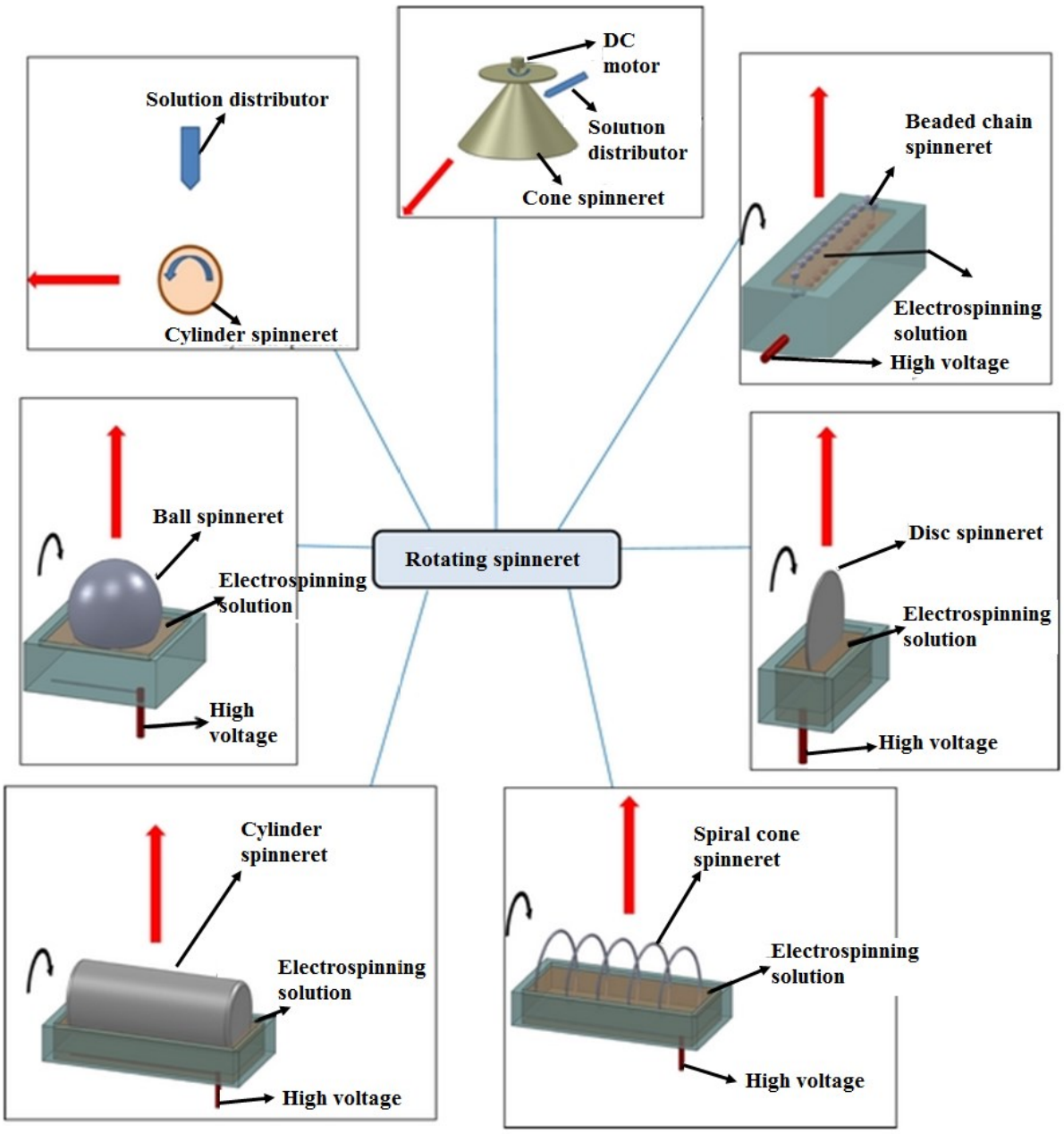

Figure 2: Schematic representation of rotating fiber generators for electrospinning (red arrows indicate direction of fiber generation) [7]

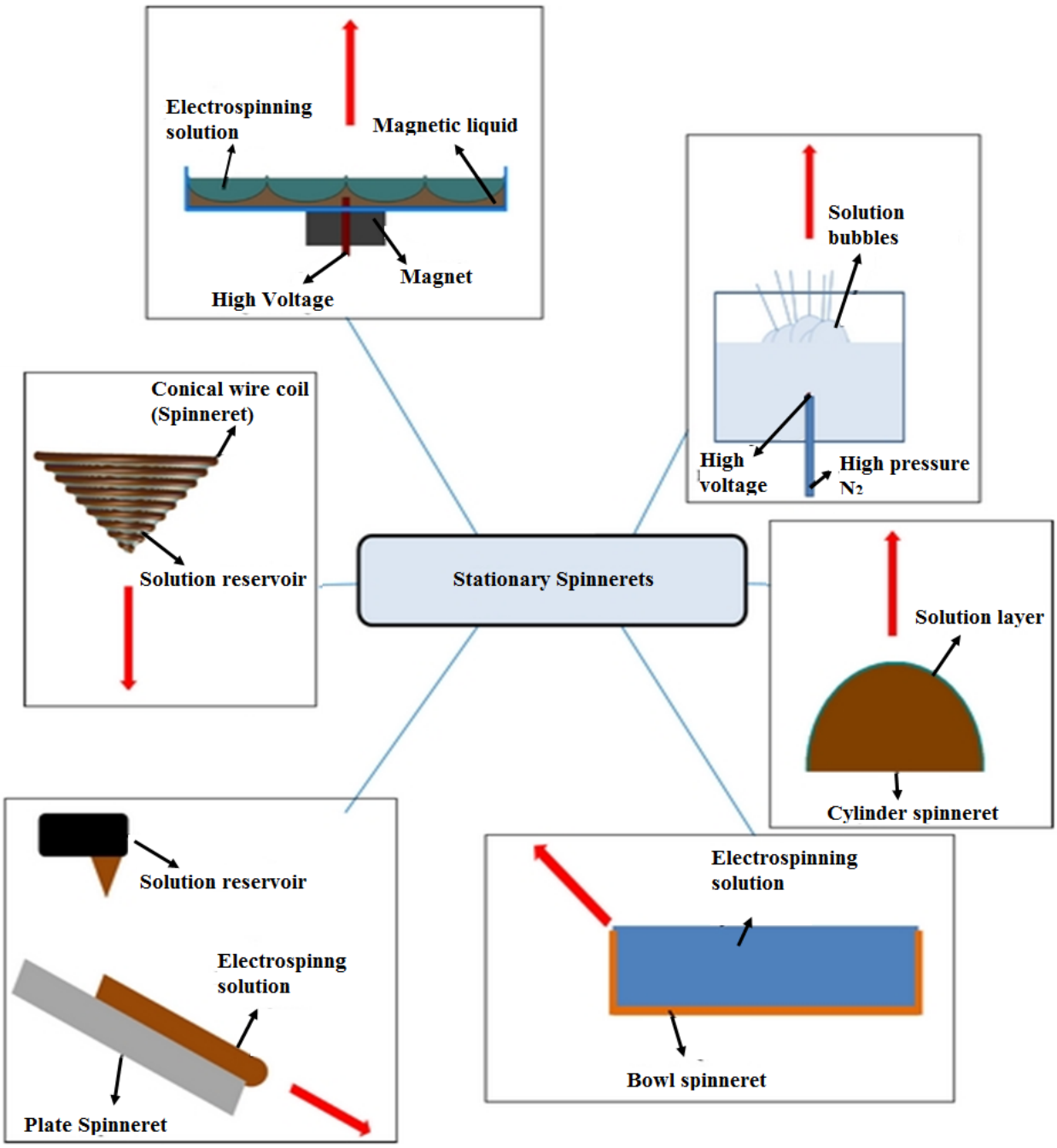

Figure 3: Schematic representation of some stationary fiber generator electrospinning setups (red arrows indicate direction of fiber generation) [7]

Nanospider™ also offers a high throughput stationary fiber generator, which employs a wire electrode that is coated directly with the polymer solution. The wire is constantly coated with solution thanks to a solution carrier, having a small orifice, through which the wire passes. As carrier moves on wire, the polymer is constantly coated over it and converted into a jet owing to high voltage electric supply. This system is one of the first commercial setups and

has been selected to perform a part of current study. The schematic diagram of this fiber generator is shown in Figure 4.

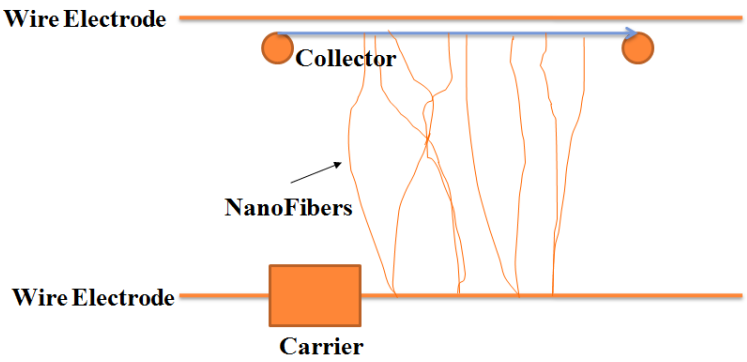

Figure 4: Schematic representation of wire electrode fiber generator needless electrospun

Meanwhile, some novel electrospinning techniques (that are not in scope of current study) have also been devised. They include Vibration electrospinning, Thermos-electrospinning, Magneto-electrospinning, Siro electrospinning and Bubble electrospinning [39, 40].

2.2 Important electrospinning parameters

Properties of the fibers produced by electrospinning are largely dependent on the different parameters, as discussed in a number of previous studies [41-46]. These parameters may be classified as solution, process and ambient parameters [19]. Some of the parameters that have stronger effect on the fiber properties are discussed in following sections.

2.2.1 Polymer solution parameters

Composition of polymer solution is considered to be the strongest factor affecting the morphology and related properties of electrospun nanofibers [47]. Some of solution parameters are discussed briefly in the following sections.

2.2.1.1 Solution Concentration

Solution concentration is the most important factor affecting the morphology and other properties of electrospun nanofibers, with major impact on fiber diameter, in terms of its magnitude and quality of fibers [19-23]. The viscosity of solution is mostly controlled by concentration of polymer in it, even though some other factors such as its molecular weight,

solvent systems and environmental conditions play a major role [41, 42]. Solution concentration is related to its viscosity by a power relationship i-e $\eta = C^{\delta}$; where, η is the solution viscosity, C is concentration and δ denotes scaling constant. From this equation, it may be concluded that solution viscosity increases, exponentially, with increasing concentration [48]. A viscosity range of 1-200 Poise (0.1- 20 Pa-sec) has been defined as suitable for electrospinning [49]; however, an optimum concentration and viscosity has to be defined for each polymer with every set of parameters being employed. At concentrations lower than that the polymer jet gets dispersed due to lower entanglement of molecular chains. This dispersed polymer forms small droplets before reaching the collector (electrospraying), failing to keep the polymer jet intact or to form beads on fibers. The formation of beads on fibers occurs due to relaxation of chains in presence of solvent because of its higher quantity, resulting in longer evaporation time, increasing the chances for molecules to relax as a result of surface tension [21]. At concentrations higher than the critical value, the molecular entanglements reach to a sufficient level to avoid the breakage of charged polymer jet thus allowing it to elongate under the columbic force [21]. Increased concentrations also result in decreased flow of solution from the spinneret (Figure 5). As the intermolecular forces and surface tension increase due to higher concentration (as a result of smaller intermolecular distance and larger intermolecular interaction), the solution resists the occurrence of rapid changes in its structure under the action of electrostatic force, thus resulting in more uniform fibers [50]. Within the critical range, an increase in concentration increases the fiber diameter due higher surface tension and greater molecular chain entanglement, that inhibits stretching of jet as it moves towards the collector [6, 51]. Moreover, the variation in diameter of fibers and irregularities in fiber morphology is higher at higher concentrations [9, 52, 53]. Solution concentration also poses a significant impact on formation of beads. Lower concentration lead to higher bead formation, which decreases as the concentration increases. Beyond a critical level of concentration, the beads are totally eliminated. At lower concentration the number of beads, that are mostly spherical in shape, increases. Beads with higher diameter have been found at lower concentrations whereas the shape of beads becomes less spherical at higher concentration [50, 53].

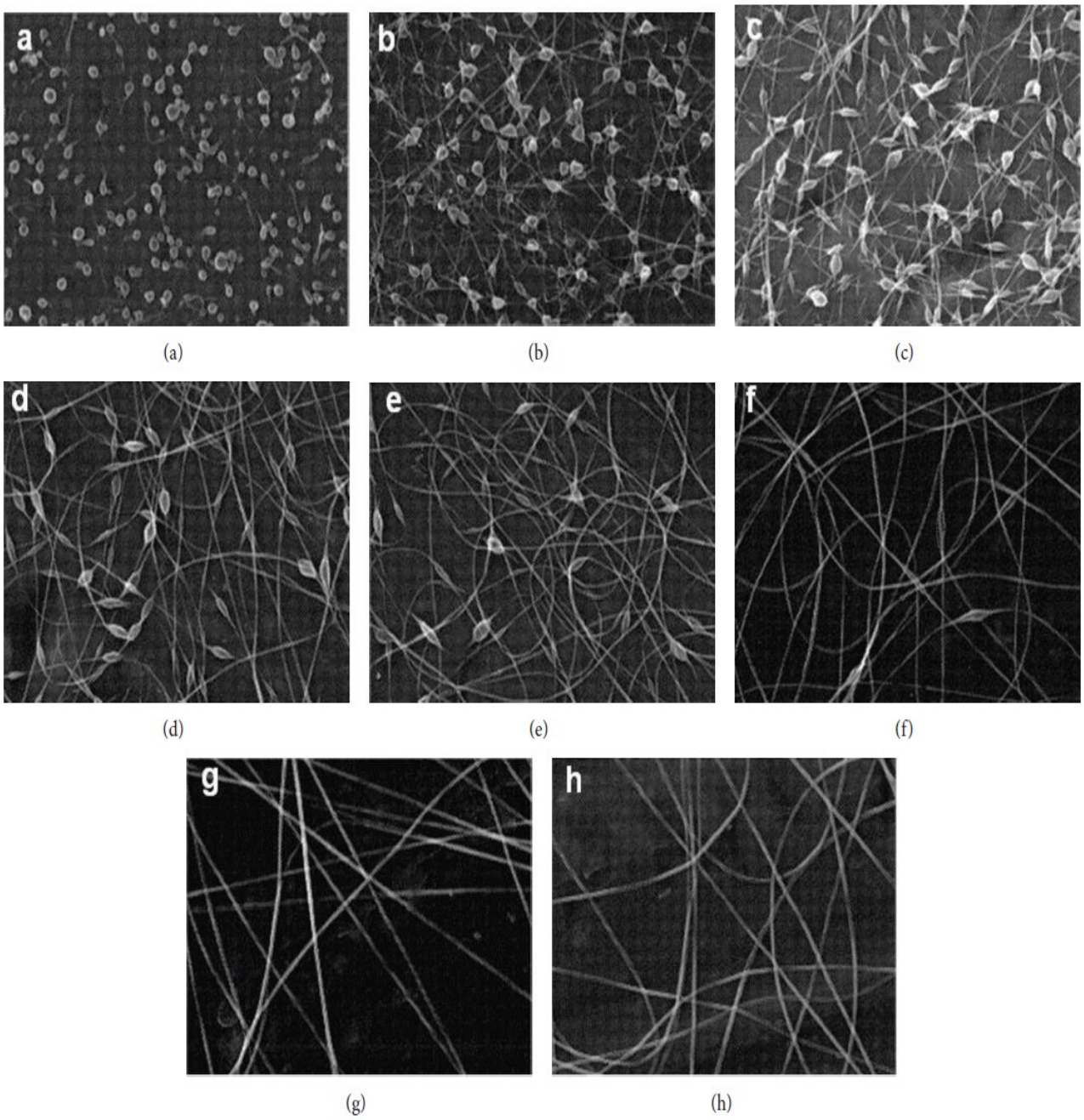

Figure 5: Morphology of PEO nanofibers at different viscosities of solution (a = 13 cp, b = 32 cp, c = 74 cp, d = 160 cp, e = 289 cp, f = 576 cp, g = 1250 cp, h = 1835 cp) [51]

2.2.1.2 Conductivity of Solution

The conductivity of solution governs the effect of electrostatic force on it. The conductivity of solutions is mostly governed by the properties of solvent employed. Solutions with higher conductivity can be pulled by the collector very easily as compared to low conductive solutions because of higher charge density in them; so, the morphology and hence the properties of fibers are also affected by it. It has been found that fiber diameter is inversely

related to cube root of conductivity [11, 50, 54]. Conductivity of electrospinning solution can be modified by varying the amount of polymer, using electrolytes, surfactants and appropriate solvent system [21, 42, 50] and it may be helpful in getting the desired morphology and defect free fibers. For instance, a beaded structure in nanofibers may be eliminated by addition of certain electrolytes and surfactants in polymer solution [50, 51]. Increasing polymer concentration also modifies the conductivity; as expected higher solution concentrations result in decreased conductivity (basically due to lower amount of solvent) and thus pose a significant impact on fiber morphology [21, 50].

Figure 6 depicts the effect of different electrolytes on electrospun fiber structures. It may be noted that increasing conductivity may also lead to decrease in diameter for certain combination of parameters because of increase of electrostatic pull on polymer. Moreover, increasing conductivity has also been observed to increase the instability in electrospinning process [47].

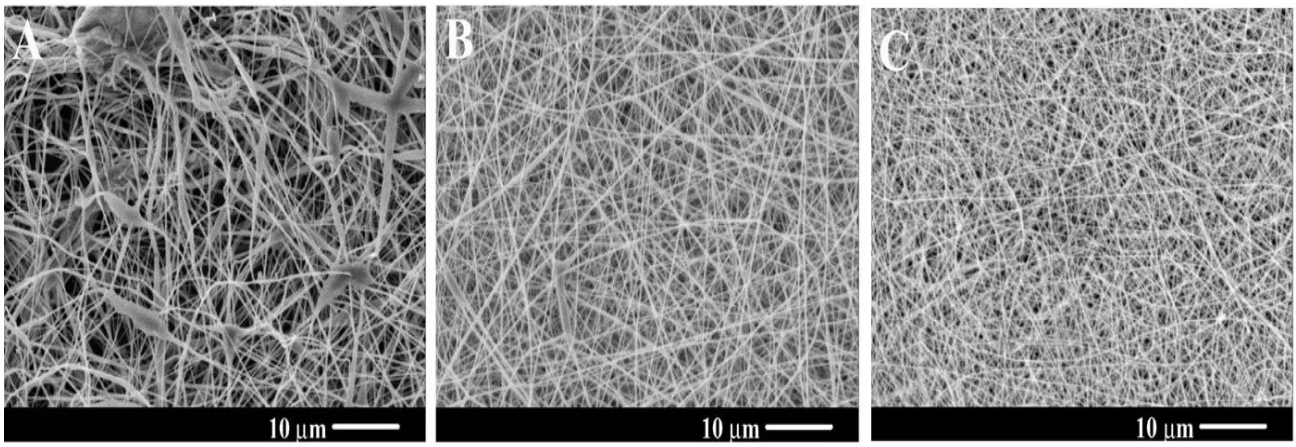

Figure 6: Effect of different electrolytes on electrospun fiber structures using A= KH_2PO_4, B = NaH_2PO_4 and C = NaCl as a solvent [55]

2.2.1.3 Nature and Properties of Solvent

The selection of solvent is one of the most important factors affecting the morphology of fiber. Solvent serves to dissolve the polymer and evaporates while the fibers pass between the needle and the collector. Thus selection of solvent is critical and depends on factors like its volatility and solubility of polymer in it. A solvent with appropriate volatility will evaporate completely just before reaching the collector. If a solvent is too volatile it will cause the polymer to dry away at the tip of nozzle, thus resulting in failure of the electrostatic force to

pull the polymer towards the collector and blockage of electrospinning needle. On the other hand, if it does not evaporate before reaching the collector, the polymer will not dry away and will result in beaded nanofibers. Similarly, the porosity of fibers also depends upon its evaporation profile at surface of the polymer [17, 44]. Mixture of solvents also affects the morphology of fibers by modifying the spinning solution viscosity, surface tension and conductivity. Such mixtures may be used to produce versatile morphologies and obtain fibers with elliptical, flat-ribbon like and core-sheath structures [42].

Other parameters related to polymer solution include molecular weight of polymer, static charge accumulation, volatility of solvent and phenomena like solution phase transition [56, 57].

2.2.2 Process parameters

Process parameters also pose considerable effect on properties of electrospun fibers, as discussed by some previous studies. Important process parameters include the rate of solution flow, voltage applied and distance between fiber generator and collector [10, 43-45, 47, 58, 59].

2.2.2.1 Solution Flow Rate

The volume of solution in the Taylor cone depends upon the rate at which the solution flows out of the capillary and magnitude of electrostatic force, which pulls it away towards the collector. If the flow rate of solution is lower than the rate at which it is taken out, then the electrostatic force gets the solution from inside the capillary. This results in development of beads in the structure [43-45]. The properties of nanofibers affected by improper flow rate of solution include non-uniform diameter, geometry and porosity in structure. Higher flow rates may result in increase in fiber diameter and may also lead to improper drying of the fiber as it reaches the collector. This is because at higher flow rates, larger amount of polymer is available to the electrostatic force to take it away to collector. Also number of bead defects and the diameters of beads were found to increase with increase in flow rate. The increase in bead defects was reasoned to occur due to incomplete drying. Moreover, a ribbon like cross section has also been observed due to incomplete drying at higher flow rates [55, 60].

2.2.2.2 Voltage

Electrostatic charge is the basic stretching force in electrospinning that decreases the diameter of the fibers to nano scale. This charge is developed and controlled by the voltage applied across the needle and the collector and the properties of fibers are strongly dependent on this voltage. A value of voltage, and hence the electrostatic charge, above or below a certain critical value may produce fibers with undesired properties. Within this critical range, higher voltage increases the fiber fineness as the jet length is directly proportional to the applied voltage; however, this change is not large as compared to that produced by change in concentration [10, 58, 59]. However, if the critical range is crossed the fibers first become finer with some defects in them but then they tend to have greater diameter with greater bead defects and drops [44]. Increase in diameter at higher voltage could be attributed to higher solution flow rates at such voltages, thus pulling additional solution from the needle [9, 61]. Higher voltage also results in formation of beads. However, beads formed at higher voltage have smaller diameter but greater density and are more spherical in shape as compared to those formed at voltage below the optimum range [55]. Higher electric field intensity is also observed to increase the productivity of electrospinning process [62].

2.2.2.3 Distance between the nozzle and Collector

The morphology and properties of electrospun nanofibers are also affected by the distance between the nozzle and the collector. Generally, at constant electric field intensity, larger the distance, finer will be the fibers [47]. The reason being the larger flight time and hence the resultant instabilities in fiber, allowing it to extend more. Increased electrostatic repulsion at larger distances also allows the fibers to have increased flight time and hence lower diameter [63]. As expected, longer spinning distances have been found to show better molecular orientation because of increase stretching time [64]. However, distance larger than optimum may result in beaded structure and oval fiber cross section. Increasing the distance even more may cause the fibers to fragment, resulting in electrospraying [65]. The smaller distances promote formation of larger fiber diameters; however, for low viscosity solutions, dripping may be observed, particularly, at lower voltages [62].

To conclude it may be inferred that process parameters are one of the most important variables that affect the electrospinning process. Optimization of these parameters and precise control over them can result in nanofibers with improved and reproducible properties. Process

parameters also include type of spinneret and diameter and (in case needle is used as spinneret), temperature of solution, polarity of applied voltage arrangement of electrodes etc. [66-68]. For current study, voltage between fiber generator and collector and solution flow rate will be focused as they are easily controllable and carry significant impact (as discussed above) on properties of nanofibers.

2.2.3 Ambient conditions

The environment, in which electrospinning is carried out, play a vital role in determining the properties of nanofibers. It may be varied to get fibers with different structure and properties. Important parameters in this category include humidity, vapor content and temperature inside electrospinning booth [69]. These variables have been discussed in following sections.

2.2.3.1 Humidity and vapor content in air

Among ambient parameters, the humidity in environment surrounding the polymer jet is amongst the most important factors. It has been found to, significantly, affect the nanofiber morphology [69]. Lower humidity can result in higher solvent evaporation rate that may result in decreased stretching, thus producing thicker fibers. Though, higher humidity also disturbs the morphology of fibers as the water condenses on the fibers surface (due to cooling resulting from solvent evaporation) and is found to produce pores on surface of fibers produced from hydrophobic polymers. The effect varies from material to material and depends, to a large extent, on composition of electrospinning solution that defines the parameters like rate of evaporation and hydrophobicity [70]. In a study carried out on polyacrylonitrile (PAN) dissolved in dimethylformamide (DMF), higher relative humidity (60%) was found to produce fibers with rough surface, while those formed at 30% humidity were much smoother [46].

Similarly, higher vapor concentration in the electrospinning chamber leads to a decreased evaporation of solvent from the polymer jet. This phenomenon can result in finer fibers if the distance from fiber generator to collector is sufficient to allow the fibers to get dried. In this case higher vapor contents will allow the jet to be stretched more because of lower solvent evaporation. However, if the jet doesn't get dry before reaching the collector some defects, such as beaded fibers, may be produced [71]. In a study carried on PA-6, the presence of solvent vapors in electrospinning chamber have also been found to affect the crystal state of

polymers constituting the fibers. This effect basically occurs due to the change in rate of solvent evaporation from the polymer jet [72].

2.2.3.2 Temperature

Effect of temperature is two multidimensional as it can alter the solution viscosity and rate of evaporation of solvent. Increasing temperature results in decreased viscosity thus resulting in finer fibers due to higher extension. On the other hand, higher the temperature, higher will be the solvent evaporation, thus increasing the viscosity of solution during its flight as a jet towards collector. This will lead to larger fibers. So, a balance in two behaviors can be achieved by selecting and maintaining the right temperature inside the electrospinning chamber [73].

From above discussion, it could be concluded that selection of best electrospinning parameters depends upon the conditions in which the process is being carried out. However, fine tuning and optimization of parameters is an important task and has to be carried out with each set of input variables. Similarly, modelling of these parameters could also be an important tool to predict the properties of fibers produced thereof. Following sections give a brief introduction about optimization and modelling techniques and their application for electrospinning.

2.3 Optimization and Modelling of Electrospinning Process

Optimization is a procedure of improving a process, system or a product to get maximum output from it [74, 75], while a model is basically a simulation of real world. It is a theoretical or an artificial representation of real world to better understand different systems, processes and phenomena in it [76]. As already discussed different parameters define properties of nanofibers produced from electrospinning. The numerical effect of these parameters, their modelling and prediction may be helpful to better understand the process and move towards better control over it. Moreover, it may also be useful to scale it up from lab to industrial level. So, one of the aim of current study was to model the electrospinning process using different statistical approaches.

Before going into the details of modelling and optimization for electrospinning process, a brief overview of these concepts is discussed in following sections.

2.3.1 General overview

In mathematics, Optimization involves maximizing or minimizing a function (a mathematical relation between inputs i-e factors or independent variables and outputs i-e responses or dependent variables) by selecting different variables and their values that affect the function. The values of input variables are normally selected from a defined range and the value of output depends on different combinations of input variable values, called levels [75]. Modelling is depiction of real world in a form that makes it easily understandable. Mathematical modeling is representation of real world systems and phenomena in mathematical form so that they can be understood well. It develops the relationship between factors and responses [76]. A model is developed by observation of the system to be modelled; analyses of that system leads to relationship between inputs and outputs. This relationship can then be used to predict the output variable for any set of input variables whenever the process is repeated in same conditions.

For modeling of scientific processes, mathematical modeling techniques are well proven tools. Some of important classes of mathematical modelling include differential equations, dynamic systems, statistical, game theoretic models, artificial neural networks and fuzzy logic. For most of the experimental works, normally statistical methods are employed as they can well utilize the data from experiments to develop a relationship between inputs and outputs [15].

2.3.1.1 Statistical modeling

Statistical models are simple way of formalizing mathematically, a phenomenon, process or a system, based on data obtained from observation and trials, with possibility to predict its results in future. There are different types of statistical modeling techniques based on the type of data available. They include one-way and multi way ANOVA (analysis of variance), single/multiple linear and nonlinear regression, ANCOVA (analysis of covariance; a blend of ANOVA and regression), MANCOVA (multivariate analysis of covariance), Poisson regression, etc. [77]. All these models work on data obtained from different situations with some input variables affecting the output variables. They determine the effect of each of the input variables on each or one of the output variables to develop a complete relationship between them. A brief description of above mentioned methodologies is discussed in following sections.

2.3.1.1.1 ANOVA

ANOVA considers if the means of population of data are different from means of another population of that data. For determining the significance of effect of a factor (or input or predictor variable) on a response (criterion variable), ANOVA compares means of response at different factor levels (values or settings) of that factor. It may negate or accept the null hypothesis (Annex I) that the mean of output obtained at all levels is equal. The negation of null hypothesis is confirmed by the P-value (probability; Annex I). If P-value is below a certain level threshold (or significance level, normally denoted by α-value and usually set at 0.5 i-e 95% possibility of negation of null hypothesis), the null hypothesis can be rejected and the difference between means of output at different levels of the factor is considered to be significant. Based on differences in means of output, a main effect plot may be generated. It plots the differences between means of output at given values of each input. If the mean is different, the factor is considered to have a main effect on response [78].

2.3.1.1.2 Single and multiple regression

Single linear regression is the relationship between the input variables and the output variables such that there is only one input variable and the plot of relationship, i-e the one obtained when output is plotted as a function of input, is a straight line. To develop a linear regression a line, best fitting the data, is plotted. This line is called regression line as it represents a regression equation and consists of predicted values of outputs for each value of input. The values predicted by regression line could be different from the actual values; the difference between the two is termed as error or residual (Annex I) and it reflects the validity of the model. The regression line should be calculated such that the errors are minimum; wherein it is called best fitting line, defined as a line with minimum sum of errors taken as squares [79]. Regression line is defined by equation $Y' = \alpha + \beta A$; where Y is the predicted value of response, α is intercept of line on y-axis, β is the slope of line and A is value of predictor.

Likewise, a multiple regression draws a linear relationship between a response and multiple predictors, at the same time. The aim is to find the combined effect of all the input parameters on output [80]. As for simple regression multiple regression also uses a fitted line that is represented by the equation $Y' = \alpha + \beta_1 A_1 + \beta_2 A_{2.....+} \beta_x A_x$, where $\beta_1 A_1$, $\beta_2 A_2$ and $\beta_x A_x$ represent the product of slopes and values of the predictor and α is the intercept of line on y-axis.

The validity of regression models is normally judged by their R-squared (R-sq; Annex I) and goodness of fit values. R-sq determines how close or how far the regression line is from data and ranges between 0 to 1 or 0 - 100%. The fit of the model is dependent on its residuals vs fits plot, i-e a plot between observed errors and predicted values. For a good model, this plot should have residuals arranged randomly throughout it. In such a case, along with a high R-sq value, the model can be considered valid or significant within the data range under study [81].

2.3.1.1.3 ANCOVA, MANCOVA and Poisson regression

ANCOVA is a blend of regression and ANOVA and evaluates relationship between the dependent and independent variables keeping in consideration some other factors, called covariates, which may also affect the process. MANCOVA, is similar to ANCOVA, however, it develops a relationship between independent variables and more than one dependent variables, while considering the effect of covariates [82]. Poisson regression is a special type of regression model that is used for count data. It combines logarithmic function with a special function called poison function to relate the independent and dependent variables [83].

2.3.1.2 Design of experiments (DOE)

To develop a relationship between dependent and independent variables/parameters, the process conditions or parameters may be selected or designed theoretically or they may be noted as they occur in nature, depending upon the type of system being studied. The systems where outputs can be controlled by controlling the inputs, can be studied by experimentation by careful selection of input parameters affecting the process, their levels (systematically arranged values) and combination of different levels of all the parameters. All these factors are crucial and define the validity of relationship of dependent and independent variables and also for the model obtained thereafter. So, a proper experimental design should be prepared before performing such experimentation.

An experimental design is a set of experiments with different level combinations (combination of values or settings) of input variables [74]. A good experimental design arranges the input variables, their levels and the combination of levels of different inputs such that it affects the output variable in a notable manner. However, selection of parameters and their levels is controlled by experimenter, and they become more precise as the area is studied consistently and systematically. The data obtained from these predesigned experiments,

normally, produces better models than that obtained from random experiments. An experimental design should produce a model that is valid, reliable, repeatable [84].

Different DOEs have been developed by statisticians, each having its own set of advantages and disadvantages and accuracy levels. Some of normally used multi-factor designs are discussed in following sections.

2.3.1.2.1 Factorial designs

A factorial design may be a full factorial or fractional factorial design. A full factorial design consists of all possible combinations of levels of two or more input variables to determine the value of output. One combination of levels of different inputs is called a run. For examples, for a system with two input variables (denoted by K), each with three levels (n) the total combinations or number of runs will be $(n)^k = (3)^2 = 9$ i-e the experiment has to be performed with 9 different settings. These combinations can be represent as shown in Figure 7. The levels of variable x_1 are (-1, 0 and +1) while that of x_2 are (-1, 0 and +1). The nine combinations are (-1,-1), (-1,0), (-1,+1), (0,-1), (0,0), (0,+1), (+1,-1), (+1,0) and (+1,+1), where "-" and "+" signs represent lower and higher values and "0" stands for middle values. A model may be developed in coded values like the one representing upper and lower levels in Figure 7. However, the actual model needs to be presented in actual values of levels i-e in uncoded units.

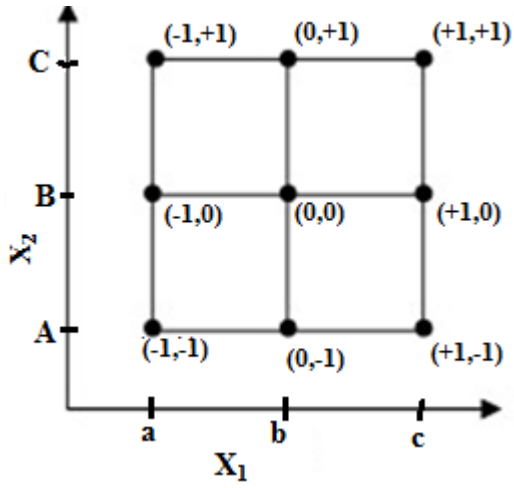

Figure 7: Different combinations of a two factor three level full factorial design [74]

The data obtained from a full factorial design of experiment, can then be analyzed using ANOVA or regression analysis. From factorial designs we can efficiently determine the "main

effects" and "interaction effects" of the inputs. A main effect is the difference produced by different levels of input. While interaction effect reflects the influence on output caused by an input in such a way that effect produced by that input depends upon the level of another input. A factorial design allows to study both these effects (except square of terms) [15, 84].

A full factorial design, however, may need a large number of runs to be performed, that may not be possible for a scientific setup. So, fractional factorial designs may be utilized to decrease the number of runs. A fractional factorial design choses only some of runs from a full factorial design to determine the effect produced by inputs on output [15, 84]. Factorial designs are a good option to study the electrospinning process, however, when studying larger number of parameters having many levels, the number of runs may exceed a feasible limit.

2.3.1.2.2 Response surface design

Response surface is a multivariate experimental design that is based on developing a polynomial equation that fits the experimental data or in other words it fits a polynomial equation on experimental data. It is considered to be a good tool for simultaneous optimization of levels of all input variables, to obtain the best response and prediction of response as a function of input variables. Response surface starts with fitting the data with linear equation (Equation (1); like a factorial design that is a first degree design) or simpler polynomial equations (Equation (2)) and may extend up to a full quadratic equation (Equation (3)) [74].

$$y = \beta_0 \sum_{i=1}^{k} (\beta_i x_i) + \varepsilon \qquad \text{Equation (1)}$$

$$y = \beta_0 + \sum_{i=1}^{k} (\beta_i x_i) + \sum_{1 \le i \le j}^{k} \left(\beta_{ij} x_i x_j\right) + \varepsilon \qquad \text{Equation (2)}$$

$$y = \beta_0 + \sum_{i=1}^{k} (\beta_i x_i) + \sum_{i=1}^{k} (\beta_{ii} x_i^2) + \sum_{1 \le i \le j}^{k} \left(\beta_{ij} x_i x_j\right) + \varepsilon \qquad \text{Equation (3)}$$

Where "y" represents the response, "k" the number of input variables, "β_0" is constant, "β_i" is coefficient of linear parameters, "β_{ij}" is coefficient of interaction parameters, "β_{ii}" is coefficient of quadratic parameters, "x_i" is the variables and "ε" is the residual (i-e error calculated from actual values and those calculated by equation). Equation (1) is a first order equation, thus it cannot represent any curvature in data, for which we use second order equations (Equation (2) and Equation (3)). There can be different types of response surface

designs; most popular are Box–Behnken and central composite designs. Box-Behnken designs use selected combinations of levels from factorial design as shown in Figure 8 [74], while, Central composite designs use some combinations that are not present in a full factorial design. They include some axial points and a central point, shown by "○" and "□", respectively, in Figure 8. So, such an approach allows efficient selection of level combinations that result in effective estimation of both the first order and second order coefficients in the model [74]. Response surface designs can be a good choice to study the effect of electrospinning parameters on outputs, optimize the process and to develop a model between them. The axial and central points, however, may sometimes become difficult to run because the values of parameters may fall in nonrealistic range. So, to run a response surface design for electrospinning, the selection of levels of each parameter is important.

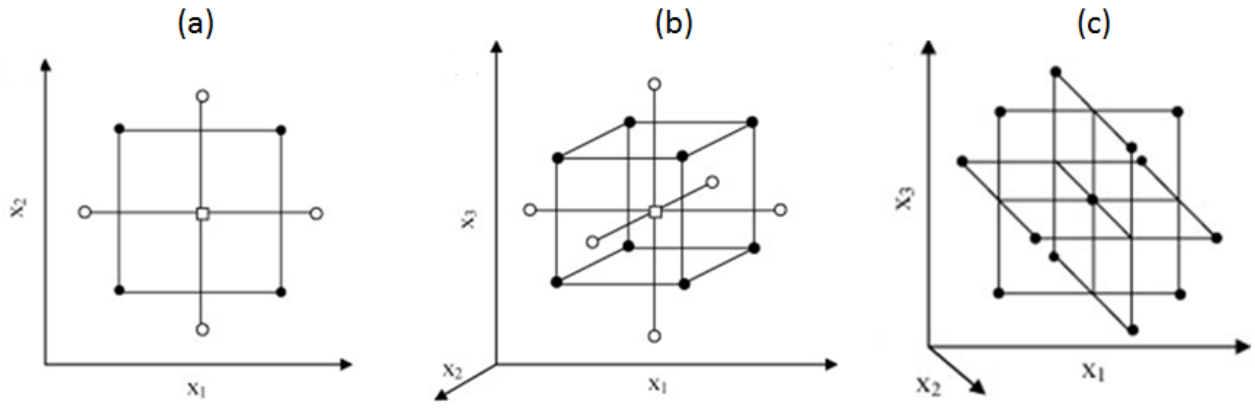

Figure 8: Combinations of levels for (a) two variable CCD (b) three variable CCD (c) three variable Box-Behnken designs [74]

2.3.1.2.3 Mixture design

Mixture designs are special case of response surface design, especially for manufactured products, where the product is composed of a number of constituents, for example process for fabric dyeing, developing blended yarns or producing a composite electrospun material. They have been formulated for processes where response is a function of proportion of input parameters that combine to make a collective total. So, in mixture designs, the inputs, when interpreted as fractions must sum up to make a total of 100% and this fact makes the analysis of such situations more complex than normal response surface designs [85, 86].

Three types of mixture designs are normally used

- Simple mixture designs are those where the response is a function of, only, the proportion of input components like recipe of a solution that is independent from other parameters.
- Mixture –process variable designs are the one where the response is dependent on the process conditions as well (like humidity and temperature) in addition to proportion of components.
- Mixture-amount designs are for systems where response depends on total amount of mixture along with the proportions of its individual components; for example, a dyeing shade not only depends on the amount of different ingredients but also the total amount of dye added in dyeing bath.

Mixture designs may be used for studies on electrospinning process, particularly, while studying the effects of various ingredients that constitute the electrospinning solution recipe.

2.3.1.2.4 Taguchi design

The Taguchi's approach for design of experiments is based on reduction of variation in process by recognizing the influence of uncontrollable factors (or noise variables; Annex I) that affect the process. Using controlled experiments (normally on lab scale), it identifies the controllable factors and their settings that can reduce the variation caused by uncontrollable factors. The experiments are designed so as to cause the variation, intentionally, due to noise factors and sort out optimum control factors to reduce that variation and implement those settings in actual process. The variation in process results can be expressed as "signal to noise ratio (S/N)". The S/N, a basic part of Taguchi approach, indicates the robustness of the process, with a higher value reflecting a more robust process and vice versa. Taguchi methodology provides three options for S/N depending upon the process, i-e "higher is the better", "lower is the better" and "nominal is the better". Using S/N ratio and ANOVA, an optimum set of parameters can be predicted and utilized for running a process with least variation in output [87, 88].

Taguchi methodology uses orthogonal arrays for designing the experiments, that allows it to consider all main and interaction effects, independently from each other. Pictorial representation of a 2^3 x 2^2 (three controllable factors with two levels multiplied by two noise

factors with two levels) is shown in Figure 9. For this design an experiment, for example, at lowest left corner will be have the setting I_1= -1 I_2= -1, I_3= -1, E_1= -1 and E_2= -1 ("+" and "–" signs show low and high levels, respectively). The total number of experiments for this design will be 2^3 x 2^2 = 32 (denoted as L32 design), at each corner of the cube with inner and outer arrays. This is an example of geometric design, while non geometric designs with mixed levels of factors may also be designed using Taguchi's orthogonal array methodology [86-88]. Taguchi designs can be considered a feasible option, particularly, for preliminary studies on a particular material or electrospinning system. Studies on a large number of parameters may also be performed using Taguchi designs that allows it to be used as a screening approach to reduce the number of factors to be studied in future works.

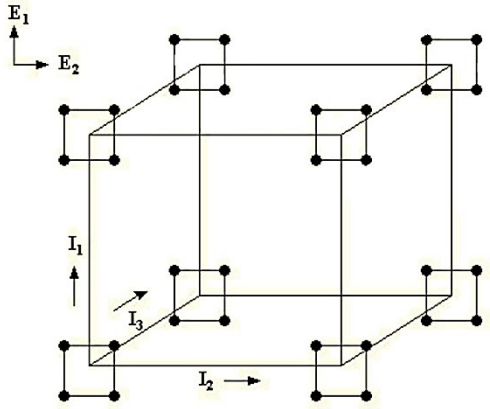

Figure 9: Taguchi 2^3x2^2 design with I representing inner arrays and E representing outer arrays [74]

2.3.2 Optimization and Modelling of nanofiber diameter as a function of electrospinning parameters

Electrospinning is a complex process, whose outputs depend on a number of variables, as discussed earlier in this chapter. Most of these variables are controllable, however, they are strongly dependent on each other. Moreover, the properties of electrospun nanofibers are, normally, not linear function of input variables. Besides, there are factors such as environmental conditions that could be controlled to a lesser extent. So, study of these relationships, optimization of process, its modeling and prediction could be valuable tools for future research on electrospun materials and their production on larger scale. Only a limited number of studies focus on these aspects of electrospinning and there hasn't been a proven theory to predict the properties of nanofibers based on solution, process and miscellaneous

variables [50]. Some of the research studies that focused on advancement of these aspects are discussed in following paragraphs.

Liu and Adanur [89], considered the prediction of PAN nanofiber diameter as function of each of the electrospinning parameters. The fiber diameter was found to increase up to a certain level by increasing voltage and then became constant. The relation between diameter (y) and voltage (x_1) was found represented by equation $y = -0.4821x_1^2 + 25.853x_1 + 65.01$ with $R^2 = 0.889$. The effect of solution flow rate on fiber diameter was not found to be significant and thus no model was developed for it. Change in needle-collector distance resulted in considerable change in diameter, however, no consistent trend was observed. Changing needle to collector distance produces change in balance between two competing factors i-e the electrostatic force and the stretching time, so it needs more detailed studies to develop a relationship for prediction of diameter as a function of distance, along with other factors involved. The effect of thickness of electrospun PAN web on mechanical strength and air permeability was also studied in same work and increase in thickness was found to result in increased tensile, tear and bursting strength. The equations obtained for tensile (y_1), tear (y_2) and bursting (y_3) strengths as a function of thickness (x_2) were $y_1 = 14.3789.x_2 - 0.8648$ (with $R^2 = 0.8315$) and $y_2 = 81.106.x_2 + 3.6858$ (with $R^2 = 0.9602$) and $y_3 = 0.105.x^{0.1126}$, respectively [89]. On the other hand, air permeability (y_4) was found to decrease with increasing thickness according to equation $y_4 = 9.5551.x^{-0.9245}$ with $R^2 = 0.9792$ [89]. This study considered only one parameter at a time for prediction of diameter.

In another similar work, the diameter of PAN nanofibers was, quantitatively, related to its concentration and viscosity employing form fitting methodology on Matlab [48]. The fiber diameter (d) was related with an exponential relation to solution concentration (C). The relation between the two was found to be $\boldsymbol{d = 0.0326.C^{3.45}}$ (with $R^2 = 0.965$), while that between diameter and viscosity (η) was observed to be $\boldsymbol{d = 0.834\ \eta^{0.827}}$ (with $R^2 = 0.972$). Both these relations are shown graphically in Figure 10.

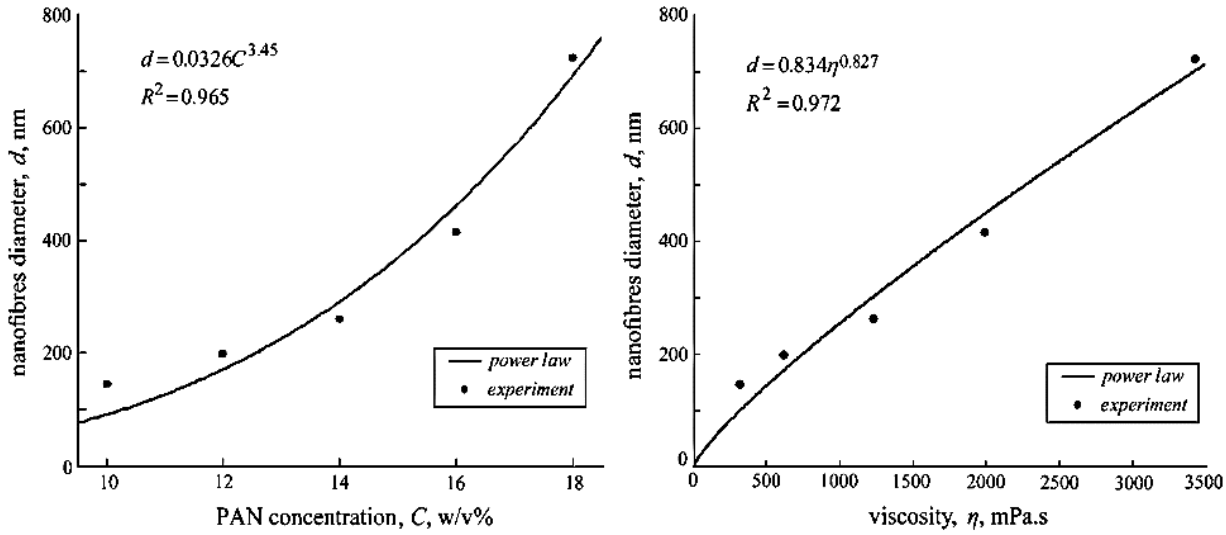

Figure 10: Relation between nanofiber diameter, solution concentration and viscosity [48]

The power law being followed for relationship between diameter with solution concentration and viscosity were found to be $d \propto C^{3.45}$ and $d \propto \eta^{0.827}$ (i-e a direct proportional relationship). Though, another study revealed the relationship between fiber diameter and concentration to follow the law $d \propto C$, with equation $y = 204.643+32.91467.x$; where, "y" is fiber diameter (nm) and "x" is the concentration (wt. %) [90]. In a couple of other similar studies carried out on Poly(Ethylene Terephthalate)-co- Polyethylenimine and polyurethane electrospun nanofibers, the diameter was found to follow the law $d \propto C^3$ [91, 92]. However, in these studies, a single electrospinning parameter was studied at a time that may not be considered sufficient to model the complex inter-related relationships of electrospinning parameters and properties of fibers achieved thereof.

In one of the studies on PA-6 nanofibers, the solution concentration was related to diameter of nanofibers for different molecular weights, with exponential equations. The molecular weights studied included 17,000, 20,000 and 32,000 Da and respective equations for diameter were $y=64.8+0.017e^{0.20x}$, $y=83.7+0.00075e^{0.28x}$, $y=83.2+0.0059e^{0.32x}$, where x is the solution concentration (w/v %) and y is fiber diameter (nm). The graphical representation of these equations is shown in Figure 11.

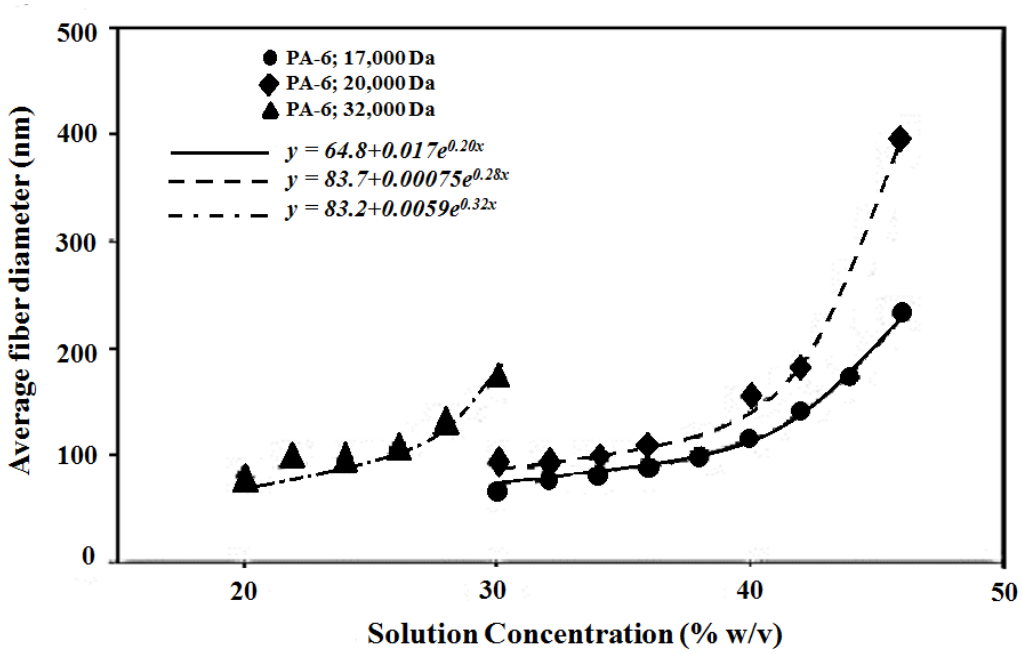

Figure 11: PA-6 fiber diameter represented as a function of solution concentration for different grades (PA-6-17 for Mw 17,000, PA-6-20 for 20,000 and PA-6-32 for 32,000) [21]

Meanwhile there are some simpler optimization studies like the one carried out for optimization of electrospinning of PA-6 nanofibers using one parameter at time while keeping the others at a constant value. The nanofibers were observed to show optimum morphology at a solution concentration of 20 wt. %, at a 15 cm needle to collector distance and an applied voltage of 15 KV with resulting fibers. However, there was no prediction equation from this study [61].

As discussed in previous section, statistical modeling is a powerful tool for understanding many complex scientific processes. Some of these methodologies have also been employed to study electrospinning process. For instance, electrospinning of PAN nanofibers was modelled, for prediction of their diameter and deviation therein, using polymer concentration and voltage as input parameters. Four equally spaced input levels, ranging between 6 and 12 wt. %, were selected for concentration; while for voltage three levels were selected, that ranged between 10 to 20 KV. The experiments were designed using full factorial method and main and interactions effect of each of the parameters was studied. The fibers were electrospun on downward needle based electrospinning setup. Data was analyzed using RSM and it was observed from ANOVA, main and interactions effect plots that only main effect of concentration posed a significant impact on diameter of PAN nanofibers while effect of voltage

and its interactions with concentration were not found to, significantly, impact the diameter (Figure 12). The model obtained for prediction of diameter in coded and uncoded units is shown in as Equation (4) and Equation (5) with R-sq of 98%. The distribution of fiber diameters was also found to be affected, significantly, by concentration only in such a way that it increased with increasing value of concentration i-e larger deviation at larger diameters. The relation between distribution of diameter and concentration, with R-sq 90%, in coded and uncoded units are reproduced as Equation (6) and Equation (7) [52].

$$Y = 321.9 + 444.80x_1 + 362.30x_1^2 \quad \text{Equation (4)}$$

$$Y = 2241.77 - 575.57x_1 + 40.25\ x_1^2 \quad \text{Equation (5)}$$

$$S_Y = 71.91 + 121.10\ x_1 + 98.25\ x_1^2 \quad \text{Equation (6)}$$

$$S_Y = 592.87 - 156.13.10\ x_1 + 10.92\ x_1^2 \quad \text{Equation (7)}$$

Where "Y" and "S_Y" are the diameter and its distribution and "x_1" is concentration. The equations show a quadratic relation between diameter and concentration. However, the distance was set constant, which otherwise could have altered the results. Moreover, better results could be achieved if the DOE was developed using RSM as it was used for data analysis.

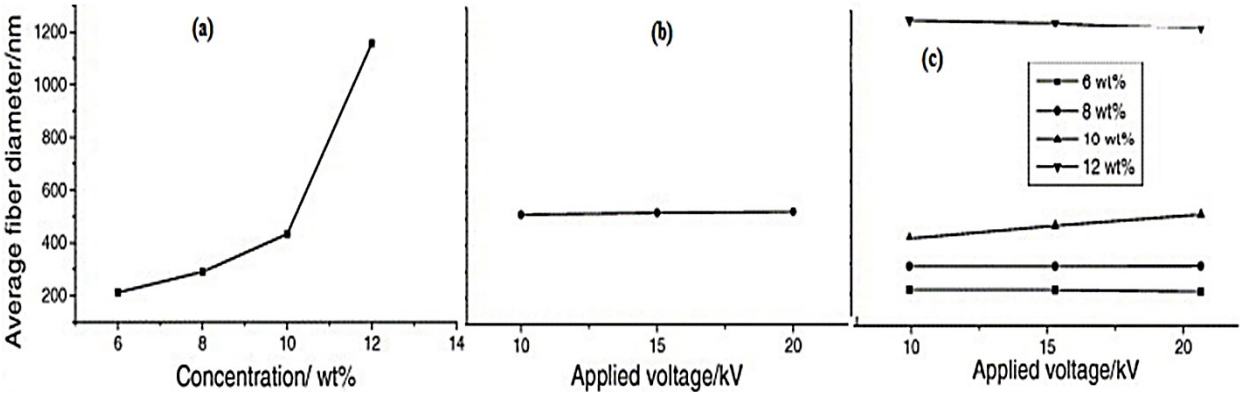

Figure 12: Main effects plot (Annex I) for (a) concentration (b) voltage and interactions plot (c) between concentration and voltage, depicting their influence on fiber diameter [52]

Electrospinning of PAN was also optimized and modelled by Yordem and co-workers [93], who utilized RSM for this purpose. They selected five concentration levels (equally spaced between 8 and 16 wt. %), five voltage levels (equally spaced between 10-30 KV). Models were developed at three different needle-distance levels (i-e 8, 12 and 16 cm). From ANOVA, the effect of concentration and voltage were found to be significant for all the three

models and R-sq for models was almost 99%, 97% and 98%, respectively, for each of above mentioned distances. The generalized model is represented in Equation (8).

$$Y = b_0 + b_1x_2 + b_2 x_3 + b_3 x_2^2 + b_4 x_2 x_3 + b_5 x_3^2 + b_6 x_2^3 + b_7 x_2^2 x_3 + b_8 x_2 x_3^2 + b_9 x_3^3 \quad \text{Equation (8)}$$

Where b1- b9 are the coefficients for each of the term and "x_2" and "x_3" denote solution concentration and applied voltage. The study suggests a different way of using RSM for modelling electrospinning process as it developed separate models for different distances. This approach was employed because the effect of distance is much higher than that of concentration and voltage, which they confirmed in their screening experiments. However, some other studies suggest that effect of distance is quite lower as compared to concentration [23, 52, 94, 95]. So this finding needs to be reconfirmed and if negated, the distance could be included in a single model with voltage and concentration, in case it is found significant.

Another similar study was carried out to optimize and model the electrospinning of silk to regenerate Bombyx Mori silk. The input parameters were concentration (5-20 wt. %; 6 levels, unequally spaced), electric field intensity (2-5 KV/cm, 4 levels, equally spaced), and electrospinning distance (5-10 cm, 3 levels, equally spaced). The DOE was developed using factorial approach and model was analyzed using response surface methodology. The mathematical relation, so obtained is shown below as Equation (9) [95].

$$Y= 7.653 - 0.668\ x1 - 2.027\ x2 + 0.346\ x12 + 2.668\ x22 + 0.325\ x1.x2 \quad \text{Equation (9)}$$

Where "Y" is the fiber diameter, "x_1" and "x_2" represent electric field intensity and concentration. The work authors didn't publish the *P-values*, however, from model it could be concluded that effect of concentration is many times higher than that of electric field intensity [95]. As already discussed, for a model analyzed by response surface better results could be achieved if its DOE has been developed by response surface DOE approach. So, results obtained in this study may be expected to improve if response surface technique is employed, both, for designing the experiments and analysis of the data so obtained.

Response surface methodology was also employed to study the electrospinning of poly(methyl methacrylate) by Chen and co-workers [96]. The input parameters selected were polymer solution concentration, needle to collector distance, applied voltage, temperature and flow rate of solution, each with five levels. ANOVA revealed that all parameters, except the

needle to collector distance, were found to affect the fiber diameter significantly with confidence interval above 95%. The non-significant factors were eliminated from further analysis to develop a model. A quadratic model (in coded values), reproduced in Equation (10) was found to fit the data with R-sq of 94.43 %.

$$Y = 301.17+74.952x_1 +46.576x_4 +21.673x_5 +41.631x_3^2 \quad \text{Equation (10)}$$

Where Y is the fiber diameter, x_1 is concentration (% w/v), x_3 is temperature in ºC, x_4 is solution flow rate in ml/hr. and x_5 is voltage in kilovolts (KV). All significant factors, except temperature, showed a linear effect; while temperature posed a quadratic impact on fiber diameter. The model was validated by confirming its prediction results through some independent experiments and was found to show mean absolute error of 3.55% only. That shows RSM to be an applicable approach for modelling of electrospinning process [96].

Taguchi orthogonal experimental design has also been employed to study the effect of different parameters on properties of electrospun PA-6 nanofibers. The input parameters for this study included the applied voltage, needle to collector distance, size of needle, polymer grade, solution viscosity, and concentration of electrolyte and the grade of formic acid used as a solvent. The solution viscosity was found to be the main parameter affecting the fiber diameter. Other important factors included needle to electric field intensity, collector distance, and content of electrolyte. The effects of different parameters are depicted in Figure 13 and Figure 14.

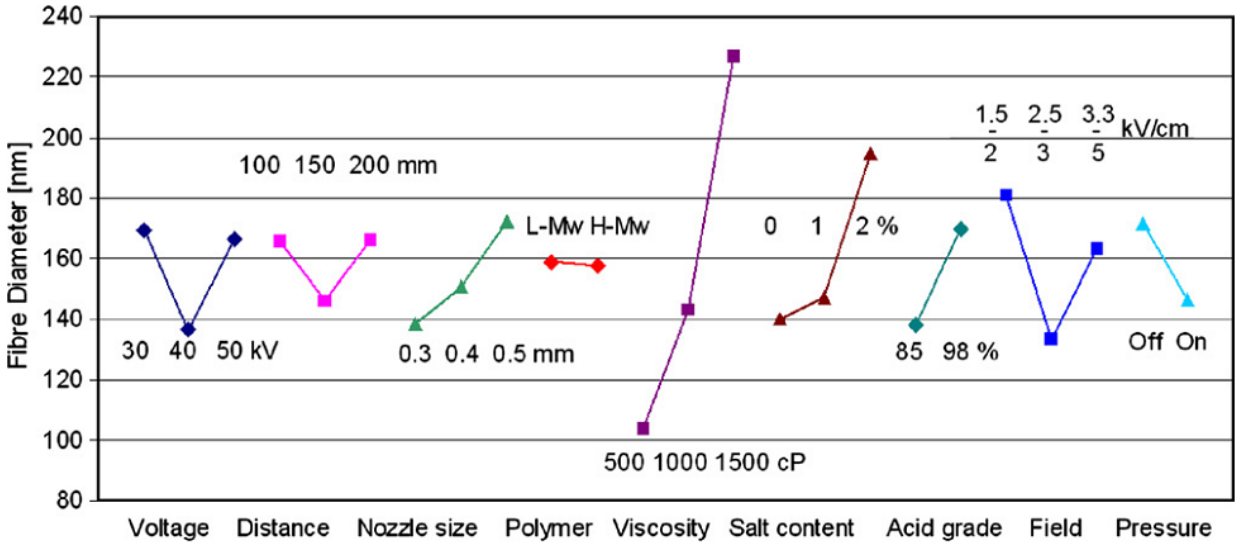

Figure 13: Effect of different input parameters on PA-6 nanofiber diameter [66]

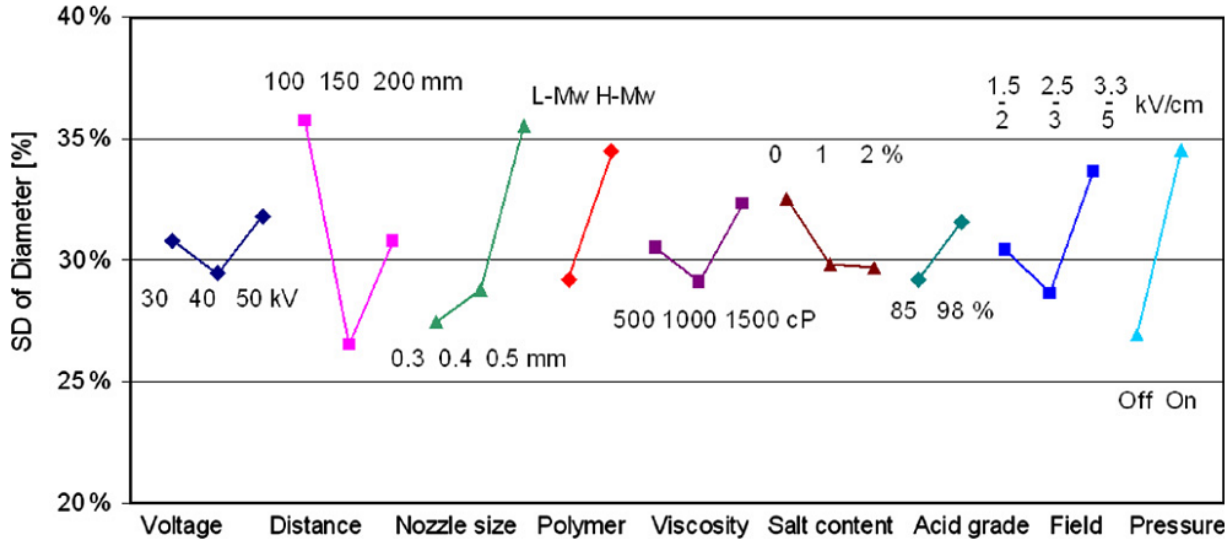

Figure 14: Effect of input parameters on distribution of PA-6 nanofiber diameter [66]

Based on these effects ranks were given to parameters with respect of their magnitude of impact on diameter as shown in Table 1 [66].

Table 1: Rank of input parameters with respect to their effect on fiber diameter and its distribution [66]

		Voltage	Distance	Nozzle	Polymer	Viscosity	Salt	Acid	Field	Pressure
Fiber Diameter [nm]	Level 1	170	166	138	159	104	140	138	181	171
	Level 2	136	146	151	157	143	147	170	133	146
	Level 3	166	166	172		227	195		163	
	Range	34	30	21	2	123	55	32	48	25
	Importance	4.	6.	8.	9.	1.	2.	5.	3.	7.
	Best level	40 kV	150 mm	0.3 mm	–	500 cP	0%	85%	–	On
SD [%]	Level 1	30.8	35.7	27.4	29.2	30.5	32.5	29.2	30.4	27.0
	Level 2	29.4	26.5	28.8	34.4	29.1	29.9	31.6	28.6	34.5
	Level 3	31.8	30.8	35.5		32.3	29.7		33.6	
	Range	2.4	9.2	8.1	5.2	3.2	2.8	2.4	5.0	7.5
	Importance	8.	1.	2.	4.	6.	7.	8.	5.	3.
	Best level	40 kV	150 mm	0.3 mm	L-M_w	1000 cP	0%	98%		Off

It is evident from above discussion that only a limited number of studies have been carried out for optimization and modeling of electrospinning process. Some of the studies employed simple approaches to develop simpler exponential models based on their plots. Such studies may not represent well the behavior of the process. They have been carried out with weak DOE or considering a single factor at a time, thus ignoring the interaction effects between different factors, While, some studies employed renowned statistical approaches such as RSM, but as mentioned earlier, DOE and analysis, if performed using a single approach (which is not the case with those studies) is expected to produce better results. For some studies DOEs were

designed using Factorial designs and data was analyzed using RSM. A more efficient approach may be a single methodology utilized for both purposes. Other than that, employing factorial DOEs increases the number of experiments, and so the time of cost for studying the process. Furthermore, a limited number of research studies have employed these statistical methodologies for optimization and modelling of electrospinning process. So the area needs to be explored to assess its advantages for it [52].

2.4 Polymers for Electrospinning

The exceptional properties of electrospun materials have encouraged the researchers to study electrospinning of more and more materials and their application as nanofibrous webs, alone or in combination with other materials. Such polymers may be classified, broadly as natural and synthetic polymers. Important natural polymers include Bombyx mori silk fibroin [97], Chitosan [98], Chitin [99], Collagen [100], Fibrinogen [101], Gelatin [102], Myoglobin and Hemoglobin [103], Lecithin [104], Pullulan [105] and starch [106]. While, a large number of synthetic polymers have also been electrospun. They include Polyamide 6 [21], Polyamide 66 [107], Polyacrylic acid [108], Polycarbonate [109], Polyacrylonitrile [110], Polyetherimide [111], Polyurethane [112], Polyvinyl chloride [113], Polyvinyl acetate [114], Polysulfone [115], Polyvinyl butyral [116] and Polyvinylidene fluoride [117] to name a few. Among the class of manmade polymers, different biodegradable polymers have also been electrospun successfully. Some notable among them include Polyhydroxystyrene [118], Poly lactic acid and Poly(L-lactic acid)-co-(glycolic acid) [119], Polycaprolactone [120] and Polyethylene glycol [121]. The current study will focus on two synthetic polymers i-e Polyacrylonitrile (PAN) and Polyamide-6 (PA-6) and one of the selected application for each. The properties, offered by these materials, that encouraged their selection for current work, have been discussed in following sections.

2.5 PAN

PAN is one of the most valuable polymers for electrospinning because of the exceptional advantages it offers; such as ease of spinnability, most viable precursor for carbon nanofiber (CNF) with high carbon yield, ease of processing for surface modification and lower cost [122, 123]. The polymer with molecular structure mentioned below (Figure 15), is relatively stable and high melting substance. It has high melting point (317 ºC) and high glass transition temperature (95 ºC), due to which it can't, normally, be used as a plastic material.

Moreover, its strong intermolecular forces and hydrogen bonding renders it good mechanical strength [122]. It has been widely used for electrospinning into nano and submicron fibers. One of the reasons for increasing interest in electrospinning of PAN is that it is one of the most suitable precursors for carbon fibers offering a yield of above 50% and can be used to produce carbon nanofibers through electrospinning and other techniques [124].

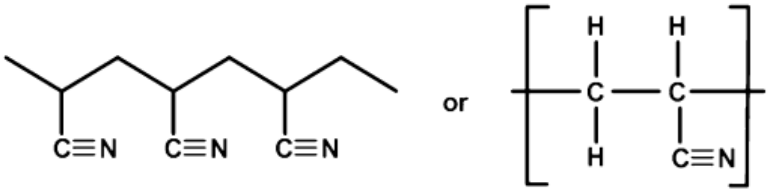

Figure 15: Molecular structure of PAN [122]

Usually the precursor for any type of carbon fibers is cellulose, PAN or Pitch, with PAN being the most commonly used material (for about 90% of carbon fiber production). This is because of the advantages it offers as compared to other precursors, which include better mechanical properties and higher yield [122, 125].

Carbon nanofibers (CNF) and the composites thereof can, normally, be produced either by vapor growth or electrospinning techniques. Vapor grown CNF are produced by gases containing carbon in presence of metallic catalysts. Such fibers, however, are shorter in length and are not well aligned with some added shortcomings, such as lower yield, complicated processing and higher production cost [18]. Electrospinning, on the other hand, has been successfully utilized to produce strong continuous carbon fibers in nanometer length dimension.

2.5.1 Electrospinning of PAN

PAN could be electrospun by dissolving the polymer (typical molecular weight 150,000) in suitable polar solvents such Dimethylformamide (DMF), Dimethylsulfoxide, Dimethylsulfone, Dimethylacetamide, Tetramethylsulfide and Ethylene carbonate (aqueous); whereas DMF is considered suitable for electrospinning because of its higher dissolving capability for PAN as well as suitability for electrospinning due to its appropriate volatility and high dielectric constant [62, 122, 126-130]. PAN can also be dissolved in ionic liquids, however, in that case the process needs to be controlled and optimized by increasing the

temperature of spinning solution [131]. Moreover, for some special fiber structures, such as porous nanofibers, liquid additives may be used along with original solvents [132].

For electrospinning uniform PAN nanofibers normally 6-13% solution of PAN is employed, that is given suitable time (normally 24 hours) to become adequately homogeneous solution at temperatures slightly higher than room temperature (40 ºC-50 ºC). The diameter of PAN nanofibers has been found to increase linearly with increasing solution concentration [50, 62, 89, 90]. At concentrations below 6%, beaded fibers are produced up to concentrations as low as 2%, below which droplets of polymers solution are deposited along with nanofibers [50, 133]. For PAN nanofibers, as for most of other polymers, concentration is found to produce very pronounced effect on fiber diameter, while effect of other factors such as voltage are much less significant [52, 134]. Addition of different additives such as surfactant, electrolytes, nanoparticles and different polymers also influences the properties of fibers produced thereof. Different salts have also been studied extensively as additives for electrospinning solutions. The increase in conductivity of electrospinning solution, by salts, is the major factor influencing electrospinning parameters. For commonly used salts, the increase in conductivity of solution has been found to be in sequence as LiCl > $NaNO_3$ > $CaCl_2$ > NaCl; so, the diameter obtained for these solutions would be as LiCl > NaNO3 > CaCl2 > NaCl, in a decreasing order [135].

For electrospinning of PAN on a typical single needle downward electrospinning machine, the electrospinning voltage between needle and collector ranges between 8-25KV with a distance of 10-25 cm between the two at a solution flow rate of 0.1-0.2 mL/hr. [122, 126, 136]. Higher distances and voltages were found to increase the mechanical strength of PAN nanofibers because of increased molecular orientation in them and reduced post-electrospinning disorientation due to presence of solvent. The voltage to distance ratio of 1 KV/cm was found to produce optimum properties such as mechanical strength and uniformity [136].

2.5.2 Carbon Nanofibers from PAN

Carbon nanofibers (CNF) may be defined as sp^2 based filaments having high aspect ratio (i-e 100) and flexibility with diameter ranging around 100 nm [137]. Based on their exceptional properties such as high surface area, they are expected to find extensive role in different areas such as aerospace, energy and a number of biomedical applications [137].

Carbon nanofibers can, normally, be produced either by vapor growth or electrospinning techniques [18, 138, 139]. Vapor grown CNF are produced by gases containing carbon in presence of metallic catalysts. Such fibers, however, are shorter in length and are not well aligned with some added shortcoming as lower yield, complicated processing and higher production cost [18]. Electrospinning, on the other hand, has been successfully utilized to produce strong continuous carbon fibers in nanometer dimension [139].

Normally, the precursors for carbon fibers are cellulose, PAN, rayon and Pitch, with PAN being the most commonly used material (for about 90% of carbon fiber production). This is because of the advantages it offers as compared to other precursors, two of most important of advantages of PAN, when used as precursor for carbon fibers, include better mechanical properties and higher yield [125, 140].

PAN nanofibers, produced by electrospinning, can be converted into carbon nanofibers by their heat treatment to carbonize them. However, the strength of such fibers is normally lower than that expected even though there is an extensive drawing and resultant molecular orientation. This may be attributed to the molecular relaxation as the fibers are collected on collector and is enhanced in the presence of traces of solvent [141].

2.5.2.1 Stabilization and Carbonization of PAN nanofibers

Before carbonization, the PAN fibers need to be stabilized to maintain their stability during subsequent carbonization stage. The stabilization process stabilizes the crystalline and amorphous phases of the polymer by converting, a basically thermoplastic polymer, to non-thermoplastic polymer with weight loss above 10% and a little decrease in diameter [124, 142]. Stabilization (or, more specifically, oxidative stabilization) is carried out by controlled heating process, wherein, the fibers are kept under tension and heated to 300 ^{o}C for almost one hour in air [18, 136, 142]. During stabilization different chemical reactions take place within the structure, they include cyclization, aromatization, dehydrogenation, oxidation and crosslinking resulting into a crosslinked ladder ring structure shown in Figure 16 [124].

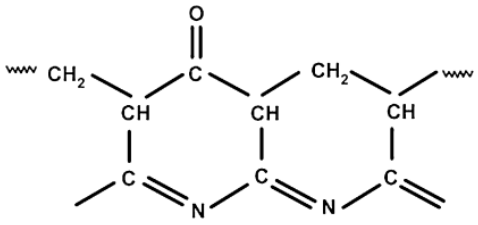

Figure 16: Ladder PAN Structure [124]

During this process, the PAN nanoweb tend to shrink up to 25% - 35% of their original dimensions and to maintain their dimensions they must be held in a support. Addition of a non-shrink additive, such as carbon nanotubes (CNTs), has also been found to decrease the thermal shrinkage [110]. Different researchers suggested different structures for thermally stabilized PAN. They include cyclic heteroaromatics [143], cyclic polyimine [144] and different crosslinked structures [145, 146]. These studies suggest that during stabilization, C≡N containing structures are converted to that containing conjugated C=N, which may result in cyclization (if it is intramolecular) or crosslinking (if it is intermolecular). Moreover, some conjugated C=C structures and carbonyl groups may also be produced due to dehydrogenation and oxidation, respectively. The summary of proposed chemistry of chemical changes occurring during carbonization is shown in Figure 17 [124].

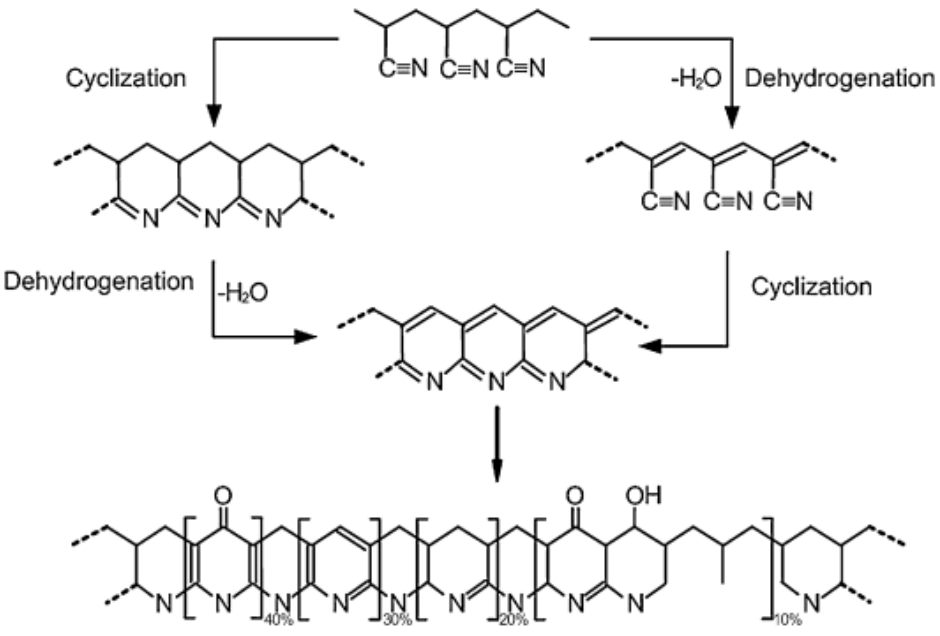

Figure 17: Proposed chemistry of chemical reactions during stabilization of PAN [124]

This thermal treatment, when performed, under tension has been found to stabilize both the crystalline and amorphous phases and thus is helpful to maintain the molecular orientation in whole bulk of material [147]. A hot-pressing pretreatment may also be carried out on PAN nanofibers to increase their density. Such pretreatments could be helpful in increasing the conductivity of carbon webs formed thereafter. The increase in conductivity may be attributed to increased number of crosslinks between fibers, resulting due to pressure and temperature and is found to increase with increase in treatment time [148].

Carbonization of PAN fibers is carried out to convert the contents to pure carbon or at least close to pure carbon. During carbonization a considerable weight loss is observed and the fiber diameter decreases to almost half of that of original PAN nanofibers [136, 142]. It is, basically, achieved by high temperature thermal treatment in inert environment, leading to polymerization resulting in aromatic growth of the molecular chains. The fiber, so obtained, can have exceptionally high modulus depending on the extent of carbonization.

Carbonization is carried in inert environment between 800-3000 °C, depending upon the degree of carbonization needed. As temperature is increased to 600 °C, dehydrogenation in already cyclized structures allows it to crosslink in lateral direction, resulting in a graphite like structure [124]. Above 600 °C, the network increases by elimination of N group from the structure leading to a highly crosslinked structure; the process continues to temperatures as high as 1300°C. The changes occurring during carbonization of stabilized structure are shown in Figure 18 [149].

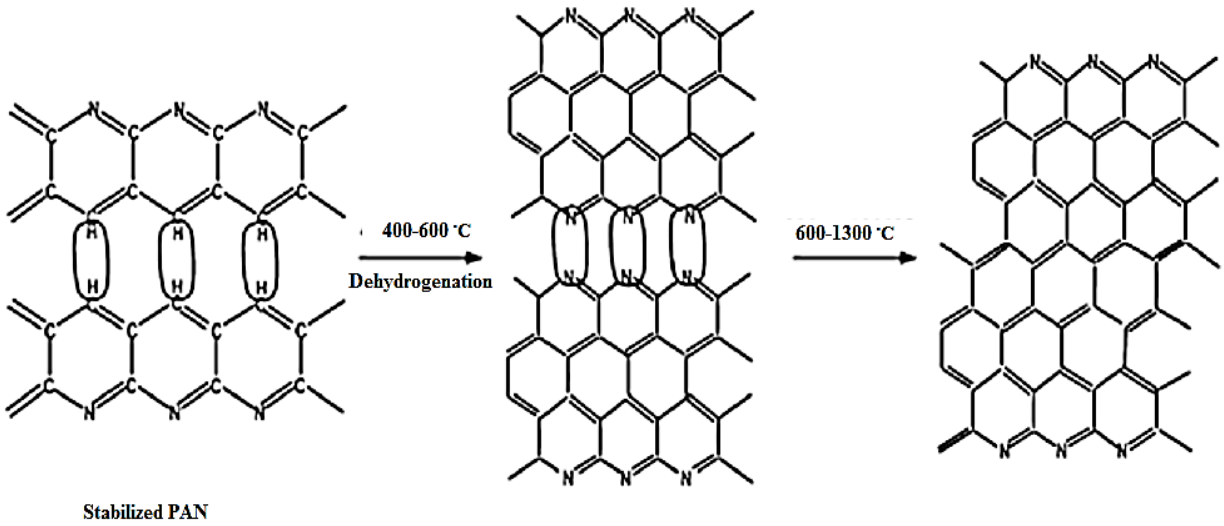

Figure 18: Structural changes during carbonization of PAN [149]

During this process, as the temperature increases above 400 °C, the non-carbon contents start to leave the structure, as a result different gases are expelled from the system; they include H_2, CH_4, CO, CO_2, H_2O, N_2, NH_3 and HCN. Over 800 °C, mostly N_2 and HCN are the dominant impurities that are evolved [150]. The evolution of these gases is the result of different reactions that increase the networking in structure. Increasing temperature further increases the carbonization and results in graphitization. The graphitized fibers have more molecular alignment and crystallized structure; thus improvement in properties has been observed. Higher the temperature, more is the growth in graphitic crystals, resulting in larger crystallites [151]. In graphitized fibers, graphene layers pileup with each other to form ribbon structure that is not visible in normal carbonized fibers having randomly arranged molecules [152]. This difference may be well viewed in TEM images of the two types of fibers as shown in Figure 19.

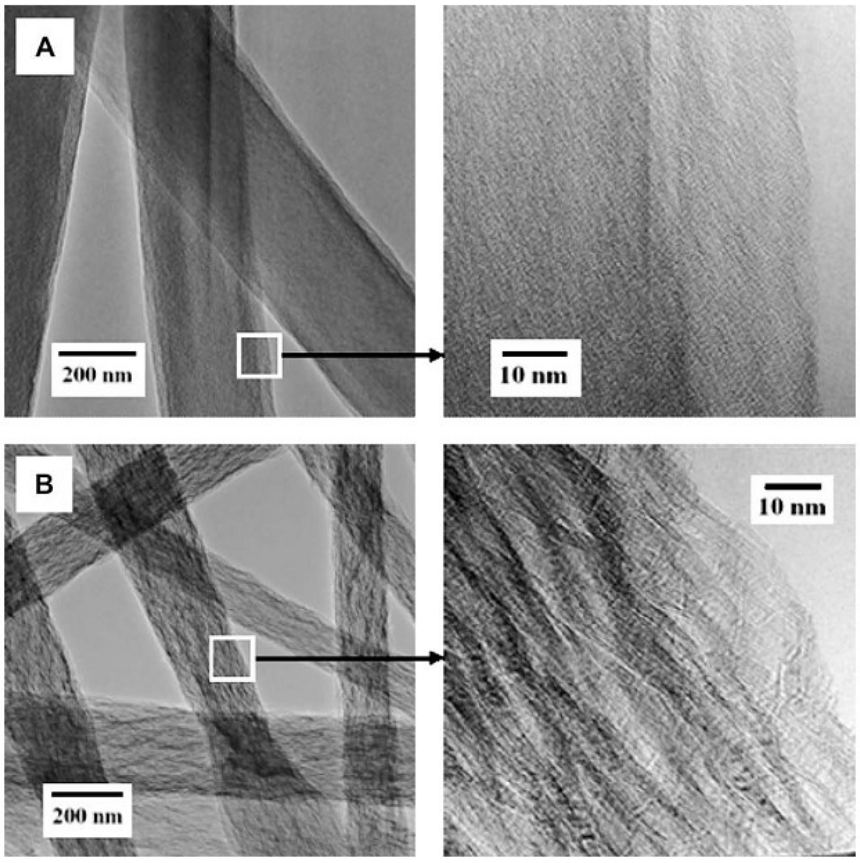

Figure 19: TEM images of carbonized fibers heat treated at (A)1000 ºC (B) 2200 ºC [152]

The rate of increase of temperature, both during stabilization and carbonization, is a very important parameter that defines the properties of the final web. Normally, the temperature is increased progressively in order to control the dimensional shrinkage and the weight loss. Some studies focused on the effect different heating rates to reach the carbonization

temperature. In one of the studies progressive stabilization and carbonization was performed by increasing the temperature at rate of 5 ^{o}C/min to reach the temperature of 230 ^{o}C, the rate was then decreased to 1 ^{o}C/min until 270 ^{o}C was achieved and then again increased to 5 ^{o}C/min to achieve the temperature of 800 ^{o}C. The process was observed to produce higher yield with lower dimensional shrinkage as compared to one without progressive heating treatment [153].

FTIR analysis of carbonized fiber has revealed considerable difference in peak intensities for different groups. The intensities of characteristic peaks of PAN at 2243 and 2929 cm^{-1} (for C≡N and CH_2, respectively) were found to decrease extensively, while that at 1591 cm^{-1} (for C=N, C=C and N-H) was found to increase; while a band at 810 (C=CH, present in aromatic ring) appeared by increasing the stabilization temperature from 250 $^{\circ}$C to 280 $^{\circ}$C. Moreover, these effects were found to intensify by increasing the treatment time [136, 142].

During heat treatment, the density of fiber was found to increase (due to compaction) up to 1000 $^{\circ}$C but then decrease; this sudden decrease has been attributed to the fact that the open pores are converted to closed pores at 1000 $^{\circ}$C [154, 155]. At lower temperatures, close to 1000 $^{\circ}$C, the strength of carbon fibers obtained is quite low and the carbon content normally reaches 95%. However, as the temperature rises above 1500 $^{\circ}$C, fibers with a high modulus could be achieved [124].

2.5.3 Electrospun PAN based Nanocomposites

Integration of different additives in electrospun nanofibers have been found to improve some of their novel properties, which include different mechanical properties, improved thermal resistance, better thermal and electrical conductance and some other novel functional properties [110].

2.5.3.1 PAN-Polymer composite nanofibers

PAN could be combined to a number of polymers to achieve specific properties or enhance the performance of PAN/CNFs produced from PAN for different applications. PAN may be mixed directly with some of the polymers. However, mixing of polymers is a complex process and depends mainly on compatibility of polymers with each other and resulting structural changes. So, different techniques may be utilized to develop some interesting polymer combinations with lower compatibility. Such options include direct mixing of

polymers in a common solvent, co-axial electrospinning or some post spinning techniques such as surface coating.

Combining through a common solvent may be useful for some polymers such as Polystyrene and Polypyrrole etc. PAN/Polystyrene composite electrospun nanofibers can be produced by dissolving both of them in a solvent such as DMF. The polymer composite can then be produced by electrospinning. Such composites can be utilized for developing porous PAN and carbon fibers by dissolving away the polystyrene component afterwards [156]. PAN combined with conductive polymer like polypyrrole renders the resulting composite excellent electrical conductivity. The said electrospun composite, when used as anode for Li-Ion battery, after carbonization, has been found to show superior electrochemical and cyclic performance [157]. Similar approach has been utilized to develop lignin/PAN based carbon fibers using an electrospinning solution produced from modified lignin and PAN, followed by carbonization to get carbon nanofibers [158].

Different bi-component core-shell fibers have also been developed using PAN as one of the components. A basic technique for producing such multicomponent fibers is co-axial electrospinning. This technique uses a needle that has two (or more) concentric tubes over one on other. The shell polymer flows in the outer needle while the core material flows in the inner needle, as shown in Figure 20 [159].

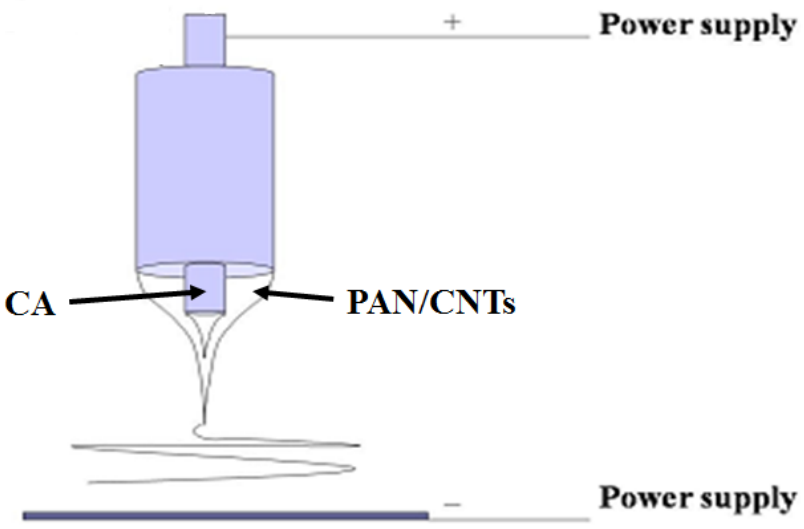

Figure 20: Basic co-axial electrospinning setup [159]

This system may be used for producing multicomponent fibers with the help of multiple concentric needles; for example, PAN has been electrospun with PMMA, Cellulose acetate (CA) and other such polymers using this system [159, 160]. Another utilization of this system is production of Nano-wire in micro-tube structure using three component core-shell arrangement and subsequently dissolving away the middle component [161].

Another system has been devised, by Bazilevsky and coworkers, by producing core-shell nanofibers with Poly(methyl methacrylate) (PMMA) core and PAN shell. They suggested the precipitation of PMMA at base of Taylor cone and resulting encapsulation of PMMA by PAN flowing over it due to electrostatic forces [162-164]. Bi-component fiber may also be produced by using two separate syringes containing different solutions with needles connected to each other to form a spinneret, as shown in Figure 21. PAN has been co-spun with such an arrangement along with polystyrene to develop a filtration system with electrically dissimilar nanofibrous composite [165].

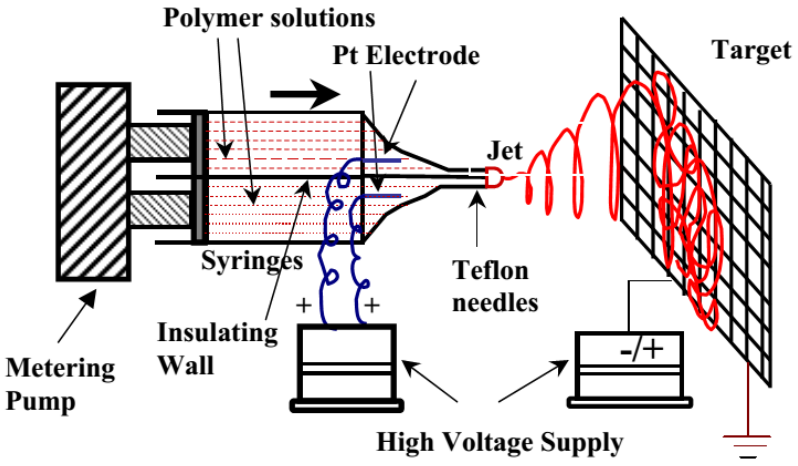

Figure 21: Double needle electrospinning setup for producing bi-component fibers [165]

Another slightly different approach has been adopted to develop self-crimp PAN/polyurethane fibers in side by side assembly. The polymers solutions were pumped to the electrospinning needle via a microfluidic device that causes only a little mixing of polymers due to their laminar flow. Ultimately the polymers were spun side by side and were found to show self-crimping property due to elastic nature of polyurethane component [166]. In one of the studies the PAN/Aniline/gold composite nanofibers, for application in transistors, were produced by coating the fibers produced from PAN/ $HAuCl_4.4H_2O$ combination with aniline by exposing them to aniline vapors [167]. Similar approach has been utilized for developing

PAN/polypyrrole core-shell fibers for elimination of hexavalent chromium in aqueous solutions [168].

2.5.3.2 PAN-Particle composite nanofibers

Nanoparticles are, nowadays, materials of interest, as they can add some interesting and novel properties in PAN nanofibers. High surface area of nanofibrous webs allows them to enhance the functionality of nanoparticles incorporated in such webs because of their accessibility. Moreover, free nanoparticles can't be reused and handled in an efficient manner unless they are immobilized on some support, for which nanofibers is one of the best options. Immobilization on nanofibers not only increases the efficiency of nanoparticles but also allows their extended and repeated usability and recycling [169].

Addition of nanoparticles in nanofibers modifies their morphology by producing larger fiber diameters, possibly, with some bead shaped structures due to agglomeration of particles [170]. Moreover, especially for PAN nanofibers, the thermal properties may also be modified thus affecting the stabilization and carbonization stages while developing carbon nanofibers [170]. Many researchers have focused on developing electrospun PAN/nanoparticles or PAN/nanotubes composites for versatile applications.

Nanoparticles may be incorporated in or on electrospun nanowebs by direct dispersion of particles in electrospinning solutions, or addition of certain agents in electrospinning solution that produce nanoparticles, *in-situ,* after some subsequent treatment or direct treatment with nanoparticle solution or agents that can generate nanoparticles. Some of examples of these routes for incorporation of nanoparticles in electrospun PAN nanofibers are discussed in following paragraphs.

The most direct route for integration of nanoparticles in nanofibers is by producing their dispersion in electrospinning solution. Using this technique, many metal/metal oxide nanoparticles have been incorporated into nanofibers. One of such examples is Palladium nanoparticles loaded in carbon nanofibers for catalysis of Sonogashria coupling reaction. A similar work focused on immobilization of bismuth oxychloride nano-sheets in PAN nanofibers for treatment of waste water and was found to show excellent efficiency for degradation of rhodamine B with UV irradiation [171]. Comparable results have also been achieved with TiO_2 immobilized on PAN nanofibers [172]. PAN/Ag_3O_4 nanofibers, for

photocatalysis, have been developed by electrospinning PAN/DMF/Ag_3O_4 solution [173]. Likewise, Fe_3O_4 nanoparticles have been integrated in PAN nanofibers to produce magnetic PAN/Fe_3O_4 nanocomposites for improved magnetic properties [174]. Silica nanoparticles may also be introduced in PAN nanofibers by adding them directly into spinning solution with an efficient dispersing setup. This technique has been used effectively for development of PAN/poly-L-lactic acid/Si, PAN/Si and PAN/SiO_2 nanofibers, especially, for energy storage [175-178]. Hollow graphitic carbon nano-spheres introduced in CNFs by electrospinning have been found to improve the storage capacity, diffusion of ions and collection of electrons in lithium ion (Li-ion) batteries [157].

In-situ development of silver nanoparticles in electrospun PAN nanofibers, by reduction of silver ions, through xenon arc and chemical reducing agents, has also been found to show significant results. The use of silver salt, in electrospinning solution for *in-situ* development of silver nanoparticles, not only results in evenly dispersed silver nanoparticles in PAN nanofibers but also has also been found to improve the electrospinning process. Such a composite shows a very good antimicrobial effect [179-182]. In another study, hollow carbon nanofibers have been developed by incorporating tetraethoxy orthosilicate in PAN nanofiber, which were converted into silica when thermal treatments for carbonization were carried out, along with evolution of various gases producing micropores in carbon fibers. The composites exhibited good performance when used as super capacitor [183]. Likewise, Sn nanoparticles have also been incorporated into PAN nanofibers by *in-situ* reduction of $SnCl_2$ and the resulting composite has been employed for energy storage applications [184]. PAN/TiO_2 nanofibrous composites for anode material for lithium ion batteries, have also been developed by *in-situ* development of TiO_2 nanoparticles [185]. Another such effort has been employed to develop Iron oxide nanoparticles in electrospun PAN fibers for utilization in capacitors [186].

In other related studies, gold nanoparticles were attached to PAN nanofibers by electrospinning a solution of PAN with a reducing agent. The fibers so obtained were treated with Hydrogen tetrachloroaurate(III) trihydrate to attach gold nanoparticles on fiber surfaces and were found to show excellent sensing capability [187]. A similar study developed gold particles doped PAN/Polyaniline nanofibers for applications in transistors [167].

2.5.3.3 PAN/ CNT based composite nanofibers

As discussed in above sections, like other nanoparticles, addition of CNTs in PAN has also been found to improve many important properties. These include solubility of polymer and tensile strength, thermal shrinkage , electrical conductivity and thermal conductivity of nanofibrous web [110].

CNTs are basically cylinders having carbon atoms bonded covalently with each other. They can be classified in two basic types, i-e single wall carbon nanotubes (SWCNTs) and multiwall carbon nanotubes (MWCNTs). As the name suggests, SWCNTs are those having a single sheet of monolayer sp^2 carbon atoms, i-e graphene, to form a cylinder. While, the MWCNTs consist of concentric layers of graphene sheets having an inter-layer distance of almost 0.34 nm. The diameter of SWCNTs normally exists in range of 1.2-1.4 nm, while, that of MWCNTs ranges from some nanometers to some 100 nanometers. The length of CNTs can vary between nanometers to centimeter range [188-191].

Properties of CNTs depend on their structure and diameter, along with some other properties. Some of their important properties are shown in Table 2. Notably, they have electrical conductivity almost equal to that of highly conductive metals (such as copper having resistivity of 1.724 μΩ.cm) but their thermal conductivity is much higher (for copper thermal conductivity is 400 W/mL) [189]. Their Young's modulus has been observed to be above 1 TPa with tensile strength of almost 30 GPa [190]. They are not soluble in current range of solvents; however, they can be dispersed in several solvents using ultra-sonication [191].

Table 2: Properties of CNTs [188]

Properties	**SWCNTs**	**MWCNTs**
Specific gravity	0.8 g/cm^3	1.8 g/cm^3
Elastic modulus	~1 TPa	~0.3-1 TPa
Strength	50-500 Gpa	10-60 Gpa
Resistivity	5-50 μΩ.cm	5-50 μΩ.cm
Thermal conductivity	3000 Wm^{-1}K^{-1}	3000 Wm^{-1}K^{-1}
Thermal stability	>700 ˚C (in air); 2800 ˚C (in vacuum)	>700 ˚C (in air); 2800 ˚C (in vacuum)
Specific surface area	~400-900 m^2/g	~200-400 m^2/g

The properties of a polymer/CNT composite is dependent on a range of factors, some of which are defined by characteristics of CNTs like their interaction with polymer matrix, the degree of dispersion in it, their dimensional properties and the contents they have in the matrix

[192]. Dispersion of CNTs is normally made in the solvent before adding the polymer. This process needs special care as normal agitation systems may not disperse the CNTs properly and specialized methodologies may be adopted for attaining a good dispersion. Poor dispersion of CNTs, especially in organic solvents, arises from strong Van der Waals forces between them, that make their separation, to individual tubes, very difficult [151]. However, the systems like sonication (normally for 1-4 hours) and high shear mixing have been found to show acceptable results [110, 193]. CNTs may be modified chemically to get dispersion; for example, their surface may be oxidized, fluorinated, functionalized by polymerization or γ-ray irradiation and plasma assisted modification to increase their affinity with solvents like DMF [110, 123, 151, 194-198]. PAN-CNT solutions for electrospinning may be produced, simply, by adding small quantity of PAN in solvent and dispersing CNTs in it through ultrasonic agitation. The initially dissolved PAN acts to keep the CNTs in dispersed form [62].

Electrospun PAN/CNT fibers can be developed by dispersion of CNTs in DMF, using one of above mentioned techniques, with subsequent dissolution of PAN. The quantity of CNTs may be varied between 2-35 wt. percent on weight of PAN, each producing its own set of properties. However, the most usual range used in research studies is between 0.5 - 10% on weight of PAN [123]. For electrospinning, the applied voltages and collector distances can be set around 30KV and 30 cm, respectively [110].

It has been observed that increasing the content of CNTs results in decreased fiber diameter [199]. It may be due the increased electrostatic force because of conductive CNTs in polymer solution, thus pulling the polymer jet more strongly into a fine fiber. However, in some other studies, it has been observed that addition of CNTs increases the overall fiber diameter with increase in fiber diameter distribution. This effect may be attributed to higher viscosities resulting due to addition of CNTs, leading to thicker fibers or due to the interaction developed between CNTs and polymer [200]. More studies, however, are needed to find the optimum parameters and range of their value in which diameter decreases with increasing CNT concentration and those where it increases with increasing CNT concentration. Loading MWCNT in PAN nanofibers has been found to increase the surface roughness of fibers with increasing trend at higher concentrations, confirming the presence of CNTs on surface. Moreover, their alignment has been confirmed to be parallel to each other and along the fiber axis, as shown in TEM images in Figure 22 [110, 151, 193].

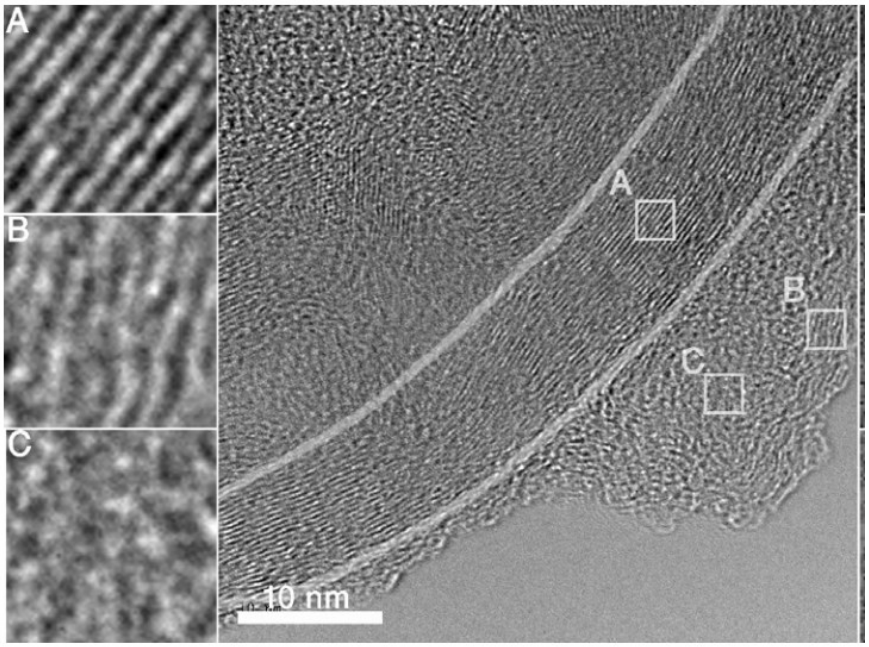

Figure 22: TEM images for PAN/CNT (95/5 %) with (A) CNTs aligned parallel to each other (B and C) areas close to CNTs [193]

However, some irregularities in arrangement of CNTs may occur as the fiber diameter changes causing some CNTs to bend, or overlap with other CNTs or protrude out of the fiber surface creating a defect on it as shown in Figure 23 [201].

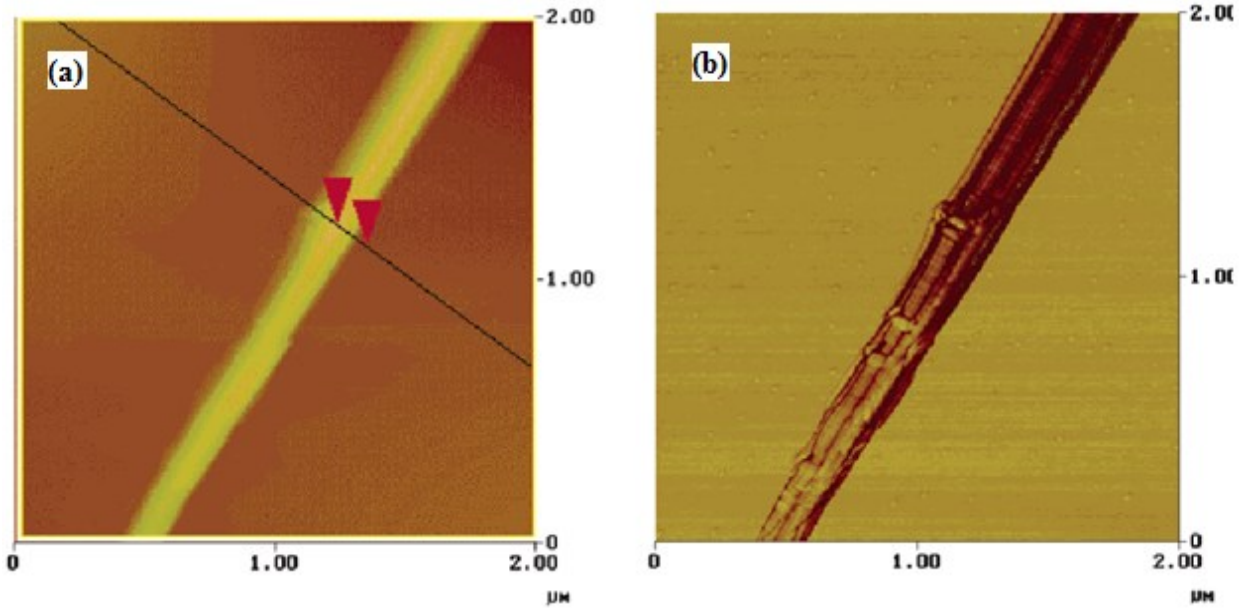

Figure 23: AFM images of PAN/MWCNT (90%/10%) fiber in tapping mode with a (a) height image and a (b) phase image [201]

Some post electrospinning treatments may also be carried out to improve the properties of composite nanofibers. Hot pressing of nanowebs may be performed to improve their mechanical, thermal and electrical properties, by bringing the CNTs and fiber close together [201]. Hot stretching, of nanowebs, close to their glass transition temperature, in order to increase the alignment of CNTs and molecular chains, have been found to improve the mechanical properties [197]. However, the area still needs extensive research as current outcomes are far from theoretically expected results [201]. Optimization of morphology and other properties of such composite systems is a challenging procedure and may need extensive experimentation and should be worked on for development of any viable product from them [202].

Carbonizing of PAN/CNT composite nanofibers to produce carbon fiber/CNT composite is carried out in the same manner as for pristine PAN nanofibers. However, addition of CNTs result in decreased thermal shrinkage, higher growth of graphitic crystals and better ordering of molecular chains (alongside the CNT walls as shown in Figure 24) to give advantage over pristine PAN. Higher the concentration of CNTs and the carbonization temperature, larger is the crystallite size.

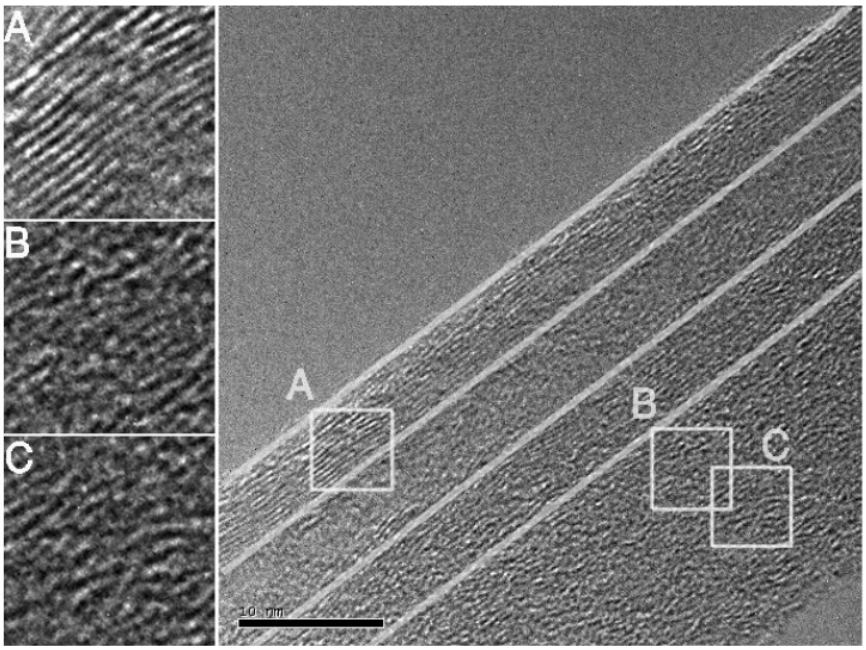

Figure 24: TEM images of electrospun PAN/CNT nanofibers with (A) regions containing CNTs aligned parallel to each other and adjacent areas (B and C) areas close to CNTs location [193]

Thus, the resulting material is more graphitic in nature than that produced from pristine PAN. However, the exact mechanism of this growth in crystal structure is not known yet and needs further research in the field [110, 123, 151]. Such a composite shows many interesting properties and numerous advantages over pristine carbon fibers. Some of important properties of carbon fiber/CNT composite nanofibers are discussed in following sections.

2.5.4 Properties

Some important properties of PAN nanofibers, PAN based carbon nanofibers and their composite with CNTs have been mentioned in following sections.

2.5.4.1 PAN nanofibers

Defect free electrospun PAN nanofibers can be achieved in diameter range of 150-500 nm. The deviation in diameter of such fibers is observed between 50-150 nm [64, 128, 130]. The deviation in diameter was found to increase for solution concentrations above 8%. However, there, have been rare studies, systematically, focusing on effect of different electrospinning parameters on deviation in diameter. Some studies, however, demonstrated the effect of some factors such as presence of electrolytes and nozzle diameters on the variation in diameters of PAN nanofibers [47].

Crystallinity of PAN nanofibers is a major factor affecting most of its properties. The degree of crystallinity of PAN nanofibers electrospun at three different needle-collector distances, between 15-25 cm, was found to fall in range of 7.3% to 16.8%, with larger distances resulting in greater crystallinity [64].

The elastic modulus and yield strength of a single electrospun PAN nanofiber, determined by a Microelectromechanical System, was found to be related to the diameter of fiber constituting it. Both these quantities were found to show a decreasing trend with increasing fiber diameter. For fibers having diameter in range of 200-800 nm the elastic modulus was found to decrease, almost uniformly, from 6 GPa to 1 GPa. Similarly, the yield strength for same diameter range was found to exist between 250 MPa to almost 50 MPa. However, when compressed, their strength increases almost by 30%-40% [64, 122, 201]. One of the studies also reported the ultimate strain to range between 60%-130% for PAN nanofibers with diameters between 300 nm – 600 nm when stretched at strain rates of 10^{-2} to 10^{-4} s^{-1} [122].

For electrospun PAN webs, with thickness between 0.1 to 0.6 mm, the tensile strength ranges between 0.2-5 N, and tear strength between 190-600 N; however, detailed work in the field is still needed to have accuracy in assessment and improvement of mechanical properties of nanofibers and to study the effect of different electrospinning parameters on fiber morphology and thus the mechanical properties [89].

2.5.4.2 PAN based carbon nanofibers

Diameter of stabilized PAN nanofibers has been found to be in same range as original unstabilized fibers; however, after carbonization it may decrease largely, in some cases up to half of original PAN fiber. Normally the diameters of carbon fibers obtained from PAN range between 100-400 nm [126, 136, 152, 203].

Carbon nanofibers from PAN have been found to have excellent electrical and thermal conductivity properties with good chemical resistance and biocompatibility. However, they exhibit a low strength which may be attributed to factors including relaxation of its macromolecular chain, the irregularities in molecular and fibrous structure and the unbalanced load distribution in electrospun webs, to name a few [18, 203]. It may also be attributed to presence of a hollow core or skin core effect, lower interaction between fibers and defects in fibers/non-homogeneous fibers [203]. The tensile strength of carbon nanofibers is estimated to range between 0.32 GPa and 0.9 GPa and Young's modulus in the range of 55-70 GPa; however, some studies showed that it could be as high as 4.5 GPa, with thicker fibers showing lower strength than thinner ones due to lower molecular orientation and presence of non-carbon contents in thicker fibers (due to lower loss of non-carbon content because of their higher bulk). The molecular orientation in fibers may be improved by increasing the stretch in fibers during electrospinning or post-stretching after electrospinning through some mechanical means [126, 136, 152, 203]. Some studies reveal that PAN copolymers have better tensile strength than PAN homopolymer that evolve lower amount of heat during oxidative stabilization, which is reason for scission of molecular chains during stabilization [126, 152]. The carbonization temperature also plays a key role in determining the strength of fibers. Temperatures lower than 1100ºC do not result in sufficient crystallite size to impact the strength in a significant manner; while at temperatures higher than 1400 ºC, the dependence of strength on diameter is not significant due to buildup of crystallite size and loss of non-carbon contents. Fibers produced at carbonization temperatures higher than 1700 ºC may result in a decreased strength due to random crystallite growth whose strength mismatches its surrounding, comparatively,

amorphous carbon, thus transferring the load on themselves to result in a rupture in structure [136].

The electrical conductivity of a single carbon nanofiber derived from electrospun PAN is almost 4.9 S/cm. The graphitized fibers have been found to have conductivity range as high as 150-600 S/m [122, 127]. In non-carbonized PAN, no conductivity has been observed; while as the carbonization process initiates, the fibers become more and more conductive. This may be attributed to presence of heteroatoms in structure of non-carbonized PAN, which are removed by increasing temperature. Moreover, presence of voids within the structure inhibits the flow of charge. Increase in temperature also reduces these void spaces and allows connection between turbostratic layers and molecular chains, thus letting them to conduct. The carbon fiber web is not conductive below 600 ºC; while at 600 ºC, it starts to conduct with conductivity of 150 S/m. As the temperature increases to 1100 ºC, the conductivity increases to 600 S/m [127]. Generally, the conductivity has been found to increase with increasing temperature and time of heat treatment [204], as shown in Figure 25. Moreover, higher conductivity has been found in direction parallel to fiber axis as compared to one perpendicular to fiber axis. The difference between the two has been found to be as high as 20 times of direction perpendicular to fiber axis. This supports the development of aligned fibers for applications that need high electrical conductivity [152].

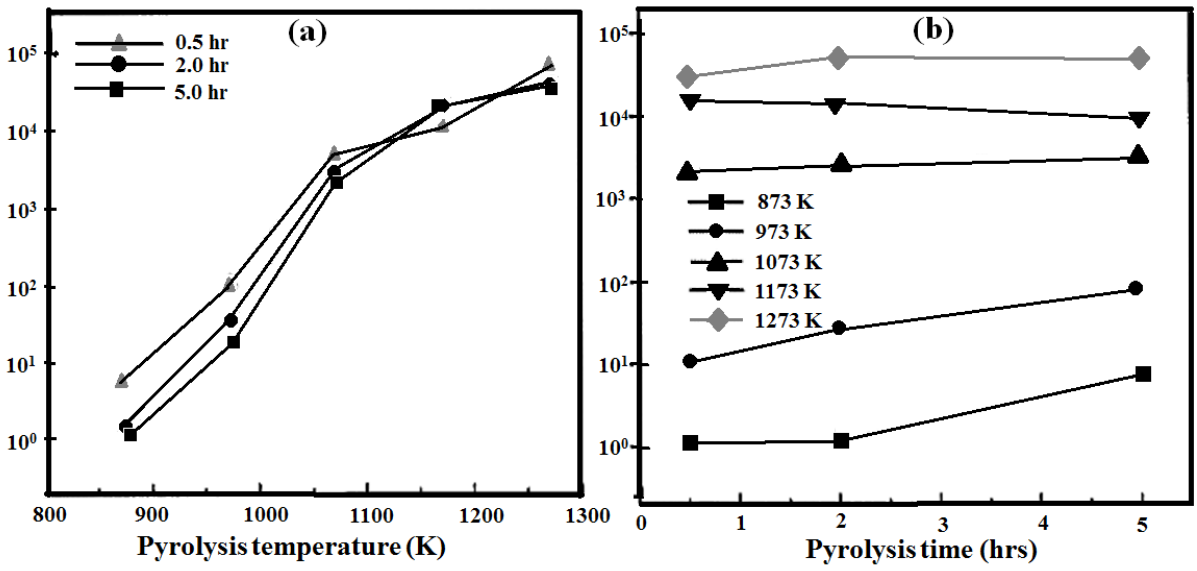

Figure 25: Effect of (a) carbonizing temperature and (b) treatment time on electrical conductivity [204]

2.5.4.3 PAN/CNT and CNF/CNT composite Nanofibers

As already discussed, addition of CNTs increases the diameters and its distribution and the surface roughness of PAN/CNT and CNF/CNT nanofibers [110]. It also improves, the mechanical, thermal and conductivity properties of these composites because of contribution of CNTs, to properties of composite, with its intrinsic characteristics. This contribution increases as the CNTs are modified by some treatments that increases their interaction with the polymer matrix. Such composites have higher strength due to efficient load transfer to CNTs from the polymer matrix. Similarly, higher conductivity for such composites results from higher interaction between the matrix and CNTs allowing better transfer of mass and energy [201].

Normally, the electrospun PAN/CNT fibers have diameters ranging between 200-600 nm and carbon nanofiber/CNT composite, based on PAN/CNT nanofibers, can be produced with diameter range of 100 nm – 500 nm, however, other sizes may also be produced by careful fine tuning of parameters. As with PAN/CNT composites, CNF/CNT composites also have higher surface roughness due to presence of CNTs inside and on surface of fibers [123, 151, 197, 201, 205].

CNTs incorporated into PAN matrix during electrospinning have been found to increase their mechanical strength because of orientation of CNTs along the fiber axis that contributes to strength of composite by interfacial interaction between CNTs and matrix. It has been observed that alignment of CNTs in electrospun PAN fibers, along the fiber axis, is much higher than that of PAN crystal matrix. So, incorporation of CNTs is expected to render better mechanical properties than that of pristine material [201]. In a study, it was observed that addition of 5 wt. % MWCNT has been observed to increase the tensile strength of PAN nanofiber web by almost 75%, reaching a value of 80 MPa, as compared to one having no CNTs, with tensile strength ranging around 40 MPa. However, when CNT concentration is increased above 5%, the tensile strength has been found to decrease. This may be attributed to higher aggregation and lower interfacial interaction between CNTs and polymer matrix. Generally, the tensile modulus for the PAN/CNT nanofibers has been found to range between 3 GPa -14 GPa, while tensile strength between 50 MPa-350 MPa [110, 197]. The highest strengths have been achieved for composites that have been compressed thus bringing the CNTs close together. There is a limited amount of work focusing the mechanical characterization of CNF/CNT based on PAN, so the area needs some extensive studies for

complete characterization of mechanical properties of electrospun PAN/CNT based CNF/CNT composite nanofibers.

Addition of CNTs also improves the thermal conductivity and reduces the thermal shrinkage and degradation of PAN nanofibers. The degradation temperature of such fibers has been found to increase to 292 ºC for PAN/CNT composites as compared to 268 ºC for pure PAN fiber [201]. Decreased thermal shrinkage for such composites is, simply, because the CNTs themselves are non-shrink material and due to their interaction with PAN matrix they hinder the shrinkage of matrix. Higher the amount of CNTs lower is the shrinkage; reducing it to values as low as 3% (for carbonizing heat treatment up to 850 ºC) for CNT concentrations around 35% (on weight of PAN) as compared to a shrinkage of 30%-40% for pristine PAN nanowebs [110]. Surface treated CNTs possess even better reduction in thermal shrinkage because of greater interfacial interaction with PAN matrix [201]. The trend of decrease in shrinkage is summarized in Figure 26.

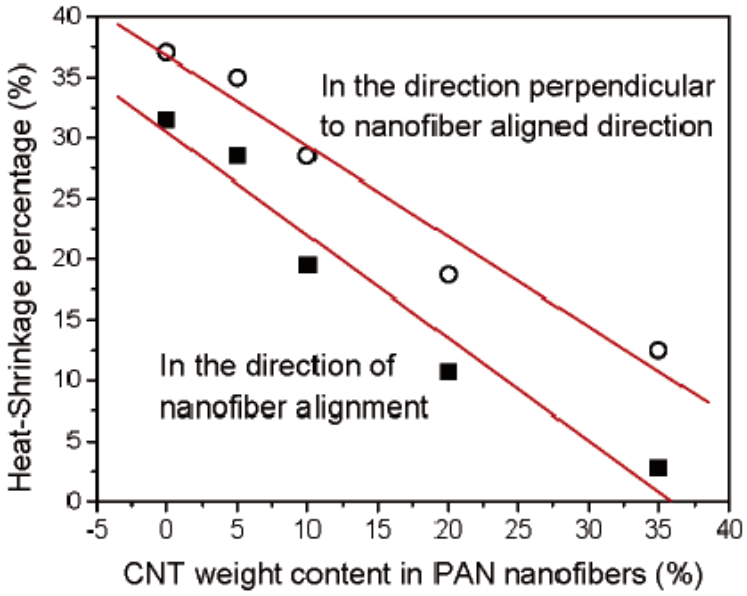

Figure 26: Decrease in thermal shrinkage with different CNT content in PAN nanofibers for carbonization at 850 ºC [110]

Addition of CNTs also increases the mass and energy transfer within and across the PAN/CNT and CNF/CNT composite fibers. The increase in conductivity of carbon fibers, due to integration of CNTs in them, is supported by the fact the CNTs present inside the fibers develop contact with each other and those on surface of nanofibers adjacent to each other make inter-fiber contact, thus allowing the flow of charge and energy [206]. As is the case for other

properties, surface modified CNTs offer better mass and energy transfer because of their better interfacial interaction with matrix [201]. The protrusion of CNTs out of the fiber surface has been found to increase with their increasing concentration, as shown in Figure 27 [205].

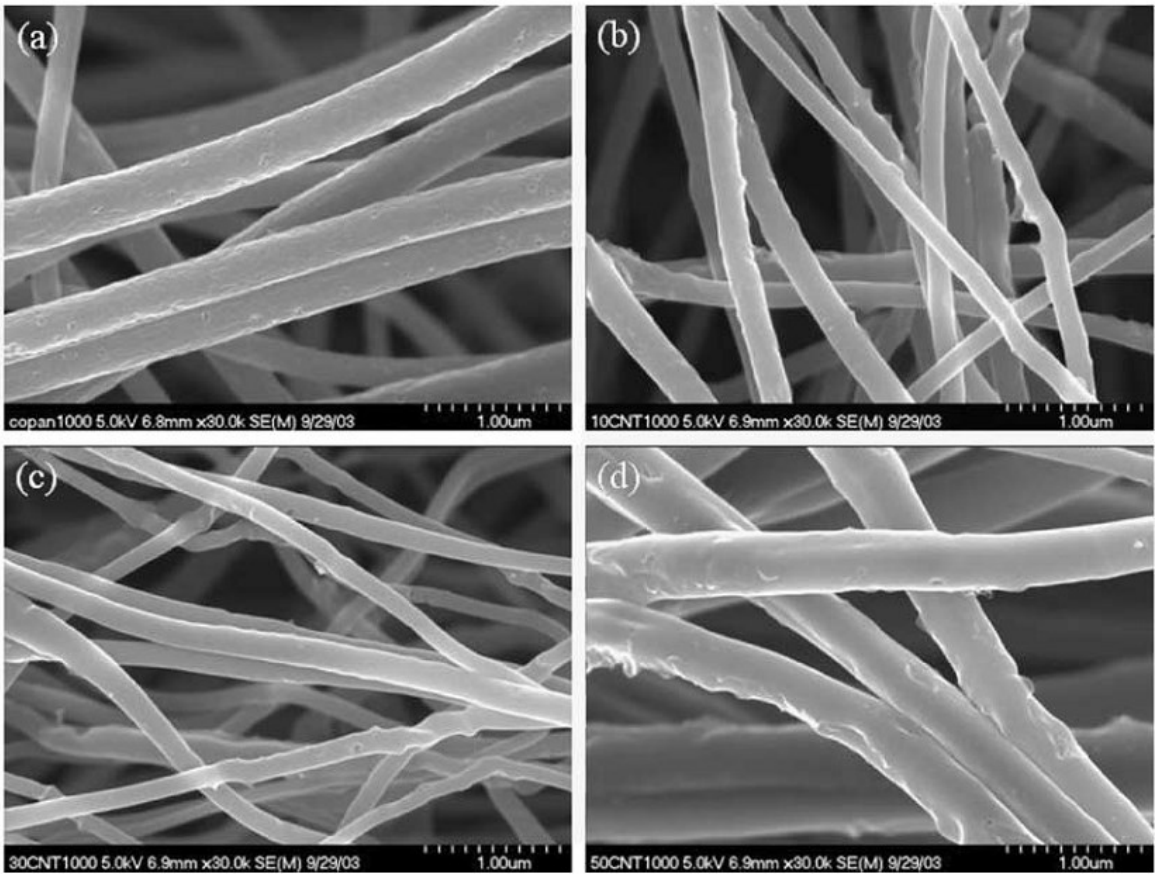

Figure 27: SEM micrograph of carbon fibers charged with (a) 0%, (b) 1%, (c) 3% and (d) 5% MWCNT [205]

Typically, the PAN/CNT composites possess electrical conductivity values between 0.1-1 S/cm with minimum percolation CNT concentration limit of 10% (MWCNTs) [199, 201]. The conductivity of single fiber of PAN/CNT composite ranges between 1.2×10^{-4} S/m to 310×10^{-4} S/m [123]; while that of CNF/CNT composite web could be as high as 35 S/cm at CNT concentration of 10 wt. %. However, it has been observed that conductivity of CNF/CNT composite nanofibers is an anisotropic property that is almost 3 times high along the fiber direction as compared to that perpendicular to it [199]. Even though, significant work has been performed to study the electrical conductivity of PAN/CNT electrospun composite fibers, most studies have been carried out with MWCNT; so, other form of CNTs (SWCNTs and double wall CNTs) still need more studies. Moreover, only limited number of studies focus,

quantitatively, the improvement in thermal conductivity; thus it may be worked on in future works in the field.

Addition of CNTs in carbon fibers is also found to render electromagnetic shielding properties to them. A CNF/CNT nanofibrous composite with thickness of 150 μm can provide a shielding effect of 30 dB at 30 MHz and 10-15 dB for frequencies as high as 3 Ghz [151]. Based on these studies, PAN/CNT and CNF/CNT can be considered as important materials for various energy applications.

2.5.5 Technical Applications

PAN nanofibers and carbon nanofibers, produced from them, find a range of applications in many fields. Most of the applications of these materials are in research phase and have shown very promising results. One of the most important usage of PAN based carbon nanofibrous materials is energy storage and conservation. Because of their high carbon content and large surface area with adjustable porosity, they show outstanding results when used as electrode materials for lithium ion batteries thanks to their high electrode-electrolyte interaction leading to excellent electrode reaction kinetics. Electrospun PAN based materials have also been studied for their potential biomedical applications and found to show exceptional results. Their important biomedical applications include different type of tissue engineering scaffolds and drug delivery systems [44, 207-210]. They have also been employed to develop different type of sensors for agents like methanol [211], dimethyl methylphosphonate [212] and some toxic gases like carbon monoxide and nitric oxide etc. [3]. In the field of electronics, some of their applications include super capacitors [18, 213, 214] and nano-electrodes [139]. Similarly, PAN and carbon nanofibrous materials have shown very promising results in the field of different protective systems like chemical [215], biological [216], thermal [217], magnetic and electromagnetic field protection [151]. Different filtration products from PAN based materials have also been studied for a number of versatile applications and have been found to show encouraging results [89, 173, 218, 219]. Other applications include different performance textiles like wind and water proof textiles, super hydrophobic textiles and antibacterial textiles, sound absorption webs and affinity membranes [220-223]

Being one of the most important source of carbon nanofibers, electrospun PAN nanofibers are very important for applications involving conductivity. Most of such studies discussed above has focused on energy storage. However, as they are conductive materials,

they can also be used for other energy related applications. The possibility to fine tune their resistivity can be utilized to produced customized products for heat generation. However, this area has not been studied in past. One of aim of current work is to study the heat generation possibility of electrospun carbon nanofibrous materials by employing their electrical resistivity. Some of the current heat generation systems are discussed in following sections for a review.

2.5.5.1 Heat generation technologies and possibility of generation through electrospun carbon fibers

Heat generation devices produce heat by employing the principle of conversion of other form of energies to heat. Current heat generation systems may be divided according to types of energy source being utilized to generate heat. Most important among them include electrical heating systems, combustion heating systems (oil, gas, waste matters) and solar heating systems. Another important and practical classification is according to type of heat transfer. According to this classification, heating systems may be divided as conduction, convection, radiation and induction systems.

Different types of above mentioned basic systems are, practically, being used for versatile heating applications. For simplicity, the current section gives an overview, of the heating techniques used in kitchenware, which may be applied in larger perspective for complex applications. Most of the current heating systems for kitchenware employ conduction, radiation and induction technologies, each having its own set of properties. Conduction systems, basically, transmit the heat through contact, so the heat source must itself be hot, opposed to radiation or induction systems that transmit the energy through radiations and electromagnetism, respectively [224]. Conduction based systems offer the advantages of being cheaper, with versatile applications and good efficiency (71.9% conversion of electrical energy into heat energy). Systems based on induction also offer good efficiencies (up to almost 73%). However, these systems are expensive and can't be used for heating all types of materials, for which they need to transfer the heat to appropriate conducting medium that in turn heats the target medium, thus resulting in lower efficiencies. Similarly, equipment using radiation as a source of heat are also very specific and pose additional risks due to radiation [224-226].

Conventionally, the conduction cooktops contain an electric coil having a predefined electrical resistivity and heat up due to that resistivity as the current flows through it. Smooth

cooktops have heating coil covered with a ceramic plate with metal at its top. Similarly, halogen cooktops contain halogen filament tube, inside ceramic case, to produce heat [227]. Other than cooktops, some software controlled intelligent cooking devices have also been developed. They use miniature heating plates connected to a circuit for heat generation that is transferred through the top ceramic covering. Such systems have been shown to produce high efficiency and can reach a temperature of up to 200 ºC in just 2 min. The key for high efficiency of such systems is the properties of these miniature heat plates. They allow to produce uniform heat as all miniature plate produce heat independently [228]. However, their efficiency may be improved by using newer material having higher conductivities and improved properties such as CNFs and CNTs and their composites.

As mentioned in above sections, carbon nanofibers can conduct heat and electricity quite well and their resistivity could be adjusted as required. This property may be utilized for efficient heat generation systems using CNFs to produce required amount of heat with lower energy consumption. CNFs may be customized for the purpose by addition of CNTs in them. As discussed in above sections, this will improve a number of properties of CNFs that may result in increased efficiency for heat generation. Such a system is expected to have tunable heat generation capacity with improved efficiency. The conductivity can be well controlled by controlling the amount of CNTs and the degree of crystallinity along with some other parameters such as extent of carbonization. Such systems are also expected to have good environmental compliance. Current literature does not mention any study with CNF/CNT nanocomposites for heat generation. So, the feasibility of this system followed by detailed quantitative evaluation could be worth-studying.

2.6 PA-6

PA-6 is a semi-crystalline synthetic polymer and used for numerous clothing and technical textile applications. It is a biodegradable polymer with good biocompatibility and mechanical properties [229]. PA-6 can be chemically represented as **H[-NH-(C_2H_5)-CO-]$_n$OH** and is normally produced from caprolactum by ring opening polymerization. As the name suggests, it opens the ring of caprolactam and joins the repeat units through amide linkages [230]. Conventional PA-6 fibers have density of 1.13 g/cm^3, glass transition and melting temperature ranges between 40-55 ˚C and 215-230 ˚C, moisture regain value of 4% and crystallinity close to 35% that may be modified according to processing conditions. Tensile strength of normal PA-6 fibers ranges between 30-220 MPa, elastic modulus between 1.1-6

GPa with elongation at break up to 150%. The covalently bonded molecular units are responsible for unique mechanical properties of PA-6 fibers. Due to their exceptional properties, they find wide applications in different fields, including clothing and apparel, canvas and parachute fabrics, sail cloth, carpets, different safety products, hoses and belts, tire cords, ropes, sutures and different types of bristles. Many techniques can be used to convert PA-6 into fibrous form; they include melt spinning, dry spinning, solution spinning, wet spinning, gel spinning and electrospinning. However, electrospinning produces nanofibers with acceptable properties and is the only technique (by now) that can produce nanofibers with acceptable production rates [230, 231].

Electrospun polyamide 6 (PA-6) nanofibers have been studied by many different researchers because of the properties offered by them; such as better formability, mechanical properties and biocompatibility. PA-6 can be dissolved in solvents like formic acid and acetic acid that renders it distinction over polymers soluble in toxic organic solvents. Moreover, its morphology can be fine-tuned as desired with option to obtain very fine to thick fibers. Furthermore, it offers some interesting technical applications that are discussed in following sections. Based on these facts, PA-6 is considered to be one of the most suitable polymers for electrospinning and has been studied by many researchers for many different properties and applications.

2.6.1 Electrospinning of PA-6

Electrospinning of PA-6 has been studied extensively by many research groups while studying its properties and applications in different fields. Electrospun PA-6 nanofibers can be formed with diameters as low as 10 nm by selection of proper electrospinning parameters. As with other polymers, mentioned in earlier sections, concentration is the most important factor having largest impact on morphology of PA-6 nanofibers [22, 61]. Usual PA-6 concentration range for electrospinning is between 15-25 wt. %; however, values around 20 wt. % have been reported to produce optimum and defect free fibers [61, 63, 232, 233]. Increasing PA-6 concentration from 10% to 46% in formic acid, the viscosity of solution rises from almost 40-4000 cp. Solution viscosities below 135 cp , i-e at concentration value of 16 wt. %, have been observed to produce only droplets. At 17% beaded fibers are produced with some droplets due to presence of higher solvent content, and above 20 % ribbon like fibers are obtained due to evaporation of all of the solvent in very short time because it is present in a small amount [61, 234]. Selection of other parameters is important in determining the diameter of fibers. Normally

used parameters include voltage between 10 to 30 KV, distance range of 15-20 cm, and feed rate of 0.1 to 0.2 mL/hr. in ambient conditions [63, 65, 232, 235]. In some of the studies it has been noticed that the effect of voltage on PA-6 nanofiber diameter is less significant than some other parameters such as concentration and needle to collector distance [71].

Formic acid has been observed to be the best solvent for PA-6. This is because of its excellent dissolution capability for PA-6 and significant conductivity due to free ions produced as a result of polyelectrolytic behavior of PA-6 in formic acid (that arise because of the partial ionization of amide groups in PA-6 chains). This property of PA-6 solutions in formic acid yields exceptional outcomes when it is electrospun [236]. This high conductivity and presence of lower mass group oligomers in PA-6/ formic acid solutions can also be utilized to produce ultrafine nanofibers with diameter between 10-30 nm, when subjected to higher voltages (Figure 28) [229, 236-238]. Electrolyte has been found to be the main determining factor of solution conductivity that is also affected, slightly, by polymer concentration and its grade [66].

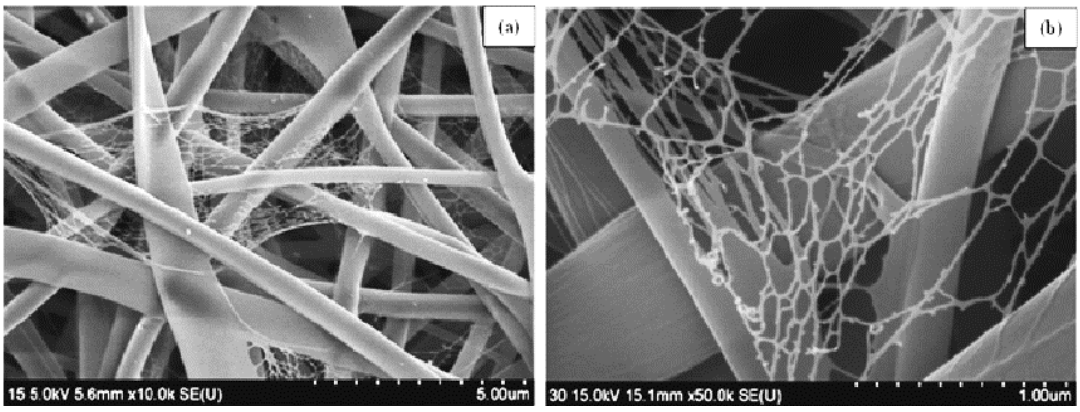

Figure 28: Ultrafine PA-6 nanofibers between the main nanofibers at (a) 10X and (b) 50X magnification [229]

The effect of solution, process and ambient parameters on electrospinning of PA-6 are similar to those discussed in opening sections of this chapter. The nanofiber diameter has been found to be affected in a directly proportional relationship with its molecular weight, viscosity of solution, concentration of electrolyte, needle size and grade of acidic solvent used. The effect of voltage, needle to collector distance and electric field on diameter is not linear and results in an initial decrease followed by an increase in diameter with increasing values of these parameters [235].

2.6.2 Properties

Using electrospinning, generally, PA-6 nanofibers with diameter range of 50-200 nm can be obtained with concentration of 15-20 wt. % [63, 232]. As discussed earlier, PA-6 can be electrospun into ultrafine fibers due to its polyelectrolytic behavior that leads to formation of lower molecular weight oligomers, initially originating from main fibers as a second layer and finally separating from it as ultrafine fibers hanging between the main fibers. The diameter of such fibers is normally between 10-30 nm [236-238].

Electrospun PA-6 fibers, normally, have poor mechanical strength, due to similar reasons as explained for PAN nanofibers [239]. The single fiber tensile strength of PA-6 fiber has been found to vary around 10 MPa to 55 MPa and the young's modulus value of almost 200 to 400 MPa at breaking strain up to 300% [41, 71, 233]. The mechanical properties have been found to be strongly affected by molecular weight, with higher molecular weights resulting in better mechanical properties [41]. Inferior mechanical properties of PA-6 nanofibers, as compared to its cast films, can be consistent with the fact that the degree of crystallinity in PA-6 nanofibers is only 38% as compared to that of cast films (almost 61%). This reduced crystallinity could be reasoned to be due to shorter time available to the molecular chains to form crystal array [71].

PA-6 nanofibers show almost the same thermal stability as compared to its raw pellet form. In one of the studies, the electrospun PA-6 nanofibers were found to degrade at 424 ºC as compared to its pellets that were found to degrade at 408 ºC. It has also been observed the electrospinning PA-6 results in a slightly decreased melting point, glass transition temperature and the degree of crystallinity [240].

2.6.3 Technical applications

Electrospun PA-6 nanofibrous materials have been studied by many researchers for numerous potential applications and found to show improved performance as compared to conventional material. One of the most important field of application of PA-6 nanofibers is in different types of filtration products, due to their inert nature to the components of filtration feed fluids, tunable filtration properties and possibility to be functionalized to make them specific to certain products that need to be screened out. They have been observed to perform very efficiently as pre filters and main filters for removal of sub-micron and micron sized

particles from different fluids [241-244]. Their use for filtration and elimination of different micro-organisms has also shown their potential significance in the field [245]. Modified and functionalized PA-6 nanowebs have been used for removal of certain toxic substances like copper ions from different fluids such as waste water [246]. They have also been utilized to study their potential for various biomedical applications. PA-6 nanofibers based materials have been found to show acceptable results as a future material for different types of drug delivery systems. Moreover, they have been found to show interesting results when used as tissue engineering scaffolds for human cells and their non-cytotoxic behavior for such cells is expected to be explored in future [104]. Studies on PA-6 nanofibrous materials, for their use as potential material for different type of sensing systems, have also revealed their potential capabilities to be used in devices in future. They have been used for sensing of different agents such as formaldehyde, copper ions, lead ions, pesticides and environmental parameters like humidity [247-251]. They can also be used in high-end electronics such as super-capacitors and versatile protective applications such as fire retardant and gas barrier products [252, 253].

As mentioned above, among many different applications of PA-6 nanofibrous materials, filtration is one of the most important application [241-244]. Current study focusses on application of PA-6 based nanofibrous materials in one of the subclasses of filtration i-e respiratory protection through filtration using optimized PA-6 nanofibers incorporated face masks. Some theoretical and practical aspects of this field are discussed in following sections.

2.6.4 Electrospun PA-6 for respiratory protection

Respiratory protection is protection of respiratory system from external agents, such as different type of particles, pollens and microbes. It is a filtration process that screens away these agents from inhalation air and inhibits them from entering into the respiratory tract. So, respiratory protection is a filtration process that filters away the harmful agents from the air entering the respiratory system.

2.6.4.1 Filtration

Filtration is separation of two more phases of matter from each other and may be categorized by the phases to be separated i-e solid-gas filtration, solid-liquid filtration, liquid-liquid filtration and solid-solid filtration [254]. It is normally carried out by a barrier, called filter media, which allows only selected components of a mixture to pass through it. A filter

media may be defined as “Any material, that under the operating conditions of the filter, is permeable to one or more components of a mixture , solution or suspension, and is impermeable to the remaining components”[255]. Filtration through a media may be the result of any type of mechanical, physical, chemical or electrical interaction of the media with the separating phases.

2.6.4.1.1 Particulate Filtration

This type of filtration may be a result of any of the following mechanisms [255];

- *Surface straining:* Here the particles due to their larger size than the filter media pores are restricted to the surface of the media.
- *Depth straining:* With this type of filtration, the filtration media has larger pore size at surface which gets much smaller in the interior of the media. So, the particle flows inside it and gets trapped as the pore diameter decreases.
- *Depth filtration:* In this case, the pore size is greater than the particle size throughout the pore length. However, the particles are still held by the pore walls with the help of Van der Waals forces.
- *Cake filtration:* The solid particles accumulated on surface of the filter media also produce a filtration effect, called cake filtration, which holds particles at the surface of media.

2.6.4.1.2 Mechanism of Particle Entrapment by Fibrous Filter Media

A particle may entrap into a filter media by impacting the fibers after overcoming the air streamlines (due to its inertia) along which it moves. This mechanism is termed as inertial impaction. In a similar process called interception, a particle does not overcome the inertial forces, however, it comes close to the fiber which attracts and captures it. While, in another process, called diffusion, a particle may leave the streamline due to Brownian motion and find a fiber in its path, which engages it. Still another mechanism is based on engagement of particles due to electrostatic attractions between fibers and particles. The mechanism that mostly governs the entrapment of smaller particles is diffusion while for larger particles is inertial impaction. The particles in range of 0.04-0.4 μm are “most penetrating particles” as they are most difficult to be engaged in filter media. This is because these particles are too large to be engaged by diffusion and too smaller to have good inertial impact [256, 257]. The

filtration process may be classified according to size of particles to be filtered, as shown in Figure 29.

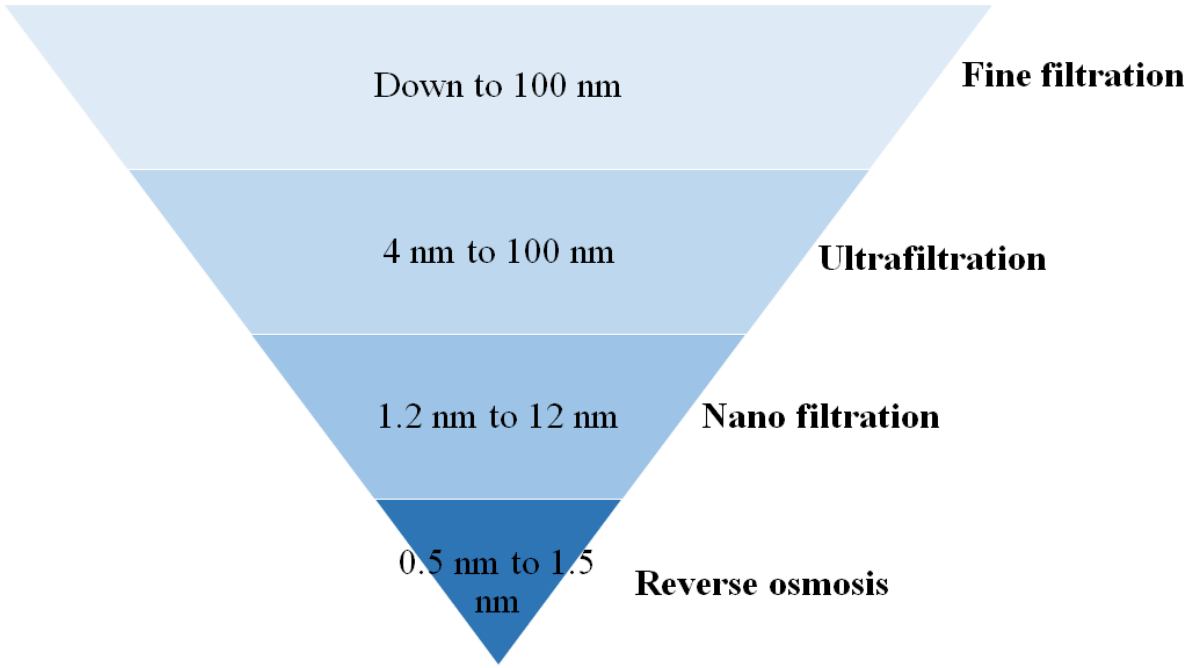

Figure 29: Classification of filtration process according to size of particles to be filtered [256]

2.6.4.1.3 Types of Filter Media

A variety of filter media have been used for filtration of different types of phases. The type of media to be employed for each of above mentioned filtration classes depends on the size, chemical and physical nature of both the phases. Following are some of types of filter media [256]:

- Adsorbent media; contains some type of adsorbing agent such as activated carbon
- Absorbent media; works by absorbing the contaminants in a structure such as a nonwoven fabric
- Coalescing media; where a fiber matrix traps one of the two immiscible liquids
- Electro-filtration media; works by capturing the contaminants by electrostatic forces
- Antimicrobial filter media; eliminates the microbes from the filtrate, filtered product and/or the media itself

For respiratory protection, mostly nonwoven filter media is employed. It is "a porous fabric composed of a random array of fibers or filaments, whose specific function is to filter and/or separate phases and components of a fluid being transported through the medium or to support the medium that does the separation" [256]. Nonwoven filter media may be classified according to their specific manufacturing technique and include spunlaid, air laid, dry laid, melt blown, spun bonded and electrospun media. One of the most recent types of nonwoven filter media is based on nonwovens produced from nanofibers. They have been discussed briefly in the following section.

2.6.4.1.4 Nanofibrous filter media

Filtration through fibrous assemblies is governed by three mechanisms namely (i) Interception, (ii) Inertial impaction (iii) Diffusion. Larger particles can normally be intercepted or caught into pores between fibers, or interaction with its surface while moving in the gaseous stream passing through the filter. For impaction, the particle should pass within one particle radius from fiber surface. Particles farther than that will not be captured by fibrous filter. Some of the particles that maintain their inertia, either due to higher speed, larger size or heavier weight, are not able to change their path and collide directly with the fibers and the mechanism is termed as inertial impaction. Some other particles lose their path by colliding with molecules of gas carrying it. Such particles move in random/zigzag path within the fibrous assembly until they find a fiber in their path and get captured by it [179, 258]. The accumulative filtration of a fibrous filter is combination of all above mechanisms taking place simultaneously. The performance of a filter media is evaluated by its filtration efficiency (η) and the resistance (ΔP) which it offers to filtrate while passing through it. Both the values are generally determined using the Equation (11) and Equation (12).

$$\eta = \frac{G1 - G2}{G1} = \frac{Q(N1 - N2)}{QN1} = 1 - \frac{N1}{N2} \qquad \text{Equation (11)}$$

$$\Delta P = \frac{2C'v^2H \propto \rho_a}{\pi {d_f}^2}\ (Pa) \qquad \text{Equation (12)}$$

Where, in Equation (11), G1 and G2 represent the amount (mg/h) of particles moving through inlet and outlet, respectively. N1 and N2 denote the particle concentration (mg/m^3) at inlet and outlet, respectively and Q signifies the wind speed (m^3/h). In Equation (12), where *C'*

denotes resistance coefficient, v is filtration velocity (in m/s), H signifies the filtration layer thickness (m), ρ_a denotes gas density (kg/m^3) and d_f represents the fiber diameter. So, from these equations it can be inferred that for higher filtration smaller fiber diameter is favorable but at the same time it will also increase the filtration resistance and this fact has also been proved practically [259].

So, nanofibrous filter media offer improved efficiency as compared to one made from macro and micro fibers because of smaller diameter fibers with smaller pores and higher surface to volume ratio thus offering greater capture sites and cohesion [179]. The porosity of nanofibrous membranes can be easily fine-tuned by optimizing the process parameters. Normally, increasing the fiber diameter increases the porosity thus affecting the permeability and quality of filtration [53]. Many different polymers have been employed for developing such a media. PA-6 is one of the most suitable materials for filtration because of stability, formability and biocompatibility other than the above mentioned properties. PA-6 nanofibrous filters have been found to show superior air filtration efficiency (almost 99.99% of impurities are removed) than High Efficiency Particulate Air (HEPA) filter at 10 times lower filter film thickness. The pressure drop, which is the measure of flow of a fluid through a filter, at face velocity of 5 cm/s (particle size 0.3 μm), however, was found to be higher than HEPA filter because of its much lower pore size. The PA-6 used in the cited study had fiber diameter between 50-200 nm, web thickness of 50 μm and base weight of 5.75 g/m^2 in comparison to 100 μm and 10.75 g/m^2, respectively, for comparative HEPA filter [63].

Similar observations were made in another study, where electrospun PA-6 nanofibrous filtration media was assessed for its filtration efficiency. Higher pressure drop was observed as compared to melt blown nonwoven media. This trend was explained to have no relation with mean fiber diameter, however, fiber diameter distribution was found to affect the pressure drop. The samples having higher percentage of thicker fibers were observed to have higher pressure drop [232]. According to Darcy's law (Equation (13)) rate of flow, and hence the pressure drop, along with other factors, depends on thickness of filter. However, in case of nanofibrous materials this phenomenon needs further studies as there are certain other factors as well.

$$q = K.\frac{\Delta P}{L} \qquad \text{Equation (13)}$$

Where “q” is the flow rate, “K” is constant for flow permeability, “ΔP” is the pressure difference between two faces and “L” is the thickness of media.

The aerosol filtration efficiency, measured by difference in concentration of filtered and unfiltered fluid, of electrospun PA-6 filter media was found to be comparable to that of commercial HEPA and ULPA (Ultra Low Penetration Air) filters, at much less thickness, especially for particles under 100 nm. Again, the filtration efficiency was found to be more related to diameter distribution than the mean diameter, with higher thick fiber distribution offering better filtration efficiency [232].

2.6.4.2 Nonwoven filter media for healthcare face masks

Respiratory protection equipment may be classified as air supplying and air purifying devices. The air supplying devices carry a system to supply air for breathing. Air purifying systems filter the air before it reaches the mouth and are meant for protection against environmental impurities that are not, immediately, dangerous to the health. They may be further classified as front/back mounted masks, chin style gas masks and escape gas masks. Front/back mounted masks and chin style masks have full face piece and containing canisters for filtration media [260]. Mechanical filter respirators, a subcategory of air purifying respirators, are those which use some entrapping technique to screen out the impurities, physically, as the air is passed through them [261].

Nonwovens are one of the most frequently used materials for different types of mechanical respirators and numerous products with nonwoven filter media have been designed and marketed [261]. They offer a suitable filtration solution required for face masks. They have a complex asymmetrical structure that suits quite well for filtration required in respiratory protection. They are efficient against different type of agents such as particles and microbes, are light weight, low cost and easy to use. Moreover, they can be designed for a maximum fit, thus ensuring only filtered air to be inhaled [260].

As for different types of filtration discussed in above sections, the performance of a nonwoven face mask (that is ultimately a filter) is evaluated based on its filtering efficiency (mostly determined by its porosity), the pressure drop and resistance to flow of air across it. They can, not only, screen out larger particles, but also smaller entities like viruses (having size as low as 10 nm to 500 nm) [262] [260]. For nonwoven face masks, the mechanism of filtration

is same as discussed in previous sections. Diffusion, impaction and interception are the main dominating mechanisms. Diffusion dominates below 1µm particles size while up to 3 µm diffusion and interception both and above 4 µm impaction and interception are the dominating modes of filtration by nonwoven for face masks [261].

Normally, the filter media of nonwoven facemask is protected by sandwiching it at both faces with nonwoven fabrics having larger fiber diameter than the filter itself (density range is almost 10-40 g/m^2). This not only prevents it from damaging but also allows a pre-filtration [262]. For loose fitting masks, the structure is pleated to allow for fitting the mouth in it for better protection. While, in case of respirators (tight fitting masks), the structure in kept in a molded frame to provide better fitting (Figure 30). Thus, respirators, because of their better fit are expected to provide better protection [263]. They may, both, be further classified as FFP1, FFP2 and FFP3 respirators. FFP1 are those that have filtration efficiency above 80%, FFP2 have above 94% and FFP3 provide filtration efficiency up to 99%. This classification has been based on European standard EN 149 (Annex I) [264], that evaluates the face mask for its performance based on filtration efficiency and breathing resistance. Filtration efficiency is measured by using sodium chloride particles dispersed in air or paraffin oil mist. Air containing these materials is passed through filter and analyzed for concentration of sodium chloride or paraffin before and after passing through filter and difference gives the filtration efficiency. Breathing resistance is determined by passing compressed air through the filter at pre-programmed rates and measuring its pressure at both faces of filter [265].

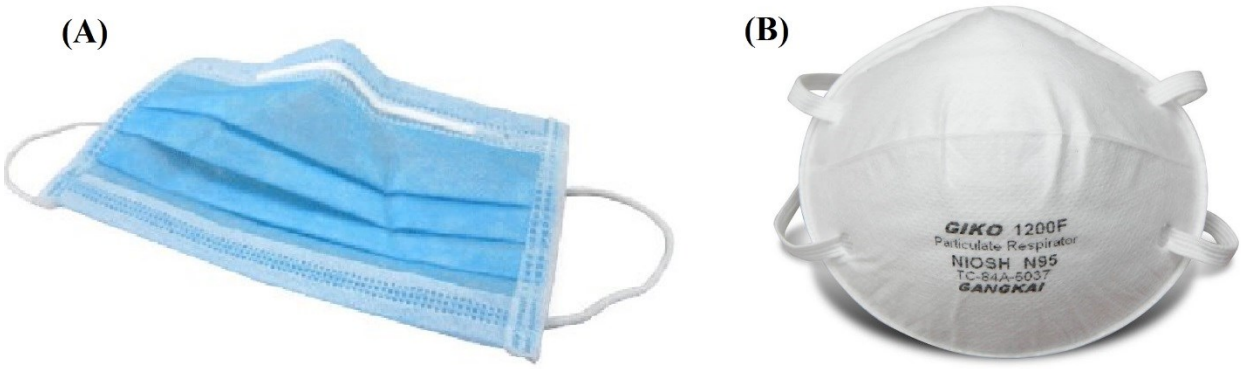

Figure 30: (A) Loose and (B) tight fitting mechanical respirator [263]

FFP2 disposable nonwoven masks are the main products used in different type of emergencies such as the recent avian influenza epidemic in Asia. As for most of the other

masks, these products are normally made of three nonwoven layers i-e two spunbond layers sandwiching a meltblown layer. Though products with more and less layers may also be developed based on the specific enduse. Meltblown (Annex I) processes allow the production of very thin fibers to capture very small particles and spunbond (Annex I) allow the production of coarse fibers in order to give mechanical strength to the complete structure. These processes use thermoplastic polymers, usually Polyethylene Terephthalate (PET), Polypropylene (PP) or Polybutylene Terephthalate (PBT). To address poor breathability, mechanism employing filtration through electrostatic charges are used to enhance the filtration properties. However, this leads to further issues associated with discharge during use of the mask. Furthermore, there is still uncertainty regarding the specific lifetime of products during storage and use. During a pandemic crisis effective products are needed to provide protection against bio-particles (viruses, bacteria), however only a few products provide adequate protection against these pathogens [260]. For this purpose, some modified nonwovens such as those coated with antimicrobial agents may be used [266]. Similarly, functionalized nonwovens containing particles like silver and Titanium dioxide embedded into them have also been developed to provide protection from screened microbes [267]. However, the area can be explored further by using pristine and functionalized nanofibrous nonwoven filters that are expected to offer better performance due to their higher surface area.

For applications like respiratory protection, comfort aspects of the filter media should also be considered as they also affect the performance and even health of the wearer. Most important factors determining the comfort properties provided by such face masks are their thermal resistance, moisture management and air permeability [266, 268].

2.6.4.3 Electrospun fibrous filter media for respiratory protection

Electrospun PA-6 nanowebs offer large surface area, finer pores sizes, good interconnectivity between pores and the fibers with adequate uniformity. They have outstanding filtration properties and may be used for filtration of air born impurities [115, 243, 269-272]. They have been shown to have good filtration properties for particles as small as nanoparticles [273, 274]. Moreover, they can be functionalized for screening of specific agents [275]. They also exhibit better mechanical properties as compared to commercial air filters [71]. Based on these properties, nanofibrous filter media can be considered as suitable material for respiratory protection masks specially those for protection against particulate entities and they can be fine-tuned to provide better comfort properties. However, no known study has

focused on performance and comfort aspects and their balance for facemasks based on nanofibrous filter media.

2.7 Aims and Objectives

From the literature reviewed, it was found that only a limited work has been done in the field of statistical modeling and optimization of electrospinning process. Specially, for needleless electrospinning, the most feasible nanofiber bulk production technique, there has been no study on modeling and optimization. Thus, before focusing on the technical applications of electrospun material it would be significant to optimize their production process and properties. An optimized electrospun material, so obtained, could be expected to be reproducible and perform better for different application. In this study we defined the optimized nanoweb as one that is free of defects and has maximum possible uniformity.

Energy and healthcare could be two of the most important application areas for electrospun materials. Within these areas, the use of electrospun nanowebs for heat generation and respiratory protection (performance and comfort) have not been studied adequately and they still need to be explored. The objective of current work is to study both these areas after optimization of electrospun webs to be used for them. It aims to assess the possibility of using nanowebs for selected applications after optimization of their morphology. This will lead to reproducible results with opportunity to focus and optimize properties, other than morphology, in subsequent studies. The specific objectives to achieve this goal are:

- Study the needleless setups for production of different types of nanowebs and compare the results produced with needle electrospinning.
    - Modelling and optimization of electrospun webs with needle and needleless techniques, using pristine polymers. Polymers selected for the current work include PAN and PA-6, because of their interesting properties discussed in previous sections
    - Modelling and optimization of electrospun nanocomposite webs with needle and needleless techniques, using PAN/CNT composite selected for current work, as they are one of the most important materials for energy applications
    - Comparison of different statistical modelling tools on needle electrospinning for selection of a better tool for needleless electrospinning

    - Comparison of models developed on needleless electrospinning with those developed with needle electrospinning
    - Development of optimized nanowebs on needleless and needle electrospinning
- Characterize optimize nanowebs from needleless electrospinning
- Employ optimized nanowebs from needleless electrospinning for selected novel technical applications
    - Study of an innovative energy application for optimized electrospun PAN nanofibrous material. For current study the technical application selected is heat generation through PAN based carbon fibers and their composites (developed and optimized in current work). Initial evaluation, of PAN based carbon fibers and PAN/CNT composite fibers, for their possibility to generate heat will be studied.
    - Study of an innovative protective healthcare application for PA-6 nanowebs (developed and optimized in current work). The area selected for this purpose is respiratory protection.

Chapter 3 METHODOLOGY

Selection of proper materials and methods were carried in order to fulfil the objectives mentioned in previous section. For both the selected end uses, different polymers were chosen. They were converted into nanofibers using needle and needleless electrospinning setups according to planned experimental designs to get optimum settings and statistical models to predict the outputs.

This section specifies the materials used for the study, along with the methodology employed to develop and characterize the samples.

3.1 Materials

3.1.1 Polymer selection

Two technical applications were selected for this study i-e heat generation through conductive nanowebs and respiratory protection. For heat generation, PAN alone and its composite with CNTs was selected as fiber forming materials. The webs so formed were converted into CNFs and CNF/CNT composites. PAN was selected for this purpose as it is a well-known source of carbon fibers with high carbon yield. Moreover, it has excellent electrospinnability, ease of processing for surface modification and lower cost [62, 122, 126-130]. PA-6 was selected for respiratory protection basically because of good mechanical strength of its nanowebs and unique fineness of fibers. Other interesting properties include its formability, biodegradability and good biocompatibility [229]. Moreover, it has long been used for different “next to skin applications” and have shown very good compatibility with skin. It has also been studied and found to show encouraging results for a number of filtration applications [115, 243, 269-272]. From modelling point of view, two polymers and a composite, as mentioned above, with entirely different natures and properties were selected. This enabled to analyze electrospinning behavior of more than one material, through well planned statistical experimental designs, in order to assess the validity of these statistical tools for different materials. The properties of polymers employed for this study are mentioned in Table 3.

Table 3: Properties of polymers used in study

S.N.		PAN	PA-6
1	Form	Powder	Pellets (3 mm)
2	Molecular weight (g/mol)	150,000	10,000
3	Density at 25 ºC (g/ml)	1.184	1.084
4	Supplier	Sigma Aldrich, France	Sigma Aldrich, France

Based on solubility and electrospinning properties investigated in different studies, mentioned earlier, N,N dimethylformamide (DMF) was selected as solvent for PAN and formic acid (FA) for PA-6. The description of these solvents is summarized in Table 4. The properties of multi-walled CNTs for development of composite nanofibers are summarized in Table 5 [276].

Table 4: Description of solvents

S.N.	Property	DMF	FA
1	Molecular weight (g/mol)	73.09	46.02
2	Density (g/ml)	0.944	1.22
3	Purity (%)	99.8%	98%
4	Supplier	Sigma Aldrich, France	Sigma Aldrich, France

Table 5: Properties of MWCNTs employed in study

Internal diameter (nm)	External diameter (nm)	Length (µm)	Chemical contents (%)						
			C	Al	Fe	H	S	N	O
2-6	10-18	0.1-10	92.8	2.95	1.71	0.71	0.3	0.18	0.0

3.1.2 Solution preparation equipment

The equipment utilized for production of electrospinning solution include sonication bath, magnetic stirrers and high shear mixer (for PAN/CNT composite fibers). Description of these equipment is summarized in Table 6.

Table 6: Solution preparation equipment

S.N.	Equipment	Model	Manufacturer
1	Sonication bath	Elmasonic S30H	Elma Schmidbauer GmbH, Germany
2	Magnetic stirrer	FB15001	Fisher Scientific, France
3	High shear mixer	T 25D	IKA, Germany

3.1.3 Sample development equipment

For comparison between results and statistical modeling and optimization with different experimental setups, the samples were developed on two different types of machines i-e needle electrospinning and wire-electrode needleless electrospinning machine. This approach may also be employed to scale up the results obtained on lab setups to a larger semi-industrial format. Both systems are described in following sections.

3.1.3.1 Needle electrospinning machine

A lab developed vertical needle electrospinning machine was used to produce samples at smaller scale. As shown in Figure 31, the machine consisted of (1) a feeding pump, for pumping the solution into electrospinning needle at a predefined rate, (2) an electrospinning needle, (3) a collector for collection of fibers, (4) high voltage generator, for generation of required voltage, (5, 6) mechanisms for horizontal and vertical motion of needle. Description of these parts is summarized in Table 7.

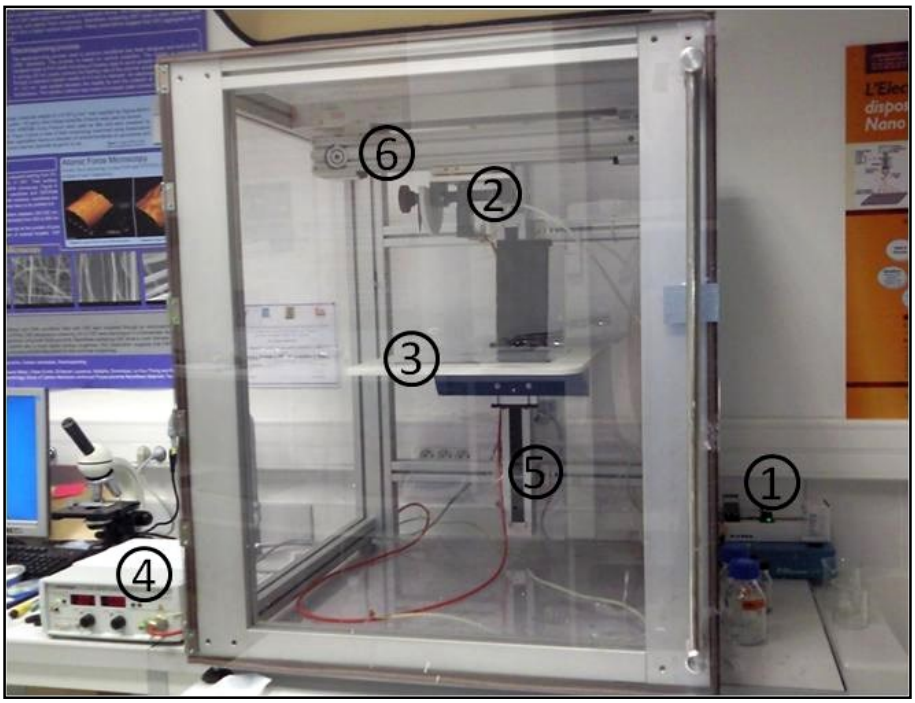

Figure 31: Needle electrospinning setup used for current study

Table 7: Description of different components of needle electrospinning setup

S.N.	Equipment	Specifications/ Model	Manufacturer
1	Solution flow pump	KD Scientific Legato 200 syringe pump	Delta Labo, France
2	High voltage generator	LNC 30 KV	Heinzinger, Germany
3	Electrospinning needles for PAN and PAN/CNT	30 mm length, 0.7 mm inner diameter, 22 gauge (bevel tip)	Terumo, Belgium
4	Electrospinning needle for PA-6	23 mm length, 0.45 mm inner diameter, 26 gauge (bevel tip)	Terumo, Belgium
5	Syringe for solution	20 mL, 2 cm inner diameter	BD Plastipak, USA
6	Nanofiber collector	Aluminum foil (thickness 0.016 mm)	Carlroth, France

3.1.3.2 Needleless electrospinning machine

Needless electrospinning machine used in this work was Elmarco's "Nanospider" (Model NS 1WS500U; Czech Republic), a wire electrode fibre generator needless electrospinning system (schematic diagram shown in Figure 4). It is based on "free surface technology" and produces nanofibers thanks to the potential difference between two wire electrodes. The polymer solution is coated on the lower wire electrode (positively charged; 0.2 mm diameter) through a solution carriage. The wire passes through an orifice (with 0.7 mm inner diameter for current work) in solution carriage that allows the solution to come in contact with wire. As the carriage moves, back and forth, on the wire, an even layer of polymer is coated on it. Under the action of electrostatic force, jets are produced on surface of wire and move towards upper wire. These jets are collected on a substrate in form of nanofibers. The substrate encounters the fibers before they reach the upper wire. The ambient conditions inside the electrospinning chamber can be controlled through the built-in system included in machine, which also maintains a proper air flow across the chamber.

3.1.3.3 Carbonization equipment

For carbonization of PAN and PAN/CNT nanowebs, two different types of ovens were employed. One of the them was used for stabilization in air and other for carbonization in nitrogen environment. Details of these ovens are mentioned in Table 8.

Table 8: Equipment used for stabilization and carbonization

S.N.	Purpose	Equipment	Model	Manufacturer
1	Stabilization	Muffle furnace	LE 14/11	Nabertherm, Germany
2	Carbonization	Tube furnace	RS 170/750/11	Nabertherm, Germany

3.1.4 Characterization equipment

PAN and PAN/CNT nanowebs were observed for their morphology, fiber structure, and alignment of CNTs, thermal degradation, electrical and thermal conductivity, and heat generation. Whereas, PA-6 nanowebs were observed for morphology and PA-6 nanoweb embedded multilayer filter for respiratory protection was evaluated for filtration efficiency, pressure drop across its faces and comfort properties. The equipment used for characterization of these structures is summarized in Table 9.

Table 9: Characterization equipment used in study

S.N.	Equipment	Model	Manufacturer	Property
1	Scanning electron microscope	S-2360N	Hitachi, Japan	Morphology
2	Transmission electron microscope	ARM-200F	JEOL, USA	Fiber structure and CNT alignment
3	Thermogravimetric analyzer	TGA Q500 V20.10 Build 36	Universal TA Instruments	Thermal degradation
4	Homemade Standard guarded electrode	----	----	Electrical conductivity
5	Homemade bridge tester	----	----	Electrical conductivity and heat generation
6	Homemade plaster heating plate	----	----	
7	Ohm meter	115 RMS	Fluke Europe, Netherlands	
8	Tera-ohm meter	H 12	Knick Tera-Ohm, France	
9	Wattmeter	F1WATT	Francais d'instrumentation, France	
10	Thermal imaging camera	Thermascan SC3000	FLIR, France	

11	High voltage converter	ALT 13A	Langlois, France	
12	Filter measuring device with filter holder	FMP 03 and FH-143/149	Lorenz Messgerätebau GmbH & Co. KG	Filtration efficiency
13	Air permeability tester	M021A	SDL Atlas, UK	Air permeability
14	Thermo Labo II	KES-F7	Kawabata Evaluation System, Japan	Thermal resistance
15	Compression tester	KES-FB3	Kawabata Evaluation System, Japan	Thickness
16	Moisture management tester	M290	SDL Atlas, UK	Liquid moisture management

As mentioned in Table 9, for determination of electrical conductivity, we designed a standard guarded electrode. The schematic diagram of this homemade standard guarded electrode is shown in Figure 32. It consisted of a guarded electrode surrounded by circular electrode B and an electrode A opposite to guarded electrode. This arrangement allows to control the error in measurements due to electric fringing at edges of normal plate electrodes, thanks to the guard electrode [277].

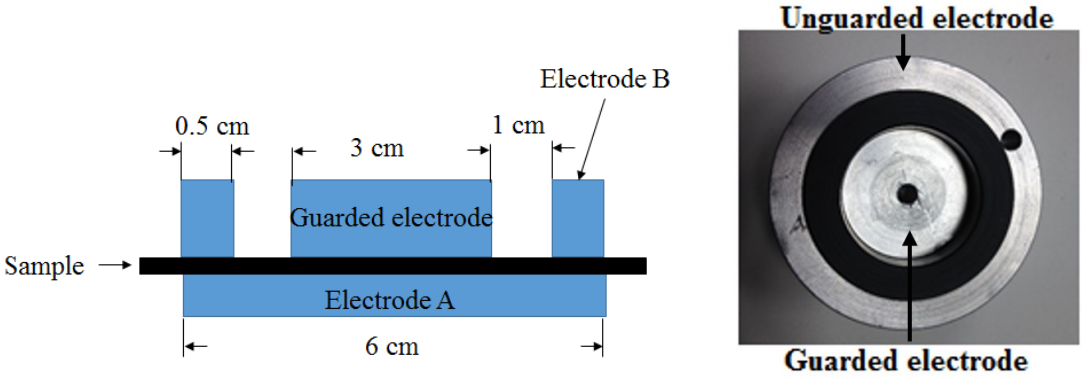

Figure 32: Schematic (left) and actual (right) image of electrode developed for measuring surface and volume resistance of webs

The home made "bridge tester" consisted of two jaw electrodes (for holding the sample) kept at a distance of 2 cm. Schematic representation and developed form of this tester, meant for measuring conductivity of webs and heat generated by them, is shown in Figure 33.

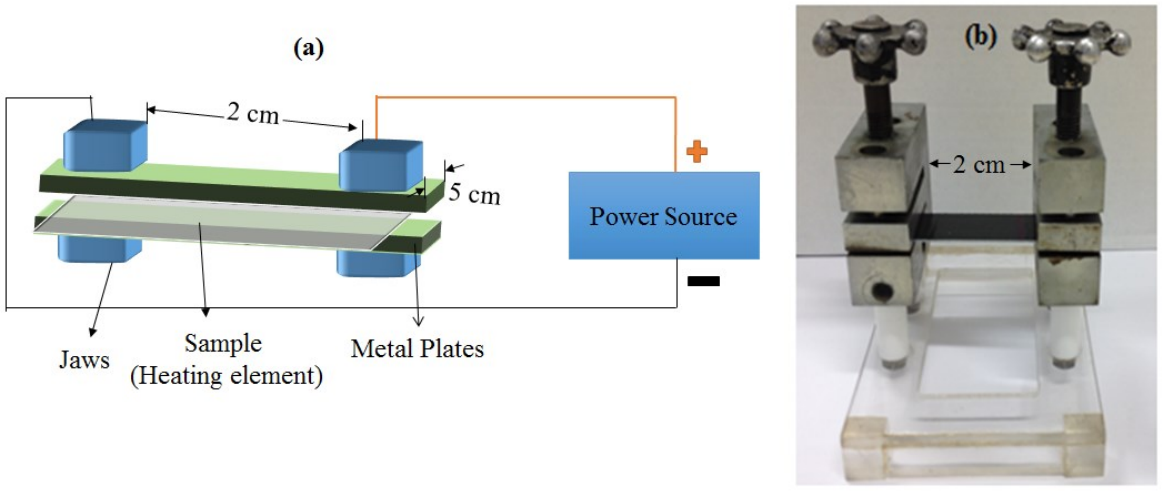

Figure 33: (a) Schematic representation of homemade bridge tester and (b) its lab developed version

Similarly, for heat generation tests, heating plates made of "Plaster of Paris" were developed. These plates contained two embedded electrodes to which the nanowebs were connected for generation of heat and evaluation of their electrical conductivity in this particular arrangement. The schematic representation and picture of actual plates developed according to that scheme are shown in Figure 34.

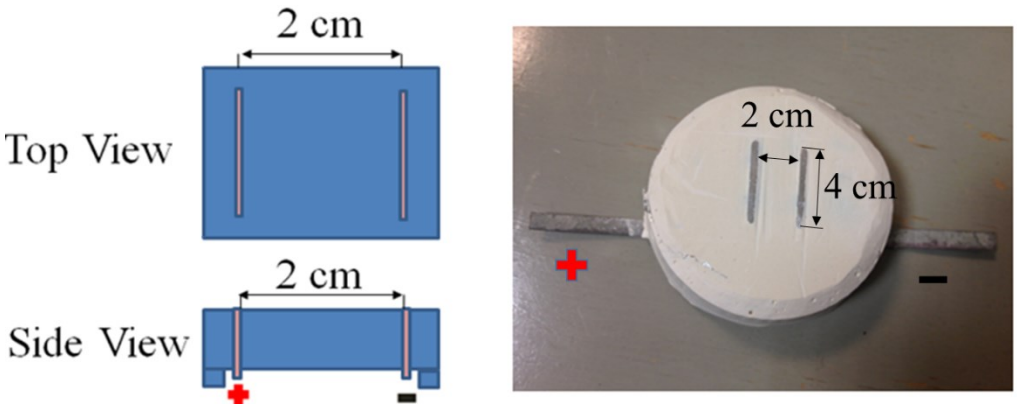

Figure 34: Schematic representation (left) and developed form (right) of heating plate

3.2 Methods

3.2.1 Sample production

For development of electrospun nanowebs, the solutions were made using the procedure mentioned in following sections. These solutions were electrospun according to

defined experimental design and the samples so produced were characterized to find the optimized settings and, subsequently, develop optimized nanowebs.

3.2.1.1 Solution preparation

3.2.1.1.1 PAN

PAN solutions were produced by dissolving the required weight of PAN as per DOE in DMF, followed by stirring on a magnetic stirrer for 24 hours at 70 ºC. The quantity of PAN to be dissolved in DMF was based on weight percentage of solution. A sample calculation for making 6 wt. % PAN solution in 30 mL DMF is shown below;

Mass of DMF = Density x Volume = 0.944 g/mL x 30 mL = 28.32 g

$$\text{Mass of PAN} = \frac{\text{Mass of DMF x weight percent of PAN}}{\text{Weight percent of DMF}}$$

$$\text{Mass of PAN (g)} = \frac{28.32 \text{ x } 6}{94} = 1.81 \text{ g}$$

According to this calculation, 1.81 g of PAN was dissolved in 30 mL of DMF and stirred for required time, resulting in 6% PAN/DMF solution.

3.2.1.1.2 PAN/CNT

Solutions for development of PAN/CNT composite nanofibers were produced based on CNT % in the fibers. For example, for 3% CNT in final dried fibers, PAN content will be 97%. For a 5% PAN solution, the calculation is mentioned below;

5% PAN in solution = 97% PAN in fibers

$$\text{CNT content in solution} = \frac{\text{CNT \% in fibers x PAN \% in solution}}{\text{PAN \% in fiber}}$$

For current situation,

$$\text{CNT \% in solution} = \frac{3\% \text{ x } 5\%}{97\%} = 0.155\%$$

Total percentage of PAN and CNT in solution = 5% + 0.155% = 5.155%

Percentage of DMF in solution = 100% - 5.155% = 95.845%

Mass of DMF = Density x Volume = 0.944 g/mL x 30 mL = 28.32 g

$$\text{Mass of PAN} = \frac{\text{Mass of DMF x weight percent of PAN}}{\text{Weight percent of DMF}}$$

$$\text{Mass of PAN (g)} = \frac{28.32 \text{ x } 5}{94.84} = 1.493 \text{ g}$$

$$\text{Mass of CNTs (g)} = \frac{28.32 \text{ x } 0.155}{94.84} = 0.0462 \text{ g}$$

For preparation of this solution, CNTs were first dispersed in DMF using high shear mixer and sonication. High shear mixing was carried out at 18000 rpm for 30 minutes, with aim to breakdown the larger CNT aggregates. Sonication was performed for 30 minutes at 37 KHz and 50 ºC. After sonication, PAN was added and stirred on magnetic stirrer at 100 rpm and 70 ºC for 24 hours. This methodology has already been evaluated and found to perform well in one of the studied carried out by our research group [278]. The solution so obtained was used for electrospinning.

3.2.1.1.3 PA-6

PA-6 was dissolved in the same manner as used for Pristine PAN. PA-6 pallets in formic acid were stirred using a magnetic stirrer at 100 rpm and 50 ºC for 24 hours. The resulting solution was used, as it was, for electrospinning.

3.2.1.2 Electrospinning of samples

For production of samples on needle and needleless electrospinning machine, different DOEs were employed. On needle machine mostly full factorial (FF) designs were used. While, for needleless machine DOEs with lower number of experimental runs were used (Response surface (RS) and Taguchi). However, to evaluate these shorter DOEs for their usability for nanowebs, they were also performed on needle electrospinning machine. So, for needle electrospinning machine, full factorial DOEs were run along with the one used for same material on needleless machines. The details of experimental design and parameters selected for each of the solutions are summarized in Table 10 and discussed in following sections.

Table 10: Summary of experimental designs and input variables along with their levels

Material	ES Mechanism	DOE	Runs	Inputs	Levels
PAN	Needle based	FF	27	PAN Concentration (wt. %)	9, 11.5, 14
				Distance (cm)	15, 20, 25
				Voltage (KV)	10, 12, 14
		RS (CCD)	20	PAN Concentration (wt. %)	9, 11.5, 14
				Distance (cm)	15, 20, 25
				Voltage (KV)	10, 12, 14
	Needleless	RS (CCD)	20	PAN Concentration (wt. %)	5, 7, 9
				Distance (cm)	15, 20, 25
				Voltage (KV)	30,35,40
PAN/CNT	Needle based	FF	27	CNT Loading (wt. %) (10% PAN solution)	3, 5, 7
				Voltage (KV)	10, 11.5, 13
				Time (min)	90, 120, 150
		RS (CCD)	20	CNT Loading (wt. %) (10% PAN solution)	3, 5, 7
				Voltage (KV)	10, 11.5, 13
				Time (min)	90, 120, 150
	Needleless	RS (CCD)	20	PAN Concentration (wt. %)	5, 6, 7
				Voltage (KV)	30, 35, 40
				Distance (cm)	15, 20, 25
		RS (CCD)	20	CNT Loading (wt. %)	3, 5, 7
				Voltage (KV)	30, 35, 40
				Distance (cm)	21, 25, 29
PA-6	Needle based	FF	27	PA-6 Concentration (wt. %)	17, 20, 23
				Voltage (KV)	22, 26, 30
				Distance (cm)	15, 20, 25
		Taguchi	9	PA-6 Concentration (wt. %)	17, 20, 23
				Voltage (KV)	22, 26, 30
				Distance (cm)	15, 20, 25
	Needleless	Taguchi	27	PA-6 Concentration (wt. %)	18, 19, 20
				Voltage (KV)	35, 45, 55
				Distance (cm)	26, 27.5, 29
				Carrier speed (mm/s)	290, 340, 390
				Substrate speed (mm/s)	15, 20, 25
				Air flow (m3/hr.)	120, 130, 140

The parameters and levels selected for this DOE were based on some pre-experimental trials and previous studies in the field. This study consisted of a total of 240 electrospun samples with almost 900 SEM images.

3.2.1.2.2 Needle electrospinning

Polymer solution was filled in the 20 mL syringe, and subsequently mounted on syringe pump, which was set to run at a solution flow rate of 0.2 mL/hr for PAN and PAN/CNT, while 0.1 mL/hr for PA-6. The needle was connected to the positive terminal of power supply and solution was fed from pump to needle through a Teflon tube. Other process parameters were set as per DOE and each sample was run for 10 minutes (unless specified in DOE). Application of voltage resulted in nanofibers that were collected on aluminum foil. However, the thicker webs (produced at optimized settings for developing heating plates) were collected on Teflon plates to remove them conveniently. The humidity and temperature (R.H. 22% ± 2% and 22 ± 2 ºC) were controlled by controlling the conditions of the room by an electronic conditioning system. In one of the previous studies of our research group, these conditions have been found to encourage the presence of CNTs on surface of PAN/CNT composite nanofibers [278]. So, they were adopted for all the samples produced in this work. DOE along with results is tabulated and discussed in next chapter.

3.2.1.2.3 Needleless electrospinning

The needleless setup employed for current work was different from the needle set up in terms that the fiber generator in it was a wire electrode, coated with polymer solution. Moreover, the direction of spinning was upward, as opposed to needle setup, where it was in downward direction. Thirdly, it had some additional parameters like speed of carriage, speed of movement of substrate, speed of movement of wire electrode (which was set in constant motion to replenish the electrospinning surface) and air flow (not present in needle setup used in current study). So, values of these parameters also needed to be defined, other than those of the basic variables i-e concentration, electrospinning distance and applied voltage.

The polymer solution was filled in reservoir of solution carrier, shown in Figure 35. The wire electrode (stainless steel 0.2 mm diameter) was passed through the orifice (0.7 mm) of the carrier, after mounting it on its support in electrospinning chamber. The wire electrode was moved at a very slow speed of 0.5 mm/s in order to replenish the electrospinning surface,

as the polymer forms a solid film over it. The carrier was moved on wire at 200±5 mm/hr., substrate was moved at 15 mm/min, while air flow into the chamber was 80 m^3/hr. and out of it was 130 m^3/hr. Humidity and temperature were kept constant as for needle electrospinning by controlling the conditions of room. However, in some of the experiments these parameters were varied, wherein the respective values are given in DOE or mentioned in discussion. All process variables under study were set as per DOE. The fibers, so obtained were collected for further analysis and characterization.

PAN and PAN/CNT fibers were, initially, collected on aluminum foil while their optimized samples were collected on Teflon coated paper (by applying a negative voltage of -5 KV at upper electrode wire, in order to compensate the insulation effect produced by Teflon sheet instead of aluminum foil) to remove them conveniently for heat generation application.

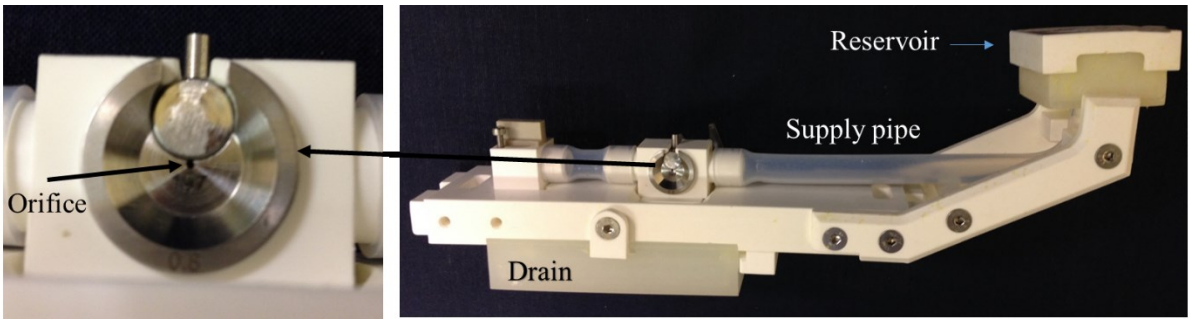

Figure 35: Solution carrier used for coating of electrospinning wire electrode fiber generator

For PA-6 the fibers were collected on nonwoven spun bond media (media 1; 35 g/m^2) and subsequently covered by nonwoven melt blown media (media 2; 38 g/m²) and then by nonwoven spun bond media (media 3; 12.5 g/m²) for evaluation of performance and comfort properties. Similar layered filter structures, (schematically, presented in Figure 36), with some variations, is already being used for production of FFP2 face masks. For current study, the exact material was provided by the project partner, Honeywell.

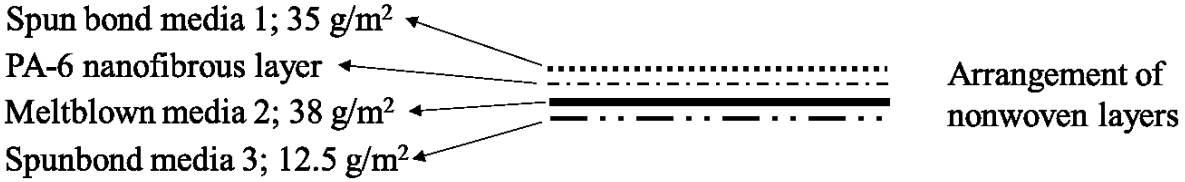

Figure 36: Components of composite filter for face mask and their arrangement

3.2.1.3 Carbonization of PAN and PAN/CNT composites nanowebs

For heat generation, the optimized PAN and PAN/CNT nanowebs were carbonized for converting them to conductive carbon nanofibers. Carbonization was preceded by stabilization process to stabilize the webs by heating them at 300 ºC in air, as shown in process profile in Figure 37. During stabilization, the webs were clamped at edges by square frames (shown in Figure 38) to avoid shrinkage and weight loss due to evolution of gases by heat treatment. After stabilization, the samples were carbonized at 1000 ºC in nitrogen environment. For both these processes, the rate of increase of temperatures was kept at 5 ºC/min, in order to avoid excessive weight loss in short time and to allow the reactions to complete, as discussed in previous chapter.

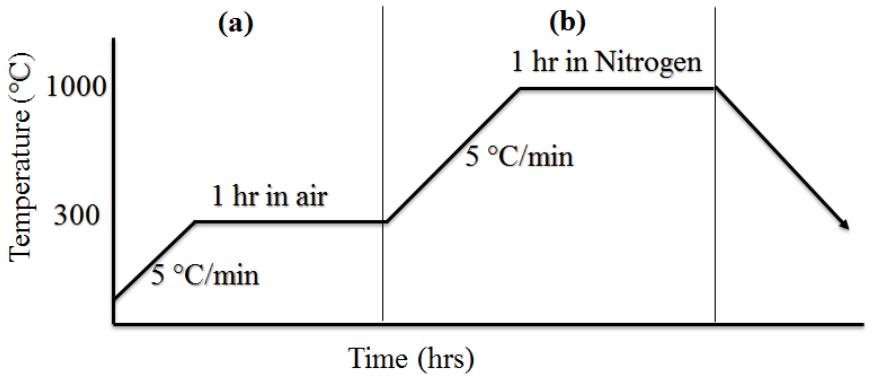

Figure 37: Process profile for (a) stabilization and (b) carbonization of PAN and PAN/CNT nanowebs

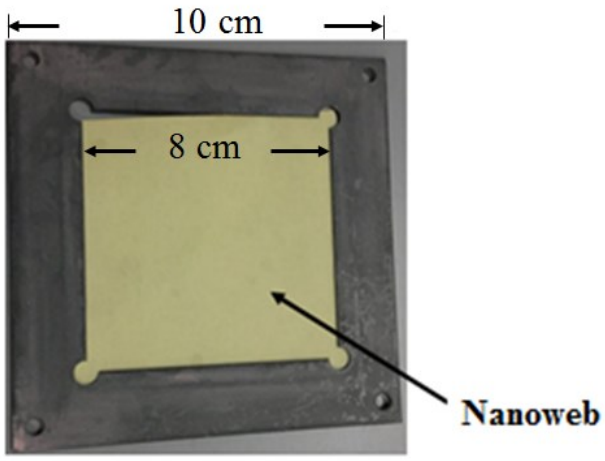

Figure 38: Stainless steel frame with stabilized nanoweb mounted on it

Based on the fact that stabilization under mechanical pressure increases the conductivity of carbon fibers due to better interfacial contact with polymer matrix [148], it was tried to stabilize the optimized PAN nanowebs in a hot press at 250 ºC, at pressure of 5 and 20 bar for 1 and 2 hours. However, it was concluded that webs stabilized under these conditions were not detachable from the support in which they were sandwiched (as shown in Figure 39). So, the process was not utilized for this study. However, more work in this direction can lead to nanowebs with improved properties.

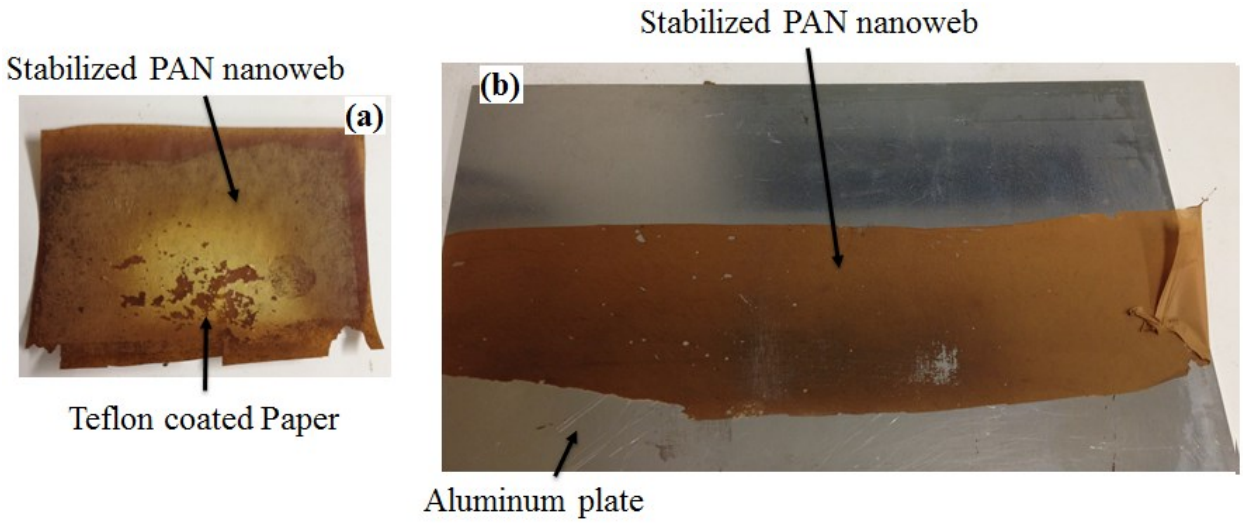

Figure 39: PAN nanowebs stabilized in hot press (at 5 bar pressure for 1 hr.) by sandwiching in (a) Teflon coated paper and (b) Aluminum plates

3.2.2 Characterization

Nanowebs, obtained after electrospinning, were analyzed for many structural and performance properties. Brief description of different tools used for this purpose is given in following sections.

3.2.2.1 Morphology

The morphology of nanowebs was analyzed using scanning electron microscopy (SEM), for which the samples were gold coated to make them conductive. These samples were then observed in SEM to obtain images at different magnifications. For each sample, five images were taken with at least three at same magnification from different locations for measurement of diameter, using “Image J” software [279]. For each sample, diameter of 50 different fibers were measured, avoiding the places having visual defects. From the results

obtained, the mean diameter and its standard deviation was calculated for further statistical analysis.

3.2.2.2 Nanofiber internal structure

To observe the arrangement of CNTS and crystalline regions inside the fibers, transmission electron microscopy (TEM) was utilized. To accomplish this, the samples were first dispersed in chloroform using ultrasonication for 30 minutes. A drop from this dispersion was dispensed on metallic grid for TEM in such a way to get individual fibers, separated from others. These fibers were then observed in TEM at 200KV with different magnifications to obtain the internal as well as surface structure of nanofibers and the crystalline regions in them.

3.2.2.3 Electrical and thermal conductivity

The ability of nanowebs to conduct electric charge was assessed by using three different types of systems, as discussed above. With guarded electrode shown in Figure 32, both surface and volume conductivity was evaluated at 10, 100 and 500 volts and electrification time of 2 minutes, using the standard testing procedure ASTM 257-61. Surface conductivity was measured by placing the samples between the guarded electrode (surrounded by electrode B) and electrode A, in such a way that guarded electrode and electrode A were connected to same terminal, while, electrode B was connected to opposite terminal. With this arrangement, electrode A acted as guard electrode to control the fringing electric field and the system measured the surface conductivity of sample in the gap between guarded electrode and electrode B. For volume conductivity, guarded electrode and electrode B were connected to same terminal while electrode A was connected to opposite terminal, so electrode B acted as guard electrode. In this case the conductivity of the sample placed between guarded electrode and guard electrode was the volume conductivity.

As the webs were also to be used for heat generation using the home made “bridge tester” shown in Figure 33, so this tester was also used to measure the electrical conductivity before evaluation of heat generation capability. For this purpose, the samples (of size 7 cm × 2.5 cm), backed by a glass slide, were mounted in jaws of tester which were connected to terminals of power source and resistance was noted using an Ohm meter or Tera-Ohm meter, as needed. Similarly, electrical conductivity was also measured by measuring the resistance offered by the samples (of size 7 cm × 2.5 cm), placed across the terminals of heating plate

shown in Figure 34. For this purpose, the samples were covered by a glass slide. With both these later systems, the measurements were made at 10, 100 and 500 V.

Thermal conductivity of samples was evaluated with Kawabata Evaluation System using its "Thermo Labo" module [280, 281]. The samples were placed on water cooled plate (20 ºC) and were covered, at the top, with BT plate maintained at 30 ºC. The heat transferred across the sample was measured in Watts and was converted to conductivity by using formula shown in Equation (14). Thickness of specimens were also measured by using the compression analysis module of the same system.

$$\text{Thermal conductivity } \left(\frac{\text{Watt}}{\text{cm.}^{\circ}\text{C}}\right) = \frac{\text{Heat transmitted (Watts)} \times \text{Sample thickness (cm)}}{\text{Sample Area (sq.cm)} \times \text{Temperature difference } (^{\circ}\text{C})}$$

Equation (14)

3.2.2.4 Thermal stability

To evaluate the thermal stability of PAN and PAN/CNT nanowebs, thermogravimetric analysis (TGA) was performed. For this purpose, samples (10 mg) were analyzed up to 800 ºC (achieved at 10 ºC/min) with nitrogen flow of 60 mL/min.

3.2.2.5 Heat generation

Heat generation capability of carbonized PAN and PAN/CNT nanowebs was assessed using the bridge tester shown in Figure 33 and the plaster plate shown in Figure 34. With bridge tester the samples were mounted between the jaws, as done for electrical conductivity. A voltage of 10 V was applied for 5 minutes and the increase in temperature was noted through a thermal imaging camera. Similarly, for plaster heating plate, the samples were placed over its electrodes and covered by a glass slide to secure it and to apply a minimal pressure for developing its contact with electrodes. A potential difference of 10 V was applied, as for bridge tester, and increase in temperature was noted through the thermal imaging camera, set to measure between 20 ºC and 50 ºC.

3.2.2.6 Filtration efficiency as respiratory protector

Face mask filters developed by coating of PA-6 nanofibers sandwiched between nonwoven layers was assessed by using the standard testing procedure EN 149+A1:2009. For

this purpose, samples were, first, molded to take the half sphere shape as shown in Figure 40. For evaluation of filtration efficiency of masks' media, their capability to filter out paraffin aerosol was assessed. The aerosol was generated by spraying paraffin and was passed through the filter. Its concentration before and after filtration was evaluated by light scattering aerosol photometer. The difference between the two was used to calculate the filtration efficiency (Annex I). The assessment was made after 3 minutes (instantaneous testing) and 60 minutes (load testing) to evaluate the performance at initial stages of exposure and after the filter became saturated with paraffin.

Figure 40: Molded filters developed from PA-6 nanofibers sandwiched between nonwoven layers

For evaluation of respiratory resistance, compressed air at different rates (30 L/min and 95 L/min for inhalation; 160 L/min and 85 L/min at exhalation) was passed through the filters and pressure drop was assessed using a pressure sensor.

3.2.2.7 Moisture vapor and air permeability

The ability of the PA-6 nanoweb incorporated filters to permeate moisture vapors across their thickness was assessed by using the standard method ASTM E96-1995. The samples were sealed to the open mouth of plastic cups having an area of 38.5 cm^2 and filled with 210 g of water. Under the standard atmospheric conditions, the rate of loss of water vapors through the samples was assessed by measuring the decrease in weight of water after 264 hours.

Air permeability of samples was evaluated by using the standard testing procedure ASTM D737. For this purpose, pressurized air was passed, perpendicularly, through an area of 38 cm^2 of specimen submitted for testing. The air flow was adjusted, automatically, by the equipment to achieve a pre-set pressure differential of 125 Pa across the two surfaces of samples. From value of air flow, air permeability was obtained.

3.2.2.8 Liquid moisture management

Moisture management properties of PA-6 nanofibers incorporated multilayer filter was evaluated using Moisture management tester, according to the standard testing procedure AATCC 195-2012. The samples were placed between circular heads of the tester having concentric circles of conductive pin sensors. A drop of water, with pre-defined conductivity, was put in center of the sample. As it moved along the surface of two faces and across the thickness of specimen, the conductive pins sensed it through its conductivity. This allowed to determine the wetting time, wetted radius, absorption rate and speed of spreading of moisture along sample's top (that is meant to touch the skin; spunbond media 3 in current study) and bottom surfaces.

3.2.3 Statistical analysis

As already mentioned in Table 10, the experiments for current study were designed using full factorial, response surface and Taguchi methodology, through statistical analysis software "Minitab 16". The results obtained were analyzed by the same tool. To accomplish this, ANOVA was performed to evaluate significance of different parameters. Those with P-value less than 0.05 were considered significant. This meant that the "null hypothesis", that a parameter does not impact the output, has probability of less than 5%. From ANOVA, the significant factors were sorted out to develop a regression model, whose significance was determined by its R-sq value, which determines whether the variation in actual output data is explained by the model or not. The effects of each of the significant input variables was elucidated, graphically, by using "Main effect plots" and "Surface plots" (Annex I). Main effect plots are normally drawn for the cases where linear effect of individual factors are significant i-e no interaction (square or product of factors) between the factors is significant. For models involving interactions, Surface plots were used.

Chapter 4 RESULTS AND DISCUSSION

Current section focusses on results obtained from experiments performed according to the methodology described in previous chapter. It will include the optimization and modelling, performed to achieve optimized electrospun nanowebs. Moreover, study on properties of nanowebs using different characterization techniques are discussed and, finally, possibility to employ the optimized nanowebs for both the selected applications, i-e heat generation and respiratory protection is described.

4.1 Optimization and modelling of electrospinning process for PAN nanofibers

To achieve the goal of modeling the electrospinning process and developing optimized nanowebs, different statistical tools were utilized. Following sections will discuss the optimization and modelling of electrospinning process for PAN nanofibers using needle and needless electrospinning mechanisms. For needle electrospinning, both full factorial and response surface designs will be deliberated, in order to understand the relationships between inputs and outputs, and to define a better experimental technique for electrospinning process. For needless setup, only response surface design will be studied because it covers more complex relationships between input and outputs (such as those governed by second degree equations) along with simpler relations and it has lower number of runs that make it more feasible for bulk scale setups.

4.1.1 PAN nanofibers from needle electrospinning

4.1.1.1 Statistical analysis using full factorial experimental design

For modelling and optimization, of needle electrospinning, using full factorial design, three input parameters were considered i-e concentration (C) of polymer solution, needle to collector distance (D) and applied voltage (V). The selection of these parameters was based on their stronger impact on morphology of nanofibers, as discussed in some previous studies [19-23, 43-45, 66]. The values for these parameters were governed by the experimental design shown in Table 11, which also gives the respective values of outputs i-e nanofiber diameter

(Dia.) and its distribution (St. Dev.). All other parameters were kept constant (as mentioned in previous chapter).

Table 11: Full factorial DOE for electrospinning of PAN nanofibers on needle electrospinning setup with resulting diameter and its distribution

S.N.	C (w/w %)	D (cm)	V (KV)	Dia. (nm)	St. Dev. in Dia. (nm)
1	9	15	10	285	43
2	9	15	12	261	23
3	9	15	14	321	54
4	9	20	10	372	56
5	9	20	12	330	64
6	9	20	14	280	70
7	9	25	10	338	74
8	9	25	12	318	53
9	9	25	14	309	53
10	11.5	15	10	763	184
11	11.5	15	12	760	193
12	11.5	15	14	559	194
13	11.5	20	10	802	132
14	11.5	20	12	732	120
15	11.5	20	14	747	353
16	11.5	25	10	858	134
17	11.5	25	12	754	122
18	11.5	25	14	757	112
19	14	15	10	1814	386
20	14	15	12	2388	402
21	14	15	14	1217	874
22	14	20	10	1549	184
23	14	20	12	1701	290
24	14	20	14	2401	711
25	14	25	10	1942	448
26	14	25	12	1618	192
27	14	25	14	2121	272

As it is evident from Table 11, the diameter for PAN nanofibers, within the selected DOE, ranged between 261 nm to 2400 nm, with standard deviation between 23 nm to 874 nm.

To determine the significance of effect of input parameters on outputs, the ANOVA of data was performed and is summarized in Table 12.

Table 12: ANOVA for full factorial design for effect of inputs on diameter and its distribution

S.N.	Term	P-value for Dia.	P-value for St. Dev. in Dia.
1	C	0.000	0.000
2	D	0.871	0.216
3	V	0.992	0.059
4	C×D	1.000	0.338
5	C×V	0.954	0.180
6	D×V	0.398	0.216

P-value in ANOVA determines the significance of impact of an input variable on an output. P-values below 0.05 indicate a significant impact with possibility of error of only 5% i-e with 95% confidence. It is clear from Table 12 that only concentration poses a significant impact on diameter, while for distribution of diameter, effect of voltage can also be considered significant with confidence interval (Annex I) of 95%. These effects have also been confirmed by some previous studies [19-23]. From P-values, it can be deduced that only concentration poses a significant impact on diameter of PAN nanofibers.

Moreover, the significance of effects may also be observed by main effect plots in Figure 41, which shows that solution concentration poses a much stronger impact, in terms of magnitude, as compared to other factors. Higher concentrations were found to increase the fiber diameter and its distribution.

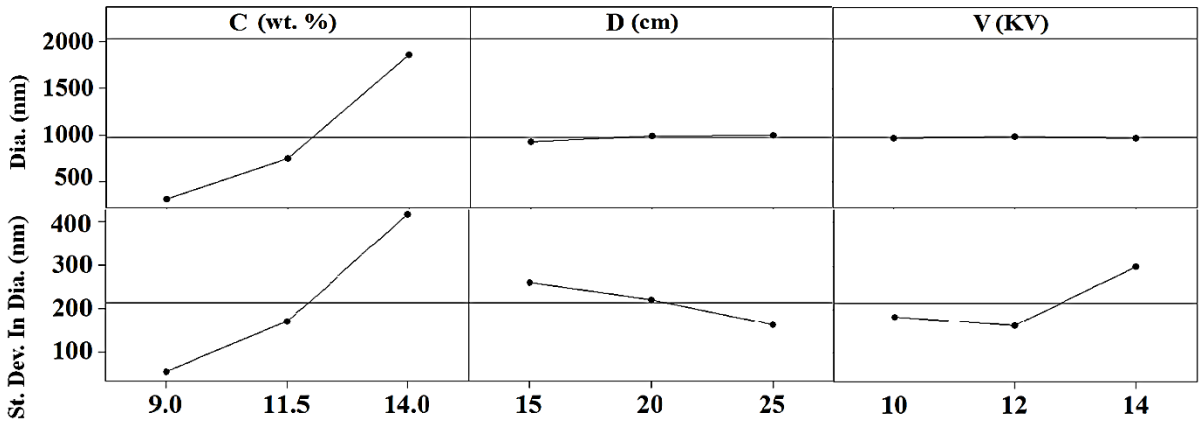

Figure 41: Main effect plots for effect of input parameters on diameter and its distribution

This fact has also been discussed in some previous studies [21, 48] as well and is also depicted in Figure 42.

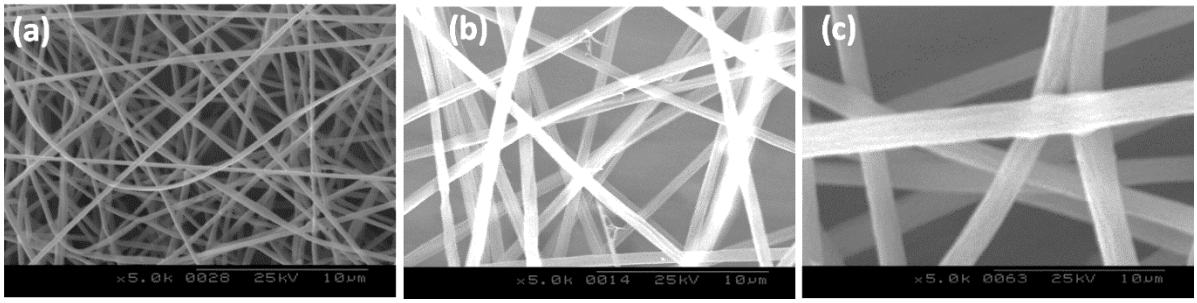

Figure 42: SEM images at (a) 9%, (b) 11.5% and (c) 14% at needle to collector distance of 20 cm and applied voltage of 12 KV (5 K i-e 5000 times, 25 KV)

As discussed in 2.2.1.1, it could be attributed to higher chain entanglement at higher concentrations, thus leading to lower stretching of polymer jet and, hence, fibers with higher diameter were produced. The effect of needle to collector distance and applied voltage, in comparison to that of concentration, is almost negligible. This is also in line with previous studies in this domain [19-23]. The effect of these factors may be magnified by considering them at constant concentration. Meanwhile, higher needle-collector distance was found to decrease the distribution of diameter. This is consistent with the fact that higher distance leads to higher stretching time [64], resulting in greater stretching uniformity in fibers.

4.1.1.2 Statistical analysis using response surface experimental design

To study the response surface experimental design and its significance for electrospinning process, the same input and output variables and their levels were selected as chosen for full factorial design. The DOE, along with resulting values of outcomes, is summarized in Table 13. It may be noted that response surface design has added some levels above and below the limits provided to it. This allows to study any second degree interactions, if present. The diameter and its standard deviation, for response surface DOE, ranged between 284 nm - 2121 nm and 42 nm – 874 nm, respectively.

Table 13: Response surface DOE for needle electrospinning of PAN nanofibers with resulting diameter and its distribution

S.N.	C (w/w %)	D (cm)	V (KV)	Dia. (nm)	St. Dev. in Dia. (nm)
1	9	15	10	285	43
2	14	15	10	1814	386
3	9	25	10	338	74
4	14	25	10	1942	448
5	9	15	14	321	54
6	14	15	14	1217	874
7	9	25	14	309	53
8	14	25	14	2121	279
9	7.3	20	12	310	71
10	15.7	20	12	2059	342
11	11.5	11.6	12	743	295
12	11.5	28.4	12	717	182
13	11.5	20	8.3	852	167
14	11.5	20	16.7	663	127
15	11.5	20	12	732	120
16	11.5	20	12	721	124
17	11.5	20	12	735	125
18	11.5	20	12	728	121
19	11.5	20	12	731	131
20	11.5	20	12	731	122

To determine the significance of input parameters, ANOVA was performed and is summarized in Table 14. It is important to note that there are terms that contain square of other terms such as “C×C” is square of concentration. These terms appear in ANOVA because of inclusion of some central points in response surface design that are meant to study second degree interactions, which are not considered in full factorial designs [74]. As with full factorial design, only concentration affects the outputs in a significant manner. However, the effect of product of distance with voltage may also be considered significant but at 93% confidence interval, so it may also be included in regression model.

Table 14: ANOVA for response surface DOE for effect of inputs on diameter and its distribution

S.N.	Term	P-value for Dia.	P-value for St. Dev. in Dia.
1	C	0.000	0.001
2	D	0.176	0.154
3	V	0.274	0.743
4	C×C	0.005	0.200
5	D×D	0.540	0.116
6	V×V	0.538	0.734
7	C×D	0.097	0.130
8	C×V	0.449	0.375
9	D×V	0.218	0.072

The effect produced by input parameters on both the outputs can be visualized by surface plots (defined in Annex I) in Figure 43, which show combined effects of two of the input variables on outputs, while keeping the third input on "hold" at a specific value.

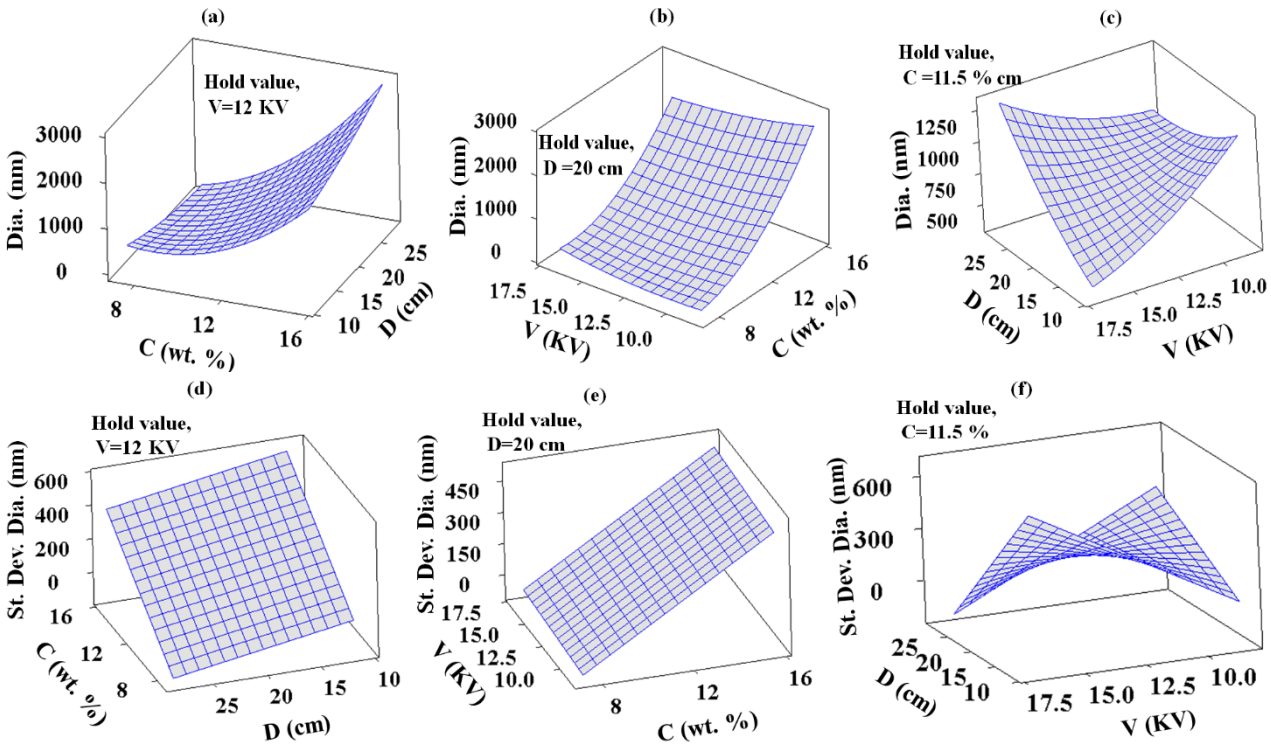

Figure 43: Surface plot (a,b,c) for effect of inputs on diameter and (c,d,e) its distribution

Moreover, these plots allow to determine effect of one variable at all values of other variable thus allowing to visualize a second degree interaction, if present. For example in Figure 43, for plot (a) increasing concentration is shown to increase the diameter at all values of voltage, however, there is steeper increase in diameter at higher voltages, which could be attributed to lower stretching time for jet and higher solution take-up at such values of voltage, due to higher electrostatic force [9, 61].

Similarly, it can be observed from plot (a) and (b) that the effect of increase in voltage and distance is much lower, in terms of magnitude, as compared to that of concentration. However, as suggested earlier, these effects may be magnified by keeping concentration constant. These low magnitude effects, at constant concertation of 11.5%, are shown in plot (c), which shows a decrease in fiber diameter at lower distance, while an increase in it at higher distance, at higher values of voltage. This may be attributed to stronger electrostatic force drawing the jet to a finer diameter at lower distance [63]. Though, at higher distance the effect is opposite due to lower drawing electrostatic force because of large distance [63]. Secondly, at higher distance the electrostatic force is much weaker as compared to that at lower distance, while keeping the voltage constant. This suggests that a lower quantity of polymer solution is pulled out of needle in such conditions. The effect of distance at lower voltages is not very evident, while, at higher voltages, increasing the needle-collector distance increased the fiber diameter, may be due to decreased effect of electrostatic force on polymer jet. These interactions confirm that a second degree interaction is present in needle based electrospinning systems that may not be covered by simpler experimental methodologies such a full factorial designs.

Similarly, fiber diameter distribution is impacted by concentration, in a directly proportional manner. It can also be observed, from plot (d) and (e), that magnitude of impact of distance and voltage is much lesser than that of concentration. Plot (f), shows an increase in diameter distribution at lower distance and a decrease in it at higher distance, with increasing value of voltage. This interaction is quite significant at 93% confidence interval and may be explained as; at lower distance increasing voltage increases the electrostatic force on polymer jet, thus attracting a larger amount of solution, forming a thicker jet. However, due to smaller distance, this jet has little time to achieve uniformity in diameter, which is achieved much better at higher distance.

4.1.1.3 Optimization results and regression models for full factorial and response surface designs

An optimized electrospun web for most of applications can be considered as, one having fine fibers, with low fiber diameter distribution and free from defects such as beads, drops, ribbon like fibers and other similar imperfections in fiber morphology. All these aspects are affected by different electrospinning parameters and can be controlled by observing impact of these parameters on imperfections. The current study also focused on these parameters to obtain an optimized PAN nanoweb.

As confirmed in previous studies [50], it was observed that lower concentration resulted in beaded fibers. Whereas, higher concentrations increased the fiber diameter distribution. Similarly, higher voltage was found to produce fibers with solvent in them because of lower time for it to evaporate. On the other hand, lower voltage resulted in drops falling directly from needle. However, this was not, always, the case and it also depended on distance and concentration.

In terms of fineness of nanofibers, lower concentration was found to produced finer fibers. Similarly, they also produced the nanowebs with lowest diameter distribution. However, beaded samples for some of the runs with 9% PAN solution were observed, even though, a number of input settings produced defect-free fibers. While, considering the beads, drops and other defects, apart from diameter and its distribution, higher concentration produced better nanowebs with lower defects but larger diameter and its distribution [9, 52, 53].

Based on these observations, three samples were selected amongst those shown in Table 11 and Table 13 (one from each concentration level) that were free of defects, having lowest diameter distribution within their respective concentration range. These samples may be considered as optimized nanowebs, for applications aimed in this work, within their own concentration level. SEM images of these samples are shown in Figure 44, depicting nanowebs with three different fiber diameters.

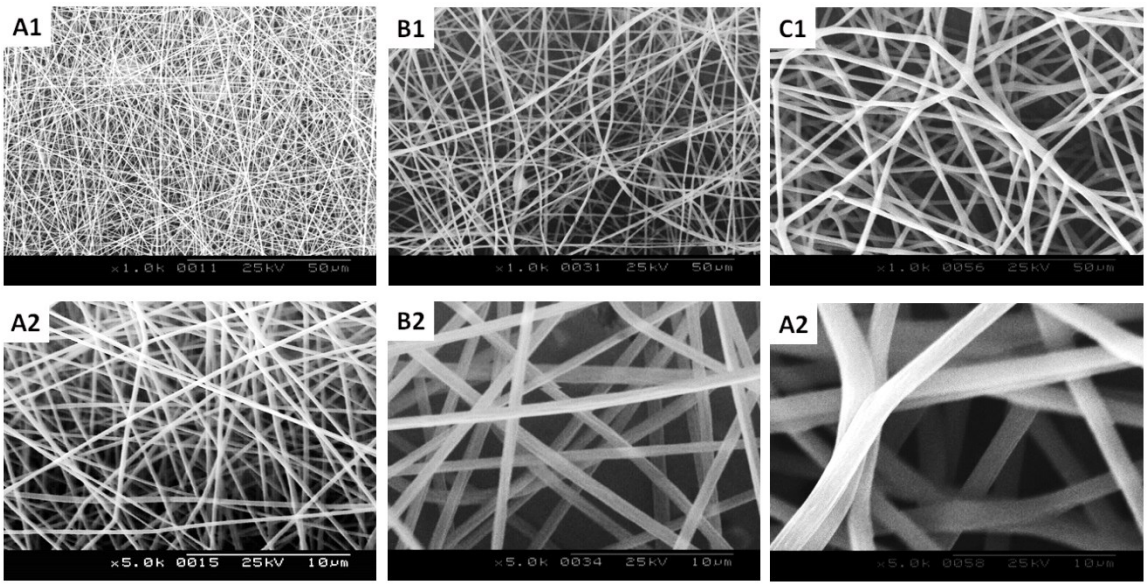

Figure 44: SEM micrographs of optimized samples with (A1, A2) 9% PAN, (B1, B2) 11.5 % PAN and (C1, C2) 14% PAN (Upper row at magnification of 1 K and lower at 5 K)

Samples in first column (A1 and A2) are for 9% concentration, needle to collector distance of 15 cm and voltage of 12 KV (with diameter of 261 nm and St. Dev. of 23 nm). Those in second column (B1 and B2) are for 11.5% PAN, needle to collector distance of 25 cm and voltage of 14 KV (with diameter of 757 nm and St. Dev. of 112 nm). While the last column (C1 and C2) represents nanowebs with 14% PAN, needle to collector distance of 20 cm and voltage of 10 KV (having diameter of 1549 nm and St. Dev. of 184 nm).

Furthermore, amongst the entire group of experiments performed, sample depicted in first column of Figure 44, may be considered as most optimized sample in current DOEs, as it fulfills the criteria of having fine fibers, with lowest diameter distribution and without any defects. So, we can conclude that even though, lower polymer concentration is known to produce beaded fibers, proper set of other important parameters may be selected to get optimized results, as obtained for the said sample by using low distance (15 cm) and medium voltage (12 KV)

The data, shown in Table 11 and Table 13, was also used to develop regression models for prediction of diameter and its distribution for needle electrospinning of PAN. The models obtained as a result of regression analysis are shown in Table 15. These models are valid only within the range of levels selected for each parameter.

Table 15: Regression model for diameter and its distribution for needle electrospinning of PAN nanofibers

S.N.	DOE	Regression model	R-sq
1	FF	Dia. = -2587.92 + 309.731 C	83.79%
2	FF	St. Dev. in Dia. = -971.178 + 72.603 C + 29.2342 V	55.83%
3	RS	Dia. = 1546.23 - 392.928 C + 28.3737 C^2	88.43%
4	RS	St. Dev. in Dia. = -2491.41+ 64.7471 C + 94.3108 D + 179.792 V - 8.71139 D×V	53.02%

For full factorial design, model for diameter contains only concentration because it is the only significant factor affecting diameter, as observed in ANOVA. R-sq for this model is quite high and shows that it can be considered a valid model for prediction of diameter of PAN nanofibers within selected range of levels. For St. Dev. in diameter, both concentration and voltage were found to show significant impacts, so they were employed to develop the model for it. However, R-sq for model is not very high and indicates presence of some noise parameters, affecting its value. These may include minor variations in environmental conditions or some experimental errors. Moreover, it also shows that controlling the fiber diameter distribution is, even, a more complex job and additional parameters should be studied to optimize it.

For response surface design, again only concentration was included in model for prediction of diameter, however, it important to note that square of concentration was also found to be significant and confirmed a second degree interaction. Though, the coefficient for it was much lesser than that of concentration, which confirms a small curvature. The addition of concentration-squared increased the R-sq of model by almost 5%, which reveals that addition of second degree terms can improve the validity of model, proving the importance of DOE methodologies like response surface DOEs. For St. Dev. in diameter, concentration was found significant (from ANOVA) along with product of distance and voltage. So, the model contained individual representation of distance and voltage. As for full factorial design, again, the R-sq is not very high, which shows that some noise parameters affect the distribution in diameter and should be identified and studied.

For validation of the models, 4 experimental runs were performed for each model and the values of diameter obtained from these experiments were compared with those predicted by model. The validation results are reported in Table 16.

Table 16: Validation of full factorial and response surface DOE for PAN nanofibers produced on needle electrospinning

DOE	C (%)	V (KV)	D (cm)	Actual		Predicted		Absolute error (Dia.)	Absolute error (St Dev.)
				Dia. (nm)	St. Dev. (nm)	Dia. (nm)	St. Dev. (nm)		
FF	11.5	11	18	800	256	974	185	174	71
	9	13	22	290	6	200	62	90	2
	14	11	24	1629	382	1748	367	120	15
	11.5	13	16	860	148	974	244	114	96
RS	11.5	11	18	800	256	780	204	20	53
	9	13	22	290	60	308	12	18	48
	14	11	24	1629	382	1606	356	22	26
	11.5	13	16	860	148	780	287	80	140

The difference between predicted and actual results (absolute error) gave an indication of validity of results. It can be observed that predictions for diameter were more valid for response surface design as they give lower absolute error. From magnitude of error, it can be deduced that models predicted by both the DOEs have good validity, as the absolute error can be considered to be in range of experimental error i-e within the standard deviation. For prediction of standard deviation, both the models gave almost similar result.

4.1.2 PAN nanofibers from needleless electrospinning

Needleless electrospinning setups are known for their higher output and have been devised for bulk scale production of nanofibers. The technique employed in current study, i-e wire electrode free surface needless electrospinning, is also meant for bulk production of nanofibers for different commercial applications. To study this technique, larger amount of material is required. So, extensive experimentation can lead to wastage of valuable material. Thus, this process needs to be optimized and modelled, in order to predict its behavior, and achieve the goals with less experimentation. For this purpose, response surface methodology fits quite well, as it generates lower number of runs. Moreover, it also covers the second degree interactions as discussed in section 4.1.1.

4.1.2.1 Statistical analysis using response surface experimental design

For subjected experimental design, same input parameters were selected, as selected for needle electrospinning. However, as the process works in different conditions, the levels of

inputs needed to be defined again. For this purpose, some pre-experimentation was performed to find the best concentration, which was varied between 5 and 13% at applied voltage of 30KV and wire to collector distance of 15 cm. From these experiments, the workable range was found to exist between 5% and 9% PAN. The voltage levels were varied between 30 KV and 40 KV. The distance was kept at same level as for needle electrospinning. The DOE generated for needleless electrospinning is shown in Table 17. It is important to note that there are some additional parameters that were kept constant, as mentioned in section 3.2.1.

Table 17: Response surface DOE for needleless electrospinning of PAN nanofibers with resulting diameter and its distribution

S.N.	C (w/w %)	D (cm)	V (KV)	Dia. (nm)	St. Dev. in Dia. (nm)
1	5.0	15.0	30.0	252	40
2	9.0	15.0	30.0	450	54
3	5.0	15.0	40.0	243	36
4	9.0	15.0	40.0	502	68
5	5.0	25.0	30.0	310	62
6	9.0	25.0	30.0	517	71
7	5.0	25.0	40.0	352	43
8	9.0	25.0	40.0	732	85
9	3.6	20.0	35.0	151	66
10	10.4	20.0	35.0	1158	52
11	7.0	20.0	26.6	243	26
12	7.0	20.0	43.4	317	42
13	7.0	12.5	35.0	272	39
14	7.0	28.4	35.0	381	58
15	7.0	20.0	35.0	394	67
16	7.0	20.0	35.0	447	79
17	7.0	20.0	35.0	414	72
18	7.0	20.0	35.0	402	64
19	7.0	20.0	35.0	390	66
20	7.0	20.0	35.0	423	78

Within the limits of parameters selected, for getting the DOE shown in Table 17, the diameter ranged between 151 nm to 1158 nm with standard deviation ranging between 26 nm to 79 nm. It shows that finer range of nanofibers were produced with needless electrospinning, basically, due to lower concentration. Such concentrations have to be selected based on results obtained from pre-experimentation, where it was observed that higher concentrations did not

produce any nanofibers or, if produced, they were found to be hanging between the upper and lower electrode wires.

To evaluate the effect of each of the input variables in DOE, shown in Table 17, ANOVA was performed and is summarized in Table 18. Visual representation of each effect is shown in Figure 45.

Table 18: ANOVA for response surface DOE for effect of inputs on diameter and its distribution

S.N.	Term	P-value for Dia.	P-value for St. Dev. in Dia.
1	C	0.000	0.017
2	D	0.096	0.669
3	V	0.279	0.901
4	C×C	0.008	0.013
5	D×D	0.247	0.270
6	V×V	0.112	0.224
7	C×D	0.658	0.998
8	C×V	0.427	0.845
9	D×V	0.464	0.971

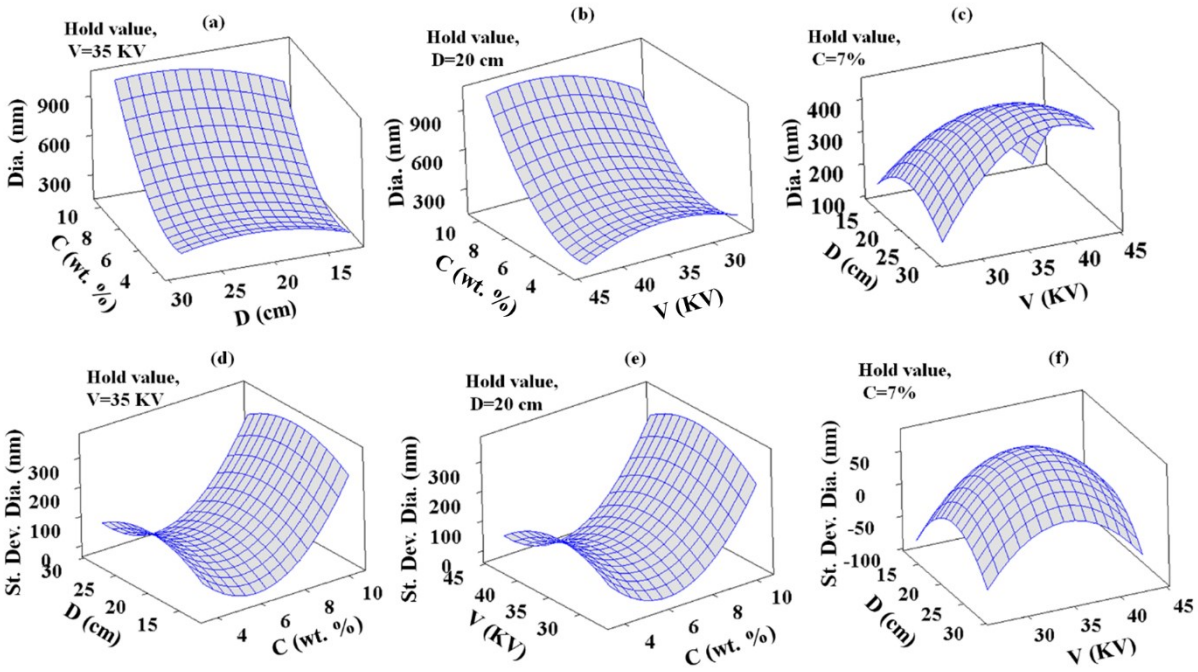

Figure 45: Surface plot (a,b,c) for effect of inputs on diameter and (c,d,e) on its distribution

For diameter of nanofibers, concentration and its square present a significant impact, with 95% (P-value below 0.05) confidence interval. However, at 91% confidence interval (P-value below 0.09), the effect of wire to collector distance can also be considered as significant. For St. Dev. in diameter, only concentration of electrospinning solution and its square show a significant influence. These observations suggest almost a similar effect, of input parameters on outputs, as that observed for needle electrospinning.

From surface plots in Figure 45, comparable effects of inputs, as witnessed for needle electrospinning, can be observed. It can be seen that effect of concentration (approximately direct proportional), both on diameter and its distribution, is much higher as compared to that of voltage and distance. For effect of voltage and distance on diameter, it can be visualized that at lower values of distance, increasing voltage decreases the diameter, however, much less steeper decrease is observed in this case than in needle electrospinning. Similarly, at higher distances, higher the voltage, higher is the diameter. Again, the slope is different from needle electrospinning. Similarly, for distance, at lower voltage values, the effect is not very evident while at higher values, increasing distance increases the diameter. Again, this impact is similar to that obtained for needle electrospinning. For diameter distribution, the effect of both the distance and voltage are much complex and follow a curve, as compared to that obtained in needle electrospinning. This may be due to additional factors affecting the variation in diameter such as air flow in needleless electrospinning etc.

Hence, it may be concluded that the effects of inputs for both the setups is similar, even though there is some difference between the magnitude of impacts and presence of curvature for needleless setup. These differences may be attributed to difference is working of both the setups, that results in inclusion of additional factors affecting the output.

4.1.2.2 Optimization results and regression models

As concentration has been proven to be the most important parameter affecting the properties of nanofibers, its optimization is important for obtaining the optimized nanofibers [19-23]. As for needle electrospinning and previous studies, low concentration resulted in finer fibers, however some of them presented defects such as beads. While, higher concentrations produced bead free fibers, but they showed higher diameter distribution. Moreover, it was observed that as the concentration increased, the hanging fibers, between the wire electrodes, also increased. On these grounds the concentration range of 5%-6% was observed to be the

optimum concentration. But still there was probability of getting beaded fibers at 5% PAN (Figure 46), so fine tuning trials were performed at 6%, that eliminated this defect, entirely.

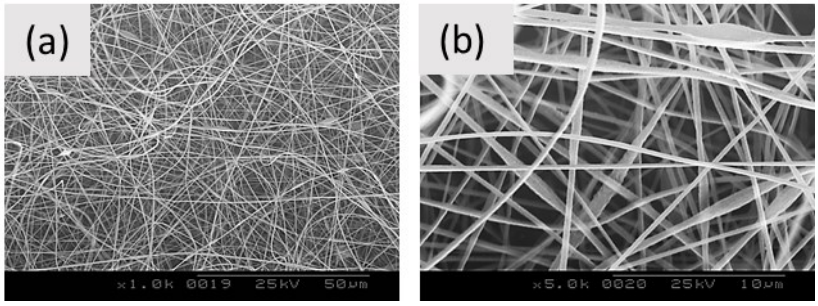

Figure 46: SEM micrographs at magnification of (a) 1K and (b) 5 K for samples obtained with 5% PAN, 25 cm and 30 KV

Samples obtained below this concentration value, mostly, produced beaded fibers, while, that above it resulted in hanging fibers or no fibers. Within this range of optimized concentration, lower voltages were observed to produce more uniform collection of nanofibers, particularly, at higher distances. At distance higher than those, the throughput was observed to decrease.

Based on above findings, fine tuning trials were performed with 6% PAN solution using three voltage levels (i-e 30, 40 and 50 KV) and two carrier speed levels (200 and 400 mm/min). However, the carrier speed was not found to result in any increase in throughput and showed that there was no such case. The optimized sample obtained after fine tuning was the one produced with 6% PAN, with wire to collector distance of 25 cm and applied voltage of 30 KV (Dia. 332 nm, St. Dev. 71 nm). SEM micrographs of this sample is shown in Figure 47.

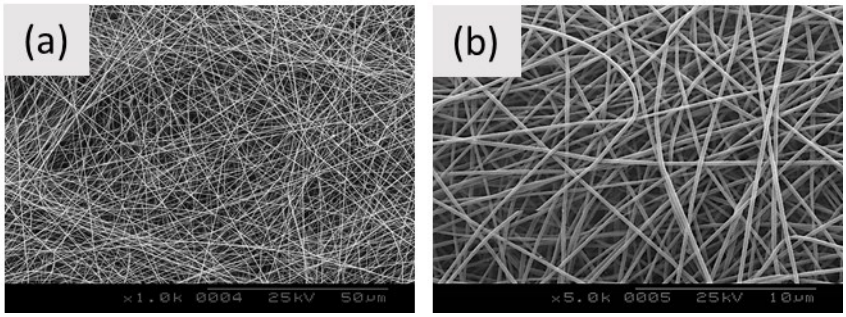

Figure 47: SEM micrographs of optimized PAN nanofiber sample at magnification of (a) 1K and (b) 5K

It is to be noted that optimized sample for only one concentration level was obtained for needleless setup as all other concentration levels produced defected fibers. This shows, that this electrospinning mechanism is more sensitive to concentration of polymer solution than needle electrospinning. This is in line with the fact that coating of solution on metallic wire strongly depends on concentration of polymer and a little variation in it can lead to a thicker or finer coating that is expected to affect the electrospinning process.

For developing regression models for diameter and its distribution, only significant terms, identified by ANOVA, were considered. The models for both these outputs is shown in Table 19.

Table 19: Regression model for diameter and its distribution for needleless electrospinning

S.N.	Regression model	R-sq
1	Dia. = 598.220 - 225.317 C + 9.66554 D + 23.253 C^2	76.83%
2	St. Dev. in Dia. = 648.951 - 206.320 C + 16.958 C^2	54.19%

R^2 of model for diameter is 76.83%, that reflects that it represents the analyzed data quite well. However, this value is lower than that obtained for needle electrospinning. It may be credited to greater number of variables, including noise variables, involved in needleless electrospinning, employed for current study. It may also be noted that square of concentration is included for model predicting diameter. This shows presence of a second degree interaction, whose magnitude is much lower than that of first degree interaction, as confirmed by their respective coefficients in model. For distribution of diameter, again, a lower R-sq is obtained that confirms the presence of additional factors impacting it, as discussed in previous sections.

For validation of models in Table 19, 4 validation runs were performed. The results of these runs are compared with the predicted results and are presented in Table 20. It can be observed that the absolute error for one of the validation experiments was a bit higher. This is in line with R-sq value for the model.

Table 20: Validation of response surface DOE for PAN nanofibers produced through needleless electrospinning

C (%)	V (KV)	D (cm)	Actual		Predicted		Absolute error (Dia.)	Absolute error (St Dev.)
			Dia. (nm)	St. Dev. (nm)	Dia. (nm)	St. Dev. (nm)		
7	30	21	480	109	363	36	117	73
9	35	23	721	169	676	166	45	3
9	35	20	600	91	647	166	47	76
7	40	20	356	101	354	36	2	65

4.2 Optimization and modelling of electrospinning of PAN/CNT composite nanofibers

For optimization and modelling of PAN/CNT composite nanofibrous webs and the process to produce them, similar strategy was employed, as used for PAN nanowebs. However, in this case polymer solution concentration was not optimized for needle setup, as our research group has, already, worked on it and found a PAN concentration range of 9%-12% to work well, when CNTs are incorporated in PAN nanofibers [278]. Instead, the CNT concentration was varied to get different CNT content (C_{CNT}) in fibers. For needleless setup, PAN concentration needed to be optimized, as it has not been worked on, previously. So, it was accomplished before optimizing CNT content.

4.2.1 PAN/CNT nanofibers from needle electrospinning

For needle electrospinning setup, both full factorial and response surface (CCD) were used to optimize the process, for the reasons mentioned in section 4.1. The details of these experiments and results obtained from them are discussed in following sections.

4.2.1.1 Statistical analysis using full factorial experimental design

The details of experimental design using full factorial methodology are summarized in Table 21. As CNTs are conductive material, electrospinning time was expected to be interesting parameter, as it is directly related to accumulation of charge, whose effect may be more pronounced in presence of CNTs. So, instead of considering the needle to collector distance (having lower impact on fiber properties), electrospinning time (T) was taken as input parameter for both the DOEs on needle based setup.

Table 21: Full factorial DOE for needle electrospinning of PAN/CNT composite nanofibers

S.N.	C_{CNT} (wt. %)	V (KV)	T (min)	Dia. (nm)	St. Dev. in Dia. (nm)
1	3	10	90	663	56
2	3	10	120	736	135
3	3	10	150	702	99
4	3	11.5	90	1055	218
5	3	11.5	120	591	99
6	3	11.5	150	528	203
7	3	13	90	703	222
8	3	13	120	650	218
9	3	13	150	615	216
10	5	10	90	513	99
11	5	10	120	366	63
12	5	10	150	398	88
13	5	11.5	90	518	149
14	5	11.5	120	467	83
15	5	11.5	150	333	61
16	5	13	90	516	159
17	5	13	120	496	76
18	5	13	150	380	61
19	7	10	90	737	201
20	7	10	120	855	192
21	7	10	150	917	164
22	7	11.5	90	933	249
23	7	11.5	120	791	144
24	7	11.5	150	964	190
25	7	13	90	1236	332
26	7	13	120	750	141
27	7	13	150	815	221

To study the significance of effect of each input parameter, mentioned in Table 21, ANOVA was performed and is tabulated in Table 22.

Table 22: ANOVA for full factorial DOE for effect of inputs on diameter and its distribution

S.N.	Term	P-value for Dia.	P-value for St. Dev. in Dia.
1	C_{CNT}	0.000	0.000
2	V	0.152	0.000
3	T	0.000	0.000
4	$C_{CNT} \times V$	0.026	0.470
5	$C_{CNT} \times T$	0.002	0.444
6	V×T	0.000	0.011
7	$C_{CNT} \times V \times T$	0.000	0.165

For diameter, all input parameters (other than voltage) and their products had significant impact, as determined by their P-values (lower than 0.05). While, for distribution of diameter, effect of some of products was not significant. This confirmed the significance of considering CNT% and electrospinning time as input factors for electrospinning of PAN/CNT composite nanofibers. The graphical representation of these effects shown in main effect plots in Figure 48.

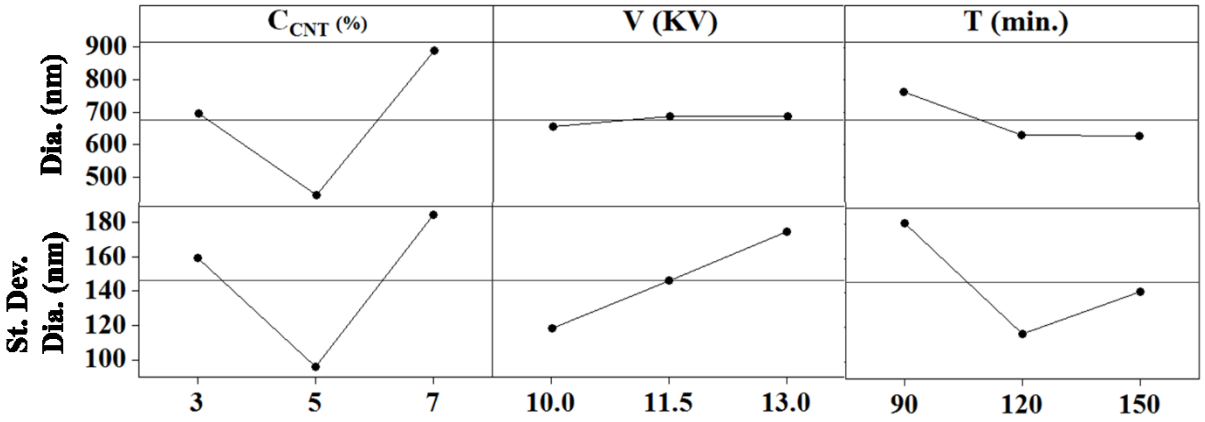

Figure 48: Main effect plots for effect of input parameters on diameter and its distribution

From the main effects plots, it was revealed that increasing CNT concentration was found to, initially, decrease the diameter and its distribution and then increase them. Higher CNT contents are expected to increase the electrostatic force on fibers, which leads to an initial decrease in diameter of composite fibers, as discussed in some previous studies [11, 50, 54]. However, addition of CNTs beyond that limit was found to result in thicker fibers. This may be credited to two factors i-e the increase in viscosity of solution and the increase in electrostatic force, beyond the optimum limit. Both these factors have the potential to increase the diameter of nanofibers [6, 51]. The effect of applied voltage on fiber diameter was not very prominent, however, for distribution in diameter, it showed a significant impact. Higher voltages were found to increase the distribution in fiber diameter, perhaps, due to lower time for fibers to stretch as discussed in section 4.1. Similar impact on diameter distribution can also be expected from increasing time of electrospinning, which may result in higher buildup of charge on solution inside the syringe, thus leading to higher electrostatic force. This increase in electrostatic force also decreases the diameter of nanofibers due to greater stretching.

4.2.1.2 Statistical analysis using response surface experimental design

To evaluate a DOE that can cover complex interactions than those covered by full factorial design, statistical analysis of PAN/CNT composite nanofiber electrospinning was performed by response surface methodology. The DOE for this purpose is shown in Table 23.

Table 23: Response surface DOE for needleless electrospinning of PAN/CNT composite nanofibers with resulting diameter and its distribution

S.N.	C_{CNT} (wt. %)	V (KV)	T (min)	Dia. (nm)	St. Dev. in Dia. (nm)
1	3.0	10.0	90.0	663	56
2	7.0	10.0	90.0	737	201
3	3.0	13.0	90.0	703	222
4	7.0	13.0	90.0	1236	332
5	3.0	10.0	150.0	702	99
6	7.0	10.0	150.0	917	164
7	3.0	13.0	150.0	615	216
8	7.0	13.0	150.0	815	221
9	1.6	11.5	120.0	750	50
10	8.4	11.5	120.0	1196	178
11	5.0	9.0	120.0	380	70
12	5.0	14.0	120.0	487	105
13	5.0	11.5	69.5	560	156
14	5.0	11.5	170.5	400	76
15	5.0	11.5	120.0	413	70
16	5.0	11.5	120.0	393	50
17	5.0	11.5	120.0	398	55
18	5.0	11.5	120.0	428	85
19	5.0	11.5	120.0	403	60
20	5.0	11.5	120.0	431	82

For determination of terms, significantly affecting the outputs in Table 23, their variance was analyzed using standard ANOVA procedure. This analysis is summarized in Table 24, which shows P-values for each term, its square and product with other terms.

Table 24: ANOVA for response surface DOE for effect of inputs on diameter and its distribution

S.N.	Term	P-value for Dia.	P-value for St. Dev. in Dia.
1	C_{CNT}	0.001	0.023
2	V	0.200	0.025
3	T	0.176	0.250
4	C_{CNT}^2	0.000	0.042
5	V^2	0.166	0.122
6	T^2	0.062	0.038
7	$C_{CNT} \times V$	0.161	0.553
8	$C_{CNT} \times T$	0.528	0.257
9	V×T	0.033	0.448

It can be observed that C_{CNT} and its square put a significant impact on diameter and its distribution. Square of time and its product with voltage also affect the diameter in a significant manner. Moreover, voltage and square of electrospinning time significantly affect the diameter distribution. Effect of these input terms can be visualized through response surface plots in Figure 49.

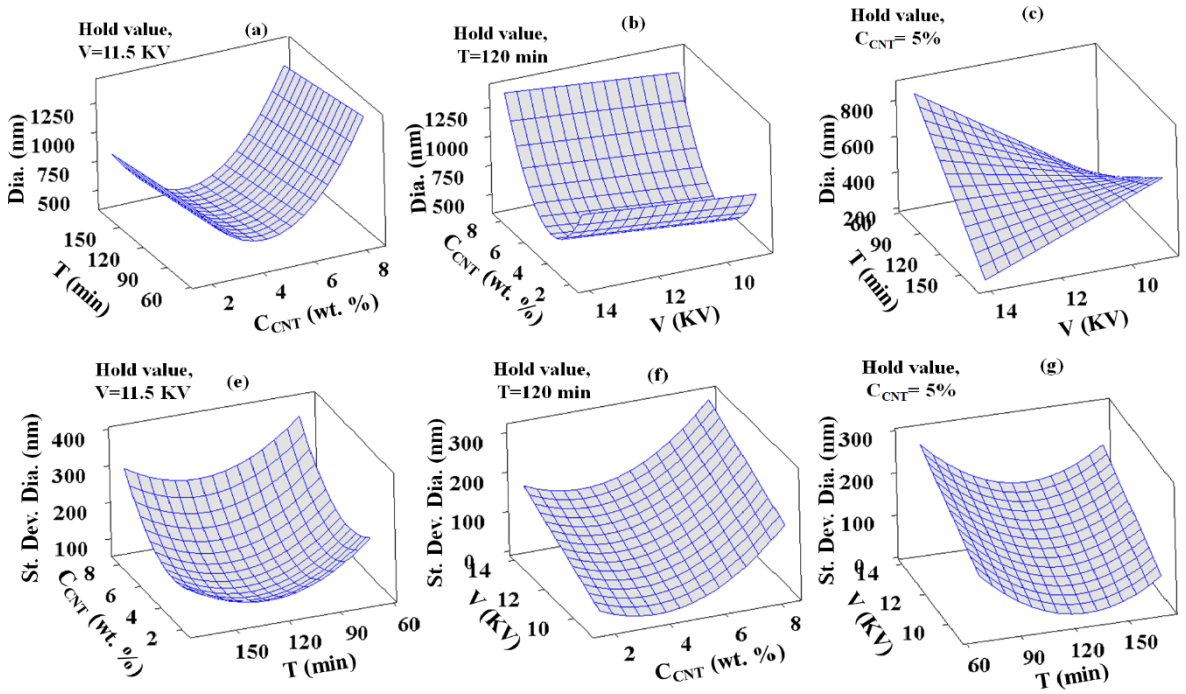

Figure 49: Surface plots (a,b,c) for effect of inputs on diameter and (c,d,e) on its distribution

Increase in CNT content in nanofibers was found to increase their diameter, after a short, initial, decrease in it. This effect could be explained due to the same reason as explained

for such a trend in section 4.1.1.1. Effect of time is different for higher and lower values of voltage. At higher voltage, higher electrospinning time decreases the diameter of nanofibers (at top), while, at lower voltage the trend is almost linear. This may be attributed to accumulation of higher charge in solution, leading to higher electrostatic force that draws the polymer jet to thinner size [11, 50, 54]. For voltage as well, the effect is different at different electrospinning times. At lower electrospinning time, increasing the voltage increases the fiber diameter, that may be attributed to take-up of higher amount of solution from needle due to stronger electrostatic force [9, 61]. However, this force doesn't draw the thicker jet it produced. For that stronger force may be needed. This strength could have been provided by charge accumulated in solution that led to, an even, greater drawing force leading to smaller diameter at longer electrospinning time, with increasing voltage.

The effect of CNT content, on distribution of diameter, followed a curved line. Increasing CNT content, resulted in less uniform diameter distribution, following a small decrease at start. The reason for this could be the same as explained in section 4.1.1.1. The trend for voltage and electrospinning time were also found to be similar as those explained in section 4.1.1.1.

4.2.1.3 Optimization results and regression models for full factorial and response surface designs

For optimization of PAN/CNT composite nanofibers, concentration of CNTs was the most important factor, as shown in Figure 48. Even though, medium levels of CNTs produced finer fibers with lower standard deviation, other concentrations also produced defect free fibers. So, the optimized samples were selected from all the three concentrations. This was also done to compare the effect of CNT concentration on other properties, needed for heat generation application. Considering the effect of voltage and time; while, lower voltages resulted in lower diameter distribution, they caused some droplets. On the other hand, higher voltages increased the diameter distribution. So, medium voltage was selected as optimized level. Similarly, higher electrospinning times resulted in finer fibers but with higher diameter distribution, thus supporting the selection of medium level as optimized value. Consequently, within each concentration level, the optimized composite webs, free from defects (such as drops and beads of polymer) were produced using applied voltage of 11.5 KV and electrospinning time of 120 minutes. SEM micrographs of samples produced at these optimized settings are shown in Figure 50.

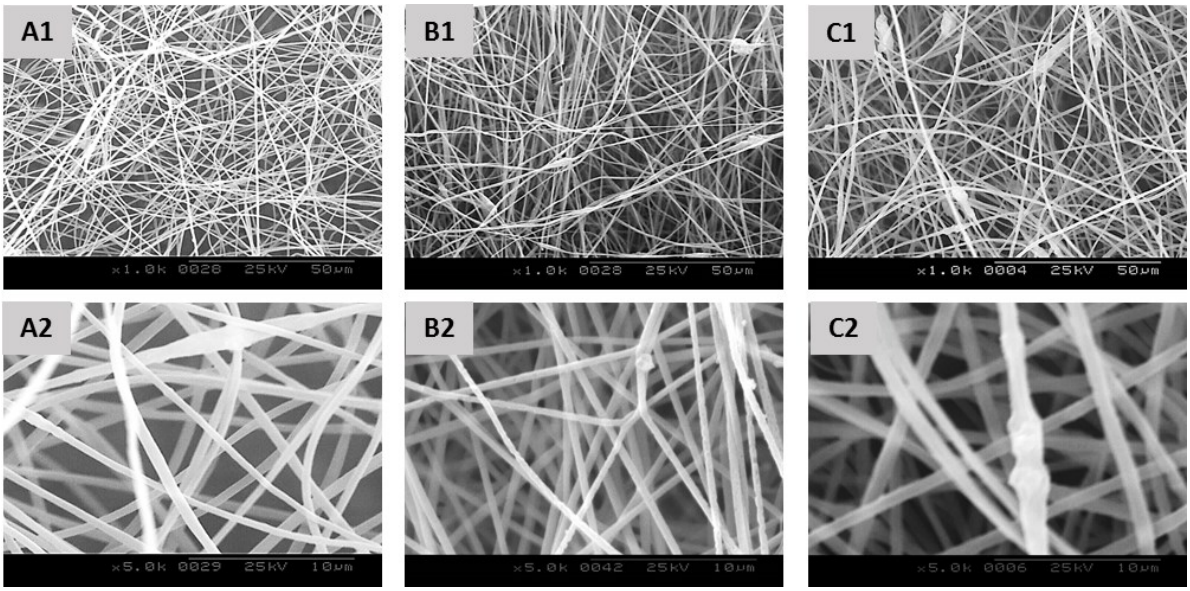

Figure 50: SEM micrographs of optimized samples of PAN/CNT nanofibers with (A1, A2) 3% CNT, (B1, B2) 5 % CNT and (C1, C2) 7% CNT (Upper row at magnification of 1K and lower at 5K)

It can be seen from micrographs, that there are some structures which look like beads. These structures have been characterized as aggregates of CNTs and are different from beads in terms of their much higher surface roughness [278]. The mean diameter of fibers in first, second and third rows was 590 nm (St. Dev. 99 nm), 466 nm (St. Dev. 83 nm), 791 nm (St. Dev. 143 nm).

Based on significance of values for their effect on output, regression analysis was performed. The equations produced from this model are summarized in Table 25.

Table 25: Regression model for diameter and its distribution for needle electrospinning

S.N.	DOE	Regression model	R-sq
1	FF	ln(Dia.) = 6.423+ 0.063 C_{CNT} + 0.013 V - 0.004 Time	12.49%
2	FF	ln(SD Dia) = 3.815 + 0.032 C_{CNT} + 0.125 V - 0.004 T	14.93%
3	RS	Dia. = -1372.150 - 492.418 C_{CNT} + 268.203 V + 21.862 T + 55.729 C_{CNT}^2 - 2.020 V.T	78.28%
4	RS	SD in Dia.= 467.501 - 58.190 C_{CNT} + 25.888 V - 9.153 T +7.802 C_{CNT}^2 + 0.035 T^2	47.89%

It is obvious that R-sq for these equations is very low for FF DOE, even though, ANOVA presented significant effect on outputs for a number of terms. It means that the model

does not fit, the data, well and better DOE is needed to study higher degree effects, as those achieved by response surface design.

The lower validity of full factorial design was also confirmed by validation experiments shown in Table 26. The absolute error shows random values with large magnitude, confirming inability of model to fit with actual data. Whereas, the regression model developed by using response surface methodology fits the data quite well, as shown by its R-sq. The validation experiments, shown in Table 26, also confirm the validity of response surface design to be better than full factorial design.

Table 26: Validation of full factorial and response surface DOE for PAN/CNT fibers using needle electrospinning

DOE	C_{CNT} (%)	V (KV)	T (min)	Actual		Predicted		Absolute error (Dia.)	Absolute error (St Dev.)
				Dia. (nm)	St. Dev. (nm)	Dia. (nm)	St. Dev. (nm)		
FF	3	11	100	575	96	575	132	0	-36
	5	12	110	440	91	635	154	-195	-62
	7	13	130	730	130	674	171	57	-41
	3	13	140	601	205	503	145	98	60
RS	5	10	120	366	63	441	36	-75	27
	7	11.5	120	791	144	832	146	-41	-2
	5	13	120	496	76	518	114	-22	-38
	3	11.5	150	528	203	531	75	-4	128

4.2.2 PAN/CNT nanofibers from needleless electrospinning

4.2.2.1 Optimization with fixed CNT content in PAN/CNT composite nanofibers

For study of needleless electrospinning of PAN/CNT composite nanofibers, initially, the PAN concentration needed to be optimized, as there was no data available in this direction. To accomplish this, response surface methodology was utilized to develop the experimental design summarized in Table 27. Throughout this part of study, CNT content was fixed at 5 wt. % (calculated on weight of fiber) and PAN concentration was varied. The data from this design was analyzed to screen out the optimized level of concentration, voltage and distance between wire and collector. These optimized values for PAN/CNT composites were, then, re-optimized by performing another experimental set (shown in Table 27) by changing CNT concentration.

Table 27: Response surface DOE for PAN/CNT nanofibers with fixed fiber CNT content

S.N.	C (w/w %)	D (cm)	V (KV)	Dia. (nm)	St. Dev. in Dia. (nm)
1	5.0	30	150	210	38
2	7.0	30	150	441	96
3	5.0	40	150	234	38
4	7.0	40	150	398	106
5	5.0	30	250	261	40
6	7.0	30	250	754	151
7	5.0	40	250	262	45
8	7.0	40	250	645	138
9	4.3	35	200	223	38
10	7.7	35	200	742	151
11	6.0	26	200	356	77
12	6.0	43	200	284	52
13	6.0	35	125	265	37
14	6.0	35	284	468	94
15	6.0	35	200	390	83
16	6.0	35	200	381	80
17	6.0	35	200	374	78
18	6.0	35	200	390	80
19	6.0	35	200	395	86
20	6.0	35	200	390	81

ANOVA of results (Table 28) show that for diameter, almost all input parameters pose a significant impact. While, for St. Dev. solution concentration, electrospinning distance and some squared and product terms show a significant impact. These terms confirm the presence of second degree interaction, supporting the fact that response surface methodology can produce better results while studying the electrospinning process.

Table 28: ANOVA for effect of input parameters on outputs of PAN/CNT composite nanofibers using needleless electrospinning

S.N.	Term	P-value for Dia.	P-value for St. Dev. in Dia.
1	C	0.000	0.000
2	V	0.001	0.253
3	D	0.000	0.000
4	C × C	0.000	0.027
5	V × V	0.000	0.109
6	D × D	0.083	0.123
7	C × V	0.001	0.761
8	C × D	0.000	0.013
9	V × D	0.051	0.498

The effect of each of the inputs is shown in Figure 51, which shows an increase in diameter and its distribution, with increasing PAN concentration. Increasing the electrospinning distance was found to increase the diameter, probably, due to reduced electrostatic attraction [65]. Similarly, decreasing the applied voltage increased the fiber diameter, due to the same reason. Higher voltages and lower distances were also found to increase the variation in diameter, mainly, because of lower time for polymer jet to become uniform, at both these conditions [63].

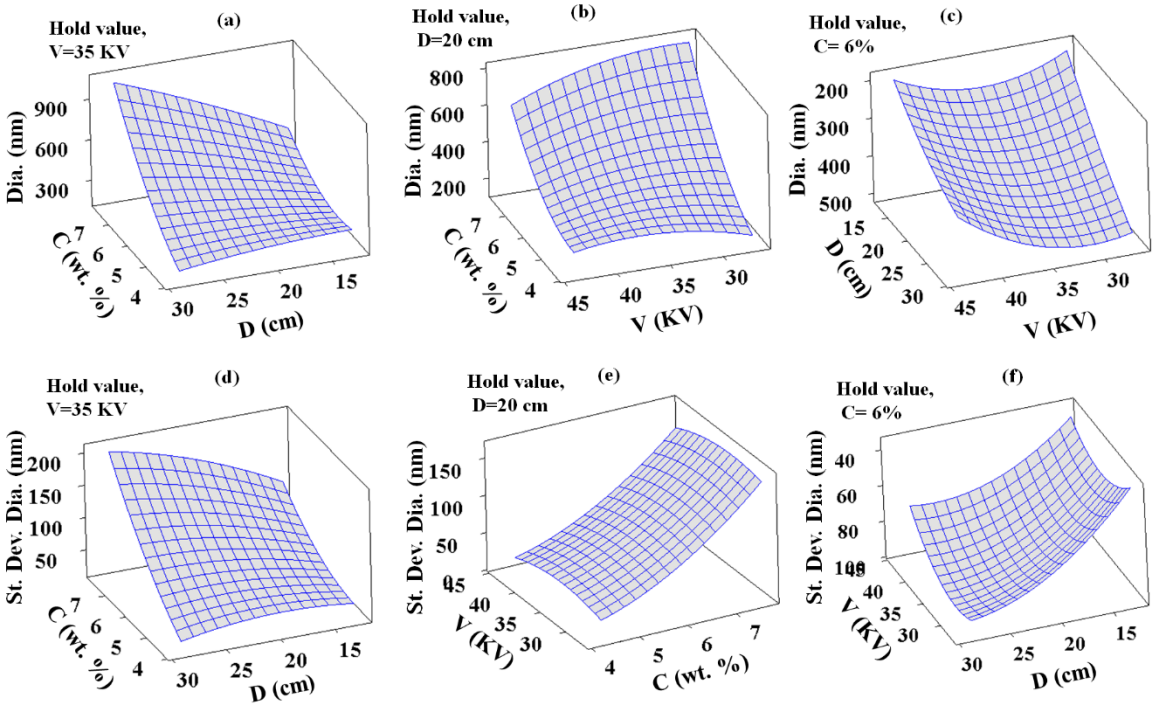

Figure 51: Surface plots (a,b,c) for effect of inputs on diameter and (c,d,e) on its distribution

4.2.2.1.2 Optimization results and regression models

From experimentation, it was observed that at concentration of PAN below 5%, droplets were produced. Even though nanofibers produced from 6% PAN solution showed better results in terms of morphology, however, at that concentration level some runs were found to produce fibers hanging between top and bottom electrode wires. Whereas, at concentrations above 6%, all settings produced hanging fibers. So, when considering overall properties and electrospinnability, 5% was considered as optimum concentration, as it did not produce hanging fibers. Similarly, higher voltage and lower distances produced finer fiber with less variation. Consequently, the optimized conditions were concluded to be: PAN concentration, 5%, wire to collector distance, 25 cm and applied voltage, 30 KV. The SEM

micrograph of composite nanoweb produced at these settings is shown in Figure 52. The optimized conditions were utilized to study optimization of PAN/CNT composite nanowebs with different CNT contents in composites.

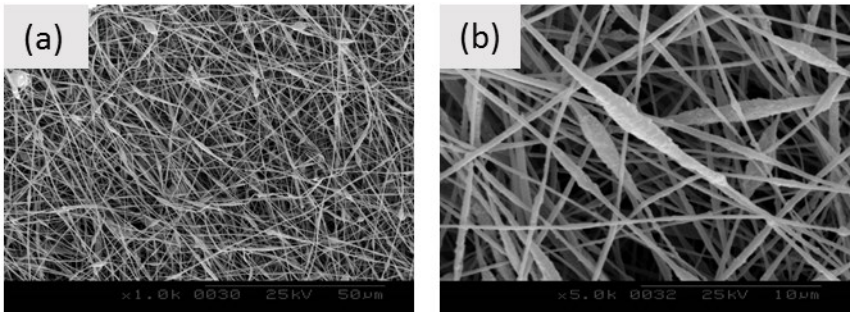

Figure 52: SEM micrographs at magnification of (a) 1K and (b) 5 K for PAN/CNT composite nanofiber samples obtained at optimized conditions

To develop prediction models for diameter and its distribution, the data was analyzed using regression modelling tool and the models so obtained are shown in Table 29. The models were found to be highly valid, based on R-sq values, so they may be used for prediction of behavior of nanocomposite fibers with CNT content of 5%. However, for other concentrations the process needs to be studied with additional levels.

Table 29: Regression model for diameter and its distribution for needle electrospinning

S.N.	Regression model	R-sq
1	Dia. = -335.091 -371.078 C + 89.908 V - 29.459 D + 36.852 C^2 - 0.830 V^2 - 0.309 D^2 - 4.420 C.V + 12.028 C.D - 0.442 V.D	99.21%
2	St. Dev. = 275.709 - 84.676 C - 8.964 D + 6.959 C^2 + 1.964 C.D	92.51%

To assess the validity of models shown in Table 29, validation experiments were performed, whose results are summarized in Table 30. It can be observed that maximum absolute error for diameter and its distribution is 48 nm and 57 nm, respectively. These values fall close to, even, the minimum standard deviation of 38 nm in data shown in Table 27, which confirms their validity.

Table 30: Validation of model for PAN/CNT nanofibers diameter and its distribution for needle electrospinning

C (%)	V (KV)	D (cm)	Actual		Predicted		Absolute error (Dia.)	Absolute error (St Dev.)
			Dia. (nm)	St. Dev. (nm)	Dia. (nm)	St. Dev. (nm)		
7	35	20	544	63	582	120	-38	-57
7	35	25	717	177	709	144	8	34
5	35	25	323	62	275	48	49	15
5	35	18	225	42	261	42	-36	0

4.2.2.2 Optimization with different CNT content in fiber

The optimized concentration, from above mentioned experimentation, was employed to study the optimization of PAN/CNT composite nanofibers by varying CNT content. For this purpose, PAN concentration, in solution, was fixed at 5% and the CNT concentration in it was changed according to its final content in fiber. The response surface DOE developed for this purpose is shown in Table 31.

Table 31: Response surface DOE for PAN/CNT nanofibers with different CNT content

S.N.	C_{CNT} (wt. %)	V (KV)	D (cm)	Diameter	SD
1	3.0	30.0	21.0	208	32
2	7.0	30.0	21.0	240	35
3	3.0	40.0	21.0	244	50
4	7.0	40.0	21.0	235	46
5	3.0	30.0	29.0	286	66
6	7.0	30.0	29.0	318	73
7	3.0	40.0	29.0	286	58
8	7.0	40.0	29.0	231	54
9	1.6	35.0	25.0	303	61
10	8.4	35.0	25.0	250	50
11	5.0	26.6	25.0	210	30
12	5.0	43.4	25.0	236	46
13	5.0	35.0	18.3	228	41
14	5.0	35.0	29.0	286	68
15	5.0	35.0	25.0	323	62
16	5.0	35.0	25.0	329	68
17	5.0	35.0	25.0	306	64
18	5.0	35.0	25.0	339	68
19	5.0	35.0	25.0	313	62
20	5.0	35.0	25.0	334	68

The ANOVA for terms in Table 31, for evaluation of statistical significance of their impact on outputs, is shown in Table 32. It can be observed that effect of voltage, CNT% and its products with voltage and distance, on diameter, is not significant. However, square of CNT% shows a significant impact, confirming a second degree interaction. For St. Dev. in diameter, the effect of CNT content, its product with voltage and distance and that of distance alone, were found to show a non-significant impact, while all other terms significantly affect St. Dev.

Table 32: ANOVA for effect of input parameters on outputs for PAN/CNT composite nanofibers with different CNT contents using needleless electrospinning

S.N.	Term	P-value for Dia.	P-value for St. Dev. in Dia.
1	C_{CNT}	0.935	0.485
2	V	0.122	0.001
3	D	0.001	0.001
4	$C_{CNT} \times C_{CNT}$	0.029	0.041
5	V × V	0.000	0.000
6	D × D	0.010	0.210
7	$C_{CNT} \times V$	0.049	0.184
8	$C_{CNT} \times D$	0.427	0.805
9	V × D	0.064	0.001

From surface plots shown in Figure 53, it can be observed that increasing CNT contents, first increased and then decreased the fiber diameter. This trend could be credited to increase in viscosity and formation of CNT aggregates at higher concentrations [110, 151, 193]. Both these factors lead to higher diameter. However, increase in C_{CNT} also increased the electrostatic pull of jet due to increased conductivity, thus, leading to a decreased diameter at higher CNT concentration. Above mentioned factors may also be considered responsible for initial increase, followed by a decrease in standard deviation in diameter. Higher viscosities are expected to result in greater resistance to drawing of jet (due surface tension), which results in lower uniformity. However, increased electrostatic force, at higher CNT contents leads, to higher drawing and greater uniformity in fibers. Whereas, increasing the electrospinning distance was found to increase the diameter, probably due to reduced effect of electrostatic force at higher distances thus leading to lower drawing of jet. The same factor could be considered responsible for higher standard deviation at higher distances. Voltage was found to put a curvilinear impact on diameter, which first increases and then decreases with increasing the applied voltage. The reason could be the same as discussed above. Increasing voltage results in increased pull on

polymer, thus. taking up higher of its quantity. However, increasing its value beyond that results in higher drawing as well, leading to lower diameter.

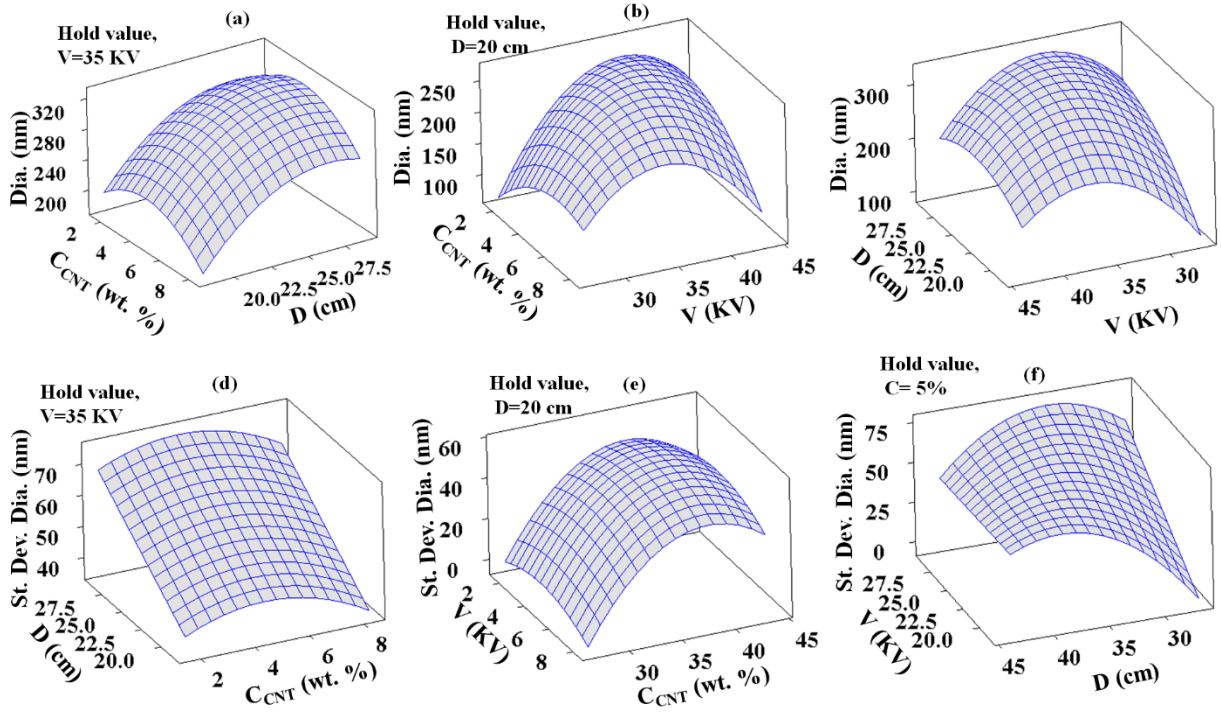

Figure 53: Surface plots (a,b,c) for effect of inputs on diameter and (c,d,e) on its distribution

4.2.2.2.2 Optimization results and regression models

This part of study was used to finalize three optimized samples, each with different CNT contents. So, the defect free fibers from each CNT concentration level were selected. For this purpose, the effect produced by voltage and distance were studied according to goal of getting optimized samples. It was observed that, lower value of wire to collector distance (i-e 21 cm) was the optimum value, as higher distances increased the deviation in diameter and resulted in thicker fibers [65], with lower outputs and, sometimes, drop formation. With lower distances, lower voltages were found to produce finest fibers with least standard deviation and free from defects. So, the optimum value, selected, for applied voltage was 30 KV. Consequently, three optimized samples (at 3%, 5% and 7% CNT content) from these results were produced in larger quantity (for characterization) at distance and voltage of 21 cm and 30 KV, respectively. The SEM micrographs of these samples are shown in Figure 54.

It can be observed in Figure 54, that CNTs are present in form of aggregates that resemble elongated beads with rough surface. The number of aggregates and their size was also found to increase with increasing the CNT concentration.

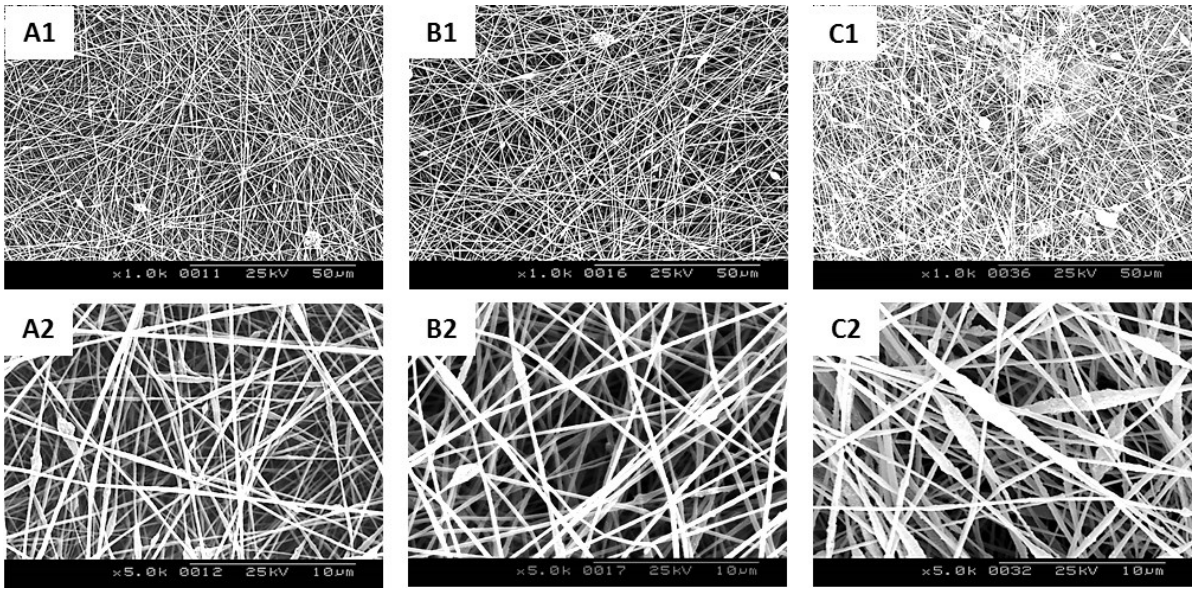

Figure 54: SEM micrographs of optimized samples PAN/CNT nanofibers with (A1, A2) 3% CNT, (B1, B2) 5 % CNT and (C1, C2) 7% CNT at 1 K and 5 K

Prediction models obtained from analysis of data in Table 31, are shown in Table 33. From R-sq. of both the models, it can be concluded that they fit the analyzed data and may be utilized to predict the outputs with acceptable error. The presence of significant second degree terms in models (i-e $(CNT\%)^2$, V^2 and D^2) signifies that electrospinning of PAN/CNT composite materials needs to be studied using DOEs, such as response surface designs, that are meant for analysis of such interactions.

Table 33: Regression model for diameter and its distribution for needle electrospinning

S.N.	Regression model	R-sq
1	Dia. = -3235.11 + 86.867 C_{CNT} + 117.681 V + 98.227 D - 3.391 C_{CNT}^2 - 1.302 V^2 - 1.342 D^2 - 1.606 V. C_{CNT} - 0.746 V.D	79.50%
2	St. Dev. in Dia. = -786.747 + 6.288 C_{CNT} + 34.573 V + 15.116 D - 0.687 C_{CNT}^2 - 0.361 V^2 - 0.353 V.D	87.79%

To validate the models presented in Table 33, additional experimental runs were performed to compare their results with those predicted by models. The levels of each of the input parameters, along with their outputs and their difference from those predicted by model is summarized in Table 34.

Table 34: Validation table for models for PAN/CNT nanofiber diameter and its distribution for needleless electrospinning

S.N.	C_{CNT} (wt.%)	V (KV)	D (cm)	Actual		Predicted		Absolute error (Dia.)	Absolute error (St Dev.)
				Dia. (nm)	St. Dev. (nm)	Dia. (nm)	St. Dev. (nm)		
1	5	30	21	305	75	233	35	72	41
2	3	35	25	300	64	314	63	-14	2
3	5	40	25	262	45	288	58	-26	-13
4	7	38	27	350	104	280	62	71	42

It can be observed that absolute error, for both, the diameter and its distribution, is close to minimum standard deviation for runs in current DOE. This shows that these models predict results within the acceptable deviation range and hence they can be used for such predictions on needleless electrospinning setups, that can be used for bulk scale production of nanofibers.

4.3 Characterization of PAN and PAN/CNT nanofiber webs

Different properties of PAN and PAN/CNT nanowebs determine their capability to produce heat. In current work, some of these properties were studied. They include internal structure, electrical and thermal conductivity and thermal stability. The internal structure of nanowebs is expected to affect their thermal properties based on arrangement of crystalline and amorphous regions and that of CNTs in case of PAN/CNT nanowebs. To determine the internal structure transmission electron microscopy (TEM) was performed. Similarly, the ability to conduct heat and electricity is expected to influence heat generation efficiency, so, they were also determined in current study. The thermal stability of nanowebs is also important for subjected application, as they will be exposed to elevated temperatures in this case. For this purpose, thermogravimetric analysis (TGA) was performed. The details of characterization are summarized in following sections.

4.3.1 Internal structure of nanowebs

As mentioned earlier, it was studied using TEM and compared to each other and to that of CNTs, used to charge them. This gave useful information about the location of CNTs inside the nanofibers, their alignment and the degree of crystallization of PAN. For needle

electrospinning, these structures have been studied extensively, so was omitted for current work.

TEM images of optimized PAN nanofibers (for images shown in Figure 47), presented in Figure 55, show the absence of significant crystallinity. This was inferred by comparison of TEM images in Figure 55 to that in Figure 22 and Figure 24, where, parallel lines signify crystalline regions. Absence of these lines in Figure 55 was used to confirm the absence of crystallinity. Moreover, it can be seen that there are some weak points in structure, pointed out by white arrows. These may be expected to result in inferior mechanical properties, which may be important in some of the applications. However, for current study, they may be accepted.

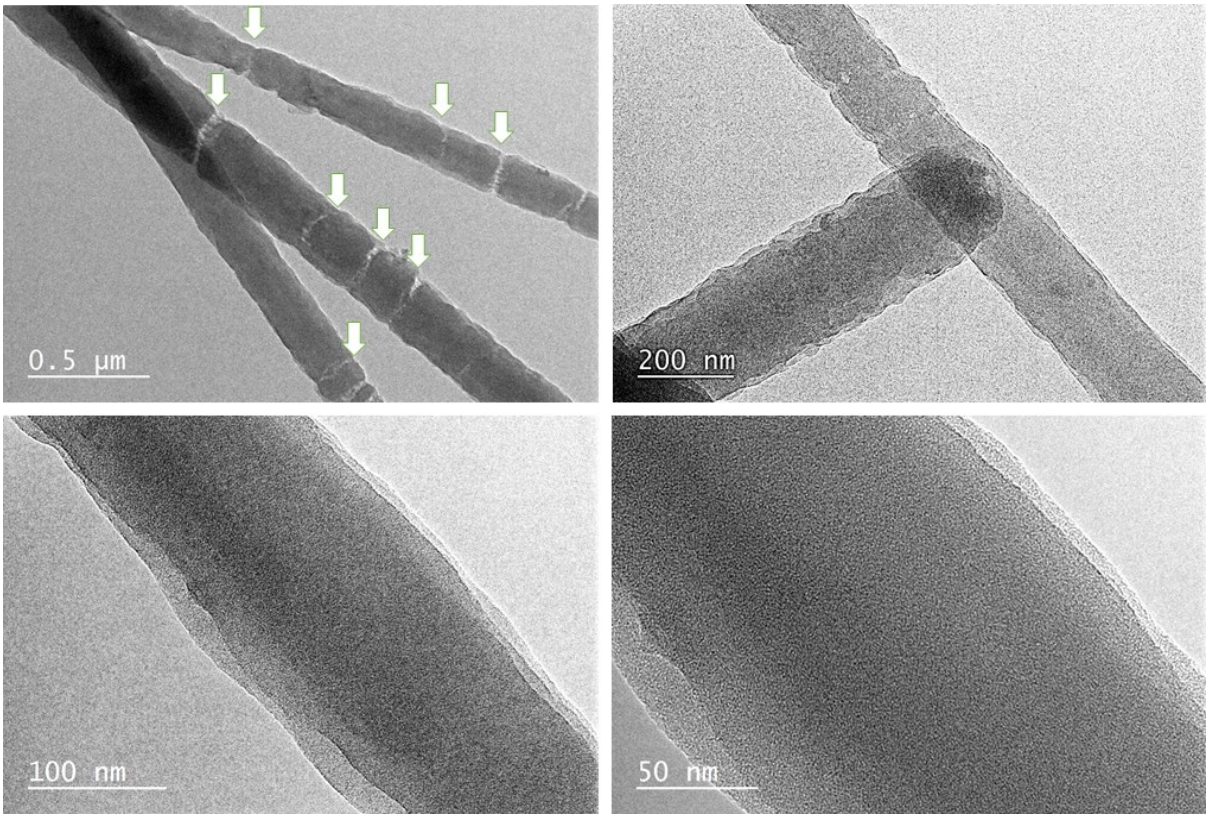

Figure 55: TEM images of pristine PAN nanofibers, from needleless electrospinning, at different magnifications

Figure 56 shows the structure of MWCNTs used in current work. It can be observed from images (a) and (b) that CNTs tend to exist as aggregates. The walls of CNTs are also visible in images (c) and (d) with a hollow central tube.

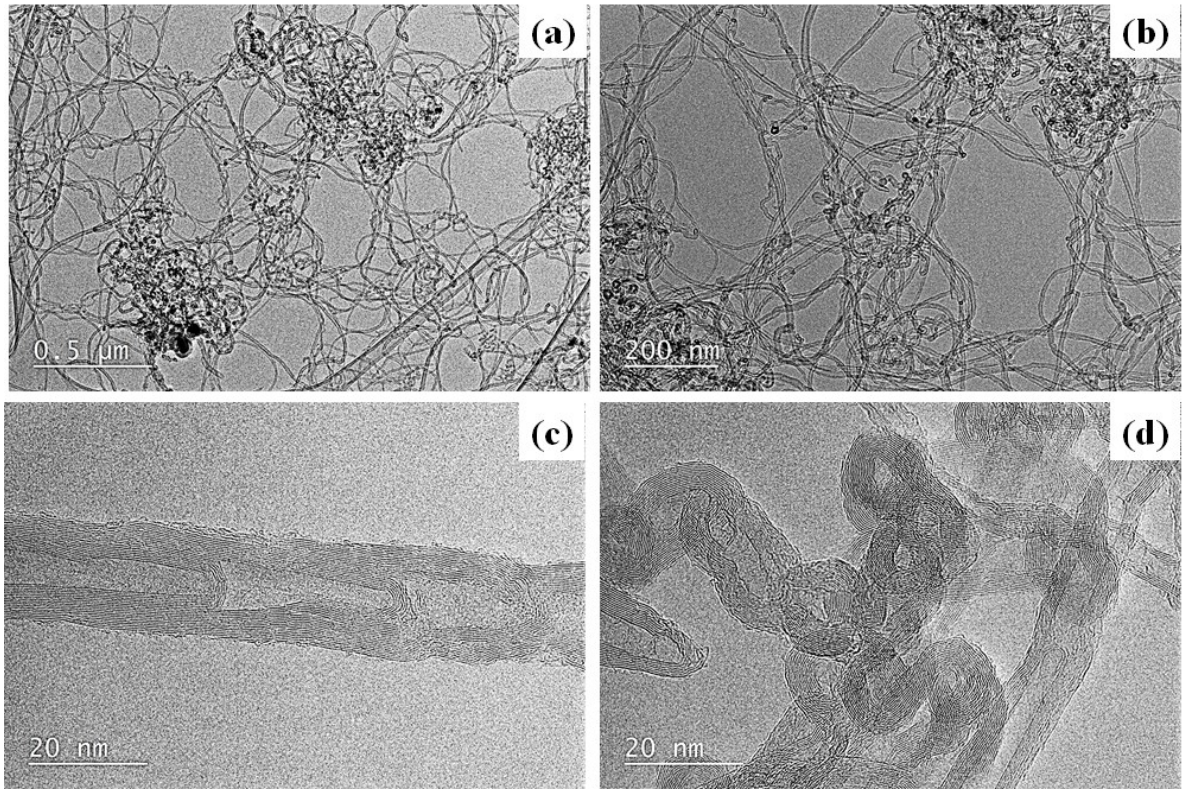

Figure 56: TEM images, of CNTs (before incorporation in nanofibers) used for current study, at different magnifications

It was noted that CNTs were aligned along the length of the fibers, as shown in Figure 57. This property of PAN/CNT nanofibers can be utilized for different mechanical applications. For such applications, the load applied on fiber is transferred to CNTs (which are much stronger than nanofibers) through the polymer matrix, thus resulting in stronger nanofibers than those produced from pure PAN. Additionally, it was also observed that CNTs were found to take spiral form inside the polymer matrix, as shown in Figure 58, where they were found to cover the whole thickness of fiber due to this spiral arrangement. This became possible due to the long length of CNTs, used in current study.

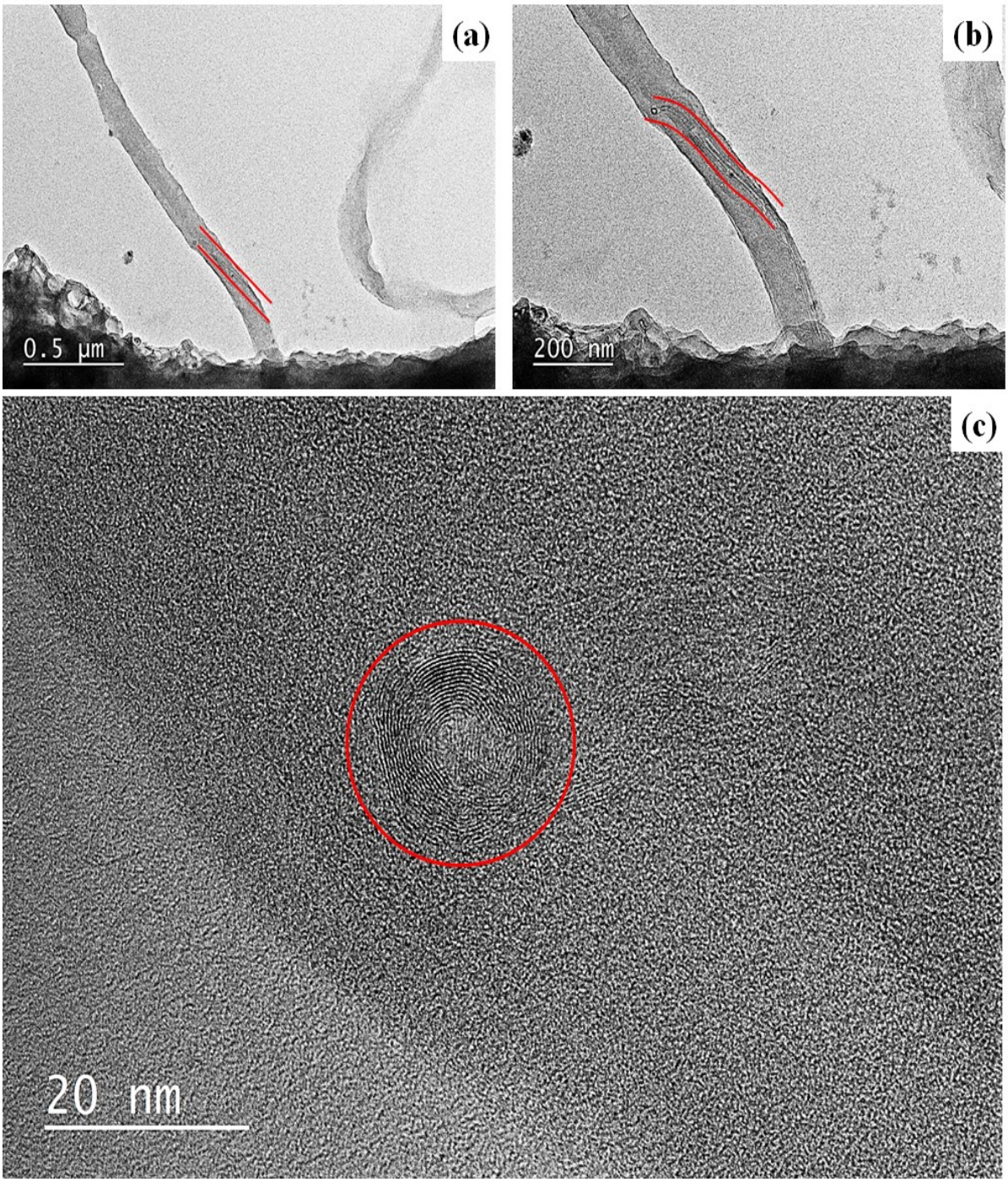

Figure 57: TEM images of PAN/CNT nanofibers from needleless electrospinning, with 7% CNT, at different magnifications

This behavior of CNTs has been noted for the first time and is expected to be formed during the spiral motion of the jet. This motion could be credited to mold the CNTs in this form. The spiral structure of CNTs is expected to have elastic properties and may be used to develop PAN/CNT composite nanofibers with elastic properties. Moreover, as the spiral is centered along the fiber axis, it is also expected to improve the strength of nanofibers.

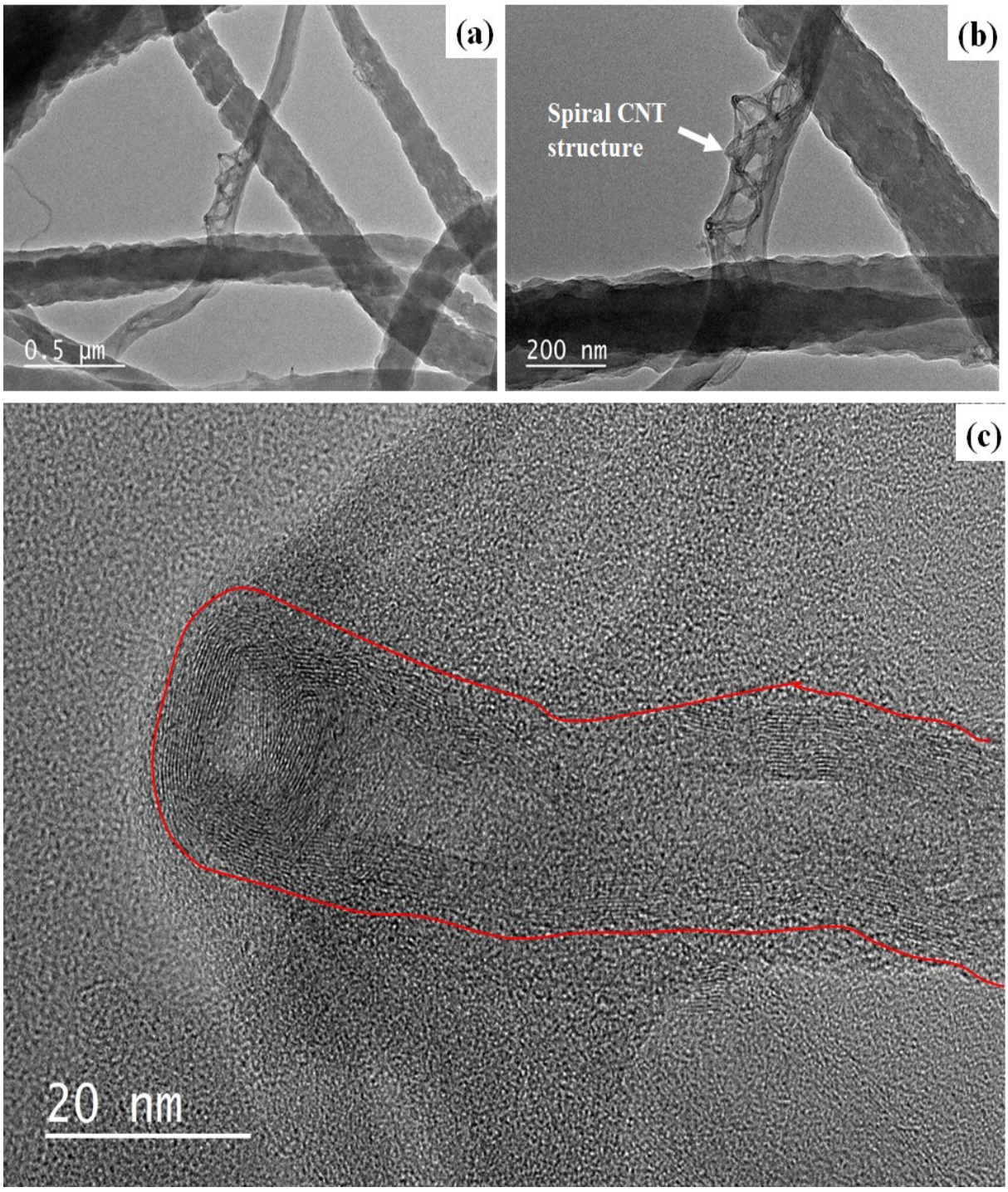

Figure 58: SEM images of PAN/CNT nanofibers with 3% CNT, from needleless electrospinning, at different magnifications

When the CNTs were loaded in PAN nanofibers, through electrospinning, it was observed that, under the conditions used in current study, CNTs were not only present inside the fibers but also at their surface (Figure 59). Moreover, comparison of structure of CNTs

before (Figure 56) and after electrospinning (Figure 57 to Figure 59) show that there is no change in crystallinity of CNTs after electrospinning.

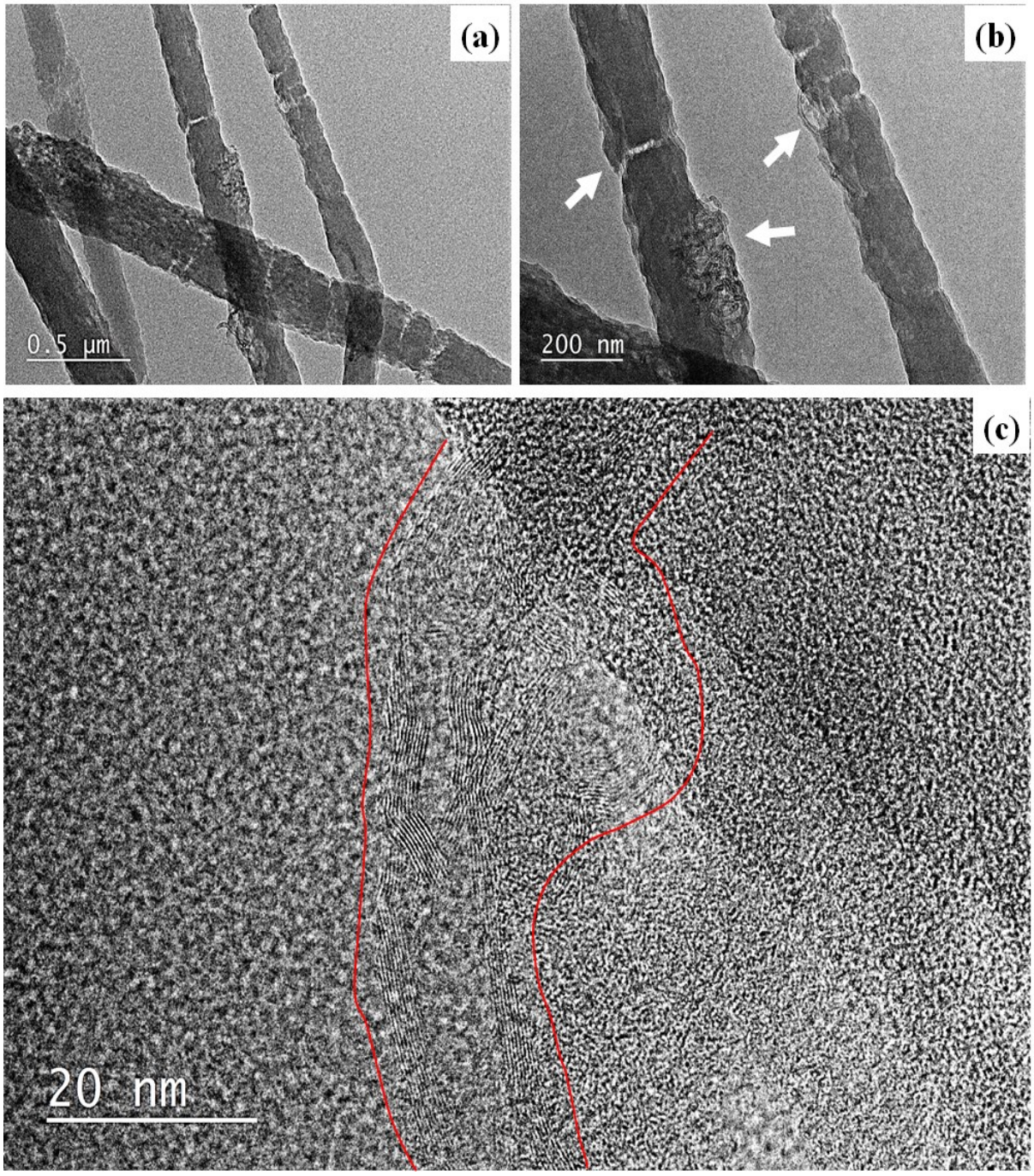

Figure 59: SEM images of PAN/CNT nanofibers, from needleless electrospinning, with 5% CNT, at different magnifications

Some of the CNTs were also found to have their end on surface of nanofibers, as shown by circular lines in Figure 57 and Figure 58. This property of PAN/CNT composite nanofibers has also been confirmed by some previous studies [278] as well as in current study for needle

electrospinning (Figure 60). Here, we proved that needleless electrospinning may be utilized to develop PAN/CNT nanofibers with CNTs on the surface. This supports the idea of using these fibers for all applications where presence of CNTs at surface is important, such as development of conductive nanowebs.

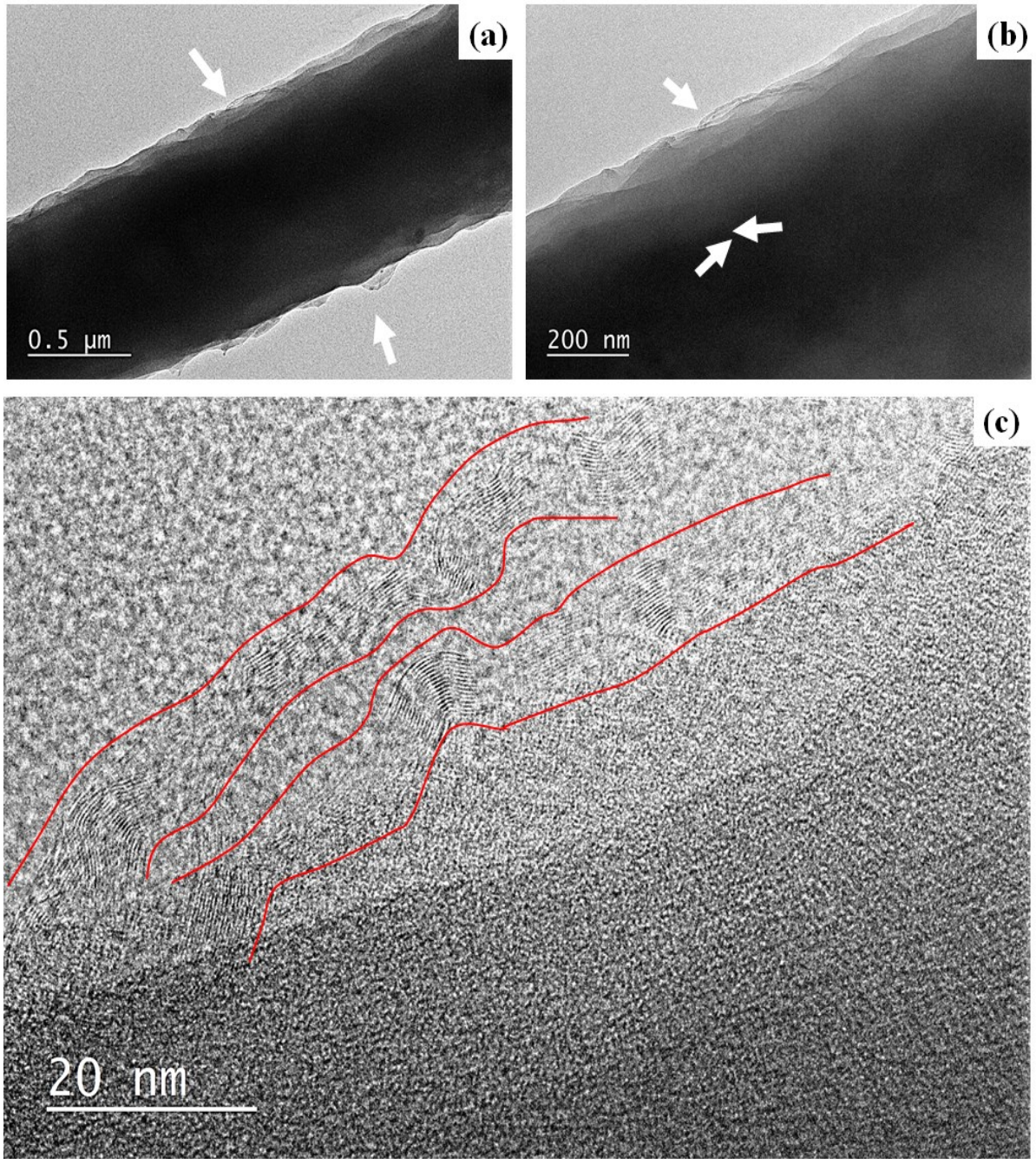

Figure 60: TEM images of PAN/CNT nanofibers from needle electrospinning, with 7% CNT, at different magnifications

So, from TEM analysis, it could be concluded that needleless electrospinning can be used to develop PAN/CNT composite nanofibers with conductive properties and improved mechanical properties.

4.3.2 Electrical conductivity

As for above study using TEM, electrical conductivity of PAN and PAN/CNT nanowebs was investigated, with focus on needleless electrospinning, as the project aimed to study the properties on needleless setups in correlation with conventional needle setups. However, for comparison, samples from needle electrospinning were also studied. The results of electrical conductivity, tested according to different procedures, mentioned in Chapter 3, have been summarized in Table 35. As the standard test procedure ASTM 257-61 recommends the measurements to be taken at 500V, all the samples were evaluated at this value. However, to mimic the commercial heating plates [282], some other setups (shown in Figure 33 and Figure 34) were also developed and tested using potential difference of only 10 V. So, all the readings were recorded at 10 V as well. It can be observed that all PAN and PAN/CNT nanowebs have very low conductivity. Though, the CNTs were found to be present on the surface of nanofibers, they are expected to be covered by a thin layer of polymer, thus insulating them from one another and leading to poor electrical conductivity. However, an increase in conductivity can be observed by addition of CNTs, which may be due to some occasional contacts between some exposed CNTs. For conductive PAN/CNT nanowebs, CNT contents in nanowebs may be increased above 7%.

Table 35: Conductivity of PAN and PAN/CNT nanowebs from needleless electrospinning

		Guarded electrode			
	C_{CNT} (%)	Surface conductivity (S/square)	Volume conductivity (S/m)	Conductivity with bridge tester (S/m)	Conductivity with plaster plate (S/m)
10 V	0	3.03E-10	8.36E-14	1.90E-07	2.54E-07
	3	4.55E-10	5.57E-14	1.90E-06	3.81E-06
	5	3.03E-10	8.36E-13	1.90E-06	1.90E-06
	7	2.27E-09	2.79E-13	4.57E-06	1.14E-06
500 V	0	3.64E-10	4.18E-08	1.69E-07	5.08E-08
	3	9.10E-09	1.11E-08	3.46E-06	1.52E-05
	5	3.03E-09	5.57E-09	2.24E-07	4.76E-05
	7	3.03E-09	3.72E-09	4.97E-06	2.86E-05

For comparison of electrical conductivity of samples from needleless electrospinning with those from needle electrospinning, the values recorded for nanowebs from needle electrospinning are summarized in Table 36.

Table 36: Conductivity of PAN and PAN/CNT nanowebs from needle electrospinning

	C_{CNT} (%)	Guarded electrode		Conductivity with bridge tester (S/m)	Conductivity with plaster plate (S/m)
		Surface conductivity (S/square)	Volume conductivity (S/m)		
10 V	0	1.30E-11	5.31E-14	2.00E-06	8.00E-06
	3	4.55E-12	5.31E-15	3.20E-06	2.96E-06
	5	4.55E-11	7.96E-14	2.86E-06	2.67E-06
	7	1.82E-10	1.59E-14	3.20E-06	3.33E-06
500 V	0	3.03E-11	1.59E-13	2.00E-06	2.00E-05
	3	3.64E-11	7.96E-15	2.86E-06	4.44E-05
	5	2.27E-11	1.99E-14	3.08E-06	2.00E-05
	7	3.03E-11	2.65E-14	3.81E-06	1.60E-05

From values in Table 35 and Table 36, it can be observed that nanowebs produced from needleless electrospinning have slightly higher conductivity than that for nanowebs from needle electrospinning. This may be reasoned to be due to greater presence of CNTs on surface of fibers for needleless electrospinning. The difference between mechanisms of the two techniques also supports this fact. For needleless electrospinning, the polymer is coated on wire electrode that repels the CNTs away from it (as CNTs acquire the same charge as that of wire), thus pushing them to surface of coated layer. However, during jet and nanofiber formation, some of CNTs may get covered by polymer layer thus reducing their overall surface presence. For needle electrospinning, the CNTs are pushed to center of needle hole, thus reducing their presence on surface of jet. However, again the jet gets modified due to stresses occurring during electrospinning. However, no proof for this proposed mechanism can be provided and further studies in this direction are needed.

4.3.3 Thermal conductivity

CNTs have been proved to carry extraordinary thermal conductivity properties [188, 206]. This characteristic of CNTs was explored in current study for development of PAN/CNT and CNF/CNT nanofiber composites, with improved heat conduction and thus better thermal uniformity throughout the mass. To evaluate improvement in thermal conductivity, PAN and

PAN/CNT nanowebs were tested and compared. The results of this testing are summarized in Figure 61.

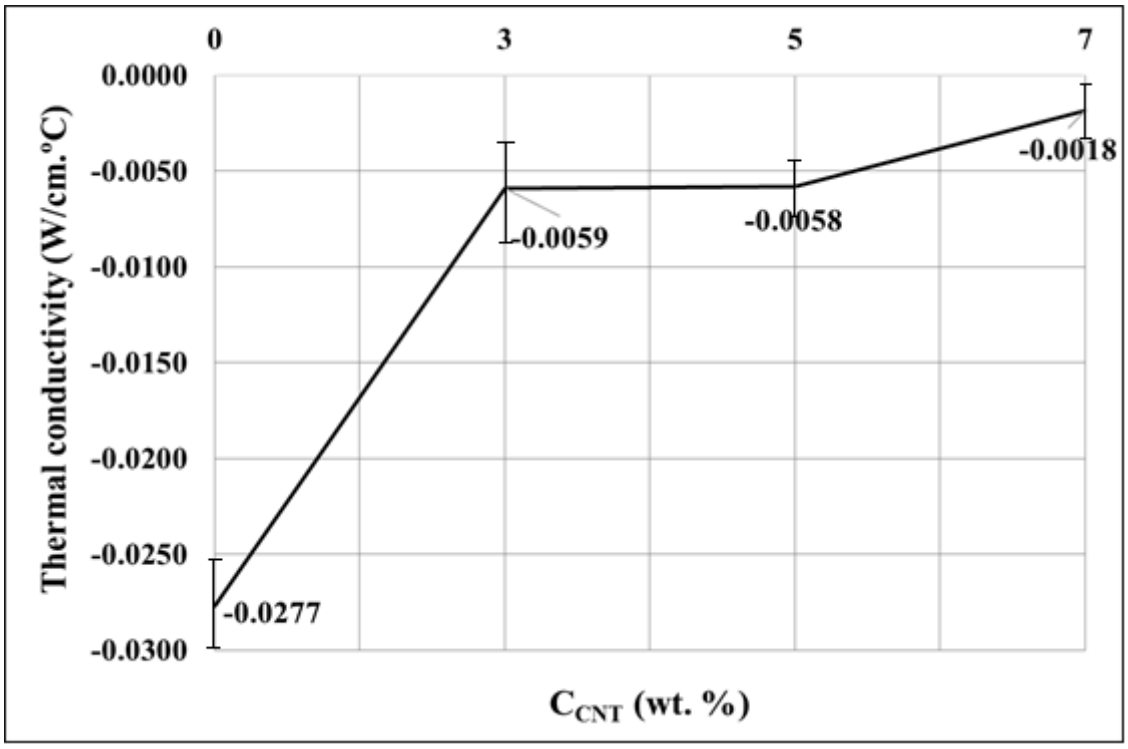

Figure 61: Thermal conductivity of PAN and PAN/CNT nanowebs with different CNT contents

Addition of CNTs was found to result in sharp increase in thermal conductivity. Moreover, higher concentration of CNTs lead to higher thermal conductivity, however, the increase of conductivity was not as high as observed when samples without CNTs and those with 3% CNTs were compared.

4.3.4 Thermal stability

4.3.4.1 TGA

Figure 62 shows TGA curve for pristine PAN nanofibers. The blue line shows the derivative curve and corresponds to the heat flow into the system. For example, glass transition temperature (Tg; a temperature above which the molecular chains in amorphous region have enough energy that can make them mobile) for pure PAN nanofibers occurs at almost 104 ºC, which is a typical temperature for PAN. It can be observed, from TGA plot (green line) in Figure 62, that there is an initial weight loss of almost 4% followed by a greater loss between 280 ºC to 320 ºC. [18, 136, 142]. This process results in many chemical changes in structure of

PAN, as discussed in section 2.5.2. The weight loss continues above this temperature up to 500 ºC. However, above this temperature, it was lower as most of non-carbon substances were removed. But still, there were some non-carbon entities that continued to leave the system up to 1300 ºC or even higher [149].

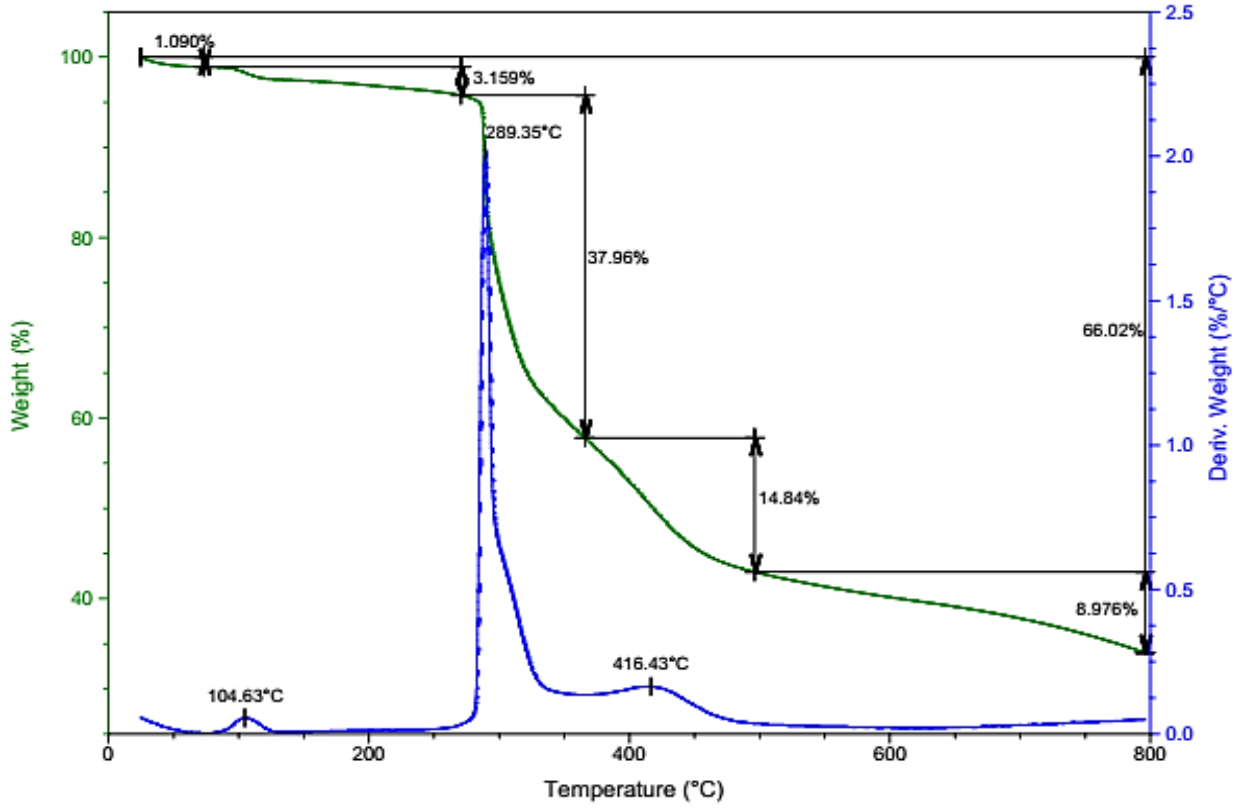

Figure 62: TGA curve for pristine PAN nanofibers

TGA plot for PAN/CNT nanofibers is shown in Figure 63. It can be observed that weight loss during stabilization was almost the same, as for pure PAN nanofibers. However, above 320 ºC, comparatively, lower weight loss occurred. This could be attributed to increased crystallinity due to CNTs in fibers. The total weight loss that occurred up to 800 ºC was 61.91% as compared to that of 66.02% for pristine PAN nanofibers. For CNT content of 5% and 7%, as well, the degradation weight was lower than that for pristine PAN as shown in Figure 64 and Figure 65. A slightly higher decrease in weight for PAN/CNT fibers with 5% CNT content was observed. However, this can be considered within the range of experimental error. It can be concluded that addition of CNTs results in improved thermal stability of PAN nanowebs. Comparison of heat flow and weight loss, during TGA, with reason of each change, is summarized in Table 37.

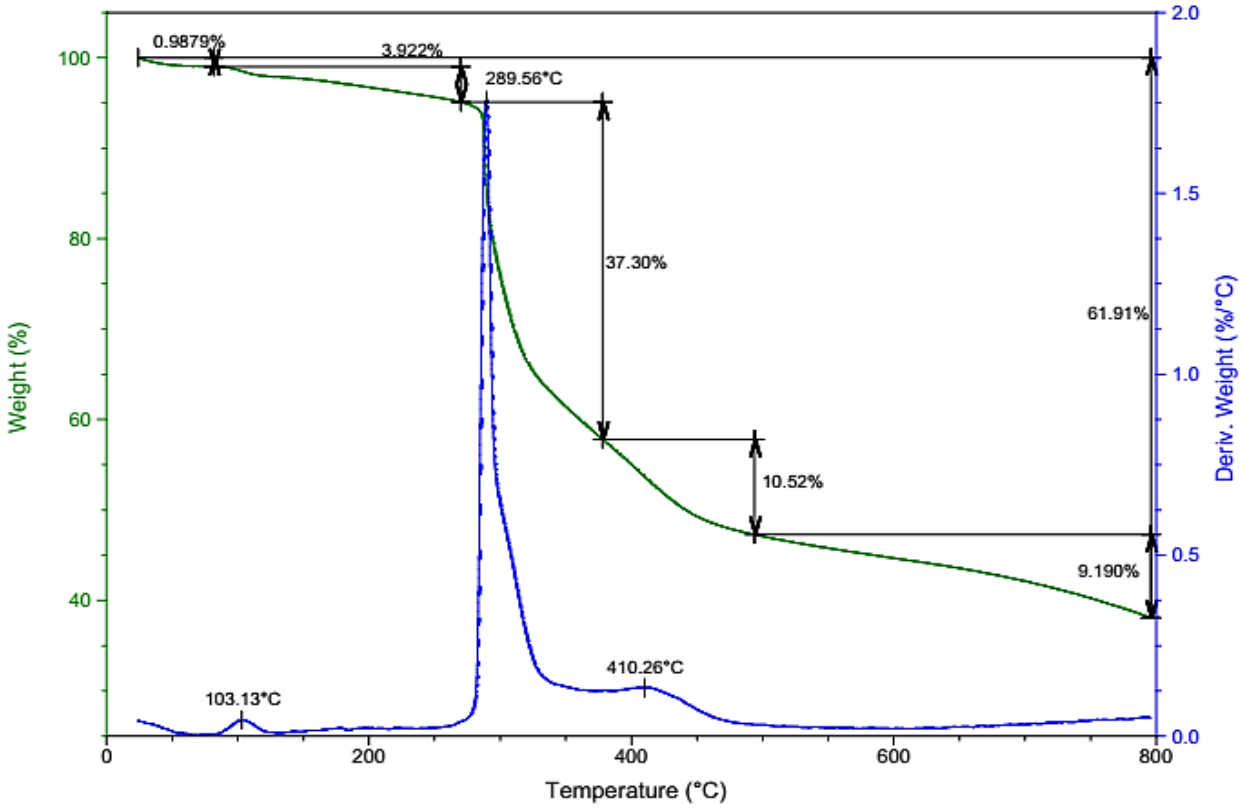

Figure 63: TGA curve for PAN/CNT nanofibers with 3% CNT contents

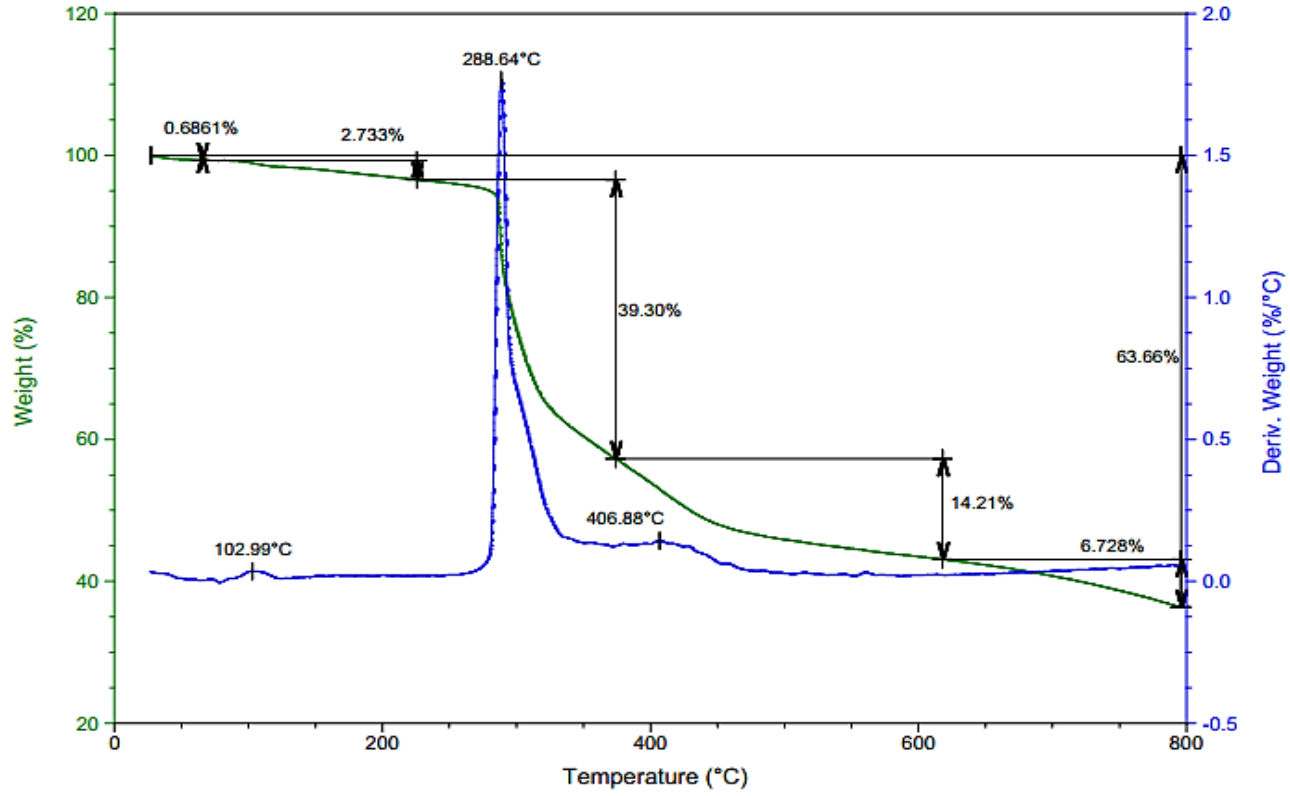

Figure 64: TGA curve for PAN/CNT nanofibers with 5% CNT contents

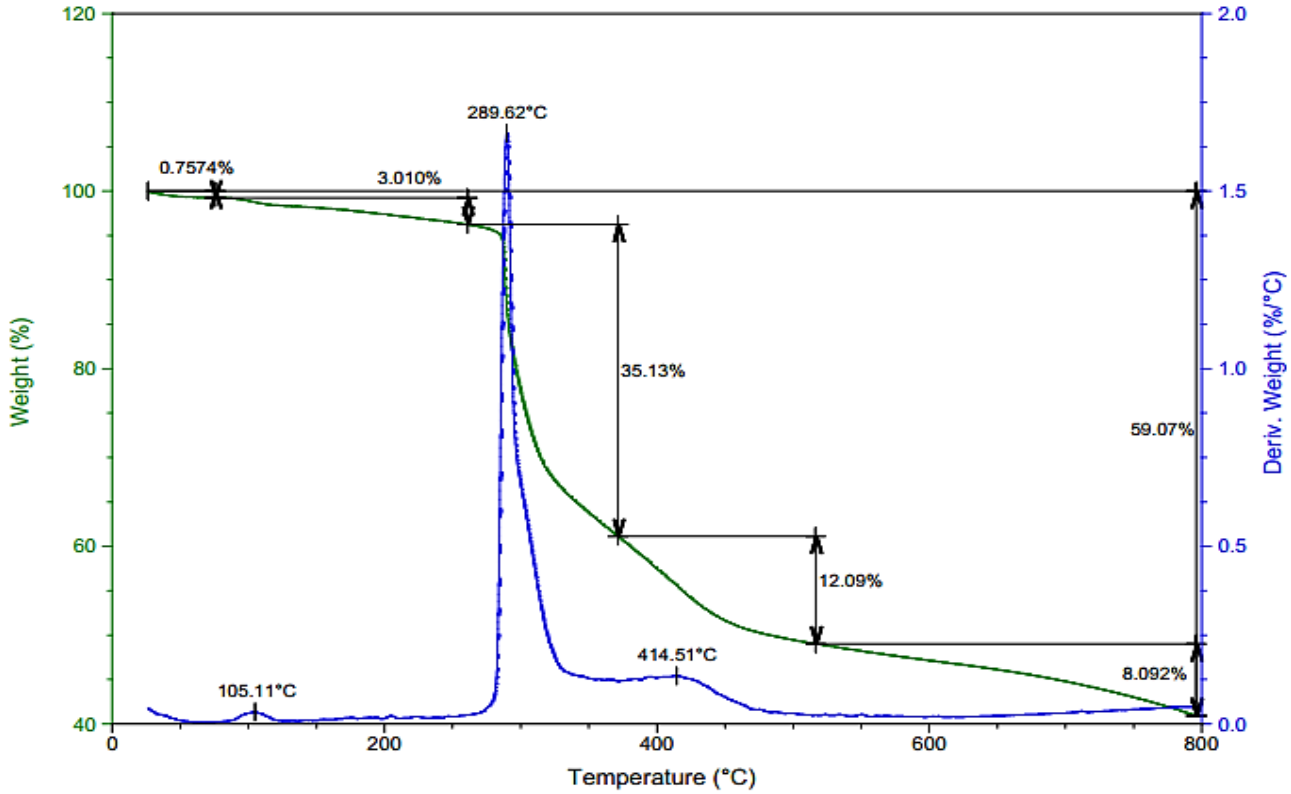

Figure 65: TGA curve for PAN/CNT nanofibers with 7% CNT contents

Table 37: Comparison of weight loss and heat flow during TGA

		CNT content in nanofibers				**Reason** [18, 136, 142, 283, 284]
		0%	***3%***	***5%***	***7%***	
Derivative weight (% / ºC)	*Peak 1*	104.6 ºC	103.1 ºC	102.9 ºC	105.1 ºC	Heat released during thermal transition at Tg
	Peak 2	289.4 ºC	289.6 ºC	288.6 ºC	289.6 ºC	Exothermic thermal degradation of PAN, with evolution of gases and cyclization
	Peak 3	416.4 ºC	410.3 ºC	406.9 ºC	414.5 ºC	Dehydrogenation and other cross linking reactions with evolution of NH_3 and HCN
Weight loss (%)	*Step 1*	1.1	0.9	0.7	0.8	Moisture evaporation
	Step 2	3.2	3.9	2.7	3.0	Solvent evaporation
	Step 3	37.9	37.3	39.3	35.1	Evolution of gases
	Step 4	14.8	10.5	14.2	12.1	Dehydrogenation reaction and other cross linking reactions
	Step 5	8.9	9.2	6.7	8.1	
	Total	66.0	61.9	63.66	59.08	-----

4.4 Heat generation through optimized carbonized PAN and PAN/CNT nanowebs

4.4.1 Properties of carbonized webs

The optimized PAN and PAN/CNT nanowebs were carbonized (after stabilization) for making them conductive. Carbonization was found to make the webs much weaker, as observed in previous studies discussed in section 2.5.4.2. This lower strength can be attributed to lack of sufficient crystalline regions, weight loss and lower fiber alignment, to name a few [18, 203].

Carbonization of PAN based nanowebs greatly decreased the diameter of nanofibers due to thermal shrinkage, that occurred during the process. This made the CNTs, embedded into PAN structure, more visible and susceptible to interaction with adjacent fibers for conduction of energy and electric charge. The decrease in diameter of nanofibers can be visualized in Figure 66 and the magnitude of decrease can be observed from Table 38. Carbon fibers without CNTs were found to show higher decrease in diameter as compared to those with CNTs. This could be credited to higher thermal stability of CNTs included in CNF/CNT composite nanofibers. It can be observed that there is a decrease in thermal shrinkage due to addition of CNTs.

When the optimized PAN and PAN/CNT nanowebs were carbonized, their electrical conductivity increased greatly (as expected). The values of conductivity for these nanowebs (with bridge tester, at 10 V) are shown in Figure 67. It can be observed that addition of CNTs, increases the conductivity. The conductivity of CNTs-incorporated webs was much higher than those without CNTs. This could be credited to superior conductivity of CNTs, as compared to that of fiber matrix [188].

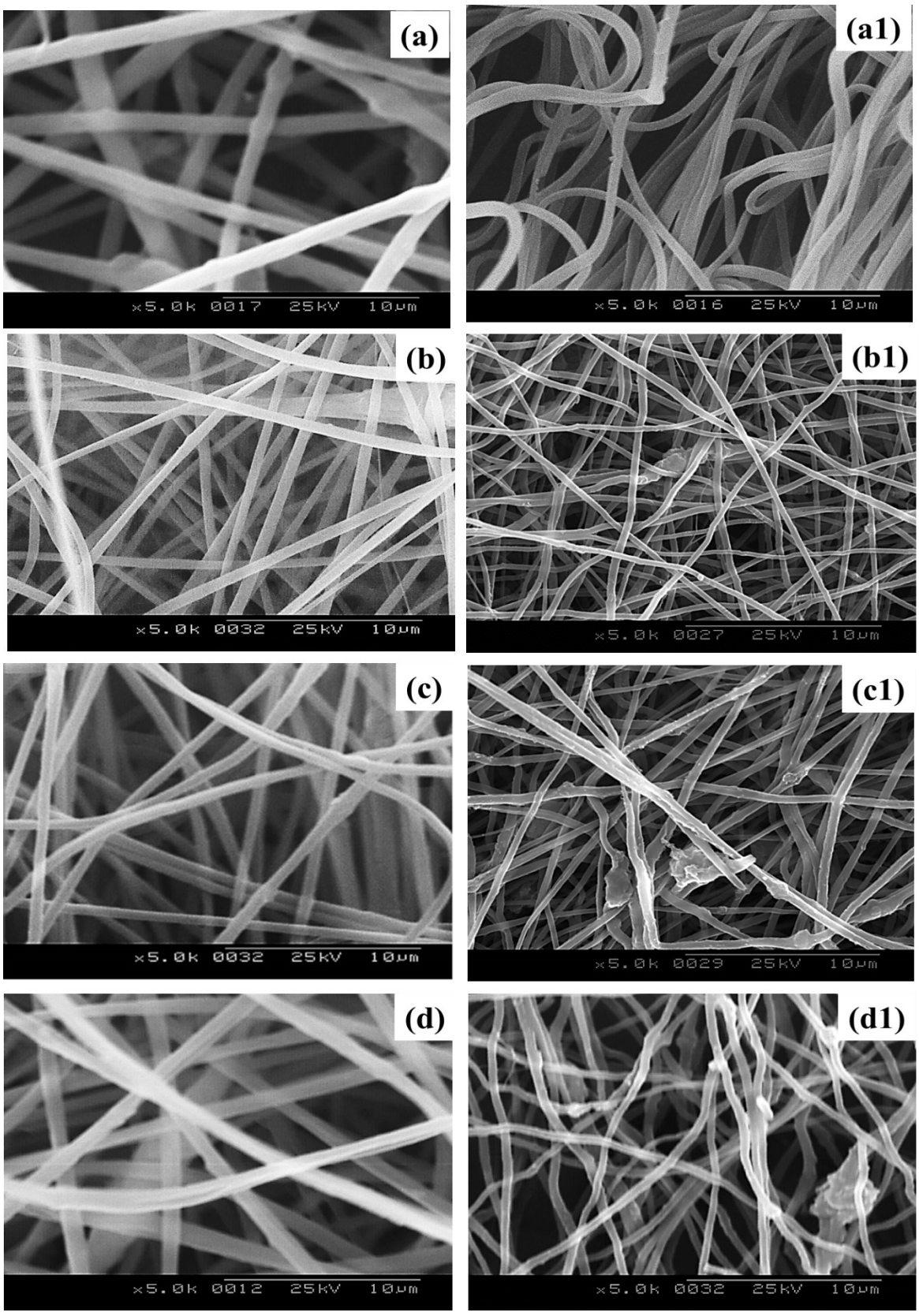

Figure 66: Comparison of (a,b,c,d) uncarbonized and (a1, b1,c1,d1) respectively carbonized PAN and PAN CNT samples with (a and a1) having 0% CNTs, (b and b1) with 3% CNTs, (c and c1) with 5% CNTs and (d and d1) with 7% CNTs

Table 38: Change in fiber diameter with carbonization

S.N.	CNT Content (%)	Fiber Diameter (Uncarbonized)	Fiber Diameter (Carbonized)	Difference (%)
1	0	1150	653	43
2	3	528	343	35
3	5	581	374	36
4	7	832	530	36

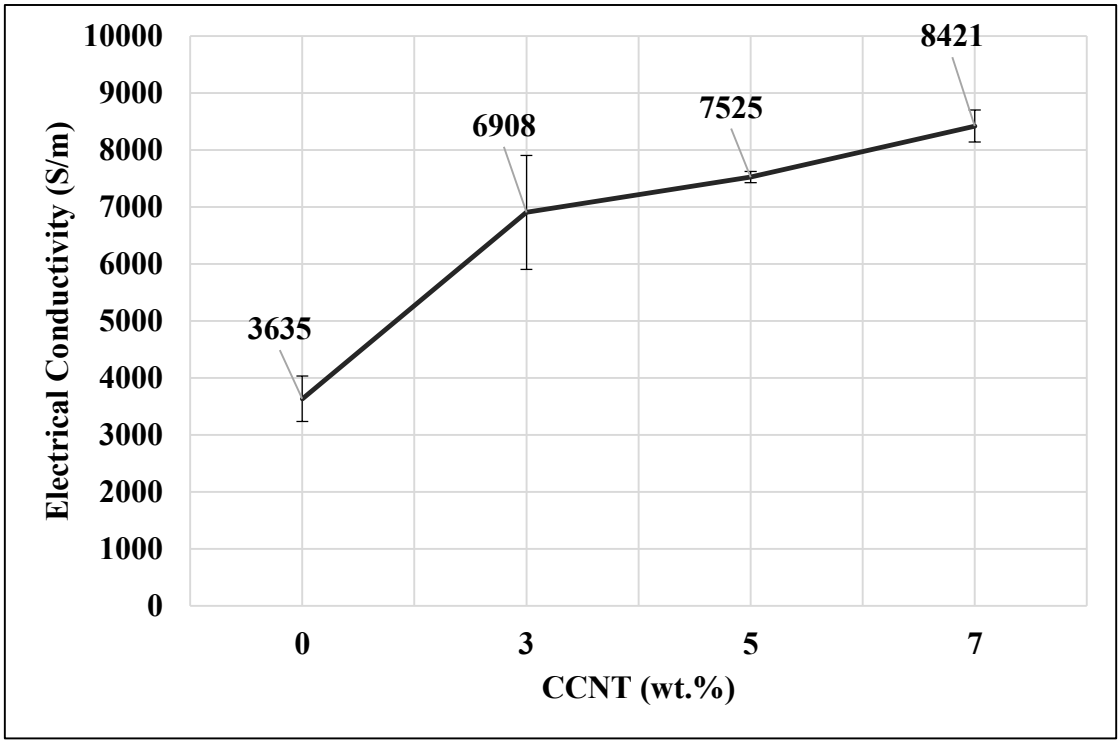

Figure 67: Electrical conductivity of carbonized nanowebs with different CNT contents (from bridge tester)

4.4.2 Heat generation with carbonized nanowebs

The carbonized nanowebs were used for generation of heat by application of voltage across their ends. This was accomplished by holding them between the jaws of bridge tester (shown in Figure 33) and applying different voltages between 10 to 40 V, across them. Voltage close to 40 V resulted in temperatures as high as 60 ºC. However, it was observed that values above 15 V degraded the webs and a visible arc was formed in them. However, this problem was not found when more than two webs were layered together. For comparison of heat generation, the webs were tested as a single layer in bridge tester. A voltage of 10 V was applied

for 5 minutes and the change in temperature was observed for 10 minutes, using a thermal imaging camera. It was found that the webs reached maximum temperature within 2 minutes after application of voltage, after which the temperature remained, almost, constant. The thermographs obtained for the four optimized nanowebs, at maximum temperature reached by each web, are shown in Figure 68.

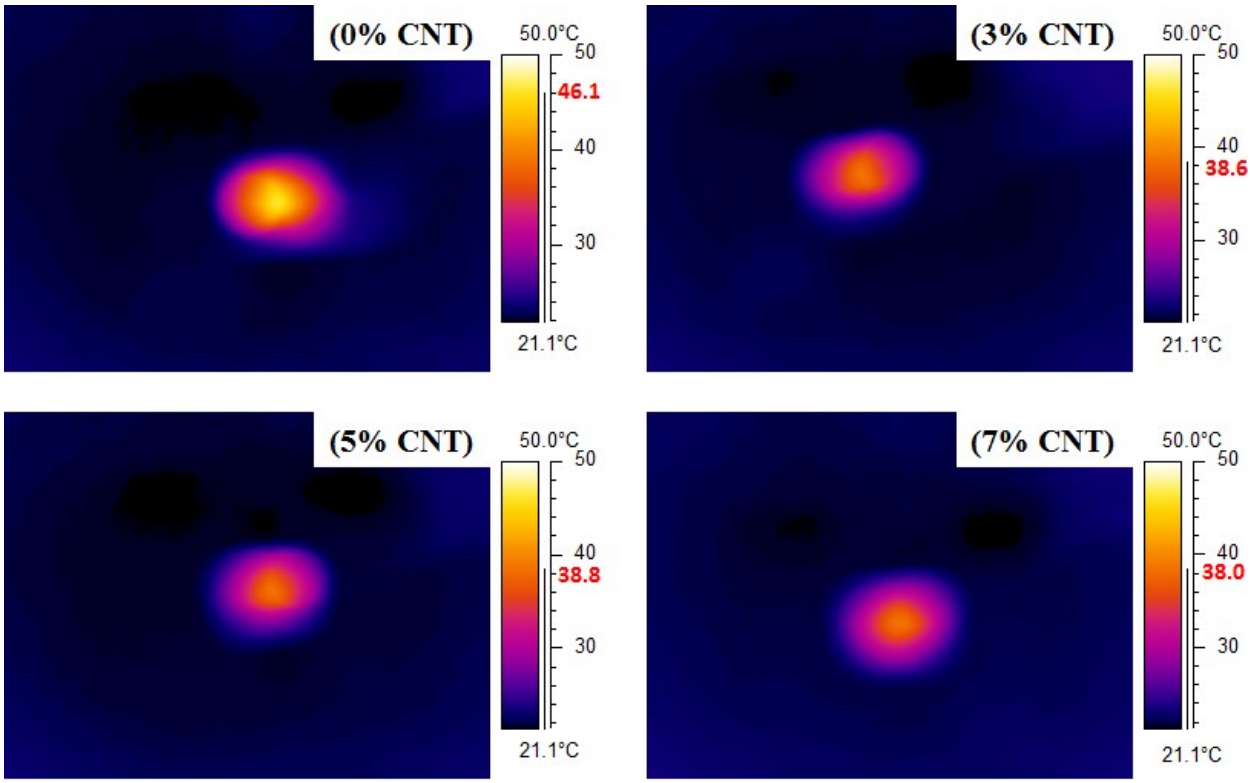

Figure 68: Comparison of thermographs obtained after application of voltage for 10 seconds and the maximum temperature reached within 5 minutes

From Figure 68, it can be observed that webs from pure PAN reached higher temperature than that achieved by those having CNTs. This could be due to lower resistance of CNT-incorporated webs (as shown by their higher conductivity in Figure 67), thus allowing lower heat to be produced. No significant difference of maximum achieved temperatures, between the webs with different CNT contents, was observed.

Although, almost all the CNF webs achieved the maximum temperature within 2 minutes, their heating profiles were different from one another. As shown in Figure 69, for CNF without CNTs, the temperature increased abruptly after remaining stable at values close to 25 ºC. This effect could be due to electrification process that may have taken longer time for pure CNF webs because of their higher resistance to flow of charge. While, smoother increase

in temperature was observed for nanowebs containing CNTs, with higher degree of uniformity, of heating profile, as the CNT content increased from 3% to 7%. This could be due to presence of CNTs, enhancing the flow of charge as well as heat. Particularly, flow of charge could lead to better electrification of webs, leading to better uniformity of heat generation with respect to time.

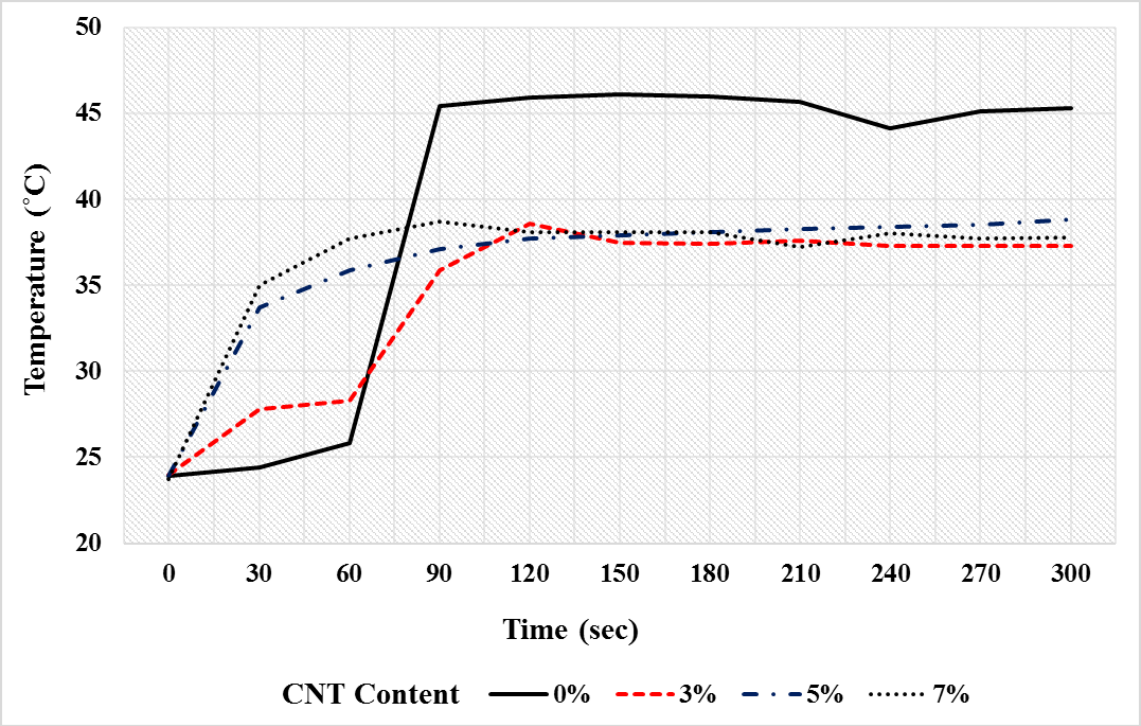

Figure 69: Comparison of heating cycle for carbon nanofiber webs with different CNT contents

The cooling cycle for nanowebs (at room temperature of 21 ºC) is described in Figure 70. Even though, the difference in cooling profiles is not too large, more uniform cooling cycle was observed for nanowebs containing CNTs as compared to those have no CNTs. Accordingly, higher CNT content was found to result in more uniform cooling cycle than that with low CNT contents. These effects could be ascribed to higher thermal conductivity due to higher CNT contents, leading to more uniform heat dissipation.

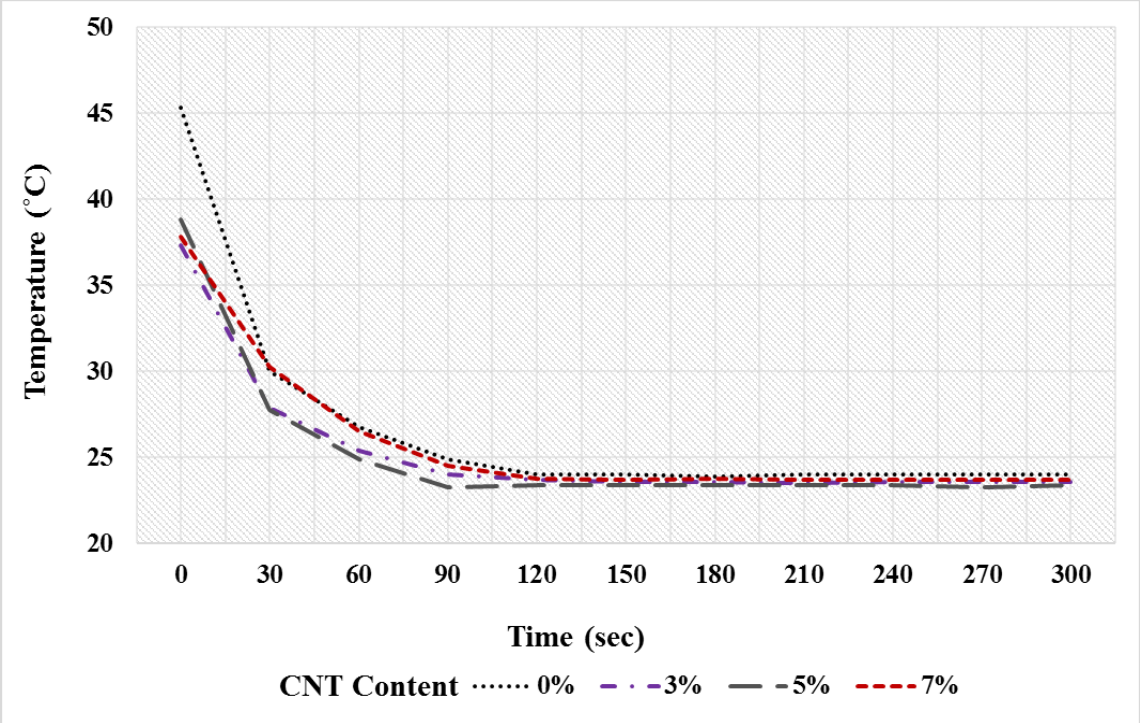

Figure 70: Comparison of heating cycle for carbon nanofiber webs with different CNT contents

Figure 71 compares the rate of change of temperature during first 2 minutes of heating and cooling cycles. It can be seen that increasing CNT content clearly increases the rate of increase in temperature for heating cycle. This could be due to better heat and charge flow in CNF containing CNTs, as compared to CNFs having no CNTs. For CNFs without CNTs, the rate was higher than that compared to CNFs with 3% CNTs. This effect could be due to contribution of abrupt increase in temperature to average value. Similarly, for cooling cycle, increasing the CNT contents, increased the rate of cooling, because of higher thermal conductivity and, thus, greater heat dissipation in webs having CNTs. This is due to higher thermal conductivity of CNTs, which allow for higher transfer of heat. However, the cooling rate was highest for webs without CNTs. This effect can be assumed to higher temperature achieved by these webs. This produced higher temperature gradient for such webs, with their surroundings, thus leading to larger heat flow as compared to cooler webs having lower temperature gradients.

It can be concluded, from above discussion, that addition of CNTs increases the heating and cooling rates of CNFs. Customized heating devices may be produced by adjusting the CNT

contents of CNF/CNT fibrous nanocomposites. These conclusions may be used for further studies and development of quick heating devices with uniform heating profiles.

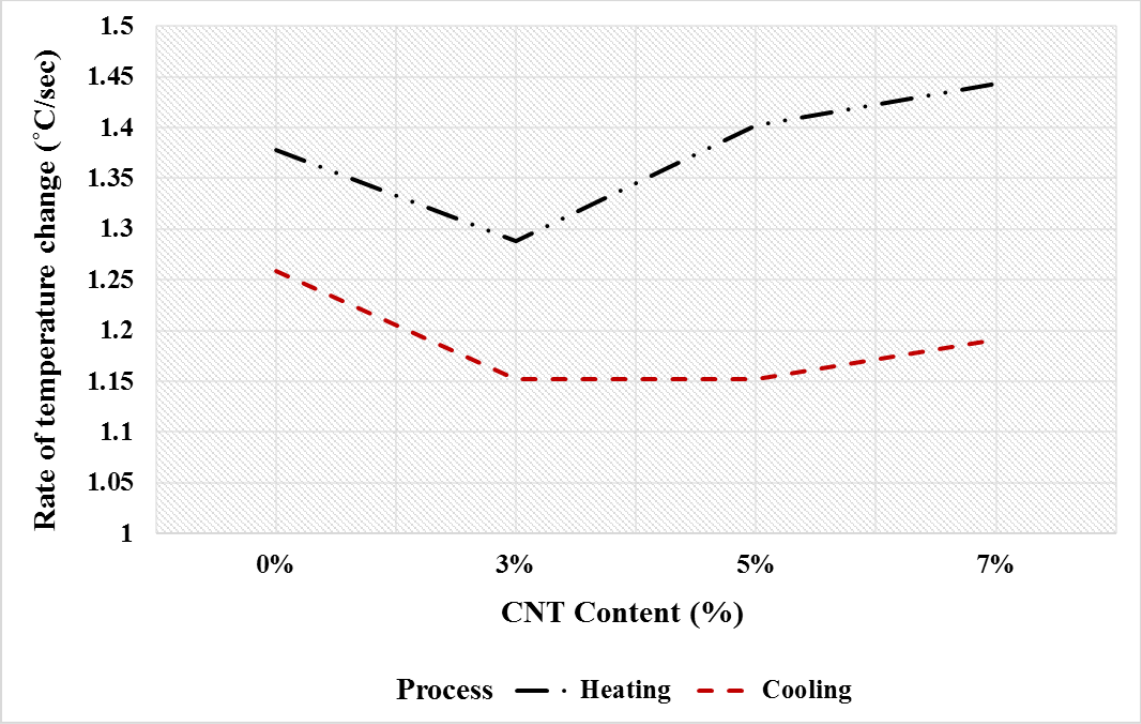

Figure 71: Comparison of rate of change of temperature during heating and cooling cycles

4.5 Optimization and modelling of electrospinning of PA-6 nanofibers

For development of optimized PA-6 nanowebs, for selected technical application i-e development of improved respiratory protection facemask filters, the electrospinning process was, first, optimized. This was accomplished, both, for needle and needleless electrospinning. For needle electrospinning, initially, full factorial experimental design was used. While, for needleless electrospinning Taguchi DOE was employed.

Taguchi DOE uses set of experiments within the full factorial design, that can effectively assess the effect of inputs on outputs. It omits the runs, in full factorial design, whose effect can be determined by other runs. This reduces the number of experiments to less than, even, half of that present in a full factorial design and produces the results almost as valid as produced by a full factorial design. Due to these facts, Taguchi has got special importance for different industrial processes. So, it was expected to be an effective tool for modelling and

optimization of electrospinning process, to optimize it on different industrial electrospinning setups [87, 88].

Taguchi design was included in this study as there were greater number of input parameters on needleless semi-industrial setup, that could have resulted in a bigger experimental design. So, a DOE with lower number of experiments was required. Taguchi DOE was expected to well serve this purpose, as it provides a smarter alternative, though, without a proper regression equation. However, the results can be predicted using the Taguchi DOE tool in Minitab software. To assess the validity of Taguchi methods for electrospinning in comparison to full factorial design, the method was, initially, evaluated on lab scale needle electrospinning, as it was not feasible to run a full factorial DOE on industrial machine.

4.5.1 PA-6 nanofibers from needle electrospinning

As mentioned above, both, the full factorial and Taguchi designs, were employed for modelling and optimization on needle electrospinning setup. Following sections discuss both these approaches, separately.

4.5.1.1 Statistical analysis using full factorial experimental design

The input parameters selected for full factorial design included concentration of PA-6 in its solution with formic acid, the voltage applied between the needle and collector and the distance between the two. The DOE developed for this purpose is tabulated in Table 39.

For determination of factors that affect the outputs, significantly, ANOVA was performed and is summarized in Table 40. It can be observed that P-value for effect of concentration and voltage is lower than (or equal to) 0.05, showing that they affect both the outputs, significantly. Additionally, for standard deviation in diameter, the product of concentration and voltage also showed a significant impact.

Table 39: Full factorial DOE for electrospinning of PA-6 nanofibers on needle setup with resulting diameter and its distribution

S.N.	C (w/w %)	D (cm)	V (KV)	Dia. (nm)	St. Dev. in Dia. (nm)
1	17	22	15	121	20
2	17	22	20	131	16
3	17	22	25	122	15
4	17	26	15	115	13
5	17	26	20	123	14
6	17	26	25	133	14
7	17	30	15	116	14
8	17	30	20	116	19
9	17	30	25	129	17
10	20	22	15	117	37
11	20	22	20	164	25
12	20	22	25	147	30
13	20	26	15	168	33
14	20	26	20	146	15
15	20	26	25	76	10
16	20	30	15	152	32
17	20	30	20	218	52
18	20	30	25	171	23
19	23	22	15	255	59
20	23	22	20	245	51
21	23	22	25	221	72
22	23	26	15	323	206
23	23	26	20	323	278
24	23	26	25	305	107
25	23	30	15	440	126
26	23	30	20	430	134
27	23	30	25	250	76

Table 40: ANOVA for full factorial design for effect of inputs on PA-6 nanofiber diameter and its distribution

S.N.	Term	P-value for Dia.	P-value for St. Dev. in Dia.
1	C	0.000	0.000
2	D	0.187	0.190
3	V	0.055	0.050
4	C×D	0.368	0.351
5	C×V	0.123	0.012
6	D×V	0.733	0.443

Main effect plots, for effect of above mentioned inputs on outputs, are shown in Figure 72.

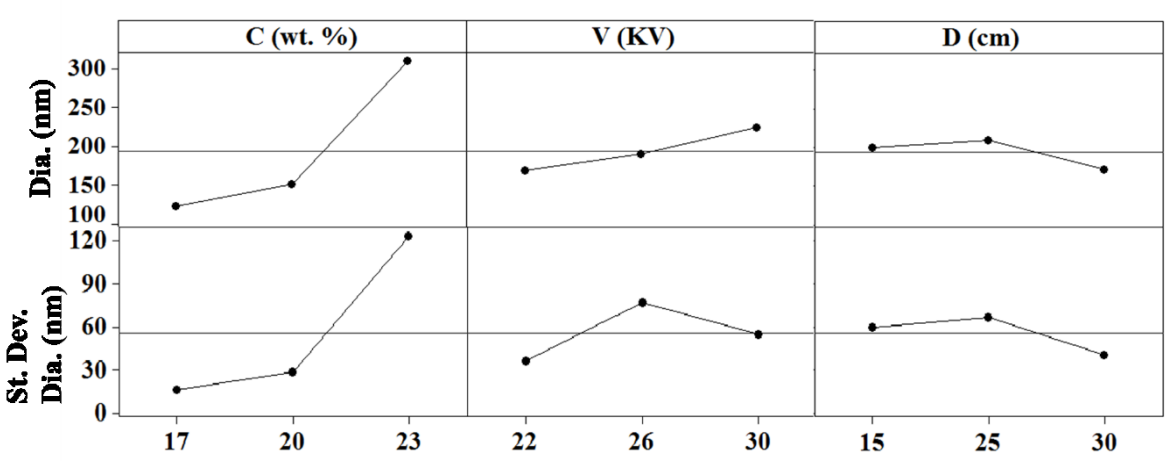

Figure 72: Main effect plots for effect of input parameters on diameter and its distribution

It can be observed that, as for PAN nanofibers, diameter of PA-6 nanofibers increased with increasing concentration of polymer solution; the reason being the same as discussed for PAN nanofibers. Increasing the voltage also resulted in higher fiber diameter, may be due to increased solution take up from the needle, as higher voltages produce stronger electrostatic pull on solution [9, 61]. The diameter of PA-6 nanofibers was found to decrease with increasing distance, as it leads to higher stretching of polymer jet before it reaches the collector [63].

Similarly, the variation in diameter also increased with increasing concentration, due to the reasons already discussed for PAN. Likewise, higher distance led to lower diameter distribution because of longer time for fibers to get uniform as they were stretched by electrostatic force [63]. However, the effect of voltage seems to follow a curve. The diameter distribution was found to, first, increase and, then, decrease with increasing voltage. This effect could be due to, larger electrostatic force on polymer solution at needle tip, thus increasing the chances of uneven take up of solution. Moreover, higher voltage could also have given lower time to jet to get uniform. On the other hand, higher voltage also increases the force to open the molecular entanglements and this effect may have become prominent after a critical level, while increasing the voltage, thus making the resultant fibers more uniform.

4.5.1.2 Statistical analysis using Taguchi experimental design

The Taguchi DOE, used for needle electrospinning is summarized in Table 41. It can be seen that some of experiments, present in full factorial DOE, were used for analysis as per Taguchi approach. Moreover, it can be seen that the DOE has only 9 runs that are much lesser that those for full factorial designs using same input parameters and their levels.

Table 41: Taguchi DOE for electrospinning of PA-6 nanofibers on needle setup with resulting diameter and its distribution

S.N.	C (w/w %)	D (cm)	V (KV)	Dia. (nm)	St. Dev. in Dia. (nm)
1	17	15	22	121	20
2	17	20	26	123	14
3	17	25	30	129	17
4	20	20	22	164	25
5	20	25	26	76	10
6	20	15	30	152	32
7	23	25	22	221	72
8	23	15	26	323	206
9	23	20	30	430	134

The ANOVA for Taguchi DOE is arranged in Table 42. It can be observed that only concentration of solution was found to affect the outputs, significantly. Also, ANOVA only shows main effect of parameters. This is because of lower number of experiments in Taguschi DOE that allow only the main effects to be studied, compared to response surface DOE, where second degree effects can also be studied, but with greater number of runs.

Table 42: ANOVA for Taguchi DOE for effect of inputs on diameter and its distribution

S.N.	**Term**	**P-value for Dia.**	**P-value for St. Dev. in Dia.**
1	C	0.043	0.095
2	D	0.285	0.583
3	V	0.196	0.409

The effect of inputs, as determined by Taguchi DOE, can be visualized by main effect plots for each of them, as shown in Figure 73. It can be observed that the trends are almost similar to those found for full factorial design. This confirms the effectiveness of Taguchi designs to study the effect of inputs and outputs for electrospinning process.

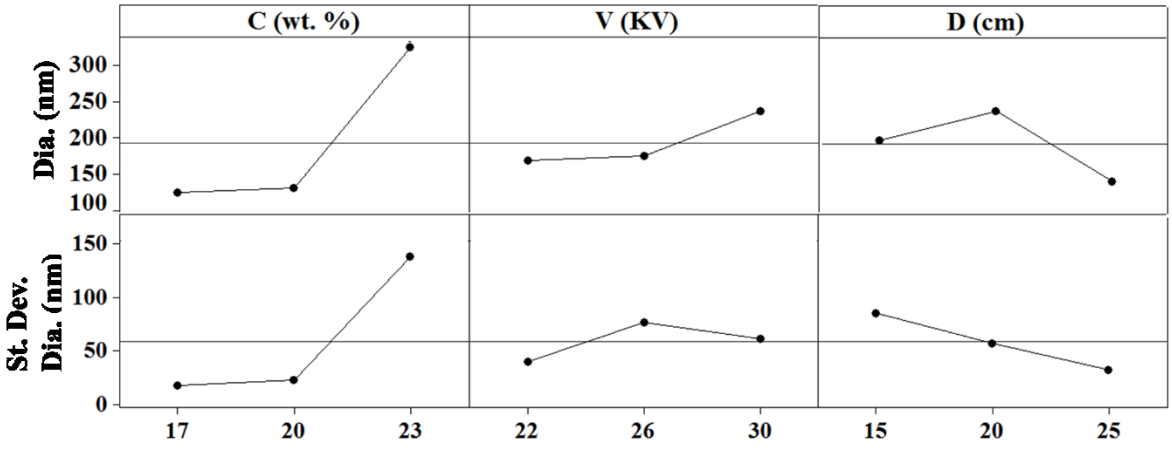

Figure 73: Main effect plots for effect of input parameters on diameter and its distribution

4.5.1.3 Optimization results and regression models for full factorial design

Selection of optimized parameters was made, keeping in view, the technical application for which they were produced i-e filter for face masks. It was expected to produce a web, that can screen out the particles, even with smallest size. This could be accomplished by development of nanowebs with very fine fiber diameter, thus, leading to a fine pore size capable of screen out a range of particle size. However, this can lead to higher pressure drop, that is expected to increase the breathing resistance. So, a balance has to be maintained between the two. Moreover, it was expected that sample should be free of defects, such as drops and beads as they can lead to some unexpectedly higher or lower efficiency.

For selection of optimized samples, the concentration level of 23% was omitted, as it resulted in fibers with ribbon like cross section and large diameter distribution. These defects were not observed in samples produced from PA-6 solution with concentration level of 17% and 20%. It was observed that nanowebs produced from 17% solutions were finer and hence can be expected to have finer pore size [285]. This could lead to better filtration efficiency but with higher pressure drop. On the other hand, samples produced from 20% solution had larger fiber diameter, and thus larger pore size. This was expected to reduce the drop in pressure but can also decrease the filtration efficiency. So, one sample from both these concentration levels was selected. It was observed that lower voltages resulted in solution drops on web, due lower force to handle the polymer flowing out of the needle. However, this problem was solved at shorter distances. The voltage value that worked well for all distance levels was 30 KV. To make the process robust, the value, selected, for distance was 15 cm. So, the optimized samples

were produced using 17% and 20% PA-6 solutions with applied voltage of 30 KV, at electrospinning distance of 15 cm. The average diameter for 17% PA-6 was 115.6 nm (St. dev., 14.3), while, for 20% solution, it was 152.4 nm (St. dev., 31.8). The SEM micrographs of these optimized samples are shown in Figure 74.

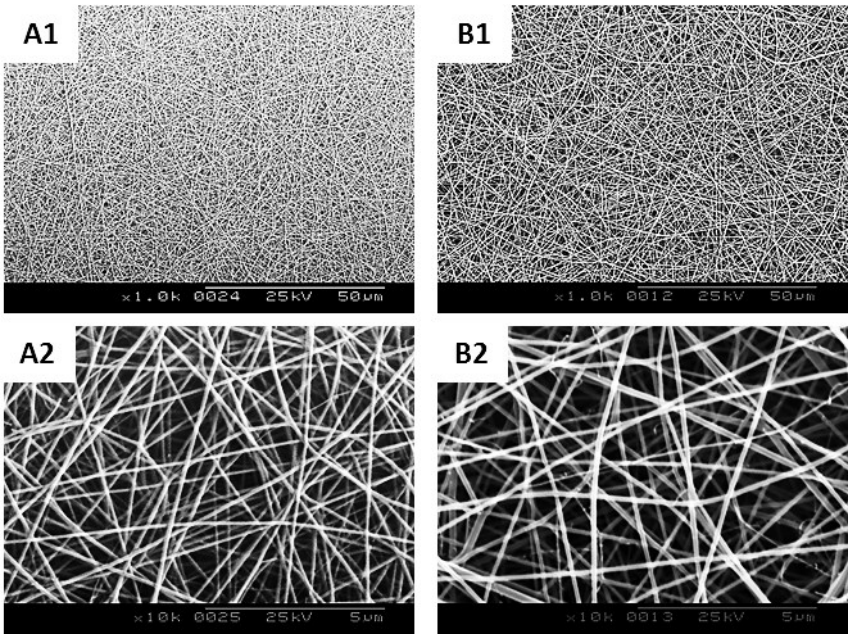

Figure 74: SEM micrographs of optimized samples with (A1, A2) 17% PA-6, and (B1, B2) 20% PA-6 (Upper row at magnification of 1 K and lower at 10 K)

The full factorial design was analyzed using the regression modelling tool in Minitab software and after removal of non-significant terms, the models so obtained are summarized in Table 43. The R-sq for the model for diameter was found to be 67.19%, that shows that it may be employed for prediction of diameter, however, with some error. While, R-sq for model for St. Dev. was very low and suggest that it doesn't represent, the data, well, and will give a large residual if used for prediction of St. Dev. in diameter.

Table 43: Regression model for diameter and its distribution for needle electrospinning of PA-6 nanofibers

S.N.	DOE	Regression model	R-sq
1	FF	Dia.= -611.3 + 31.2 C + 6.9 V	67.19%
2	FF	St. Dev. in Dia.= -362.1 + 17.9 C + 2.3 V	44.92%

The output of Taguchi design is in form of a response table that is based on Delta statistics i-e it assigns the ranks to input parameters with respect to the difference in values of

output at extreme levels of inputs. The input corresponding to maximum difference in output is ranked higher as compared to one producing lower difference in value of output. For example, for current data, the value of diameter at high and low values of concentration were 124 nm and 324.5 nm, with a difference if 200.5 nm (as shown in Table 44).

Table 44: Response table for Dia. and St. Dev. in Dia., as predicted by Taguchi DOE

			C	D	V
Dia.	Level	1	124.0	168.4	198.5
		2	130.8	173.9	238.8
		3	324.5	237	141.9
	Delta		200.5	68.6	96.9
	Rank		1	3	2
St. Dev. in Dia.	Level	1	16.94	85.88	39.27
		2	22.28	57.77	76.32
		3	137.46	33.02	61.07
	Delta		120.52	52.86	37.05
	Rank		1	2	3

This difference is highest as compared to that produced by different levels of needle-collector distance and applied voltage. So, concentration was ranked first, followed by applied voltage and distance between needle and collector. While, for St. Dev. in diameter, order of ranking was Concentration > Distance > Voltage.

The modelling results, obtained by using full factorial and Taguchi DOE, were assessed for their validity by carrying out some validation runs. The output of these runs were compared with those predicted by models and are summarized in Table 45.

Table 45: Validation of FF and Taguchi DOE for PA-6 nanofibers using needle setup

DOE	C (%)	V (KV)	D (cm)	Actual		Predicted		Absolute error (Dia.)	Absolute error (St Dev.)
				Dia. (nm)	St. Dev. (nm)	Dia. (nm)	St. Dev. (nm)		
FF	17	25	25	165	32	92	0	74	32
	20	28	22	338	108	206	60	133	47
	23	24	24	256	84	272	105	16	21
	20	27	25	249	57	199	58	50	1
Taguchi	17	30	15	116	14	173	9	58	6
	20	26	15	168	33	117	46	50	13
	23	30	15	440	126	374	167	66	41
	17	26	15	115	13	110	61	5	48

For Taguchi DOE, as there was no regression equation, the outputs were predicted by putting different set of input values from prediction experiment and comparing the results with those predicted by model. It may be noted that Taguchi analysis allows only the levels of inputs used for corresponding full factorial deign. So, separate prediction experiments were not needed and the model was assessed by using the values in 4 different runs from full factorial design, such that they were not present in Taguchi design.

For full factorial design, it can be observed that absolute error does not fall in the range of minimum St. Dev. shown in Table 39, thus the residual error for both the models is higher and may be taken into account if they are used for prediction of respective outputs. For Taguchi design as well, the absolute error is higher than the standard deviation shown in Table 41. However, it is similar to that observed for full factorial DOE, as it is a subset DOE of full factorial DOE. So, it may be concluded that Taguchi design can give acceptable results for prediction of, comparatively, linear relations. However, its main advantage is that it determines the magnitude of impact that each input puts on output. This allows to modify the process to get the optimized results with minimum number of inputs. So, it was decided to use Taguchi DOE for modelling and optimization of needleless electrospinning process, where greater number of parameters were to be studied.

4.5.2 PA-6 nanofibers from needleless electrospinning

4.5.2.1 Statistical analysis using Taguchi experimental design

For needleless electrospinning of PA-6 nanofibers, for face mask filters, six different parameters were selected, as they were expected to affect the properties of the nanoweb. They included solution concentration, distance between fiber generator wire and collector, applied voltage, speed of movement of polymer coating carrier (Cs), speed of substrate (Ss) and outward air flow through chamber (Af; inward flow was kept constant at 80 m^3/hr). The levels for each parameter were selected based on some pre-experimentation that led to an initial estimate of input values. Using these ranges of values, a DOE was developed using Taguchi design and is shown in Table 46. The ANOVA for these inputs is tabulated in Table 47.

Table 46: DOE for electrospinning of PA-6 nanofibers on needleless electrospinning

S.N.	C (%)	D (cm)	V (KV)	Cs (mm/s)	Ss (mm/min)	Af (m^3/hr)	Dia. (nm)	SD in Dia. (nm)
1	18	26.0	35	290	15	120	136	23
2	18	26.0	35	290	20	130	134	27
3	18	26.0	35	290	25	140	201	68
4	18	27.5	45	340	15	120	198	77
5	18	27.5	45	340	20	130	183	52
6	18	27.5	45	340	25	140	167	47
7	18	29.0	55	390	15	120	160	37
8	18	29.0	55	390	20	130	147	23
9	18	29.0	55	390	25	140	181	41
10	19	26.0	45	390	15	130	138	23
11	19	26.0	45	390	20	140	215	58
12	19	26.0	45	390	25	120	269	81
13	19	27.5	55	290	15	130	149	37
14	19	27.5	55	290	20	140	173	49
15	19	27.5	55	290	25	120	167	60
16	19	29.0	35	340	15	130	172	42
17	19	29.0	35	340	20	140	172	31
18	19	29.0	35	340	25	120	183	38
19	20	26.0	55	340	15	140	190	62
20	20	26.0	55	340	20	120	218	124
21	20	26.0	55	340	25	130	214	92
22	20	27.5	35	390	15	140	239	82
23	20	27.5	35	390	20	120	275	111
24	20	27.5	35	390	25	130	192	55
25	20	29.0	45	290	15	140	176	39
26	20	29.0	45	290	20	120	221	73
27	20	29.0	45	290	25	130	234	72

From ANOVA, it can be observed that, statistically, only concentration of solution poses a significant impact on diameter of nanofibers and its distribution. This reconfirms the comparative importance of solution concentration. While, for St. Dev. in diameter, even the effect of concentration is not significant. It shows that there are some other contributing factors that affected it, more strongly, than factors studied here. This leads to idea of extensive study in the field with larger number of input parameters.

Table 47: ANOVA for Taguchi design for effect of inputs on PA-6 nanofiber diameter and its distribution produced by needleless electrospinning

S.N.	Term	Dia.	St. Dev. in Dia
		P-value for Dia.	P-value for St. Dev. in Dia.
1	C	0.014	0.126
2	D	0.485	0.267
3	V	0.635	0.854
4	Cs	0.414	0.683
5	Ss	0.164	0.436
6	Af	0.123	0.272

To visualize the effects produced by each of the input parameters, their main effect plots are shown in Figure 75 and Figure 76.

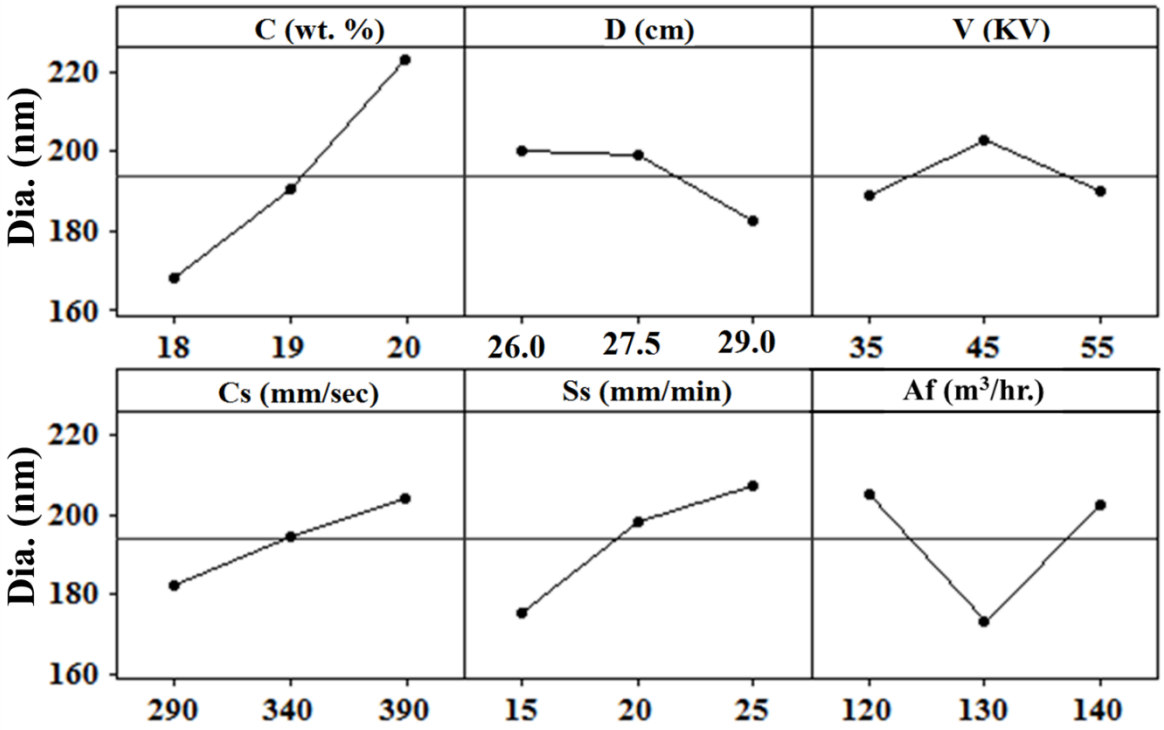

Figure 75: Effect of input parameters on diameter of PA-6 nanofibers

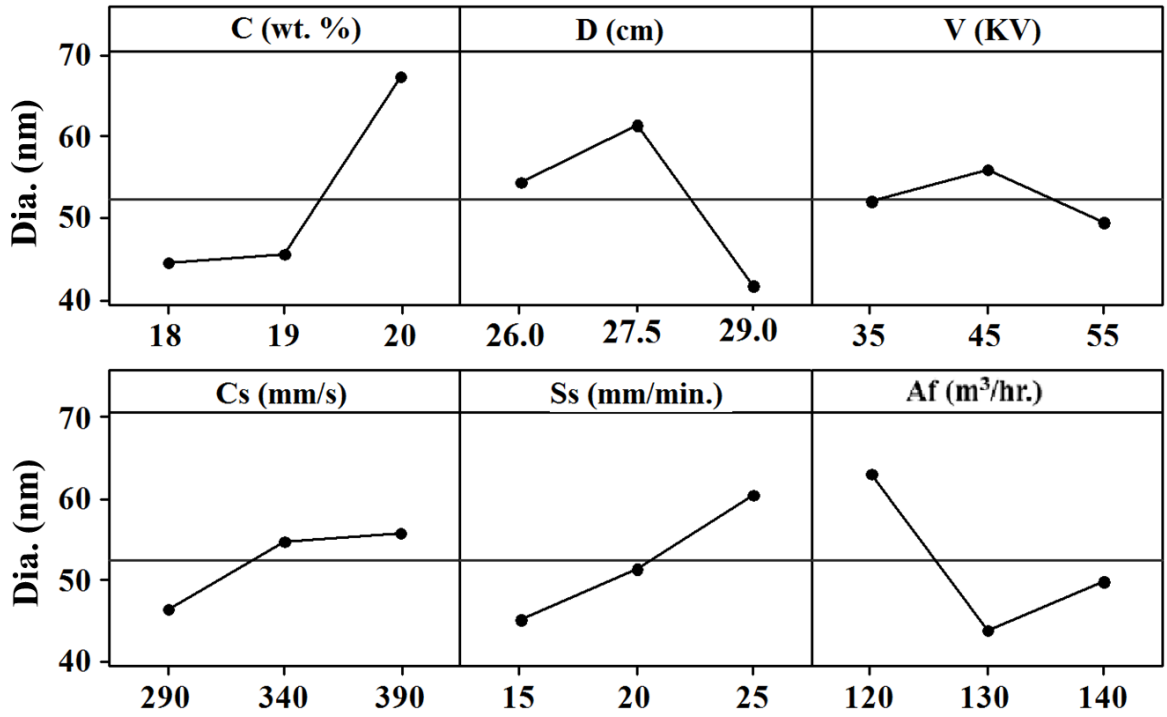

Figure 76: Effect of input parameters on diameter and St. Dev. in diameter of PA-6 nanofibers

It can be observed that higher concentration resulted in higher diameter and its distribution, due to the reasons already discussed in preceding sections and some previous studied on the subject [6, 51]. It can be observed that concentrations beyond an optimum limit produced larger variation in diameter. This could be attributed to higher increase in solution viscosity, above a certain concentration range, as discussed in section 2.2.1.1. Similarly, it could be observed that higher distance between the wire electrode and collector resulted in lower fiber diameter and its distribution. Higher decrease in diameter was observed as the distance between electrodes was increased beyond a critical level. This could be inferred to be due to solvent evaporation, that increases, greatly, due to initiation of bending instabilities. These instabilities cause much larger decrease in diameter after a critical fight time [18]. Nevertheless, increasing voltage was found to, first increase and then decrease the diameter, as well as its variation. As already discussed, this could be due to multidimensional effect of higher solution take-up and increased electrostatic forces on increasing the voltage [9, 10, 44, 58, 59, 61].

Higher carriage speed was found to increase diameter of nanofibers with a directly proportional relationship. The effect produced by higher carriage speeds can be considered to

be similar to that produced by higher feed rates in needled electrospinning. At higher carriage speeds, replenishment frequency of polymer coating increases, thus resulting in a thicker layer of solution and hence larger polymer take-up by electrostatic force. The variation in diameter was found to increase with increase in carrier speed [43-45]. This may be considered to occur because of improper drying in thicker jets, that are produced at higher carrier speed and lower smoothing effect of electrostatic force due to higher thickness of such jets [55, 60].

To the best of our knowledge, no significant work has been reported on the effect non-conductive substrate speed on the diameter of electrospun fibers. In the present work, the substrate speed was found to have a strong linear impact on fiber diameter such that by increasing the speed of substrate, the fibers turned coarser. This suggests that there are some factors, defined by substrate speed, that have a strong impact on diameter. In some previous works, it has been observed that higher charge density, as a result of lower charge drainage on non-conductive substrate, decreases the number of fibers or their density on such collectors due to repulsive forces and decrease in potential difference between the emitter and collector [286, 287]. For certain polymers, the fibers collected on a substrate are known to carry a charge as high as 1 kV, even after 20 hours [287]. Moreover, it has been found that growing deposition of charged fibers increases the overall charge of deposited fibers [288]. In current study, moving substrate out of the electric field can be expected to have reduced the growth of charge on it by reducing the deposition of nanofibers at a single location. So, at higher substrate speed there was higher decrease in rate of charge growth. This means an increase in potential difference occurred, leading to a lower repulsion to on-flight fibers from charges on collected fibers, thus decreasing the flight time and hence the drawing during shorter time for bending instability to operate. Moreover, it also leads to higher polymer solution take-up from fiber generator wire. For lower substrate speeds, larger amount of charge accumulation on substrate and collected fibers takes place thus repelling the incoming fibers and causing them to “fly” for longer time and getting more stretched. However, more work in area is needed to confirm these observations and authors intend to carry out these studies in near future.

The effect of air flow is quite complex. Increasing air flow can be expected to enhance evaporation of solvent, thus allowing the bending instabilities to operate earlier. This may result in thinner fibers (due to higher solvent evaporation [70, 71]). On the other hand, it also increases the viscosity of solution present on wire electrode thus increasing diameter of the

solution jet and thus that of fibers. From Figure 75, it can be observed, that the diameter of fibers was decreased below air flow of 130 m^3/hr., beyond which it started to increase.

4.5.2.2 Optimization results and model validation

From Figure 75, it can be observed that diameter of PA-6 nanofibers, produced by needleless electrospinning, is mostly defined by concentration of solution. So, it was used as basic parameter for defining the optimized conditions for electrospinning. It can be observed that concentration level of 20% produced much higher variation in diameter of fibers. So, it was omitted, and the experimental runs containing only 18% and 19% PA-6 solutions were considered for optimized settings. However, some of the trends may also be studied using 20% solution concentration. Both these concentration levels produced fibers below 200 nm. So, the optimized samples from both these were sorted out. This also allowed to have filters with different filtration efficiency and pressure drop. Within these concentration range, no defects such as drops and beads were observed. However, considerable change in variation in diameter was observed. The samples selected as optimized samples were those against S.N. 1 and 10 in Table 46. The SEM images of these samples are shown in Figure 77. The mean fiber diameter for these samples was 135.8 nm and 268.5 nm. However, as the samples within the optimized concentration range were free from other defects, all of them were considered for study of performance and comfort properties of the filters obtained from them.

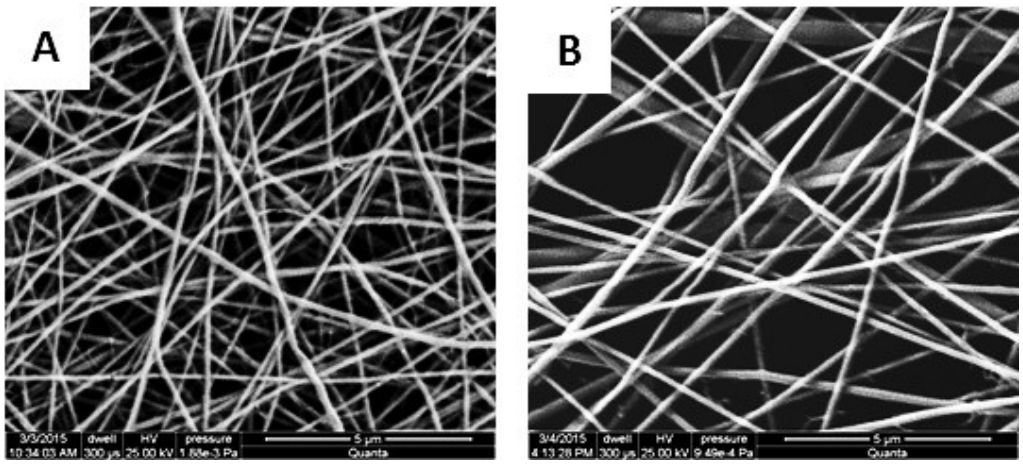

Figure 77: SEM micrographs of optimized samples with (A) 18% and (B) 19, at magnification of 12.5 K

As mentioned earlier, Taguchi approach do not generate a regression equation. Instead it gives rankings to different terms in form of response table, while the prediction may be done

using the Minitab software itself. For current part of study, the response table for diameter and its distribution is shown in Table 48. It can be observed that effect of concentration is ranked first, both for diameter and its distribution, and effect of voltage on diameter and its distribution is ranked last. The results obtained by Taguchi DOE analysis were validated by 4 experimental runs. The values for diameter obtained from these runs were compared with that predicted by Taguchi model, through Minitab software. The comparison of actual and predicted results is shown in Table 49. It can be observed that the absolute error for diameter is very close to the minimum variation in diameter (22.8 nm), shown in Table 46. This suggests that the model predicted the values very close to that obtained by actual experiments. Considering, even the minimum standard deviation, the model performed quite well and may be used for prediction of results for future studies.

Table 48: Response table for Dia. and St. Dev. in Dia., as predicted by Taguchi DOE

			C	D	V	Cs	Ss	Af
Dia.	Level	1	168	200	189	182	176	205
		2	190	200	203	194	198	173
		3	223	182	190	204	207	203
	Delta		54.6	17.7	14.1	22	31.8	32.1
	Rank		1	5	6	4	3	2
St. Dev. in Dia.	Level	1	44	54	52	46	45	63
		2	46	61	56	55	51	44
		3	67	42	49	56	61	50
	Delta		22.8	19.7	6.6	9.5	15.5	19.4
	Rank		1	2	6	5	4	3

Table 49: Validation of Taguchi DOE for PA-6 nanofibers using needle electrospinning

C (%)	V (KV)	D (cm)	Cs (mm/s)	Ss (mm/ min)	Af (m^3/hr)	Actual		Predicted		Absolute error (Dia.)	Absolute error (St Dev.)
						Dia. (nm)	St. Dev. (nm)	Dia. (nm)	St. Dev. (nm)		
18	29	35	390	15	140	141	28	153	27	12	1
20	26	55	290	25	120	276	122	239	79	37	43
19	27.5	45	340	20	130	170	33	189	51	20	18
20	29	35	390	15	140	210	100	208	50	3	50

4.5.3 Respiratory protection through PA-6 coated nonwoven filter media

According to the standard selected for current work, i-e EN 149 +A, the performance of a face mask filter is assessed by its efficiency to block particulate species (paraffin mist in this case) along with the resistance it offers during inhalation and exhalation. The resistance is evaluated by pressure drop across filter, when air is passed through it, at different rates. Numerical values for all these properties, for a range of filters containing nanowebs (sandwiched between nonwoven layers) are shown in Table 50. The samples are numbered according to serial number mentioned in Table 46, with results for a sample (denoted by "0") that contains no nanoweb. The bottom row of table gives the minimum requirements to be met according to the standard followed. The highlighted rows show the results for samples that conform to the minimum limits prescribed by EN 149 +A. It may be noted that paraffin screening properties of these samples is, exceptionally, high.

Table 50: Performance properties of nonwoven filters containing nanowebs

			Paraffin penetration (%)		Inhalation pressure drop (mB)		Exhalation pressure drop (mB)	
S.N.	Mean Dia.	St. Dev. in Dia.	Initial	Maximum for 120 mg Paraffin	Inhalation at 30 L/min	Inhalation at 95 L/min	Exhalation at 85 L/min	Exhalation at 160 L/min
0	--	--	1.705	2.457	0.267	0.843	0.732	1.336
1	135.8	22.8	0.28	0.383	0.595	1.859	1.608	2.943
2	134.3	26.6	0.262	0.416	0.481	1.503	1.311	2.398
3	200.8	68.0	0.363	1.134	0.438	1.367	1.192	2.19
4	197.7	77.0	0.159	0.28	0.742	2.316	2.026	3.78
5	183.4	52.3	1.105	2.103	0.374	1.176	1.028	1.887
6	167.4	47.0	1.075	1.606	0.315	0.979	0.834	1.512
7	160.4	37.0	0	0	0.696	2.179	1.876	3.431
8	146.8	23.3	0.246	1.278	0.595	1.851	1.058	2.877
9	180.6	40.7	0.277	1.122	0.567	1.777	1.509	2.76
10	138.1	23.3	0.106	0.875	0.782	2.44	2.068	3.765
11	215.3	58.3	0.213	2.059	0.657	2.054	1.794	3.3
12	268.5	80.6	0.349	1.124	0.498	1.569	1.386	2.544
13	148.9	36.9	0.076	0.535	0.897	2.851	2.416	4.428
14	173.1	48.7	0.243	1.146	0.599	1.884	1.595	2.912
15	167.4	59.6	0.37	1.047	0.492	1.531	1.294	2.374
16	172.0	41.5	0.339	1.052	0.472	1.465	1.293	2.374
17	171.7	30.8	0.531	1.139	0.402	1.248	1.095	1.997
18	182.8	38.2	0.66	1.146	0.354	1.101	0.953	1.729
FFP2 Limit (EN 149 +A)			6.00	3.00	0.70	2.40	1.20	3.00

4.5.3.1 Effect of inputs on filtration performance

To determine the effect produced by inputs on different filtration performance properties, correlation analysis was performed using Minitab software and is summarized in Table 51. Each analysis cell shows two values i-e Pearson correlation coefficient (top) and P-value (bottom). Pearson correlation coefficient (Annex I) gives information about the impact of factor on response and P-value signifies its importance [289]. In current study, only applied voltage and speed of substrate affected the outputs significantly, as reflected by their P-value (less than 0.05). The significant terms are highlighted in Table 51.

Table 51: Correlation analysis of different factors in filtration properties

Properties	C	D	V	Cs	Ss	Af	Dia.	St. Dev. in Dia.
Initial Penetration of Paraffin	-0.165 0.512	0.111 0.662	-0.282 0.257	-0.093 0.714	0.492 0.038	0.204 0.418	0.139 0.584	0.113 0.654
Max. Penetration of Paraffin	0.183 0.466	-0.032 0.901	-0.018 0.944	0.224 0.371	0.506 0.032	0.527 0.025	0.38 0.12	0.223 0.375
Inhalation at 30 L/min	0.126 0.617	-0.161 0.522	0.488 0.04	0.13 0.608	-0.672 0.002	-0.176 0.484	-0.217 0.386	-0.111 0.661
Inhalation at 95 L/min	0.129 0.609	-0.163 0.517	0.492 0.038	0.122 0.63	-0.667 0.002	-0.174 0.491	-0.213 0.396	-0.107 0.672
Exhalation at 150 L/min	0.12 0.635	-0.177 0.483	0.461 0.054	0.128 0.612	-0.681 0.002	-0.191 0.448	-0.175 0.488	-0.068 0.788
Exhalation at 85 L/min	0.191 0.448	-0.254 0.31	0.37 0.131	0.044 0.862	-0.663 0.003	-0.181 0.472	-0.121 0.632	0.003 0.992

It was observed that increasing the applied voltage for electrospinning, increased the drop in inhalation and exhalation pressures. This was indicated by a positive value for Pearson correlation coefficient (showing a direct relationship) and is also shown in Figure 78. This increase in pressure drop can be inferred to higher compaction of nanowebs due to increased electrostatic force at higher voltages. Thus producing a denser web with more resistance to inhalation and exhalation.

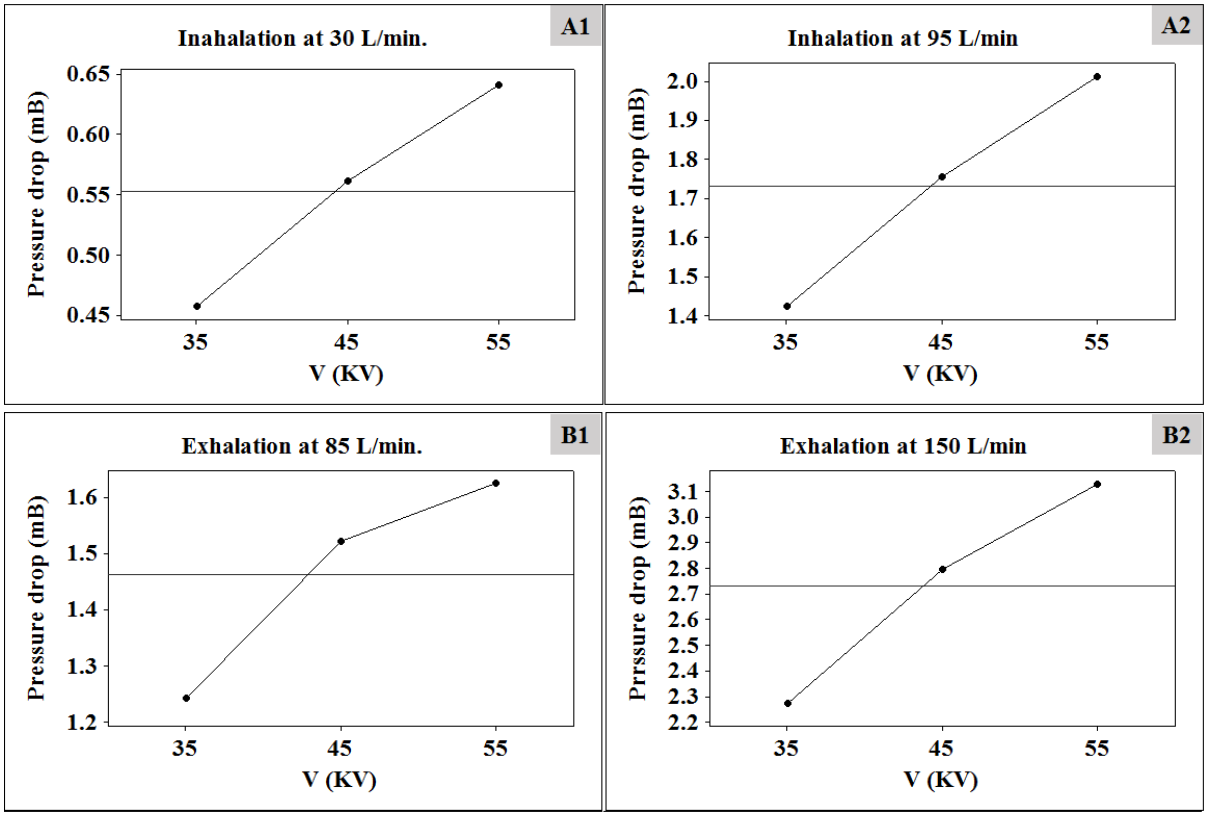

Figure 78: Correlation of electrospinning voltage with filtration properties

Speed of movement of substrate was found to influence all the filtration properties. As already discussed, higher substrate speed could lead to lower buildup of static charge on collected nanofibers. This may result in formation of nanowebs with higher fiber diameter and pore size, which allow more paraffin mist to pass through it, as shown in Figure 79 (A1 and A2). Due to the same reason, i-e higher pore size, decreased pressure drop could also be expected, as shown in Figure 79 (B1, B2, C1 and C2).

Even though, the secondary input parameters, i-e diameter and its distribution were expected to, systematically, affect the filtration properties, as discussed in section 2.6.4.1.4 and some previous research studies [179, 259], these affects were not significant for current study. This can be confirmed by P-value in Table 51. However, some combinations of diameter and its distribution were found to impact the paraffin filtration more strongly than others. Nevertheless, study of diameter and its distribution may be carried out with better group of their values, according to a predefined DOE, so as to consider them as primary inputs.

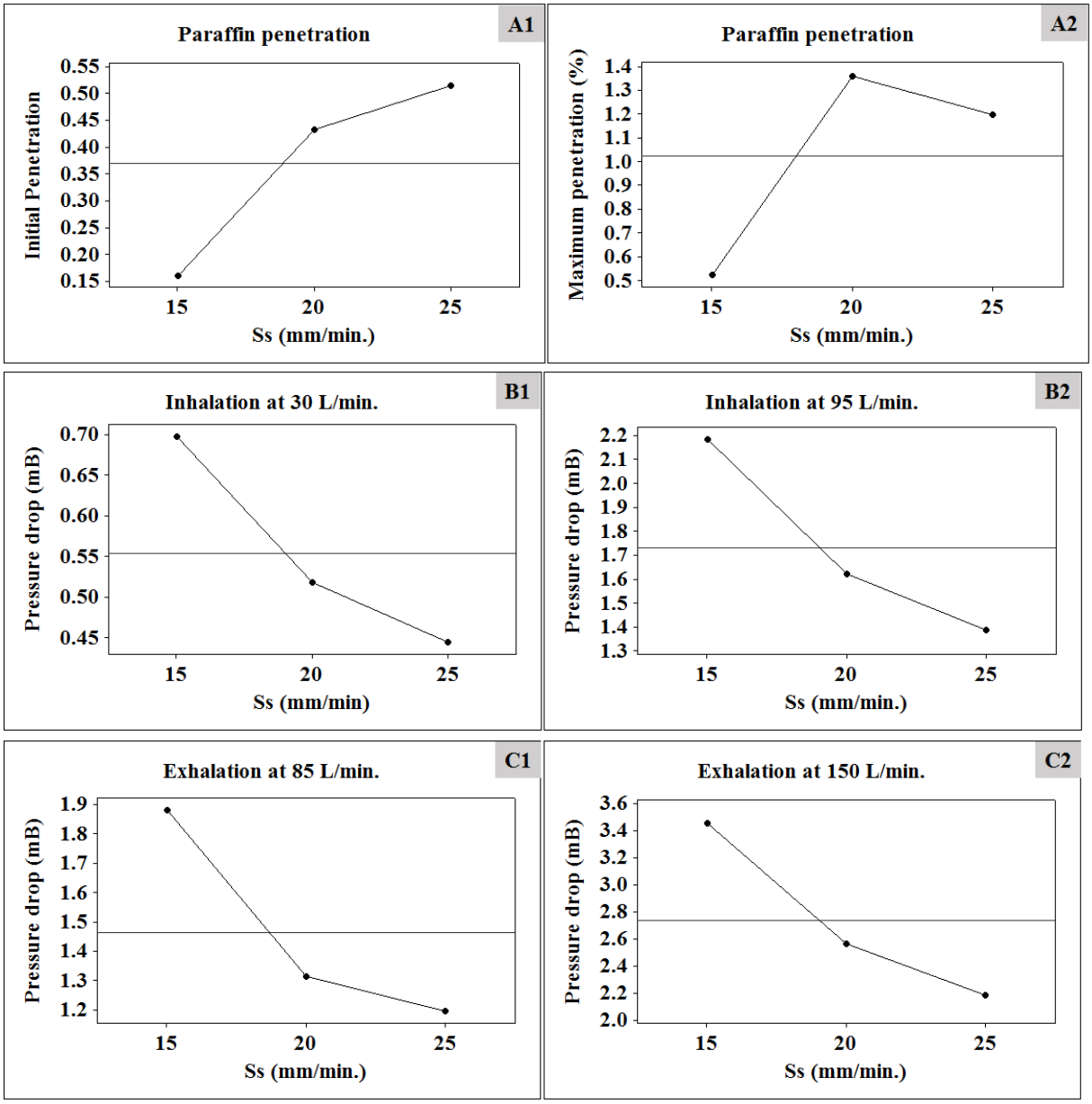

Figure 79: Correlation of substrate speed while electrospinning with filtration properties

Correlation of fiber diameter and its distribution, with paraffin screening efficiency, can be visualized in Figure 80. It can be seen that there are specific combinations of these values that produce higher screening potential. These regions may be linked with factors like higher porosity and low density, however, this needs to be studied further to reach a final conclusion. It can be concluded that different electrospinning input parameters affect the filtration properties of nanowebs. Hence, these properties may be optimized by fine tuning the inputs of electrospinning process.

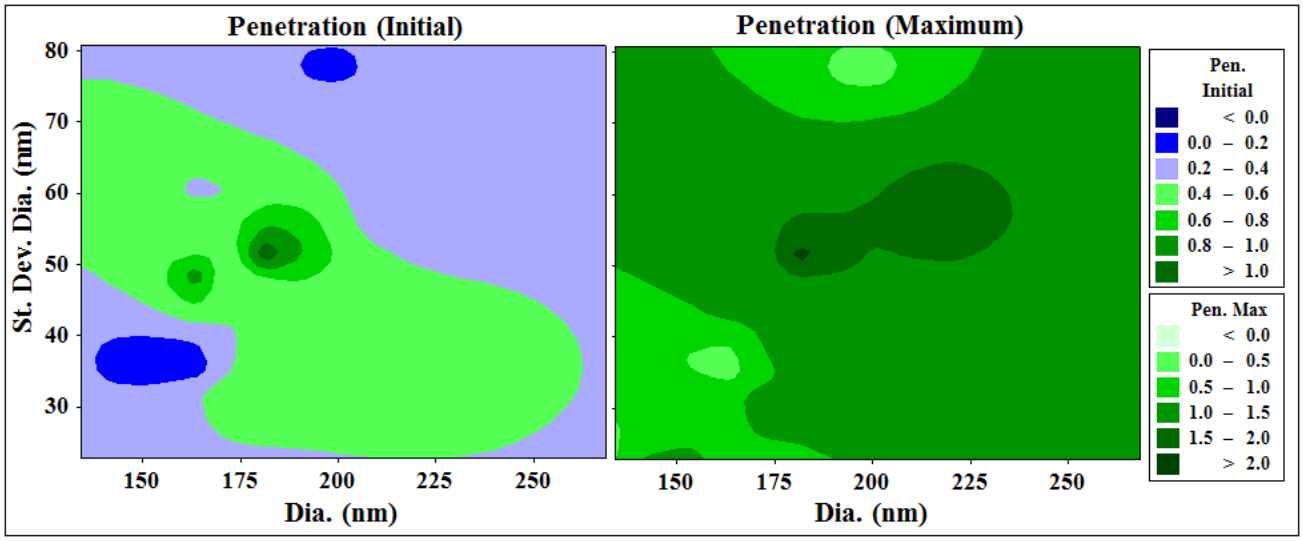

Figure 80: Correlation of nanofiber diameter and its distribution with paraffin penetration

4.5.3.2 Performance of nanoweb containing filters for face mask application

Figure 81 shows the decrease in penetration of paraffin for filters containing nanowebs. It can be observed that all the filters containing nanowebs improved the filtration efficiency, as confirmed by lower penetration of paraffin mist through them. The penetration was decreased by up to 100%, as compared to that for filter without nanoweb. Even, the minimum decrease in penetration was close to 20%, all values being much higher than minimum value defined by EN 149+A for FFP2 (filtering face pieces class 2) facemasks. This shows that inclusion off nanowebs, can, drastically, increase the filtration efficiency of face mask filters. However, other factors such as drop in inhalation and exhalation pressure also need to be considered.

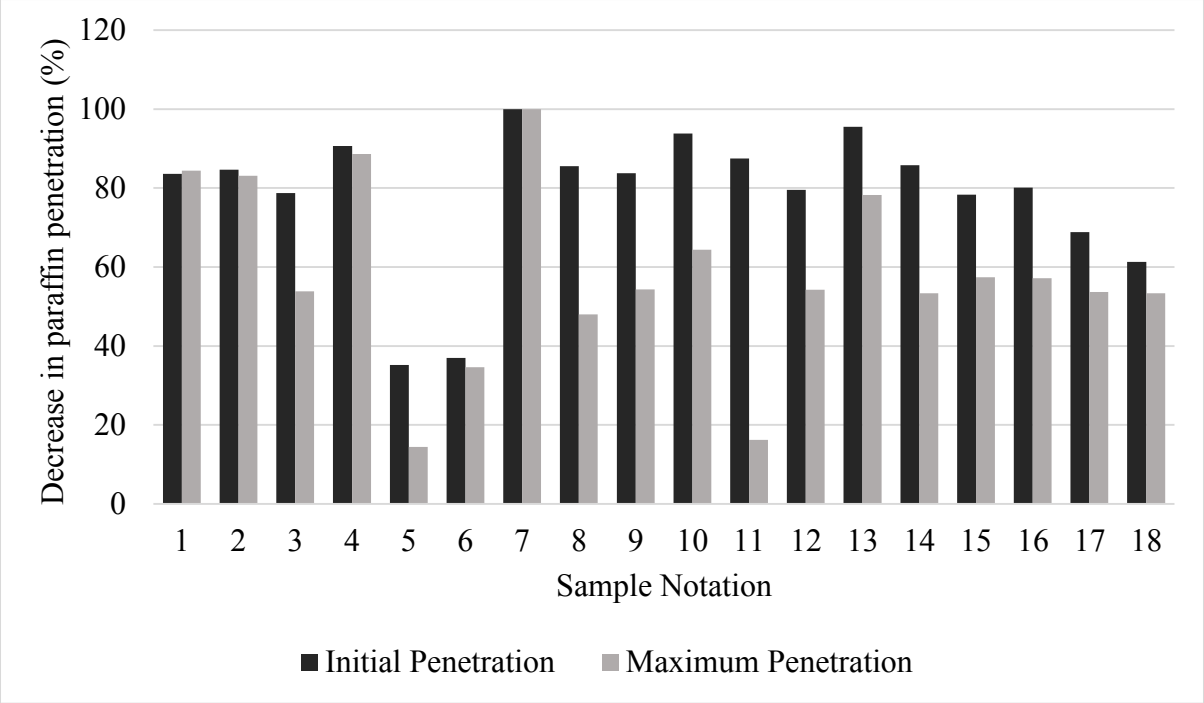

Figure 81: Percentage decrease in Paraffin penetration for filters containing nanowebs

Figure 82 and Figure 83 show increase in pressure drop, for nanoweb containing filters, expressed as a percentage of pressure drop for filter without nanowebs. All the nanoweb containing filters showed that their inclusion in filters resulted in significant increase in pressure drop. The highest increase was up to almost 240% as compared to original filter. This corresponds to value of 0.897 mB and 2.851 mB for inhalation at 30 L/min and 95 L/min, compared to an allowed value of 0.7 mB and 2.4 mB, respectively. However, there were some samples that showed a pressure drop within the allowed limits of FFP2 masks, as highlighted in Table 50. Similar observations could also be made for exhalation pressure drop. This confirmed that, although, addition of nanowebs increases the drop in pressure, it can be fine-tuned to get the pressure drop within the allowed limit, with much higher filtration efficiency. This fact could be utilized to develop high efficiency filters complying with normally implemented standards.

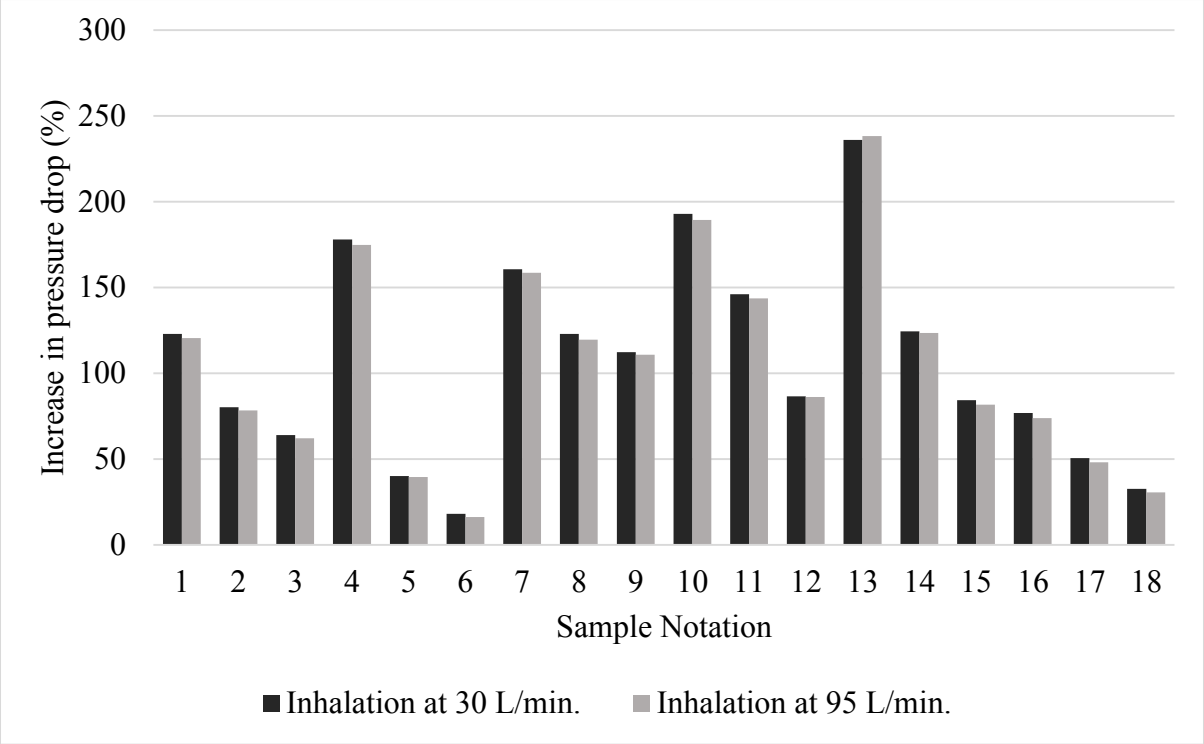

Figure 82: Percentage increase in inhalation pressure drop for filters containing nanowebs

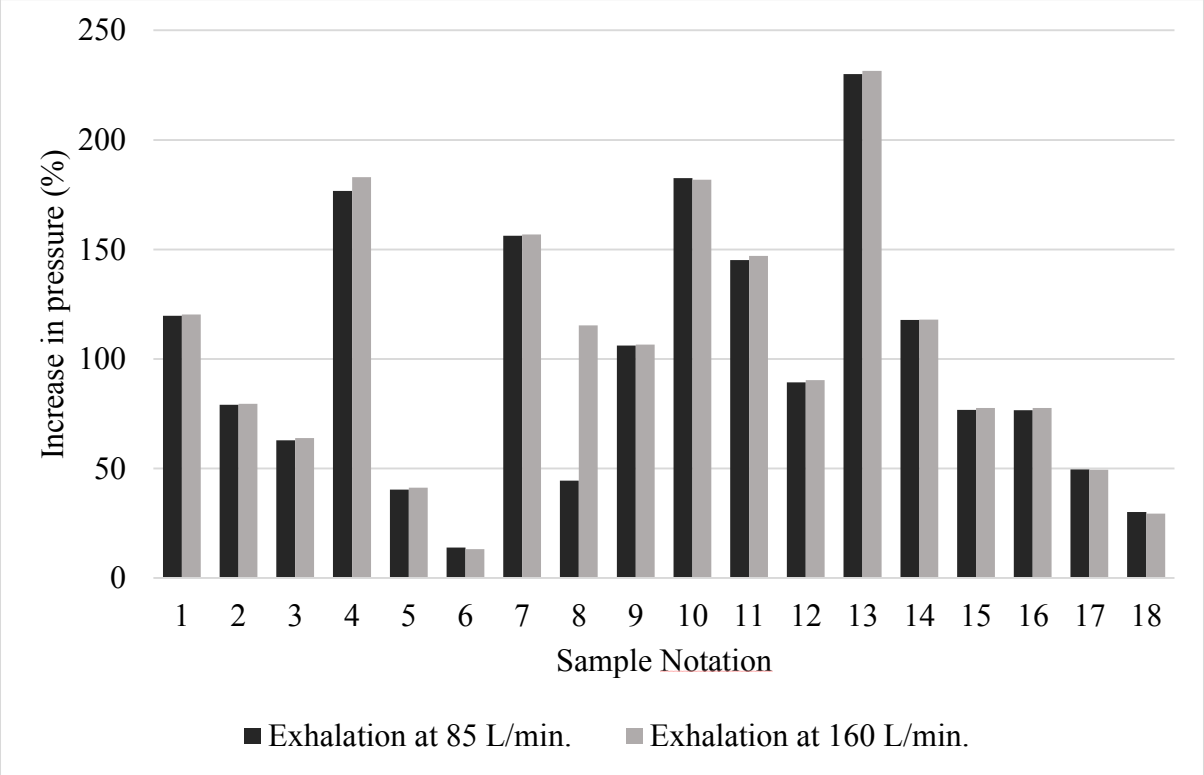

Figure 83: Percentage increase in Exhalation pressure drop for filters containing nanowebs

4.5.4 Comfort properties

Products, like face masks, are normally worn in conditions that are not very conducive and comfortable. They are, mostly, used for conditions with considerable physical activity like for emergency services, in manufacturing facilities, for surgical applications and other such activities. So, they also need to be studied for their comfort properties. By now, the authors did not find any study relating to different comfort properties for nanofiber incorporated products. Therefore, this part of study is dedicated to different comfort related properties of nanofiber-incorporated filter media for face mask applications. For this purpose, four important properties will be discussed. They include thermal resistance, air and water permeability and liquid moisture management.

The primary parameters for electrospinning were found to impact the above mentioned comfort properties, by affecting the morphology of nanofibers. They were correlated to comfort properties by ANOVA, that is shown, separately, for each of the properties in, following sections.

4.5.4.1 Thermal conductivity

Thermal conductivity is one of the basic property that defines the comfort of a wearable products. It, not only defines the comfort properties, but also affects the performance of wearer. Specially, for applications like emergency response service and surgical activities, it must be considered [290-292].

During current study, it was observed that thermal conductivity is significantly affected by different electrospinning parameters, as a result of their impact on fiber morphology. It is important to mention here that evaluation of impact of adding nanoweb on thermal conductivity of complete sandwiched filter was not possible. This was due to higher impact of thickness of other components of sandwich filter, which was much greater than that of nanoweb. So, the impact was studied by removing the nonwoven filter media 2 and 3 from sandwich (shown in Figure 36). The remaining structure included the nonwoven media 1 on which the nanoweb was coated.

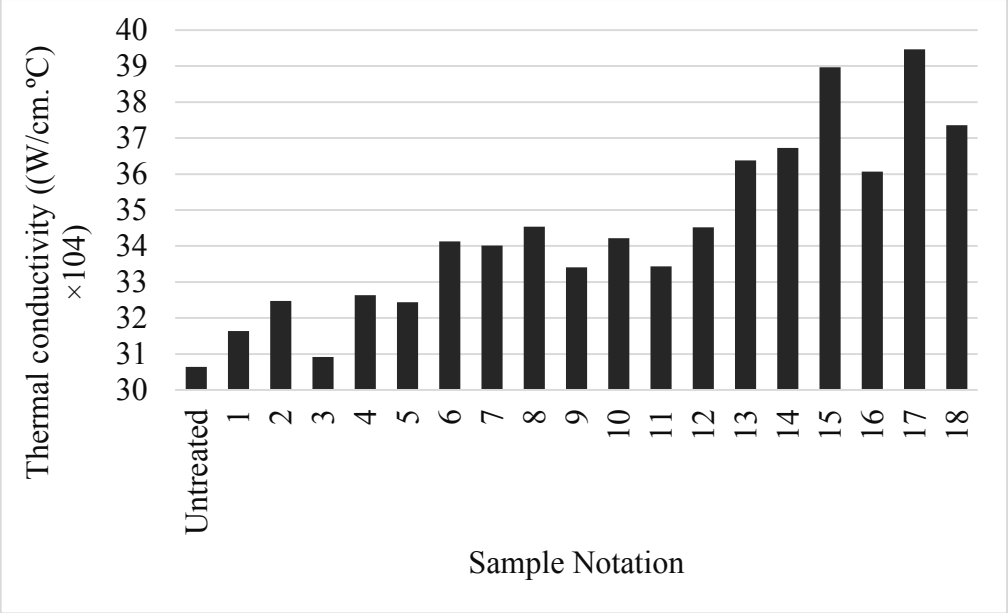

Figure 84: Influence of adding nanoweb on thermal conductivity of spunbond nonwoven

Figure 84 shows the effect of coating the spunbond nonwoven media 1 (as per Figure 36) with PA-6 nanowebs. It can be observed that addition of nanowebs resulted in improved thermal conductivity, as compared to the spunbond media alone, denoted by "0" in Figure 84. This could be attributed to higher density, resulting from filling of pores in spunbond media by nanofibers. To evaluate important parameters affecting thermal conductivity of facemask, ANOVA was performed and is summarized in Table 52. It can be observed that polymer solution concentration, electrospinning voltage and speed of carrier, pose a significant impact on thermal conductivity of facemask filter (P-value < 0.05). This impact can, actually, considered to take place due to the effect that these parameters put on morphology of nanoweb. The effects produced by significant terms is discussed in following paragraphs.

Table 52: ANOVA for effect of input parameters on thermal conductivity of sandwich filter

S.N.	Term	P-value
1	C	0.000
2	D	0.949
3	V	0.000
4	Cs	0.001
5	Ss	0.745
6	Af	0.266
7	Dia.	0.780
8	St. Dev. in Dia.	0.666

Before discussing the effect of primary input factors, it may be useful to discuss the impact produced by nanofiber diameter on thermal conductivity, as it may allow to justify some of the trends posed by primary inputs. Even though, according to ANOVA, fiber diameter was not found to impact the thermal conductivity, in a significant way, it may be interesting to observe its impact from Figure 84. It can be observed that thermal conductivity, gradually, increased from sample 1 through 18. It was discussed previously, that within this range of samples, diameter of fibers increased, thus leading to lower bulkiness and, thus, higher density. The increase in density has been known to be one of the strongest factors affecting the thermal conductivity [293].

It can be observed from Figure 85, that increasing the solution concentration increased the thermal conductivity of nanofiber coated nonwoven. This could be attributed to a lower bulkiness produced due to thicker fibers resulting from increase in concentration.

Thermal conductivity was found to have a nonlinear relation with voltage with an overall increase in it, as the voltage was increased from 35 KV to 55 KV. This effect could also be related to the difference in bulkiness, as affected by change in voltage between fiber generator and collector. Higher attracting forces on fibers, at higher voltages during electrospinning, and lower bulkiness of nanoweb, could be expected to increase the resultant conductivity. However, a lower conductivity at intermediate voltages may be attributed to the static charges playing a role to make the nanowebs bulkier by inter-fiber repulsion. This impact may be considered to reduce at higher voltages due to stronger pulling forces in that range.

Carrier speed was also found to pose a significant effect on fiber properties and hence the thermal conductivity of resulting nanofibrous nonwoven produced thereof. As shown in Figure 85, the thermal conductivity first increased and then decreased, as the carrier speed was increased.

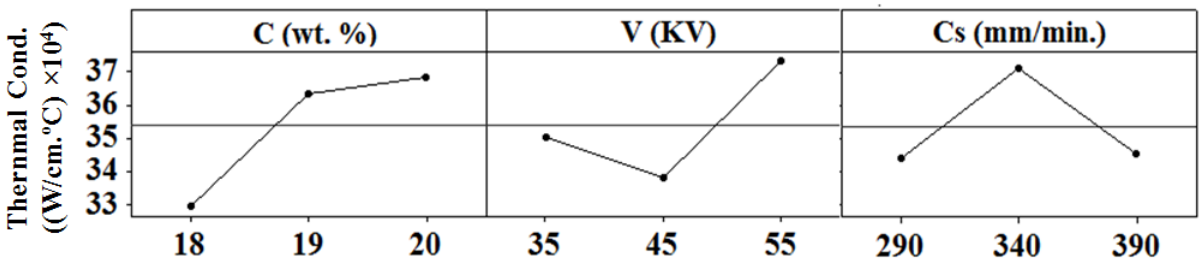

Figure 85: Effect of significant inputs on thermal conductivity of nanoweb-coated filter

This trend may be explained to be due to competing impacts of higher static charge at lower speeds (leading to higher bulkiness) and higher fiber diameter (leading to lower bulkiness) at higher carrier speeds, as shown in Figure 75.

From above discussion, it may be concluded that addition of nanoweb in nonwoven filter media is expected to increase its thermal conductivity. This fact may be useful in warmer working environments (i-e lower than the body temperature), where the face mask filter will allow to better conduct the body heat to outside environment. This heat may also be transferred though convection by the air passing in and out of the filter. This property of depends on air permeability if filter, which described in next section.

4.5.4.2 Air permeability

As for any wearable product, air permeability, of a respiratory face mask is a major factor that decides its comfort properties. It defines the movement of air across the filter, thus allowing the exchange of heat and mass through it. Incorporation of nanoweb, between the layers of facemask filter, was found to affect its air permeability. It can be observed from Figure 86, that addition of nanoweb between the layers of filter media resulted in decrease in air permeability.

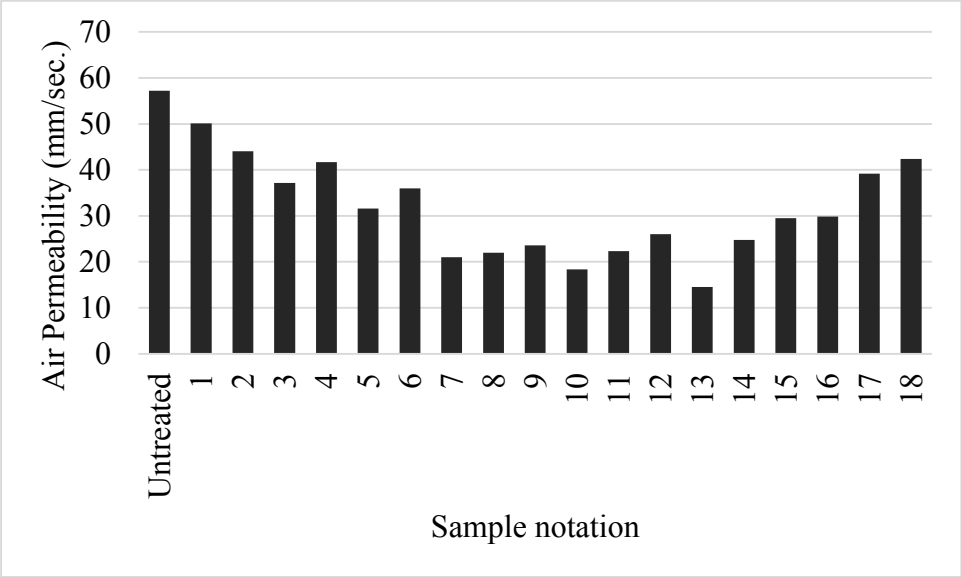

Figure 86: Influence of adding nanoweb on air permeability of sandwich filter

This is, obviously, due to increased hindrance that nanoweb offered to air crossing the filter media. The difference in air permeability can be considered to be due to difference in

porosity, resulting from factors like change in diameter, its distribution, density of web and its bulkiness. However, these factors need extensive studies with sophisticated testing facilities to define a proper relationship, they have with air permeability. To study the relationship between different primary (i-e C, V, D, Cs, Ss and Af) and secondary factors (Dia., St. Dev. in Dia. and other parameters, not studied in current work) on air permeability, ANOVA was utilized and is shown in Table 53.

Table 53: ANOVA for effect of input parameters on thermal conductivity of sandwich filter

S.N.	Term	P-value
1	C	0.021
2	D	0.746
3	V	0.003
4	Cs	0.263
5	Ss	0.580
6	Af	0.427
7	Dia.	0.063
8	St. Dev. in Dia.	0.043

The presence of dark areas at top right column of figure shows that air permeability is higher for thicker fibers with larger standard deviation. This could be credited to larger pores created by both these conditions. However, this needs to be studied further, in order to define the factors resulting from change in diameter and its distribution, and consequently, the air permeability of sandwich filter. As shown in Figure 87, higher diameter and its distribution were observed to result in higher air permeability.

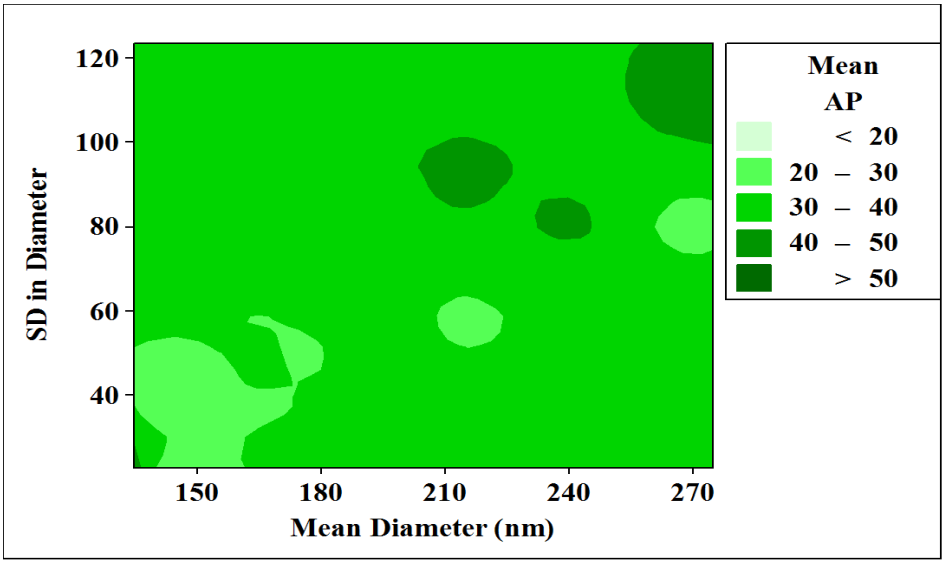

Figure 87: Effect of nanofiber diameter and its St. Dev. on air permeability of sandwich filter

The effect of significant electrospinning parameters on air permeability of sandwich filter can be depicted from Figure 88. Increasing concentration was observed to have an, overall, increasing impact on air permeability. This could be due to the fact that increasing concentration, normally, resulted in thicker fibers with higher standard deviation. Both these factors lead to increased air flow because of larger inter-fiber spaces. However, the drop of air permeability, at intermediate concentrations, need to be studied further. Meanwhile, increasing voltage was found to decrease the air permeability of sandwich media. This could be credited to production of thinner fibers at higher voltages, thus reducing the pore size and resultant air flow.

It may be concluded from above discussion that, inclusion of nanowebs, significantly decreases the air permeability of layered structure in which it was incorporated. However, as mentioned above, the area needs further investigations to define different secondary factors that define the air permeability. These factors may include porosity, pore size distribution and bulkiness (and density) of nanowebs etc.

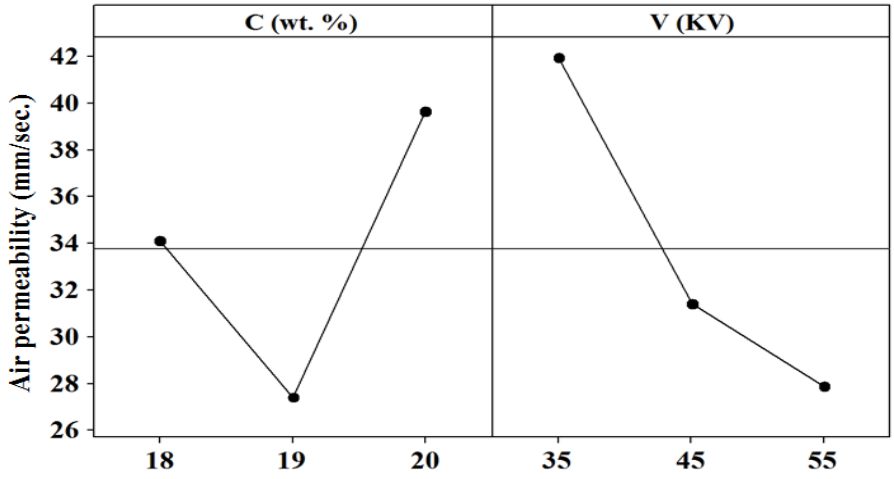

Figure 88: Effect of significant electrospinning parameters on air permeability

4.5.4.3 Water vapor permeability

Water vapor permeability defines the ability of a product to transfer out the sweat vapors, produced by human body. As compared to air permeability, it is a complex parameter, as it also depends on nature of material under study i-e its hydrophilic or hydrophobic characteristic and the size of vapors as compared to pore size etc.

Figure 89 shows effect of adding nanowebs on vapor permeability of sandwich filters. Inclusion of nanoweb in filter media was found to improve the water vapor permeability of nanoweb. This improvement may be due to small capillaries that could have re-evaporated the moisture deposited on nanowebs. It has been known that decreasing the capillary diameter increases the wicking of moisture through it [294]. The same could considered to be responsible for improvement in water vapor permeability in current case, as the nanowebs have much smaller capillaries than the nonwoven substrates on which they are deposited. However, capillaries smaller than optimum may result in lower wicking among other capillary sizes of their class.

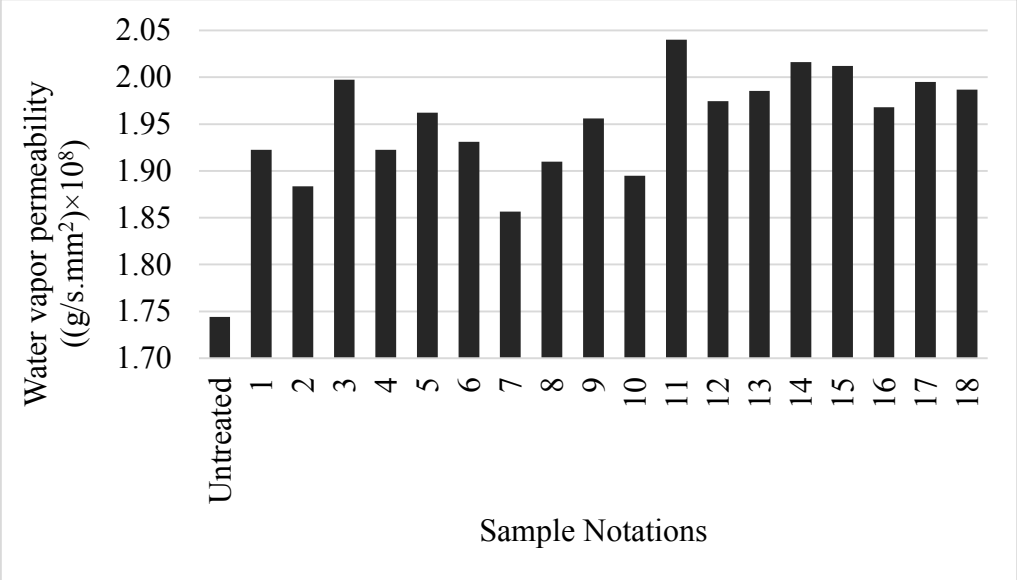

Figure 89: Influence of adding nanoweb on vapor permeability of sandwich filter

As for other output parameters, water vapor permeability was expected to be affected by the factors under study. Their impact can be assessed by ANOVA shown in Table 54. It suggests that electrospinning solution concentration and air flow in electrospinning chamber affect the water vapor permeability, in a significant manner. While, among secondary factors, both the diameter and its distribution, significantly, affect the vapor permeability.

Table 54: ANOVA for effect of inputs on water vapor permeability of sandwich filter

S.N.	Term	P-value
1	C	0.001
2	D	0.392
3	V	0.717
4	Cs	0.972
5	Ss	0.764
6	Af	0.075
7	Dia.	0.007
8	St. Dev. in Dia.	0.009

The impact posed by diameter and its distribution is summarized in Figure 90. As for air permeability, it can be observed that higher fiber diameter increased the vapor permeability of nanoweb, though, webs with higher diameter fibers have higher capillary size, that should decrease the vapor permeability. For nonwoven webs, the capillary size was much higher than that for nanowebs, thus leading to lower permeability of vapors through them. Addition of these finer capillaries increased the overall vapor permeability. While, within the range of diameters of nanowebs under study, increasing fiber diameter, and hence the capillary size, increased the vapor permeability. This suggests that there is an optimum value of fiber fineness (may be between "micro" and "nano") that have highest vapor permeability and beyond which it starts to decrease, as observed in case of current diameter range.

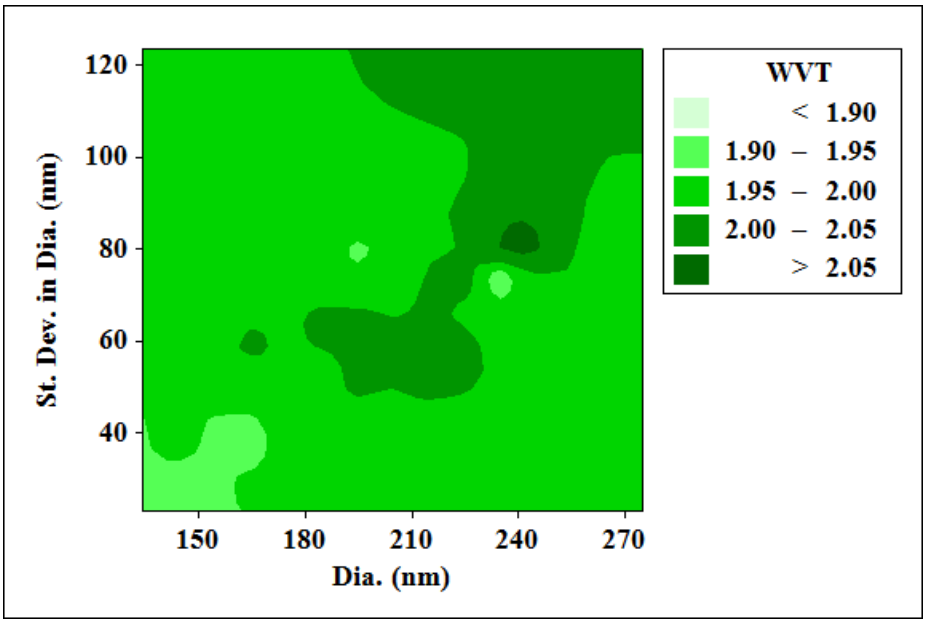

Figure 90: Effect of nanofiber diameter and its distribution on water vapor permeability of sandwich filter

The effect of solution concertation and air flow in electrospinning chamber is shown in Figure 91.

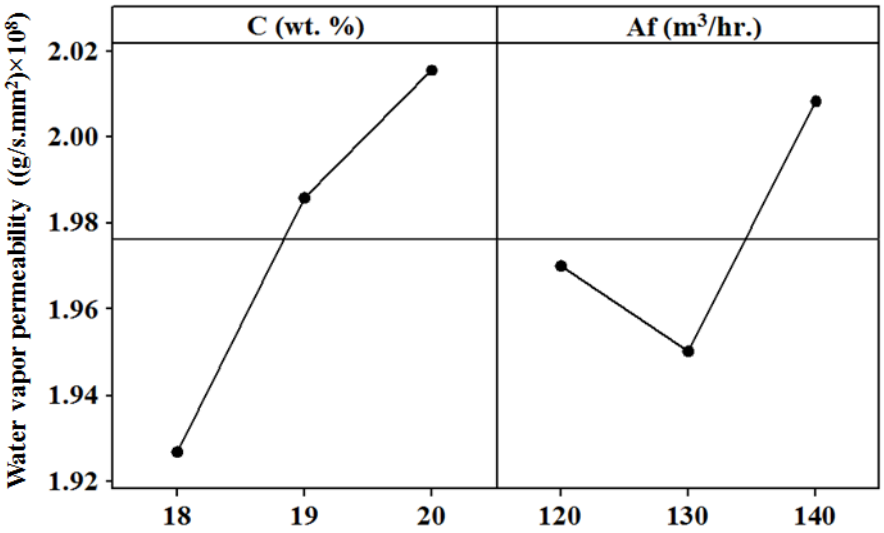

Figure 91: Effect of significant electrospinning parameters on air permeability

Both, higher solution concentration and air flow, were found to increase the vapor permeability. Increase of solution concentration, increased the fiber diameter and hence the capillary size, that was expected to be below its optimum range. Increasing diameter increased and took the capillary size and vapor permeability closer to optimum value, beyond which further increase in diameter could be expected to decrease these outputs. However, further studies in this regard, with wider range of fiber diameter, can give more detailed view of these trends.

Increase in air flow was also found to increase the vapor permeability, may be due to fiber loss at higher air flows, thus producing thinner webs. However, this trend needs to be studied further, as the P-value for air flow, in Table 54, suggests that its effect is not as significant as that of concentration of solution.

From these results, it may be inferred that inclusion of nanowebs, significantly, impact the water vapor permeability of sandwich filters. Moreover, the vapor permeability can be fine-tuned by adjusting different electrospinning parameters.

4.5.4.4 Liquid moisture management

Liquid moisture management of a fibrous material is a complex phenomenon defined by many different parameters. They include the wetting time, absorption rate, wetted radius and spreading speed. The samples shortlisted in current part of study were tested for these properties and the results obtained are plotted in Figure 92 to Figure 95. The significance of impact of input parameters on these outputs is summarized in Table 55. It can be observed that the electrospinning parameters did not impact most of the moisture management properties, as the sandwiched nanoweb has very little role to play in this case. Though, some terms showed significant impact, but that also can be considered to be due to some noise variables affecting the process. Moreover, the trends obtained for these terms didn't give any logical correlation with properties of nanoweb. So, these terms were ignored for further discussions.

Table 55: ANOVA for effect of inputs on moisture management by sandwich filter

		P-values							
		Wetting time		Absorption rate		Wetted radius		Spreading speed	
S.N.	Terms	Top	Bottom	Top	Bottom	Top	Bottom	Top	Bottom
1	C	0.969	0.746	0.051	0.779	0.375	0.762	0.152	0.074
2	D	0.609	0.027	0.345	0.584	0.627	0.105	0.160	0.105
3	V	0.070	0.144	0.887	0.065	0.100	0.096	0.025	0.133
4	Cs	0.416	0.851	0.162	0.240	0.298	0.744	0.194	0.313
5	Ss	0.278	0.195	0.172	0.499	0.722	0.212	0.647	0.568
6	Af	0.341	0.034	0.756	0.778	0.254	0.089	0.630	0.387
7	Dia.	0.450	0.665	0.703	0.606	0.840	0.929	0.497	0.854
8	St. Dev. in Dia.	0.946	0.983	0.365	0.896	0.894	0.990	0.865	0.256

It can be observed that most of the factors related to nanoweb do not impact the outputs, significantly. Specially, the effect of diameter and its distribution are far from significance. This may be attributed to stronger influence of top and bottom surfaces, made of nonwoven materials. So, these properties are more affected by properties of these nonwoven materials. It may not be very useful to study the impact of these inputs. However, a general observation may be made from plots in Figure 92 to Figure 95. The top side is the one intending to touch the skin i-e spunbond media 3 and bottom side is the one whose inner face is coated with nanoweb i-e spunbond media 1.

It can be observed that there was no trend for effect of addition of nanowebs on wetting properties. This, again, is because, these properties are more dependent of surface characteristics that are defined by the nonwoven webs at top and bottom side.

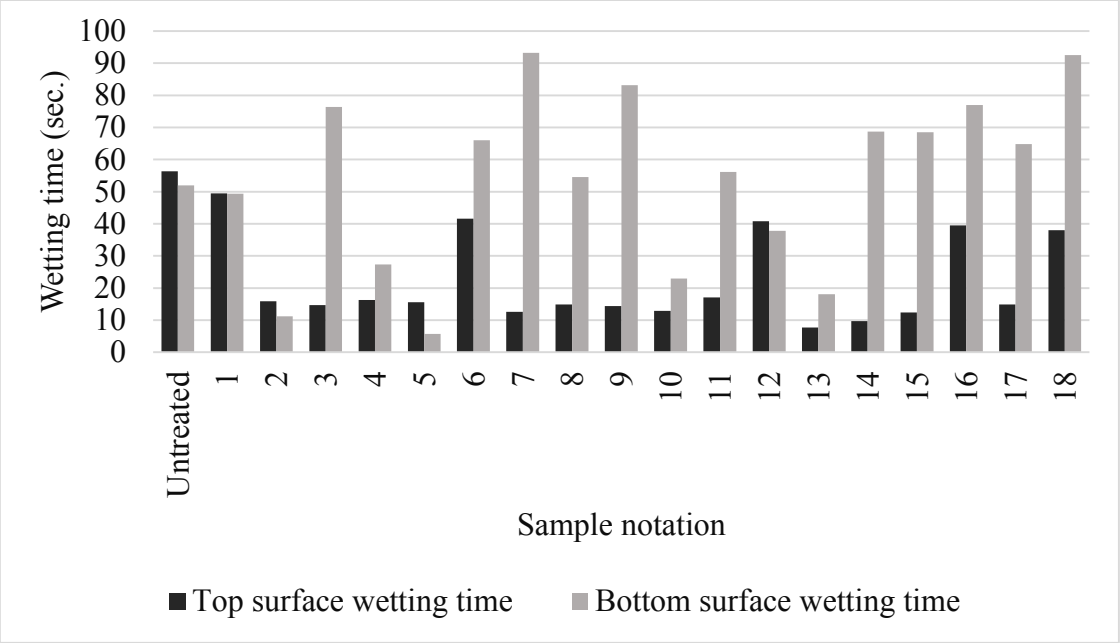

Figure 92: Influence of adding nanoweb on wetting behavior of sandwich filter

For absorption rates, it seemed to be increased by addition of nanoweb. It may be credited to the dissipation of any moisture reaching the nanoweb, as it has greater wicking potential because of its finer fibers [295]. Similar observation could be made for maximum wetted radius of top surface, that increased after addition of nanoweb. However, for spreading speed, the trend was not very clear.

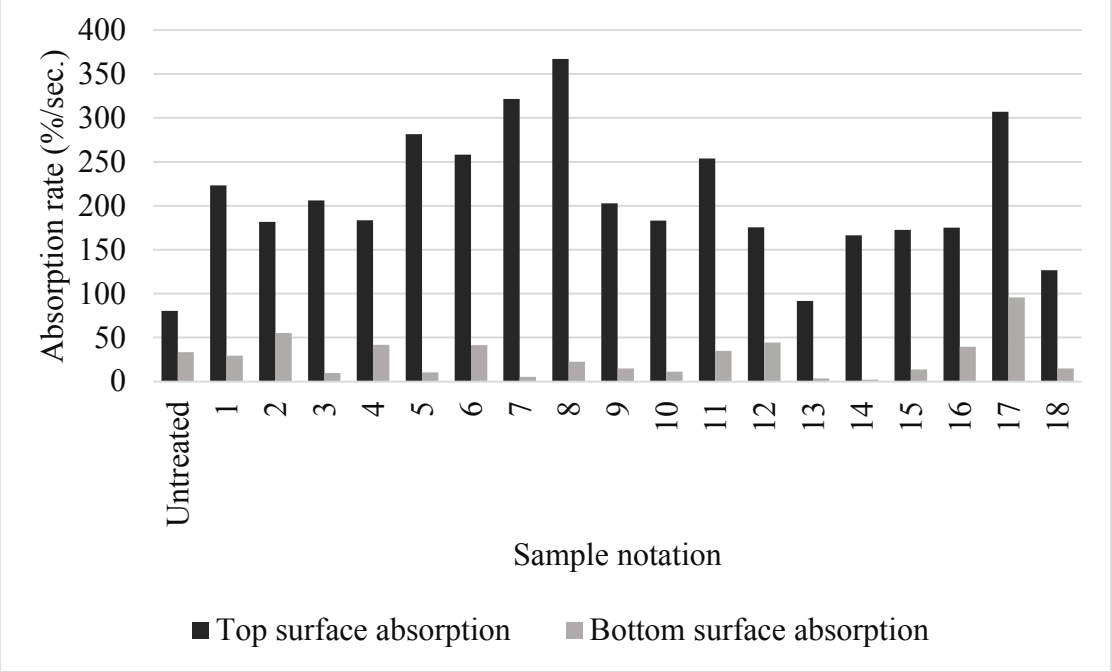

Figure 93: Influence of adding nanoweb on moisture absorption of sandwich filter

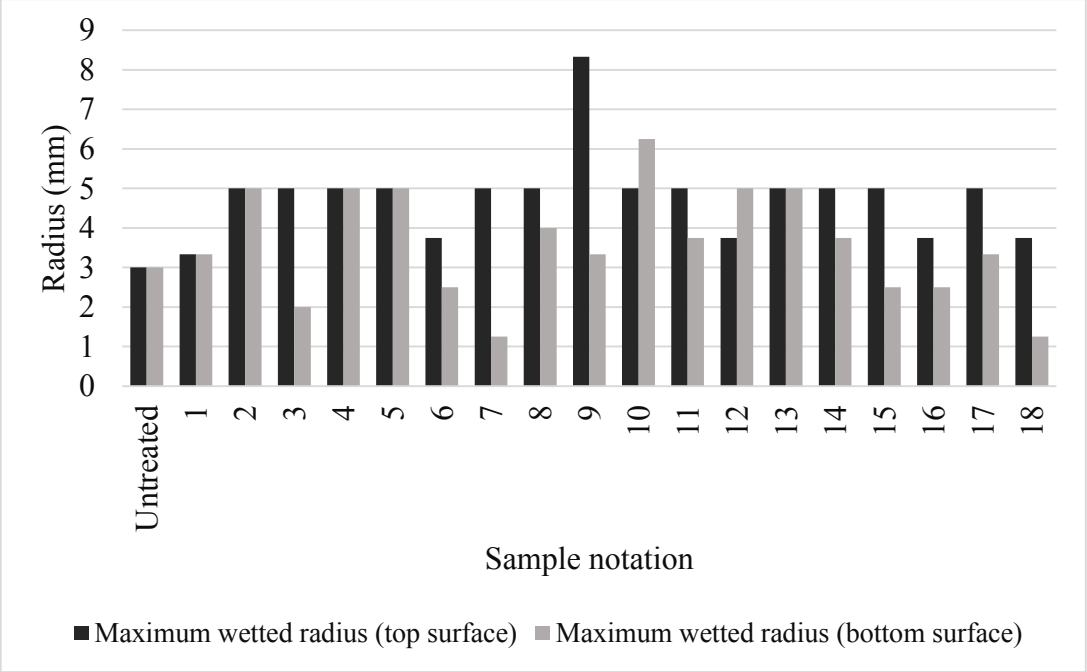

Figure 94: Influence of adding nanoweb on wetting extent of sandwich filter

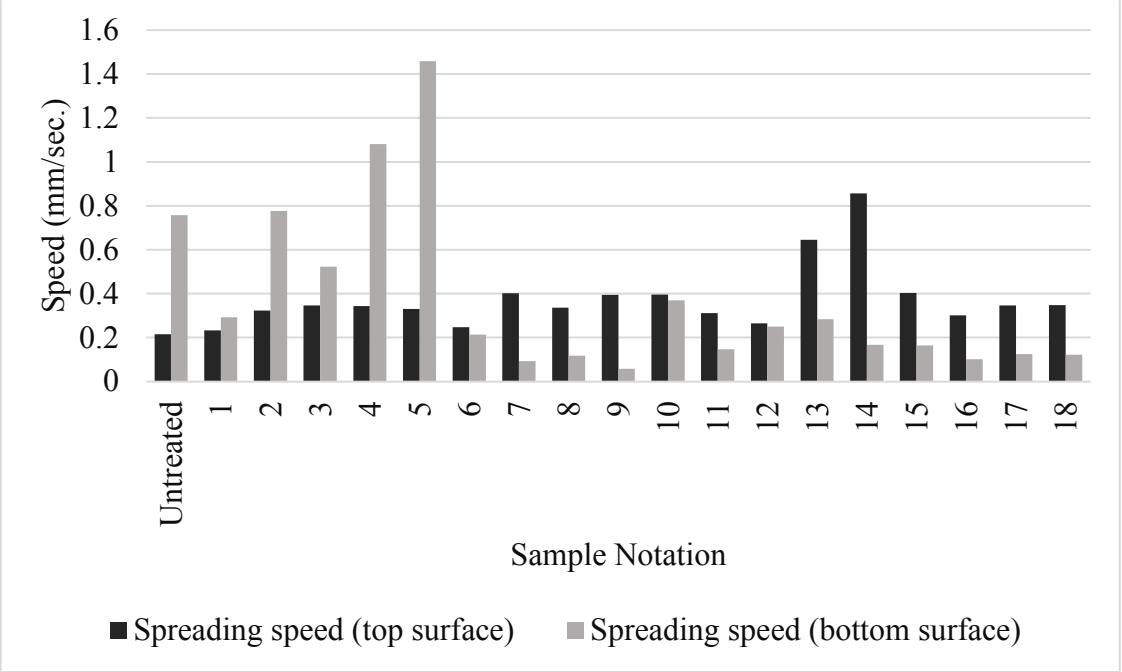

Figure 95: Influence of adding nanoweb on speed of moisture spreading on sandwich filter

From above discussion, it may be concluded that addition of nanowebs affect the moisture management properties of sandwich filter media. However, the trends of this impact were not very clear. This suggests that further studies may be carried out to understand these relationships.

Chapter 5 CONCLUSIONS AND PERSPECTIVES

5.1 Conclusions

Modelling and optimization of electrospinning process have been carried out in order to give a start point for two novel technical applications for electrospun nanofibers i-e heat generation and filtration for respiratory protection. Heat generation was studied by using PAN and PAN/CNT composite nanowebs, while respiratory protection by utilizing PA-6 nanowebs incorporated in nonwoven filter media. Moreover, the electrospinning process was also studied with different types of setups i-e needle and needleless electrospinning. This was accomplished to compare the processes and develop optimized webs, particularly, on needleless setup (which may be utilized for bulk scale production of nanowebs) as it has not been studied, adequately.

The nanowebs were modelled and optimized in order to define a range of parameters that can produce defect free nanofibrous nonwoven and that may be utilized in further studies for fine tuning of properties for selected applications. This was expected to develop the products with optimized morphology and, thus, with better repeatability, reproducibility and predictability of performance properties. Moreover, it was expected that optimization of morphology will allow to focus and better optimize other performance related properties for both the end uses.

To achieve the goals, the electrospinning process and morphological properties of nanowebs were studied using different DOEs. For PAN and PAN/CNT nanowebs, full factorial and response surface designs were utilized. While, for PA-6 nanowebs full factorial and Taguchi designs were used. The input parameters, mostly used, were, solution concentration, applied voltage and distance between fiber generator and collector, as their qualitative impact was already known through previous studies in the field. For heat generation CNT content and electrospinning time were also studied because of their impact on some of the outputs, as determined by pre-experimental trials. Similarly, for respiratory protection some process parameters included in needleless setup (such as air flow rate, substrate speed and polymer

carrier speed), were also considered. The morphological outputs studied in this work were nanofiber diameter, its distribution and defects in nanowebs such as beads and drops etc.

Among different parameters studied, it was observed that magnitude of effect of electrospinning solution concentration was much higher as compared to others. Increasing concentration was found to increase the nanofiber diameter and its distribution. So, lower concentrations may be employed to produce finer fibers with lower fiber diameter distribution. Defects in fibers for such concentrations may be controlled by proper selection of other parameters controlling the process, such as voltage and fiber generator to collector distance. Although, higher magnitude of impact of concentration diminished the effect of other parameters. However, when studied at constant concentration, they also showed significant impact in some of the cases. The effect of voltage and distance was found to be much more complex than concentration. The proportionality of impact of each of them was strongly affected by value of the other. So, it was concluded that they must be optimized simultaneously. In most of the cases increasing voltage and time of electrospinning and decreasing fiber generator to collector distance was found to increase the diameter. However, these trends were mostly not linear and these judgements depended on range of values selected for each of them as well as the settings of other affecting parameters. Another important parameter for PAN/CNT composite nanofibers was content of CNTs in them. It was observed that higher CNT contents increased the diameter of fibers, thus putting a significant impact on fiber morphology.

For fiber parameter distribution, a general observation was that nanofibers with higher diameter had higher standard deviation in it. Fiber diameter distribution can be considered sensitive to parameters other than concentration of solution, distance between fiber generator and collector and the voltage applied between needle and collector. So, these parameters need be identified and studied along with basic parameters normally considered.

It was observed that the impact of most of the parameters under study was not linear i-e they had second degree interaction with diameter and its distribution. This observation may be considered to suggest the use of experimental designs, like response surface DOEs, that cover such second degree interactions. Experimental settings included in such DOEs are expected to allow better study the behavior of processes, especially the complex interactions between parameters. Moreover, such DOEs are expected to improve the significance and prediction efficiency of the regression models developed from them. Furthermore, the shorter

DOEs, such as those developed using Taguchi approach, were found to give satisfactory results with much lesser number of experiments than that used for full factorial and response surface DOEs. Such DOEs can be considered effective in scenarios, where more important inputs have to be screened out from those having lesser importance.

Additionally, it can be concluded that, although, needleless electrospinning is, somewhat, complex process as compared to needle electrospinning, both showed similar trend for impact of inputs on outputs. However, the magnitude of impact was found to be much different in both cases. The numerical relationship between the processes was not drawn, as it needed separate DOEs, developed, specifically for this purpose, which was out of scope of current study.

Based on results produced by different experimental settings according to DOEs, optimized levels for all the input parameters were defined. These settings were used to develop optimized samples for further characterization. Statistical analysis of data resulted in regression equation for all the DOEs (other than Taguchi). These models were found to be reasonably significant in most of the cases, which was also confirmed by validation experiments. It was also observed that the models developed for response surface DOEs were more significant than those developed by full factorial DOEs. This could be credited to the presence of second degree interactions, that cannot be defined well by DOEs that consider only linear interactions (such as full factorial and Taguchi DOEs).

Optimized PAN and PAN/CNT nanowebs and the resulting CNF and CNF/CNT nanowebs, from needleless electrospinning, were characterized for some important properties. TEM analysis of PAN/CNT nanowebs confirmed the alignment of CNTs along the fiber axis. This aspect may be important for applications where mechanical properties are important. Moreover, it was observed that CNTs were also present on surface of nanowebs. However, negligible electrical properties of such webs suggested that they were covered by a film of polymer. Another important finding in this regard was the spiraled arrangement of CNTs along the fiber axis. This arrangement showed that CNTs were affected by the instabilities in polymer jet. Moreover, this may be considered important for production of nanowebs with good elasticity and toughness.

As mentioned above, addition of CNTs in PAN nanofibers didn't render them considerable electrical conductivity, may be due to the presence of very fine polymer layer on

CNTs present at surface of fibers. However, their thermal conductivity was found to increase, substantially. Similarly, it also resulted in noticeable improvement in thermal stability.

Carbon fiber nanowebs produced from optimized PAN and PAN/CNT nanowebs, when subjected to a voltage as low as 10 V, were found to generate heat. Due to their higher electrical resistance, pure PAN nanowebs were found to achieve higher temperature, as compared to that achieved by PAN/CNT nanowebs. In this regard, addition of CNTs was found to increase the heating and cooling rates of CNF/CNT nanowebs, in addition to generation of smoother profiles for heating/cooling cycles. This gave a start point for further studies with focus on optimization of properties of nanowebs other than their morphology.

The optimized PA-6 nanowebs, sandwiched between the layers of nonwoven filter media, were found to produce a significant improvement in filtration efficiency of the sandwich filters. The incorporation of nanowebs increased the filtration efficiency of face mask filters by a value as high as 200%. However, it also resulted in increase in inhalation and exhalation pressure drops. But a number of options resulted in acceptable pressure drop, with much higher increase in filtration performance.

Inclusion of PA-6 nanowebs in sandwich filter was also found to affect their comfort properties, as well. For example, they were found to increase their thermal conductivity and water vapor permeability, that can be expected to improve their overall comfort characteristics. Meanwhile, it was also observed that, when PA-6 nanowebs were sandwiched between the layers of nonwoven filter media, their air permeability was found to decrease. However, further studies in this direction are expected to improve these deficiencies. So, it may be concluded that PA-6 nanowebs can be used, effectively, for development of improved facemask filters with better filtration and comfort properties.

5.2 Perspectives

Even though the electrospinning parameters have been studied extensively, in last decade, still, they need to be investigated further. Specially, the parameters having lower impacts on properties of nanowebs are important for fine tuning their properties. For instance, as discussed above, higher magnitude of impact of solution concentration diminishes the magnitude of effects produced by other parameters. To study effects produced by these low impact factors, further studies in this direction may be carried out, by selecting lower difference

in levels of concentration. This is expected to fine tune the process with improved validity of models produced thereof. Moreover, the parameters like, substrate speed and air flow in electrospinning chamber, were also found to influence properties of resulting nanowebs. Further studies on these parameters can result in improved nanowebs with fine-tuned properties. Similarly, fiber diameter distribution can be considered much sensitive to some variables other than concentration of solution, distance between fiber generator and collector and the voltage applied between needle and collector. So, these variables need be identified and studied, along with basic parameters, normally considered.

The properties of nanowebs other than morphology also need further investigations. For example, in case of PAN/CNT composite nanofibers, the spiral arrangement of CNTs can be used in development of nanowebs with better mechanical characteristics. Electrospinning of such nanowebs needs to be explored further to understand this phenomenon and make further developments in the field. Similarly, inclusion of CNTs in nanowebs was found to result in an ignorable increase in electrical conductivity. This also needs to be studied further with more number of levels of CNT concentration. Moreover, the properties of nanowebs such as air permeability, water vapor transmission and liquid moisture management also need to be studied in detail.

Considering diameter and its distribution as input parameters can also give some interesting correlations amongst different properties. However, this can be accomplished by producing nanowebs to group them according to predefined DOEs. Similarly, such studies with diameter and its distribution as inputs, are expected to develop correlations between different lab and bulk scale electrospinning setups. This will allow to scale up the electrospinning process for better performance of industrial setups.

Finally, current study created a starting point for research on utilization of nanowebs for heat generation and respiratory protection. Use of optimized nanowebs will allow to focus and optimize other important properties that can enhance their performance in above mentioned applications. For example, heating systems with PAN/CNT based carbon nanofibers may be explored with higher CNT content, thicker nanowebs and optimized carbonization. Similarly, the filtration and comfort properties of respiratory protection mask studied in current work, may be correlated with porosity and other such characteristics to better understand these factors. Such investigations will not only improve the end use properties but also provide better control over electrospinning for these applications.

References

[1] Philadelphia University. *Textiles defined* (2016, 02 July). Available: http://faculty.philau.edu

[2] S. Ramakrishna, *An Introduction to Electrospinning and Nanofibers*: World Scientific, 2005.

[3] J. Fang, H. Niu, T. Lin, and X. Wang, "Applications of electrospun nanofibers," *Chinese Science Bulletin,* vol. 53, pp. 2265-2286, 2008.

[4] F. L. Zhou and R. H. Gong, "Manufacturing technologies of polymeric nanofibres and nanofibre yarns," *Polymer International,* vol. 57, pp. 837-845, 2008.

[5] H. S. Wang, G. D. Fu, and X. S. Li, "Functional polymeric nanofibers from electrospinning," *Recent Pat Nanotechnol,* vol. 3, pp. 21-31, 2009.

[6] A. Greiner and J. H. Wendorff, "Electrospinning: a fascinating method for the preparation of ultrathin fibers," *Angewandte Chemie International Edition,* vol. 46, pp. 5670-703, 2007.

[7] H. Niu and T. Lin, "Fiber generators in needleless electrospinning," *Journal of nanomaterials,* vol. 2012, p. 12, 2012.

[8] V. Pillay, C. Dott, Y. E. Choonara, C. Tyagi, L. Tomar, P. Kumar*, et al.*, "A Review of the Effect of Processing Variables on the Fabrication of Electrospun Nanofibers for Drug Delivery Applications," *Journal of Nanomaterials,* vol. 2013, p. 22, 2013.

[9] J. M. Deitzel, J. Kleinmeyer, D. Harris, and N. C. Beck Tan, "The effect of processing variables on the morphology of electrospun nanofibers and textiles," *Polymer,* vol. 42, pp. 261-272, 2001.

[10] P. K. Baumgarten, "Electrostatic spinning of acrylic microfibers," *Journal of Colloid and Interface Science,* vol. 36, pp. 71-79, 1971.

[11] L. Huang, K. Nagapudi, R. P. Apkarian, and E. L. Chaikof, "Engineered collagen-PEO nanofibers and fabrics," *Journal of Biomaterials Science, Polymer Edition,* vol. 12, pp. 979-93, 2001.

[12] Y. Wang, Y. Li, G. Sun, G. Zhang, H. Liu, J. Du*, et al.*, "Fabrication of Au/PVP nanofiber composites by electrospinning," *Journal of Applied Polymer Science,* vol. 105, pp. 3618-3622, 2007.

[13] M. M. Demir, M. A. Gulgun, Y. Z. Menceloglu, B. Erman, S. S. Abramchuk, E. E. Makhaeva*, et al.*, "Palladium Nanoparticles by Electrospinning from Poly(acrylonitrile-co-acrylic acid)−PdCl2 Solutions. Relations between Preparation Conditions, Particle Size, and Catalytic Activity," *Macromolecules,* vol. 37, pp. 1787-1792, 2004.

[14] M. M. Khan, M. Tsukada, X. Zhang, and H. Morikawa, "Preparation and characterization of electrospun nanofibers based on silk sericin powders," *Journal of Materials Science,* vol. 48, pp. 3731-3736, 2013.

[15] P. D. Cha, J. J. Rosenberg, and C. L. Dym, *Fundamentals of modeling and analyzing engineering systems*: Cambridge University Press, 2000.

[16] L. Y. Yeo and J. R. Friend, "Electrospinning carbon nanotube polymer composite nanofibers," *Journal of Experimental Nanoscience,* vol. 1, pp. 177-209, 2006.

[17] L. Wannatong, A. Sirivat, and P. Supaphol, "Effects of solvents on electrospun polymeric fibers: preliminary study on polystyrene," *Polymer International,* vol. 53, pp. 1851-1859, 2004.

[18] L. Zhang, A. Aboagye, A. Kelkar, C. Lai, and H. Fong, "A review: carbon nanofibers from electrospun polyacrylonitrile and their applications," *Journal of Materials Science,* vol. 49, pp. 463-480, 2014.

[19] Z. Li and C. Wang, "Effects of working parameters on electrospinning," in *One-Dimensional Nanostructures*: Springer, 2013, pp. 15-28.
[20] Z.-M. Huang, Y.-Z. Zhang, M. Kotaki, and S. Ramakrishna, "A review on polymer nanofibers by electrospinning and their applications in nanocomposites," *Composites Science and Technology,* vol. 63, pp. 2223-2253, 2003.
[21] C. Mit-uppatham, M. Nithitanakul, and P. Supaphol, "Ultrafine electrospun polyamide-6 fibers: effect of solution conditions on morphology and average fiber diameter," *Macromolecular Chemistry and Physics,* vol. 205, pp. 2327-2338, 2004.
[22] M. Chowdhury and G. Stylios, "Effect of experimental parameters on the morphology of electrospun Nylon 6 fibres," *International Journal of Basic & Applied Sciences,* vol. 10, pp. 116-131, 2010.
[23] D. S. Katti, K. W. Robinson, F. K. Ko, and C. T. Laurencin, "Bioresorbable nanofiber-based systems for wound healing and drug delivery: Optimization of fabrication parameters," *Journal of Biomedical Materials Research Part B: Applied Biomaterials,* vol. 70, pp. 286-296, 2004.
[24] J. Lyons, C. Li, and F. Ko, "Melt-electrospinning part I: processing parameters and geometric properties," *Polymer,* vol. 45, pp. 7597-7603, 2004.
[25] P. D. Dalton, D. Grafahrend, K. Klinkhammer, D. Klee, and M. Möller, "Electrospinning of polymer melts: phenomenological observations," *Polymer,* vol. 48, pp. 6823-6833, 2007.
[26] S. Lee and S. Kay Obendorf, "Developing protective textile materials as barriers to liquid penetration using melt-electrospinning," *Journal of Applied Polymer Science,* vol. 102, pp. 3430-3437, 2006.
[27] J. Doshi and D. H. Reneker, "Electrospinning process and applications of electrospun fibers," in *Industry Applications Society Annual Meeting, 1993., Conference Record of the 1993 IEEE*, 1993, pp. 1698-1703.
[28] J. Pu, X. Yan, Y. Jiang, C. Chang, and L. Lin, "Piezoelectric actuation of direct-write electrospun fibers," *Sensors and Actuators A: Physical,* vol. 164, pp. 131-136, 2010.
[29] D. Rodoplu and M. Mutlu, "Effects of electrospinning setup and process parameters on nanofiber morphology intended for the modification of quartz crystal microbalance surfaces," *Journal of Engineered Fibers and Fabrics,* vol. 7, pp. 118-123, 2012.
[30] F. Abdel-Hady, A. Alzahrany, and M. Hamed, "Experimental validation of upward electrospinning process," *ISRN Nanotechnology,* vol. 1, 2011.
[31] H. Niu, X. Wang, and T. Lin, "Upward needleless electrospinning of nanofibers," *Journal of engineered fibers and fabrics,* vol. 7, pp. 17-22, 2012.
[32] A. Yarin and E. Zussman, "Upward needleless electrospinning of multiple nanofibers," *Polymer,* vol. 45, pp. 2977-2980, 2004.
[33] F. Abdel-Hady, A. Alzahrany, and M. Hamed, "Experimental Validation of Upward Electrospinning Process," *ISRN Nanotechnology,* vol. 2011, p. 14, 2011.
[34] Bioinicia. *Fluidnatek LE-1000* (2015, 06 April). Available: http://www.bioinicia.com/products/fluidnatek-le-1000/
[35] H. Jiang, Y. Hu, Y. Li, P. Zhao, K. Zhu, and W. Chen, "A facile technique to prepare biodegradable coaxial electrospun nanofibers for controlled release of bioactive agents," *Journal of Controlled Release,* vol. 108, pp. 237-243, 2005.
[36] B. Lu, Y. Wang, Y. Liu, H. Duan, J. Zhou, Z. Zhang*, et al.*, "Superhigh-Throughput Needleless Electrospinning Using a Rotary Cone as Spinneret," *Small,* vol. 6, pp. 1612-1616, 2010.
[37] C. Huang, H. Niu, J. Wu, Q. Ke, X. Mo, and T. Lin, "Needleless electrospinning of polystyrene fibers with an oriented surface line texture," *Journal of nanomaterials,* vol. 2012, p. 7, 2012.

[38] H. Niu, T. Lin, and X. Wang, "Needleless Electrospinning: Developments and Performances," in *Nanofibers – Production, Properties and Functional Applications*: INTECH Open Access Publisher, 2011, pp. 17-36.
[39] J.-H. He, Y. Liu, and L. Xu, "Apparatus for preparing electrospun nanofibres: a comparative review," *Materials Science and Technology,* vol. 26, pp. 1275-1287, 2010.
[40] Y. Liu and J.-H. He, "Bubble electrospinning for mass production of nanofibers," *International Journal of Nonlinear Sciences and Numerical Simulation,* vol. 8, pp. 393-396, 2007.
[41] P. Supaphol, C. Mit-Uppatham, and M. Nithitanakul, "Ultrafine electrospun polyamide-6 fibers: Effect of emitting electrode polarity on morphology and average fiber diameter," *Journal of Polymer Science Part B: Polymer Physics,* vol. 43, pp. 3699-3712, 2005.
[42] W. Wei, J. T. Yeh, P. Li, M. R. Li, W. Li, and X. L. Wang, "Effect of nonsolvent on morphologies of polyamide 6 electrospun fibers," *Journal of applied polymer science,* vol. 118, pp. 3005-3012, 2010.
[43] J. Zeleny, "The role of surface instability in electrical discharges from drops of alcohol and water in air at atmospheric pressure," *Journal of the Franklin Institute,* vol. 219, pp. 659-675, 1935.
[44] T. J. Sill and H. A. von Recum, "Electrospinning: Applications in drug delivery and tissue engineering," *Biomaterials,* vol. 29, pp. 1989-2006, 2008.
[45] W. K. Son, J. H. Youk, T. S. Lee, and W. H. Park, "The effects of solution properties and polyelectrolyte on electrospinning of ultrafine poly (ethylene oxide) fibers," *Polymer,* vol. 45, pp. 2959-2966, 2004.
[46] S. N. Arshad, "High strength carbon nanofibers derived from electrospun polyacrylonitrile," University of Illinois at Urbana-Champaign, 2010.
[47] A. K. Haghi and M. Akbari, "Trends in electrospinning of natural nanofibers," *Physica status solidi (a),* vol. 204, pp. 1830-1834, 2007.
[48] K. Nasouri, A. M. Shoushtari, and A. Kaflou, "Investigation of polyacrylonitrile electrospun nanofibres morphology as a function of polymer concentration, viscosity and Berry number," *Micro & Nano Letters, IET,* vol. 7, pp. 423-426, 2012.
[49] J. Kleinmeyer, J. Deitzel, and J. Hirvonen, "Electrospinning of submicron diameter polymer filaments," ed: Google Patents, 2003.
[50] T. Lin, H. Wang, H. Wang, and X. Wang, "Effects of polymer concentration and cationic surfactant on the morphology of electrospun polyacrylonitrile nanofibres," *Journal of materials science & technology,* vol. 21, pp. 1-4, 2005.
[51] H. Fong, I. Chun, and D. H. Reneker, "Beaded nanofibers formed during electrospinning," *Polymer,* vol. 40, pp. 4585-4592, 1999.
[52] S. Gu, J. Ren, and G. Vancso, "Process optimization and empirical modeling for electrospun polyacrylonitrile (PAN) nanofiber precursor of carbon nanofibers," *European polymer journal,* vol. 41, pp. 2559-2568, 2005.
[53] Y. J. Ryu, H. Y. Kim, K. H. Lee, H. C. Park, and D. R. Lee, "Transport properties of electrospun nylon 6 nonwoven mats," *European Polymer Journal,* vol. 39, pp. 1883-1889, 2003.
[54] W. K. Son, J. H. Youk, T. S. Lee, and W. H. Park, "The effects of solution properties and polyelectrolyte on electrospinning of ultrafine poly(ethylene oxide) fibers," *Polymer,* vol. 45, pp. 2959-2966, 2004.
[55] X. Zong, K. Kim, D. Fang, S. Ran, B. S. Hsiao, and B. Chu, "Structure and process relationship of electrospun bioabsorbable nanofiber membranes," *Polymer,* vol. 43, pp. 4403-4412, 2002.

[56] M. Yousefzadeh, M. Latifi, M. Amani-Tehran, W.-E. Teo, and S. Ramakrishna, "A note on the 3D structural design of electrospun nanofibers," *Journal of Engineered Fabrics & Fibers (JEFF),* vol. 7, 2012.
[57] J.A. Knopf, " Investigation of Linear Electrospinning Jets," University of Delaware, 2009.
[58] A. G. Sener, A. S. Altay, and F. Altay, "Effect of voltage on morphology of electrospun nanofibers," in *Electrical and Electronics Engineering (ELECO), 2011 7th International Conference on*, 2011, pp. I-324-I-328.
[59] Y. Li, Z. Huang, and Y. Lǔ, "Electrospinning of nylon-6, 66, 1010 terpolymer," *European Polymer Journal,* vol. 42, pp. 1696-1704, 2006.
[60] S. Megelski, J. S. Stephens, D. B. Chase, and J. F. Rabolt, "Micro- and Nanostructured Surface Morphology on Electrospun Polymer Fibers," *Macromolecules,* vol. 35, pp. 8456-8466, 2002.
[61] M. B. Bazbouz and G. K. Stylios, "Alignment and optimization of nylon 6 nanofibers by electrospinning," *Journal of Applied Polymer Science,* vol. 107, pp. 3023-3032, 2008.
[62] P. Heikkilä and A. Harlin, "Electrospinning of polyacrylonitrile (PAN) solution: Effect of conductive additive and filler on the process," *Express Polymer Letters,* vol. 3, pp. 437-445, 2009.
[63] Y. Ahn, S. Park, G. Kim, Y. Hwang, C. Lee, H. Shin*, et al.*, "Development of high efficiency nanofilters made of nanofibers," *Current Applied Physics,* vol. 6, pp. 1030-1035, 2006.
[64] M. Naraghi, S. Arshad, and I. Chasiotis, "Molecular orientation and mechanical property size effects in electrospun polyacrylonitrile nanofibers," *Polymer,* vol. 52, pp. 1612-1618, 2011.
[65] C. Thompson, G. Chase, A. Yarin, and D. Reneker, "Effects of parameters on nanofiber diameter determined from electrospinning model," *Polymer,* vol. 48, pp. 6913-6922, 2007.
[66] P. Heikkilä and A. Harlin, "Parameter study of electrospinning of polyamide-6," *European Polymer Journal,* vol. 44, pp. 3067-3079, 2008.
[67] C. Wang, H.-S. Chien, K.-W. Yan, C.-L. Hung, K.-L. Hung, S.-J. Tsai*, et al.*, "Correlation between processing parameters and microstructure of electrospun poly (D, L-lactic acid) nanofibers," *Polymer,* vol. 50, pp. 6100-6110, 2009.
[68] C. J. Angammana, "A Study of the Effects of Solution and Process Parameters on the Electrospinning Process and Nanofibre Morphology," 2011.
[69] H. I. Icoglu and R. T. Ogulata, "Effect of ambient parameters on morphology of electrospun polyetherimide (PEI) fibers," *TEKSTIL VE KONFEKSIYON,* vol. 23, pp. 313-318, 2013.
[70] E. S. Medeiros, L. H. C. Mattoso, R. D. Offeman, D. F. Wood, and W. J. Orts, "Effect of relative humidity on the morphology of electrospun polymer fibers," *Canadian Journal of Chemistry,* vol. 86, pp. 590-599, 2008.
[71] E. Marsano, L. Francis, and F. Giunco, "Polyamide 6 nanofibrous nonwovens via electrospinning," *Journal of applied polymer science,* vol. 117, pp. 1754-1765, 2010.
[72] C. B. Giller, D. B. Chase, J. F. Rabolt, and C. M. Snively, "Effect of solvent evaporation rate on the crystalline state of electrospun nylon 6," *Polymer,* vol. 51, pp. 4225-4230, 2010.
[73] S. Vrieze, T. Camp, A. Nelvig, B. Hagström, P. Westbroek, and K. Clerck, "The effect of temperature and humidity on electrospinning," *Journal of Materials Science,* vol. 44, pp. 1357-1362, 2008.

[74] M. A. Bezerra, R. E. Santelli, E. P. Oliveira, L. S. Villar, and L. A. Escaleira, "Response surface methodology (RSM) as a tool for optimization in analytical chemistry," *Talanta,* vol. 76, pp. 965-977, 2008.
[75] N. A. Gershenfeld, *The Nature of Mathematical Modeling*: Cambridge University Press, 1999.
[76] A. Ford, *Modeling the Environment, Second Edition*: Island Press, 2009.
[77] XLSTAT. *What is statistical modeling?* (2015, 02 April). Available: https://help.xlstat.com
[78] *ANOVA analyses in Minitab* (2016, 03 April). Available: http://support.minitab.com/
[79] S. Weisberg, *Applied Linear Regression*: Wiley, 2013.
[80] X. Yan, *Linear Regression Analysis: Theory and Computing*: World Scientific Publishing Company, 2009.
[81] *Regression Analysis: How Do I Interpret R-squared and Assess the Goodness-of-Fit?* (2016, 05 April). Available: http://blog.minitab.com/
[82] A. French, M. Macedo, J. Poulsen, T. Waterson, and A. Yu, "Multivariate analysis of variance (MANOVA)," ed, 2008.
[83] University of California, Los Angeles. *R Data Analysis Examples: Poisson Regression* (2016, 04 April). Available: http://www.ats.ucla.edu/stat
[84] G. E. Box, J. S. Hunter, and W. G. Hunter, *Statistics for experimenters: design, innovation, and discovery*, vol. 2: Wiley-Interscience New York, 2005.
[85] Minitab Inc. *What is a mixture design?* (2016, 05 April). Available: http://support.minitab.com/
[86] NIST. (2012, 05 April, 2016). *Engineering Statistics handbook*. Available: http://www.itl.nist.gov/div898/handbook/
[87] K. D. Kim, D. N. Han, and H. T. Kim, "Optimization of experimental conditions based on the Taguchi robust design for the formation of nano-sized silver particles by chemical reduction method," *Chemical Engineering Journal,* vol. 104, pp. 55-61, 2004.
[88] M. Nalbant, H. Gökkaya, and G. Sur, "Application of Taguchi method in the optimization of cutting parameters for surface roughness in turning," *Materials & Design,* vol. 28, pp. 1379-1385, 2007.
[89] W. Liu and S. Adanur, "Properties of electrospun polyacrylonitrile membranes and chemically-activated carbon nanofibers," *Textile Research Journal,* 2009.
[90] J.-H. He, Y.-Q. Wan, and J.-Y. Yu, "Effect of concentration on electrospun polyacrylonitrile (PAN) nanofibers," *Fibers and Polymers,* vol. 9, pp. 140-142, 2008.
[91] M. G. McKee, G. L. Wilkes, R. H. Colby, and T. E. Long, "Correlations of solution rheology with electrospun fiber formation of linear and branched polyesters," *Macromolecules,* vol. 37, pp. 1760-1767, 2004.
[92] M. M. Demir, I. Yilgor, E. Yilgor, and B. Erman, "Electrospinning of polyurethane fibers," *Polymer,* vol. 43, pp. 3303-3309, 2002.
[93] O. S. Yördem, M. Papila, and Y. Z. Menceloğlu, "Effects of electrospinning parameters on polyacrylonitrile nanofiber diameter: An investigation by response surface methodology," *Materials & Design,* vol. 29, pp. 34-44, 2008.
[94] D. H. Reneker, A. Yarin, E. Zussman, S. Koombhongse, and W. Kataphinan, "Nanofiber manufacturing: toward better process control," in *ACS symposium series*, 2006, pp. 7-20.
[95] S. Sukigara, M. Gandhi, J. Ayutsede, M. Micklus, and F. Ko, "Regeneration of Bombyx mori silk by electrospinning—part 1: processing parameters and geometric properties," *Polymer,* vol. 44, pp. 5721-5727, 2003.

[96] J.-P. Chen, K.-H. Ho, Y.-P. Chiang, and K.-W. Wu, "Fabrication of electrospun poly (methyl methacrylate) nanofibrous membranes by statistical approach for application in enzyme immobilization," *Journal of Membrane Science,* vol. 340, pp. 9-15, 2009.
[97] J. Ayutsede, M. Gandhi, S. Sukigara, M. Micklus, H.-E. Chen, and F. Ko, "Regeneration of Bombyx mori silk by electrospinning. Part 3: characterization of electrospun nonwoven mat," *Polymer,* vol. 46, pp. 1625-1634, 2005.
[98] X. Zhuang, B. Cheng, W. Kang, and X. Xu, "Electrospun chitosan/gelatin nanofibers containing silver nanoparticles," *Carbohydrate Polymers,* vol. 82, pp. 524-527, 2010.
[99] Y. Zhang, B. Su, J. Venugopal, S. Ramakrishna, and C. Lim, "Biomimetic and bioactive nanofibrous scaffolds from electrospun composite nanofibers," *International Journal of Nanomedicine,* vol. 2, pp. 623–638.
[100] L. Fagundes, T. Sousa, A. Sousa, V. Silva, and E. Sousa, "SBA-15-collagen hybrid material for drug delivery applications," *Journal of non-crystalline solids,* vol. 352, pp. 3496-3501, 2006.
[101] G. E. Wnek, M. E. Carr, D. G. Simpson, and G. L. Bowlin, "Electrospinning of nanofiber fibrinogen structures," *Nano Letters,* vol. 3, pp. 213-216, 2003.
[102] X. Xu and M. Zhou, "Antimicrobial gelatin nanofibers containing silver nanoparticles," *Fibers and polymers,* vol. 9, pp. 685-690, 2008.
[103] C. P. Barnes[1], M. J. Smith[1], G. L. Bowlin[1], S. A. Sell[1], T. Tang[1], J. A. Matthews*, et al.*, "Feasibility of electrospinning the globular proteins hemoglobin and myoglobin," 2006.
[104] R. Nirmala, H.-M. Park, R. Navamathavan, H.-S. Kang, M. H. El-Newehy, and H. Y. Kim, "Lecithin blended polyamide-6 high aspect ratio nanofiber scaffolds via electrospinning for human osteoblast cell culture," *Materials Science and Engineering: C,* vol. 31, pp. 486-493, 2011.
[105] M. R. Karim, H. W. Lee, R. Kim, B. C. Ji, J. W. Cho, T. W. Son*, et al.*, "Preparation and characterization of electrospun pullulan/montmorillonite nanofiber mats in aqueous solution," *Carbohydrate polymers,* vol. 78, pp. 336-342, 2009.
[106] L. Kong and G. R. Ziegler, "Role of molecular entanglements in starch fiber formation by electrospinning," *Biomacromolecules,* vol. 13, pp. 2247-2253, 2012.
[107] L. M. Guerrini, M. C. Branciforti, T. Canova, and R. E. S. Bretas, "Electrospinning and characterization of polyamide 66 nanofibers with different molecular weights," *Materials Research,* vol. 12, pp. 181-190, 2009.
[108] B. Ding, M. Yamazaki, and S. Shiratori, "Electrospun fibrous polyacrylic acid membrane-based gas sensors," *Sensors and Actuators B: Chemical,* vol. 106, pp. 477-483, 2005.
[109] N. Kattamuri and C. Sung, "Uniform polycarbonate nanofibers produced by electrospinning," *Macromolecules,* vol. 3, p. 425, 2004.
[110] H. Hou, J. J. Ge, J. Zeng, Q. Li, D. H. Reneker, A. Greiner*, et al.*, "Electrospun polyacrylonitrile nanofibers containing a high concentration of well-aligned multiwall carbon nanotubes," *Chemistry of Materials,* vol. 17, pp. 967-973, 2005.
[111] S. Moon, J. Choi, and R. J. Farris, "Preparation of aligned polyetherimide fiber by electrospinning," *Journal of applied polymer science,* vol. 109, pp. 691-694, 2008.
[112] M. S. Khil, D. I. Cha, H. Y. Kim, I. S. Kim, and N. Bhattarai, "Electrospun nanofibrous polyurethane membrane as wound dressing," *Journal of Biomedical Materials Research Part B: Applied Biomaterials,* vol. 67, pp. 675-679, 2003.
[113] H. Zhu, S. Qiu, W. Jiang, D. Wu, and C. Zhang, "Evaluation of electrospun polyvinyl chloride/polystyrene fibers as sorbent materials for oil spill cleanup," *Environmental science & technology,* vol. 45, pp. 4527-4531, 2011.

[114] M. Jannesari, J. Varshosaz, M. Morshed, and M. Zamani, "Composite poly (vinyl alcohol)/poly (vinyl acetate) electrospun nanofibrous mats as a novel wound dressing matrix for controlled release of drugs," *Int J Nanomedicine,* vol. 6, pp. 993-1003, 2011.
[115] R. Gopal, S. Kaur, C. Y. Feng, C. Chan, S. Ramakrishna, S. Tabe*, et al.*, "Electrospun nanofibrous polysulfone membranes as pre-filters: Particulate removal," *Journal of Membrane Science,* vol. 289, pp. 210-219, 2007.
[116] S. Imaizumi, H. Matsumoto, K. Suzuki, M. Minagawa, M. Kimura, and A. Tanioka, "Phenolic resin-based carbon thin fibers prepared by electrospinning: additive effects of poly (vinyl butyral) and electrolytes," *Polymer journal,* vol. 41, pp. 1124-1128, 2009.
[117] C. Yang, Z. Jia, Z. Guan, and L. Wang, "Polyvinylidene fluoride membrane by novel electrospinning system for separator of Li-ion batteries," *Journal of Power Sources,* vol. 189, pp. 716-720, 2009.
[118] E.-R. Kenawy, A. E.-R. R. El-Shanshoury, N. Omar Shaker, B. M. El-Sadek, A. H. Khattab, and A. Elzatahry, "Synthesis and Biocide Activity of Polymers Based on Poly (hydroxy styrene) and Poly (hydroxy styrene-co-2-hydroxyethyl methacrylate)," *Main Group Chemistry,* vol. 12, pp. 293-306, 2013.
[119] A. G. Mikos, M. D. Lyman, L. E. Freed, and R. Langer, "Wetting of poly (L-lactic acid) and poly (DL-lactic-co-glycolic acid) foams for tissue culture," *Biomaterials,* vol. 15, pp. 55-58, 1994.
[120] C. Luo, E. Stride, and M. Edirisinghe, "Mapping the influence of solubility and dielectric constant on electrospinning polycaprolactone solutions," *Macromolecules,* vol. 45, pp. 4669-4680, 2012.
[121] C. Chen, L. Wang, and Y. Huang, "Electrospinning of thermo-regulating ultrafine fibers based on polyethylene glycol/cellulose acetate composite," *Polymer,* vol. 48, pp. 5202-5207, 2007.
[122] S. Nataraj, K. Yang, and T. Aminabhavi, "Polyacrylonitrile-based nanofibers—a state-of-the-art review," *Progress in polymer science,* vol. 37, pp. 487-513, 2012.
[123] T. Maitra, S. Sharma, A. Srivastava, Y.-K. Cho, M. Madou, and A. Sharma, "Improved graphitization and electrical conductivity of suspended carbon nanofibers derived from carbon nanotube/polyacrylonitrile composites by directed electrospinning," *Carbon,* vol. 50, pp. 1753-1761, 2012.
[124] M. S. A. Rahaman, A. F. Ismail, and A. Mustafa, "A review of heat treatment on polyacrylonitrile fiber," *Polymer Degradation and Stability,* vol. 92, pp. 1421-1432, 2007.
[125] P. Morgan, *Carbon Fibers and Their Composites*: CRC Press, 2005.
[126] C. Lai, G. Zhong, Z. Yue, G. Chen, L. Zhang, A. Vakili*, et al.*, "Investigation of post-spinning stretching process on morphological, structural, and mechanical properties of electrospun polyacrylonitrile copolymer nanofibers," *Polymer,* vol. 52, pp. 519-528, 2011.
[127] F. Agend, N. Naderi, and R. Fareghi-Alamdari, "Fabrication and electrical characterization of electrospun polyacrylonitrile-derived carbon nanofibers," *Journal of applied polymer science,* vol. 106, pp. 255-259, 2007.
[128] R. Jalili, M. Morshed, and S. A. H. Ravandi, "Fundamental parameters affecting electrospinning of PAN nanofibers as uniaxially aligned fibers," *Journal of applied polymer science,* vol. 101, pp. 4350-4357, 2006.
[129] N. Li, Q. Hui, H. Xue, and J. Xiong, "Electrospun Polyacrylonitrile nanofiber yarn prepared by funnel-shape collector," *Materials Letters,* vol. 79, pp. 245-247, 2012.
[130] S.-F. Li, J.-P. Chen, and W.-T. Wu, "Electrospun polyacrylonitrile nanofibrous membranes for lipase immobilization," *Journal of Molecular Catalysis B: Enzymatic,* vol. 47, pp. 117-124, 2007.

[131] T. Yang, Y. Yao, Y. Lin, B. Wang, R. Xiang, Y. Wu*, et al.*, "Electrospinning of polyacrylonitrile fibers from ionic liquid solution," *Applied Physics A,* vol. 98, pp. 517-523, 2010.
[132] X. Yu, H. Xiang, Y. Long, N. Zhao, X. Zhang, and J. Xu, "Preparation of porous polyacrylonitrile fibers by electrospinning a ternary system of PAN/DMF/H 2 O," *Materials Letters,* vol. 64, pp. 2407-2409, 2010.
[133] T. Wang and S. Kumar, "Electrospinning of polyacrylonitrile nanofibers," *Journal of applied polymer science,* vol. 102, pp. 1023-1029, 2006.
[134] D. H. Reneker and I. Chun, "Nanometre diameter fibres of polymer, produced by electrospinning," *Nanotechnology,* vol. 7, p. 216, 1996.
[135] X. H. Qin, E. L. Yang, N. Li, and S. Y. Wang, "Effect of different salts on electrospinning of polyacrylonitrile (PAN) polymer solution," *Journal of applied polymer science,* vol. 103, pp. 3865-3870, 2007.
[136] S. N. Arshad, M. Naraghi, and I. Chasiotis, "Strong carbon nanofibers from electrospun polyacrylonitrile," *Carbon,* vol. 49, pp. 1710-1719, 2011.
[137] T. H. Yoong Ahm Kim, Morinobu Endo, Mildred S. Dresselhaus, "Carbon Nanofibers," in *Handbook of Nanomaterials*: Springer Berlin Heidelberg, 2013.
[138] G. Che, B. Lakshmi, C. Martin, E. Fisher, and R. S. Ruoff, "Chemical vapor deposition based synthesis of carbon nanotubes and nanofibers using a template method," *Chemistry of Materials,* vol. 10, pp. 260-267, 1998.
[139] M. Adabi, R. Saber, R. Faridi-Majidi, and F. Faridbod, "Performance of electrodes synthesized with polyacrylonitrile-based carbon nanofibers for application in electrochemical sensors and biosensors," *Materials Science and Engineering: C,* vol. 48, pp. 673-678, 2015.
[140] H. Ono and A. Oya, "Preparation of highly crystalline carbon nanofibers from pitch/polymer blend," *Carbon,* vol. 44, pp. 682-686, 2006.
[141] J. Liu, Z. Yue, and H. Fong, "Continuous nanoscale carbon fibers with superior mechanical strength," *Small,* vol. 5, pp. 536-542, 2009.
[142] M. Wu, Q. Wang, K. Li, Y. Wu, and H. Liu, "Optimization of stabilization conditions for electrospun polyacrylonitrile nanofibers," *Polymer Degradation and Stability,* vol. 97, pp. 1511-1519, 2012.
[143] R. Houtz, "" Orlon" Acrylic Fiber: Chemistry and Properties," *Textile Research Journal,* vol. 20, pp. 786-801, 1950.
[144] N. Grassie, J. N. Hay, and I. C. McNeill, "Coloration in acrylonitrile and methacrylonitrile polymers," *Journal of Polymer Science,* vol. 31, pp. 205-206, 1958.
[145] N. Grassie and J. Hay, "Thermal coloration and insolubilization in polyacrylonitrile," *Journal of Polymer Science,* vol. 56, pp. 189-202, 1962.
[146] J. Schurz, "Discoloration effects in acrylonitrile polymers," *Journal of Polymer Science,* vol. 28, pp. 438-439, 1958.
[147] S. Dalton, F. Heatley, and P. M. Budd, "Thermal stabilization of polyacrylonitrile fibres," *Polymer,* vol. 40, pp. 5531-5543, 1999.
[148] Y. Yang, F. Simeon, T. A. Hatton, and G. C. Rutledge, "Polyacrylonitrile-based electrospun carbon paper for electrode applications," *Journal of Applied Polymer Science,* vol. 124, pp. 3861-3870, 2012.
[149] D. Zhu, C. Xu, N. Nakura, and M. Matsuo, "Study of carbon films from PAN/VGCF composites by gelation/crystallization from solution," *Carbon,* vol. 40, pp. 363-373, 2002.
[150] B. O. Donnet JB, "Encyclopedia of Physical Science and Technology," vol. 2, ed: New York: Acedamic Press Inc, 1987.

[151] I.-H. Chen, C.-C. Wang, and C.-Y. Chen, "Fabrication and structural characterization of polyacrylonitrile and carbon nanofibers containing plasma-modified carbon nanotubes by electrospinning," *The Journal of Physical Chemistry C,* vol. 114, pp. 13532-13539, 2010.
[152] Z. Zhou, C. Lai, L. Zhang, Y. Qian, H. Hou, D. H. Reneker*, et al.*, "Development of carbon nanofibers from aligned electrospun polyacrylonitrile nanofiber bundles and characterization of their microstructural, electrical, and mechanical properties," *Polymer,* vol. 50, pp. 2999-3006, 2009.
[153] L. Zhang and Y.-L. Hsieh, "Carbon nanofibers with nanoporosity and hollow channels from binary polyacrylonitrile systems," *European Polymer Journal,* vol. 45, pp. 47-56, 2009.
[154] T. H. Ko, "The influence of pyrolysis on physical properties and microstructure of modified PAN fibers during carbonization," *Journal of applied polymer science,* vol. 43, pp. 589-600, 1991.
[155] T. H. Ko and L. C. Huang, "The influence of cobaltous chloride modification on physical properties and microstructure of modified PAN fiber during carbonization," *Journal of applied polymer science,* vol. 70, pp. 2409-2415, 1998.
[156] S. Moon, J. Choi, and R. J. Farris, "Highly porous polyacrylonitrile/polystyrene nanofibers by electrospinning," *Fibers and Polymers,* vol. 9, pp. 276-280, 2008.
[157] Y. Chen, Z. Lu, L. Zhou, Y.-W. Mai, and H. Huang, "In situ formation of hollow graphitic carbon nanospheres in electrospun amorphous carbon nanofibers for high-performance Li-based batteries," *Nanoscale,* vol. 4, pp. 6800-6805, 2012.
[158] R. Ding, H. Wu, M. Thunga, N. Bowler, and M. R. Kessler, "Processing and characterization of low-cost electrospun carbon fibers from organosolv lignin/polyacrylonitrile blends," *Carbon,* vol. 100, pp. 126-136, 2016.
[159] M. Lisunova, A. Hildmann, B. Hatting, V. Datsyuk, and S. Reich, "Nanofibres of CA/PAN with high amount of carbon nanotubes by core–shell electrospinning," *Composites Science and Technology,* vol. 70, pp. 1584-1588, 2010.
[160] S.-H. Park, B.-K. Kim, and W.-J. Lee, "Electrospun activated carbon nanofibers with hollow core/highly mesoporous shell structure as counter electrodes for dye-sensitized solar cells," *Journal of Power Sources,* vol. 239, pp. 122-127, 2013.
[161] H. Chen, N. Wang, J. Di, Y. Zhao, Y. Song, and L. Jiang, "Nanowire-in-Microtube Structured Core/Shell Fibers via Multifluidic Coaxial Electrospinning," *Langmuir,* vol. 26, pp. 11291-11296, 2010.
[162] N. E. Zander, K. E. Strawhecker, J. A. Orlicki, A. M. Rawlett, and T. P. Beebe Jr, "Coaxial Electrospun Poly (methyl methacrylate)–Polyacrylonitrile Nanofibers: Atomic Force Microscopy and Compositional Characterization," *The Journal of Physical Chemistry B,* vol. 115, pp. 12441-12447, 2011.
[163] A. V. Bazilevsky, A. L. Yarin, and C. M. Megaridis, "Co-electrospinning of Core−Shell Fibers Using a Single-Nozzle Technique," *Langmuir,* vol. 23, pp. 2311-2314, 2007.
[164] C. Kim, Y. I. Jeong, B. T. N. Ngoc, K. S. Yang, M. Kojima, Y. A. Kim*, et al.*, "Synthesis and characterization of porous carbon nanofibers with hollow cores through the thermal treatment of electrospun copolymeric nanofiber webs," *Small,* vol. 3, pp. 91-95, 2007.
[165] P. Gupta, "The Effect of Cooperative Charging On Filtration Properties Of Electrically Dissimilar Electrospun Nanofibers Of Polymers," PhD, Chemical Engineering, Virginia Polytechnic Institute And State University, United states, 2004.
[166] T. Lin, H. Wang, and X. Wang, "Self-crimping bicomponent nanofibers electrospun from polyacrylonitrile and elastomeric polyurethane," *Advanced Materials,* vol. 17, pp. 2699-2703, 2005.

[167] W. Wang, Z. Li, X. Xu, B. Dong, H. Zhang, Z. Wang, *et al.*, "Au-Doped Polyacrylonitrile–Polyaniline Core–Shell Electrospun Nanofibers Having High Field-Effect Mobilities," *Small,* vol. 7, pp. 597-600, 2011.
[168] J. Wang, K. Pan, Q. He, and B. Cao, "Polyacrylonitrile/polypyrrole core/shell nanofiber mat for the removal of hexavalent chromium from aqueous solution," *Journal of hazardous materials,* vol. 244, pp. 121-129, 2013.
[169] Y. Chou, C. Shao, X. Li, C. Su, H. Xu, M. Zhang, *et al.*, "BiOCl nanosheets immobilized on electrospun polyacrylonitrile nanofibers with high photocatalytic activity and reusable property," *Applied Surface Science,* vol. 285, pp. 509-516, 2013.
[170] L. Ji and X. Zhang, "Ultrafine polyacrylonitrile/silica composite fibers via electrospinning," *Materials Letters,* vol. 62, pp. 2161-2164, 2008.
[171] L. Chen, S. Hong, X. Zhou, Z. Zhou, and H. Hou, "Novel Pd-carrying composite carbon nanofibers based on polyacrylonitrile as a catalyst for Sonogashira coupling reaction," *Catalysis Communications,* vol. 9, pp. 2221-2225, 2008.
[172] C. Su, Y. Tong, M. Zhang, Y. Zhang, and C. Shao, "TiO 2 nanoparticles immobilized on polyacrylonitrile nanofibers mats: a flexible and recyclable photocatalyst for phenol degradation," *RSC Advances,* vol. 3, pp. 7503-7512, 2013.
[173] H. Yu, Z. Jiao, H. Hu, G. Lu, J. Ye, and Y. Bi, "Fabrication of Ag 3 PO 4–PAN composite nanofibers for photocatalytic applications," *CrystEngComm,* vol. 15, pp. 4802-4805, 2013.
[174] D. Zhang, A. B. Karki, D. Rutman, D. P. Young, A. Wang, D. Cocke, *et al.*, "Electrospun polyacrylonitrile nanocomposite fibers reinforced with Fe 3 O 4 nanoparticles: fabrication and property analysis," *Polymer,* vol. 50, pp. 4189-4198, 2009.
[175] L. Ji, Z. Lin, A. J. Medford, and X. Zhang, "Porous carbon nanofibers from electrospun polyacrylonitrile/SiO2 composites as an energy storage material," *Carbon,* vol. 47, pp. 3346-3354, 2009.
[176] L. Ji and X. Zhang, "Electrospun carbon nanofibers containing silicon particles as an energy-storage medium," *Carbon,* vol. 47, pp. 3219-3226, 2009.
[177] J. Liwen, S. Carl, A. K. Saad, and Z. Xiangwu, "Preparation and characterization of silica nanoparticulate – polyacrylonitrile composite and porous nanofibers," *Nanotechnology,* vol. 19, p. 085605, 2008.
[178] H.-R. Jung, D.-H. Ju, W.-J. Lee, X. Zhang, and R. Kotek, "Electrospun hydrophilic fumed silica/polyacrylonitrile nanofiber-based composite electrolyte membranes," *Electrochimica Acta,* vol. 54, pp. 3630-3637, 2009.
[179] X. H. Qin and S. Y. Wang, "Filtration properties of electrospinning nanofibers," *Journal of Applied Polymer Science,* vol. 102, pp. 1285-1290, 2006.
[180] D. Y. Lee, K.-H. Lee, B.-Y. Kim, and N.-I. Cho, "Silver nanoparticles dispersed in electrospun polyacrylonitrile nanofibers via chemical reduction," *Journal of sol-gel science and technology,* vol. 54, pp. 63-68, 2010.
[181] Y. Wang, Q. Yang, G. Shan, C. Wang, J. Du, S. Wang, *et al.*, "Preparation of silver nanoparticles dispersed in polyacrylonitrile nanofiber film spun by electrospinning," *Materials Letters,* vol. 59, pp. 3046-3049, 2005.
[182] G. N. Sichani, M. Morshed, M. Amirnasr, and D. Abedi, "In situ preparation, electrospinning, and characterization of polyacrylonitrile nanofibers containing silver nanoparticles," *Journal of Applied Polymer Science,* vol. 116, pp. 1021-1029, 2010.
[183] B.-H. Kim, K. S. Yang, and H.-G. Woo, "Thin, bendable electrodes consisting of porous carbon nanofibers via the electrospinning of polyacrylonitrile containing tetraethoxy orthosilicate for supercapacitor," *Electrochemistry Communications,* vol. 13, pp. 1042-1046, 2011.

[184] Y. Yu, Q. Yang, D. Teng, X. Yang, and S. Ryu, "Reticular Sn nanoparticle-dispersed PAN-based carbon nanofibers for anode material in rechargeable lithium-ion batteries," *Electrochemistry Communications,* vol. 12, pp. 1187-1190, 2010.
[185] Z. Yang, G. Du, Q. Meng, Z. Guo, X. Yu, Z. Chen*, et al.*, "Synthesis of uniform TiO 2@ carbon composite nanofibers as anode for lithium ion batteries with enhanced electrochemical performance," *Journal of Materials Chemistry,* vol. 22, pp. 5848-5854, 2012.
[186] S. Nataraj, B. Kim, M. dela Cruz, J. Ferraris, T. Aminabhavi, and K. Yang, "Free standing thin webs of porous carbon nanofibers of polyacrylonitrile containing iron-oxide by electrospinning," *Materials Letters,* vol. 63, pp. 218-220, 2009.
[187] Z. Liu, C. Zhou, B. Zheng, L. Qian, Y. Mo, F. Luo*, et al.*, "In situ synthesis of gold nanoparticles on porous polyacrylonitrile nanofibers for sensing applications," *Analyst,* vol. 136, pp. 4545-4551, 2011.
[188] Y. T. Ong, A. L. Ahmad, S. H. S. Zein, and S. H. Tan, "A review on carbon nanotubes in an environmental protection and green engineering perspective," *Brazilian Journal of Chemical Engineering,* vol. 27, pp. 227-242, 2010.
[189] J. Choy and Y. Zhang, "Properties and Applications of Single-, Double-and Multi-Walled Carbon Nanotubes," *Sigma-Aldrich,* 2014.
[190] Nanowerk. *Carbon Nanotubes 101 – Properties* (9 April). Available: http://www.nanowerk.com/
[191] M. Moniruzzaman and K. I. Winey, "Polymer nanocomposites containing carbon nanotubes," *Macromolecules,* vol. 39, pp. 5194-5205, 2006.
[192] H. Guo, M. L. Minus, S. Jagannathan, and S. Kumar, "Polyacrylonitrile/carbon nanotube composite films," *ACS applied materials & interfaces,* vol. 2, pp. 1331-1342, 2010.
[193] S. Prilutsky, E. Zussman, and Y. Cohen, "The effect of embedded carbon nanotubes on the morphological evolution during the carbonization of poly (acrylonitrile) nanofibers," *Nanotechnology,* vol. 19, p. 165603, 2008.
[194] X. Pei, W. Liu, and J. Hao, "Functionalization of multiwalled carbon nanotube via surface reversible addition fragmentation chain transfer polymerization and as lubricant additives," *Journal of Polymer Science Part A: Polymer Chemistry,* vol. 46, pp. 3014-3023, 2008.
[195] G. Mountrichas, S. Pispas, and N. Tagmatarchis, "Grafting-to approach for the functionalization of carbon nanotubes with polystyrene," *Materials Science and Engineering: B,* vol. 152, pp. 40-43, 2008.
[196] A. Shanmugharaj, J. Bae, R. R. Nayak, and S. H. Ryu, "Preparation of poly (styrene-co-acrylonitrile)-grafted multiwalled carbon nanotubes via surface-initiated atom transfer radical polymerization," *Journal of Polymer Science Part A: Polymer Chemistry,* vol. 45, pp. 460-470, 2007.
[197] J. Ji, G. Sui, Y. Yu, Y. Liu, Y. Lin, Z. Du*, et al.*, "Significant improvement of mechanical properties observed in highly aligned carbon-nanotube-reinforced nanofibers," *The Journal of Physical Chemistry C,* vol. 113, pp. 4779-4785, 2009.
[198] J. S. Im, S. J. Kim, P. H. Kang, and Y.-S. Lee, "The improved electrical conductivity of carbon nanofibers by fluorinated MWCNTs," *Journal of Industrial and Engineering Chemistry,* vol. 15, pp. 699-702, 2009.
[199] E. J. Ra, K. H. An, K. K. Kim, S. Y. Jeong, and Y. H. Lee, "Anisotropic electrical conductivity of MWCNT/PAN nanofiber paper," *Chemical Physics Letters,* vol. 413, pp. 188-193, 2005.

[200] G. Mathew, J. P. Hong, J. M. Rhee, H. S. Lee, and C. Nah, "Preparation and characterization of properties of electrospun poly(butylene terephthalate) nanofibers filled with carbon nanotubes," *Polymer Testing,* vol. 24, pp. 712-717, 2005.
[201] J. J. Ge, H. Hou, Q. Li, M. J. Graham, A. Greiner, D. H. Reneker*, et al.*, "Assembly of well-aligned multiwalled carbon nanotubes in confined polyacrylonitrile environments: electrospun composite nanofiber sheets," *Journal of the American Chemical Society,* vol. 126, pp. 15754-15761, 2004.
[202] P. Heikkilä, "Nanostructured Fibre Composites, and Materials for Air Filtration," PhD, Department of Materials Science, Tampere University of Technology, Finland, 2008.
[203] E. Zussman, X. Chen, W. Ding, L. Calabri, D. Dikin, J. Quintana*, et al.*, "Mechanical and structural characterization of electrospun PAN-derived carbon nanofibers," *Carbon,* vol. 43, pp. 2175-2185, 2005.
[204] Y. Wang, J. J. Santiago-Aviles, R. Furlan, and I. Ramos, "Pyrolysis temperature and time dependence of electrical conductivity evolution for electrostatically generated carbon nanofibers," *Nanotechnology, IEEE Transactions on,* vol. 2, pp. 39-43, 2003.
[205] K. Chakrabarti, P. Nambissan, C. Mukherjee, K. Bardhan, C. Kim, and K. Yang, "Positron annihilation spectroscopy of polyacrylonitrile-based carbon fibers embedded with multi-wall carbon nanotubes," *Carbon,* vol. 44, pp. 948-953, 2006.
[206] J. Che, T. Cagin, and W. A. Goddard III, "Thermal conductivity of carbon nanotubes," *Nanotechnology,* vol. 11, p. 65, 2000.
[207] W. J. Li, C. T. Laurencin, E. J. Caterson, R. S. Tuan, and F. K. Ko, "Electrospun nanofibrous structure: a novel scaffold for tissue engineering," *Journal of biomedical materials research,* vol. 60, pp. 613-621, 2002.
[208] Z. Ma, M. Kotaki, R. Inai, and S. Ramakrishna, "Potential of nanofiber matrix as tissue-engineering scaffolds," *Tissue engineering,* vol. 11, pp. 101-109, 2005.
[209] R. L. Mauck, B. M. Baker, N. L. Nerurkar, J. A. Burdick, W.-J. Li, R. S. Tuan*, et al.*, "Engineering on the straight and narrow: the mechanics of nanofibrous assemblies for fiber-reinforced tissue regeneration," *Tissue Engineering Part B: Reviews,* vol. 15, pp. 171-193, 2009.
[210] C. Xu, R. Inai, M. Kotaki, and S. Ramakrishna, "Electrospun nanofiber fabrication as synthetic extracellular matrix and its potential for vascular tissue engineering," *Tissue engineering,* vol. 10, pp. 1160-1168, 2004.
[211] T.-S. Jun, T. A. Ho, M. Rashid, and Y. S. Kim, "A novel methanol sensor based on gas-penetration through a porous polypyrrole-coated polyacrylonitrile nanofiber mat," *Journal of nanoscience and nanotechnology,* vol. 13, pp. 6249-6253, 2013.
[212] J. S. Lee, O. S. Kwon, S. J. Park, E. Y. Park, S. A. You, H. Yoon*, et al.*, "Fabrication of ultrafine metal-oxide-decorated carbon nanofibers for DMMP sensor application," *ACS nano,* vol. 5, pp. 7992-8001, 2011.
[213] C. Kim, B. T. N. Ngoc, K. S. Yang, M. Kojima, Y. A. Kim, Y. J. Kim*, et al.*, "Self-Sustained Thin Webs Consisting of Porous Carbon Nanofibers for Supercapacitors via the Electrospinning of Polyacrylonitrile Solutions Containing Zinc Chloride," *Advanced Materials,* vol. 19, pp. 2341-2346, 2007.
[214] C. Kim and K. Yang, "Electrochemical properties of carbon nanofiber web as an electrode for supercapacitor prepared by electrospinning," *Applied physics letters,* vol. 83, pp. 1216-1218, 2003.
[215] L. Chen, L. Bromberg, H. Schreuder-Gibson, J. Walker, T. A. Hatton, and G. C. Rutledge, "Chemical protection fabrics via surface oximation of electrospun polyacrylonitrile fiber mats," *Journal of Materials Chemistry,* vol. 19, pp. 2432-2438, 2009.

[216] L. Zhang, J. Luo, T. J. Menkhaus, H. Varadaraju, Y. Sun, and H. Fong, "Antimicrobial nano-fibrous membranes developed from electrospun polyacrylonitrile nanofibers," *Journal of Membrane Science,* vol. 369, pp. 499-505, 2011.
[217] C. L. Phillip W. Gibson, Frank Ko, Darrell Reneker, "Application of Nanofiber Technology to Nonwoven Thermal Insulation," *Journal of Engineered Fibers and Fabrics,* vol. 2, pp. 32-40, 2007.
[218] K. J. Lee, N. Shiratori, G. H. Lee, J. Miyawaki, I. Mochida, S.-H. Yoon, *et al.*, "Activated carbon nanofiber produced from electrospun polyacrylonitrile nanofiber as a highly efficient formaldehyde adsorbent," *Carbon,* vol. 48, pp. 4248-4255, 2010.
[219] K. Saeed, S. Y. Park, and T. J. Oh, "Preparation of hydrazine-modified polyacrylonitrile nanofibers for the extraction of metal ions from aqueous media," *Journal of Applied Polymer Science,* vol. 121, pp. 869-873, 2011.
[220] H.-f. Xiang, S.-x. Tan, X.-l. Yu, Y.-h. Long, X.-l. Zhang, and N. Zhao, "Sound absorption behavior of electrospun polyacrylonitrile nanofibrous membranes," *Chinese Journal of Polymer Science,* vol. 29, pp. 650-657, 2011.
[221] H. Zhang, H. Nie, D. Yu, C. Wu, Y. Zhang, C. J. B. White, *et al.*, "Surface modification of electrospun polyacrylonitrile nanofiber towards developing an affinity membrane for bromelain adsorption," *Desalination,* vol. 256, pp. 141-147, 2010.
[222] R. Bagherzadeh, M. Latifi, S. S. Najar, M. Gorji, and L. Kong, "Transport properties of multi-layer fabric based on electrospun nanofiber mats as a breathable barrier textile material," *Textile Research Journal,* vol. 82, pp. 70-76, 2012.
[223] A. P. S. Sawhney, B. Condon, K. V. Singh, S. S. Pang, G. Li, and D. Hui, "Modern Applications of Nanotechnology in Textiles," *Textile Research Journal,* vol. 78, pp. 731-739, 2008.
[224] B. Johnson and K. Standiford, *Practical Heating Technology*: Cengage Learning, 2008.
[225] *Heat Transfer and Cooking* (2007, 09 April). Available: http://www.cookingforengineers.com
[226] 0097-6326, "Energy Conservation Program: Test Procedures for Conventional Cooking Products; Proposed Rule," vol. 232, ed. United States: Office of the Federal Register, National Archives and Records Service, General Services Administration, 2014.
[227] *The Science of Cooktops* (9 April, 2016). Available: http://www.finecooking.com/
[228] Frima. *VarioBoost™: the patented heating system will really speed up your cooking* (2015, 9 April). Available: https://www.frima-online.com
[229] H. R. Pant, M. P. Bajgai, C. Yi, R. Nirmala, K. T. Nam, W.-i. Baek, *et al.*, "Effect of successive electrospinning and the strength of hydrogen bond on the morphology of electrospun nylon-6 nanofibers," *Colloids and Surfaces A: Physicochemical and Engineering Aspects,* vol. 370, pp. 87-94, 2010.
[230] B. L. Deopura, R. Alagirusamy, M. Joshi, and B. Gupta, *Polyesters and Polyamides*: Elsevier Science, 2008.
[231] R. Sinclair, *Textiles and Fashion: Materials, Design and Technology*: Elsevier Science, 2014.
[232] S. Zhang, W. S. Shim, and J. Kim, "Design of ultra-fine nonwovens via electrospinning of Nylon 6: Spinning parameters and filtration efficiency," *Materials & Design,* vol. 30, pp. 3659-3666, 2009.
[233] M. B. Bazbouz and G. K. Stylios, "The tensile properties of electrospun nylon 6 single nanofibers," *Journal of Polymer Science Part B: Polymer Physics,* vol. 48, pp. 1719-1731, 2010.
[234] C. Mit-uppatham, M. Nithitanakul, and P. Supaphol, "Effects of Solution Concentration, Emitting Electrode Polarity, Solvent Type, and Salt Addition on

Electrospun Polyamide-6 Fibers: A Preliminary Report," in *Macromolecular Symposia*, 2004, pp. 293-300.
[235] S. S. Ojha, M. Afshari, R. Kotek, and R. E. Gorga, "Morphology of electrospun nylon-6 nanofibers as a function of molecular weight and processing parameters," *Journal of applied polymer science,* vol. 108, pp. 308-319, 2008.
[236] R. Nirmala, H. R. Panth, C. Yi, K. T. Nam, S.-J. Park, H. Y. Kim*, et al.*, "Effect of solvents on high aspect ratio polyamide-6 nanofibers via electrospinning," *Macromolecular Research,* vol. 18, pp. 759-765, 2010.
[237] R. Nirmala, R. Navamathavan, M. H. El-Newehy, and H. Y. Kim, "Preparation and characterization of electrospun ultrafine polyamide-6 nanofibers," *Polymer International,* vol. 60, pp. 1475-1480, 2011.
[238] R. Nirmala, K. T. Nam, S.-J. Park, Y.-S. Shin, R. Navamathavan, and H. Y. Kim, "Formation of high aspect ratio polyamide-6 nanofibers via electrically induced double layer during electrospinning," *Applied Surface Science,* vol. 256, pp. 6318-6323, 2010.
[239] J. H. Park, B. S. Kim, Y. C. Yoo, M. S. Khil, and H. Y. Kim, "Enhanced mechanical properties of multilayer nano-coated electrospun nylon 6 fibers via a layer-by-layer self-assembly," *Journal of applied polymer science,* vol. 107, pp. 2211-2216, 2008.
[240] C. Carrizales, S. Pelfrey, R. Rincon, T. M. Eubanks, A. Kuang, M. J. McClure*, et al.*, "Thermal and mechanical properties of electrospun PMMA, PVC, Nylon 6, and Nylon 6, 6," *Polymers for Advanced Technologies,* vol. 19, pp. 124-130, 2008.
[241] D. Aussawasathien, C. Teerawattananon, and A. Vongachariya, "Separation of micron to sub-micron particles from water: electrospun nylon-6 nanofibrous membranes as pre-filters," *Journal of Membrane Science,* vol. 315, pp. 11-19, 2008.
[242] Y. Guibo, Z. Qing, Z. Yahong, Y. Yin, and Y. Yumin, "The electrospun polyamide 6 nanofiber membranes used as high efficiency filter materials: Filtration potential, thermal treatment, and their continuous production," *Journal of Applied Polymer Science,* vol. 128, pp. 1061-1069, 2013.
[243] P. Heikkilä, A. Taipale, M. Lehtimäki, and A. Harlin, "Electrospinning of polyamides with different chain compositions for filtration application," *Polymer Engineering & Science,* vol. 48, pp. 1168-1176, 2008.
[244] J. Matulevicius, L. Kliucininkas, D. Martuzevicius, E. Krugly, M. Tichonovas, and J. Baltrusaitis, "Design and characterization of electrospun polyamide nanofiber media for air filtration applications," *J. Nanomaterials,* vol. 2014, pp. 14-14, 2014.
[245] S. De Vrieze, N. Daels, K. Lambert, B. Decostere, Z. Hens, S. Van Hulle*, et al.*, "Filtration Performance of Electrospun Polyamide Nanofibres Loaded With Bactericides," *Textile Research Journal,* 2011.
[246] A. Aluigi, C. Tonetti, C. Vineis, C. Tonin, and G. Mazzuchetti, "Adsorption of copper(II) ions by keratin/PA6 blend nanofibres," *European Polymer Journal,* vol. 47, pp. 1756-1764, 2011.
[247] B. Ding, Y. Si, X. Wang, J. Yu, L. Feng, and G. Sun, "Label-free ultrasensitive colorimetric detection of copper (II) ions utilizing polyaniline/polyamide-6 nano-fiber/net sensor strips," *Journal of Materials Chemistry,* vol. 21, pp. 13345-13353, 2011.
[248] B. Ding, X. Wang, J. Yu, and M. Wang, "Polyamide 6 composite nano-fiber/net functionalized by polyethyleneimine on quartz crystal microbalance for highly sensitive formaldehyde sensors," *Journal of Materials Chemistry,* vol. 21, pp. 12784-12792, 2011.
[249] Y. Li, Y. Si, X. Wang, B. Ding, G. Sun, G. Zheng*, et al.*, "Colorimetric sensor strips for lead (II) assay utilizing nanogold probes immobilized polyamide-6/nitrocellulose nano-fibers/nets," *Biosensors and Bioelectronics,* vol. 48, pp. 244-250, 2013.

[250] J. E. Oliveira, V. P. Scagion, V. Grassi, D. S. Correa, and L. H. Mattoso, "Modification of electrospun nylon nanofibers using layer-by-layer films for application in flow injection electronic tongue: Detection of paraoxon pesticide in corn crop," *Sensors and Actuators B: Chemical,* vol. 171, pp. 249-255, 2012.
[251] X. Wang, B. Ding, J. Yu, and M. Wang, "Highly sensitive humidity sensors based on electro-spinning/netting a polyamide 6 nano-fiber/net modified by polyethyleneimine," *Journal of Materials Chemistry,* vol. 21, pp. 16231-16238, 2011.
[252] K. Devarayan, D. Lei, H.-Y. Kim, and B.-S. Kim, "Flexible transparent electrode based on PANi nanowire/nylon nanofiber reinforced cellulose acetate thin film as supercapacitor," *Chemical Engineering Journal,* vol. 273, pp. 603-609, 2015.
[253] A. Liu, A. Walther, O. Ikkala, L. Belova, and L. A. Berglund, "Clay nanopaper with tough cellulose nanofiber matrix for fire retardancy and gas barrier functions," *Biomacromolecules,* vol. 12, pp. 633-641, 2011.
[254] T. C. Dickenson, *Filters and Filtration Handbook*: Elsevier Advanced Technology, 1997.
[255] D. B. Purchas and K. Sutherland, *Handbook of Filter Media*: Elsevier Advanced Technology, 2002.
[256] I. M. Hutten, *Handbook of Nonwoven Filter Media*: Butterworth-Heinemann, 2007.
[257] K. R. Spurny, *Advances in Aerosol Gas Filtration*: Taylor & Francis, 1998.
[258] S. Yang and G. W. Lee, "Filtration characteristics of a fibrous filter pretreated with anionic surfactants for monodisperse solid aerosols," *Journal of aerosol science,* vol. 36, pp. 419-437, 2005.
[259] H. Fong, W. Liu, C.-S. Wang, and R.A. Vaia, "Generation of electrospun fibers of Nylon 6 and Nylon 6-montmorillonite nanocomposite," *Polymer,* vol. 43, pp. 775-780, 2002.
[260] I. M. Hutten, *Handbook of Nonwoven Filter Media*: Elsevier Science, 2015.
[261] 3M, Respirators Direct. *About respirators* (2015, 10 April). Available: http://www.respiratorsdirect.net/
[262] N. Jaksic, D. Jaksic, and H.-Y. Jeon, "Novel Theoretical Approach to the Filtration of Nano Particles Through Non-Woven Fabrics," in *Woven Fabrics*. vol. 1: Intechopan, 2012, pp. 205-234.
[263] Wearamask. *Face Masks vs. Respirators* (2009, 10 April). Available: http://www.wearamask.org/
[264] A. Bałazy, M. Toivola, A. Adhikari, S. K. Sivasubramani, T. Reponen, and S. A. Grinshpun, "Do N95 respirators provide 95% protection level against airborne viruses, and how adequate are surgical masks?," *American Journal of Infection Control,* vol. 34, pp. 51-57, 2006.
[265] EN 149:2001, "Respiratory protective devices – Filtering half masks to protect against particles – Requirements, testing, marking," ed: European committee for standardization, 2001.
[266] B. Demir, I. Cerkez, S. D. Worley, R. M. Broughton, and T.-S. Huang, "N-Halamine-Modified Antimicrobial Polypropylene Nonwoven Fabrics for Use against Airborne Bacteria," *ACS Applied Materials & Interfaces,* vol. 7, pp. 1752-1757, 2015.
[267] B. J. McCarthy, *Textiles for Hygiene and Infection Control*: Elsevier Science, 2011.
[268] I. Laird, R. Goldsmith, R. Pack, and A. Vitalis, "The effect on heart rate and facial skin temperature of wearing respiratory protection at work," *Annals of Occupational Hygiene,* vol. 46, pp. 143-148, 2002.
[269] Y. Wang, W. Li, Y. Xia, X. Jiao, and D. Chen, "Electrospun flexible self-standing [gamma]-alumina fibrous membranes and their potential as high-efficiency fine

particulate filtration media," *Journal of Materials Chemistry A,* vol. 2, pp. 15124-15131, 2014.
[270] F. Dotti, A. Varesano, A. Montarsolo, A. Aluigi, C. Tonin, and G. Mazzuchetti, "Electrospun porous mats for high efficiency filtration," *Journal of Industrial Textiles,* vol. 37, pp. 151-162, 2007.
[271] L. Li, M. W. Frey, and T. B. Green, "Modification of air filter media with nylon-6 nanofibers," *Journal of Engineered Fibers and Fabrics,* vol. 1, pp. 1-24, 2006.
[272] R. Barhate, C. K. Loong, and S. Ramakrishna, "Preparation and characterization of nanofibrous filtering media," *Journal of Membrane Science,* vol. 283, pp. 209-218, 2006.
[273] Y.-Y. Kuo, F. C. Bruno, and J. Wang, "Filtration Performance Against Nanoparticles by Electrospun Nylon-6 Media Containing Ultrathin Nanofibers," *Aerosol Science and Technology,* vol. 48, pp. 1332-1344, 2014.
[274] M. Faccini, D. Amantia, S. Vázquez-Campos, C. Vaquero, J. L. de Ipiña, and L. Aubouy, "Nanofiber-based filters as novel barrier systems for nanomaterial exposure scenarios," in *Journal of Physics: Conference Series*, 2011, p. 012067.
[275] C.-N. Kuo, H.-F. Chen, J.-N. Lin, and B.-Z. Wan, "Nano-gold supported on TiO2 coated glass-fiber for removing toxic CO gas from air," *Catalysis Today,* vol. 122, pp. 270-276, 2007.
[276] S. A. Muhamed, "Study and development of nonwovens made of electrospun composite nanofibers," PhD, Laboratory of Textile Physics and Mechanics (LPMT), Univerdity de Haute Alsace, France, 2016.
[277] B. Tony and B. David, "Electrical properties of polymers," ed: Campridge University press, 2005.
[278] S. AlMuhamed, "Study and development of nonwovens made of electrospun composite nanofibers," PhD, Laboratory od Textile Physics and Mechanics, University of Haute Alsace, Mulhouse, France, 2016.
[279] National Insititute of health. *Image J, Image processing and analysis in Java* (21 May). Available: https://imagej.nih.gov
[280] X.-l. HOU and W.-d. GAO, "Development of kawabata evaluation system-fabric (KES-F)[J]," *Wool Textile Journal,* vol. 3, pp. 46-48, 2005.
[281] J. Yip and S.-P. Ng, "Study of three-dimensional spacer fabrics:: Physical and mechanical properties," *Journal of materials processing technology,* vol. 206, pp. 359-364, 2008.
[282] Frima. *Product highlights* (10 May). Available: www.frima-online.com
[283] S. Lee, J. Kim, B.-C. Ku, J. Kim, and H.-I. Joh, "Structural evolution of polyacrylonitrile fibers in stabilization and carbonization," 2012.
[284] I. M. Alarifi, A. Alharbi, W. S. Khan, A. Swindle, and R. Asmatulu, "Thermal, electrical and surface hydrophobic properties of electrospun polyacrylonitrile nanofibers for structural health monitoring," *Materials,* vol. 8, pp. 7017-7031, 2015.
[285] S. Sell, C. Barnes, D. Simpson, and G. Bowlin, "Scaffold permeability as a means to determine fiber diameter and pore size of electrospun fibrinogen," *Journal of Biomedical Materials Research Part A,* vol. 85, pp. 115-126, 2008.
[286] L. Liu and Y. A. Dzenis, "Analysis of the effects of the residual charge and gap size on electrospun nanofiber alignment in a gap method," *Nanotechnology,* vol. 19, p. 355307, 2008.
[287] H. L. Schreuder-Gibson, P. Gibson, P. Tsai, P. Gupta, and G. Wilkes, "Cooperative charging effects of fibers from electrospinning of electrically dissimilar polymers," DTIC Document2005.

[288] G. Collins, J. Federici, Y. Imura, and L. H. Catalani, "Charge generation, charge transport, and residual charge in the electrospinning of polymers: A review of issues and complications," *Journal of Applied physics,* vol. 111, p. 044701, 2012.
[289] Minitab Inc. *Basics of correlation and covariance* (2016, 05 April). Available: http://support.minitab.com/
[290] A. Wong and Y. Li, "Relationship between thermophysiological responses and psychological thermal perception during exercise wearing aerobic wear," *Journal of Thermal Biology,* vol. 29, pp. 791-796, 2004.
[291] K. Prasad, W. Twilley, and J. R. Lawson, "Thermal Performance of Fire Fighters' Protective Clothing. 1. Numerical Study of Transient Heat and Water Vapor Transfer," *National Institute of Standards and Technology, Gaithersburg, MD,* 2002.
[292] L. Yi, L. Fengzhi, and Z. Qingyong, "Numerical simulation of virus diffusion in facemask during breathing cycles," *International journal of heat and mass transfer,* vol. 48, pp. 4229-4242, 2005.
[293] M. Matusiak, "Investigation of the thermal insulation properties of multilayer textiles," *Fibres & Textiles in Eastern Europe,* vol. 14, pp. 98-102, 2006.
[294] M. Sampath, S. Mani, and G. Nalankilli, "Effect of filament fineness on comfort characteristics of moisture management finished polyester knitted fabrics," *Journal of Industrial Textiles,* vol. 41, pp. 160-173, 2011.
[295] B. Das, A. Das, V. Kothari, R. Fanguiero, and M. De Araújo, "Effect of fibre diameter and cross-sectional shape on moisture transmission through fabrics," *Fibers and Polymers,* vol. 9, pp. 225-231, 2008.

Appendix A

1. Spunbond nonwoven

The nonwoven structure produced by bonding filaments (produced by melt spinning), as they move out of a spinneret. The bonding of filaments is normally achieved by application of heat through calendaring.

2. Meltblown nonwoven

They are similar to spunbond nonwoven in that they are also produced from filaments obtained from molten polymer passing through a spinneret. However, here the filaments are further meltblown to get finer filaments, that are deposited on a suitable media and bonded together by heat treatment. The nonwoven produced in this manner are finer and softer than spun bond nonwoven.

3. Confidence interval

It gives the range of values that is likely to include an unknown parameter and describes the uncertainty related to an estimate of the population parameter. For example, 95% confidence interval means we can expect 95% of intervals to contain the population parameter.

4. Null hypothesis

Null hypothesis is a form of hypothesis testing where an initial claim is considered to be true and then this clam is tested by sample data. A null hypothesis claims that there is no significant difference between specified populations. When negated, it means that there is significant difference between specified populations. Thus, the populations are confirmed to be different from each other. This methodology is employed to assess the effect produced by different levels of a parameter. If the levels produce statistically different outputs the parameter is considered to have significant impact on outputs.

5. P-value

Frequently used in ANOVA, the P-value determines whether a relation between variables is significant or not. If P-value is less than or equal to the α-level (referred to as level

of significant usually considered as 0.05 i-e 95% confidence interval), the relationship can be considered to be significant.

6. Main effects plot

Used to visualize the effect of input variables on output variables. It determines the differences between output means obtained on each level of input. A main effect is considered to be present when different input levels affect the output differently.

7. Surface plot

It represents the relationship between two of the factors (input variables) with the response (output variable), keeping all other factors at constant value. It allows to visualize the changes in response as values of both the factors are changed and is based on model equation developed from data.

8. Residual

It is the difference between observed values and those calculated from data. It determines the effectiveness of any model

9. R-sq

It represents the variation in response data as explained by the predictors and determines the extent to which the model fits experimental data. Higher value of R-sq shows better fit of model for the data.

10. Noise variables

The parameters that can cause a change in response but cannot be controlled during a process are called noise variables. However, experimental setups on lab scale may be designed to simulate noise variables so that the process could be studied.

11. Pearson correlation coefficient

Ranging between -1 and +1, Pearson correlation coefficient is used to determine the strength and direction (direct or inverse proportionality) of correlation between variables. It is

normally employed to assess the relationship between variables that are linearly related to each other.

12. EN 149 +A, Keywords : Modelling, optimization, electrospinning, heat generation, respiratory protection, morphological characterization, nanocomposite, nanofibres

A standard test method for determination of filtration efficiency and breathing resistance (along with some other related properties such as inward leakage, extended exposure and flammability) of filtering half mask for respiratory protection. For measurement of filtration resistance, sodium chloride particles or aerosol of paraffin oil droplets (generated by spraying the paraffin oil) is passed through the filter media. The concentration of particles or aerosol is measured upstream and downstream of the filter under test using appropriate sensors, as shown in figure A.1. The difference between the upstream and downstream concentrations corresponds to the percentage of their penetration. For breathing resistance, compressed air is passed through the filter at preprogrammed rates. Pressure sensors placed before and after the filter are used to determine the pressure drop.

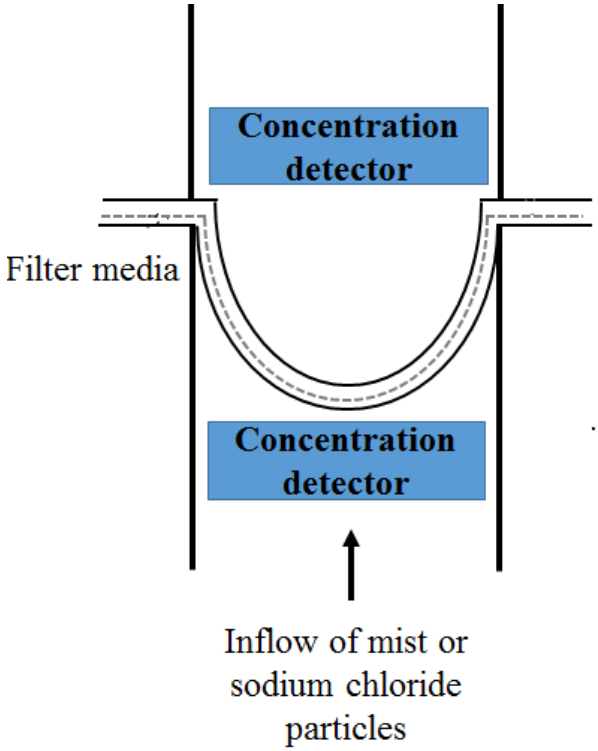

Figure A.1: Schematic representation for measurement of filtration performance as defined by EN 149 +A-2001